Effect of Fuel Composition on Aldehyde Emissions from Spark Ignition Engines

Varun Shankar

Pembroke College

University of Oxford

A thesis submitted for the degree of

Doctor of Philosophy

Hilary 2024

This thesis is dedicated to my mum, dad, and brother
for their endless love, invaluable wisdom, and unwavering support.

Acknowledgements

First and foremost, I extend my deepest gratitude to my supervisor, Prof. Felix Leach, for giving me the opportunity to pursue this research under his guidance. His invaluable advice, constant support, and mentorship have been pivotal in overcoming challenges and reaching project milestones.

I also wish to express my sincere thanks to Dr. Roger Cracknell, for his mentorship and guidance, especially valuable during the initial stages of defining the project's scope.

Special appreciation is due to Prof. Richard Stone, for his practical assistance and advice in building and rectifying issues with the single-cylinder engine test cell, a critical component of my project. My gratitude extends to Prof. Martin Davy, Prof. XiaoHang (Leo) Fang, Dr. Nathan Hinton, and Dr. Nikola Sekularac, for their support with the laminar burning velocity work, which has significantly enriched my research knowledge and capability. I am also thankful to Dr. Christopher Willman for serving as the interim supervisor, providing guidance and support during a crucial phase of my project.

My heartfelt thanks go to the current and previous members of the Thermal Propulsion Systems Research Group (TPSRG) including Samuel White, Samuel Baker, Tejo Jehart, Ruixuan Zhu, Qichi He, Daniel Bundred, Dr. Priyav Shah, Dr. Li Shen, and Dr. Abdullah Bajwa, Dr. Hannah Rana, Dr. Maruthi Malladi, Dr. Karthick Chakravarthy, for their collaboration and efforts to foster a supportive and dynamic working environment.

I am grateful to Nick Molden and Dr. Ime Usen from Emissions Analytics for their support and collaboration with the real-driving work which added great value to this project.

I am deeply grateful to the Rhodes Trust for significantly enhancing my personal and professional development, in addition to providing financial support throughout my DPhil.

I would also like to thank the John Fell Fund for their support in acquiring the emissions analyser and fuels, which have been pivotal to my research.

Last but certainly not least, I must express my profound gratitude to my family and friends. Their unwavering support, encouragement, and faith have been the foundation of my journey.

Abstract

The transport sector is a substantial contributor to global greenhouse gas emissions. To address this, governments are pursuing policies including vehicle electrification and the promotion of renewable fuels. Ethanol stands out as a promising alternative fuel due to its low-carbon potential and compatibility with current infrastructure.

However, aldehydes, particularly formaldehyde and acetaldehyde, are both observed emissions and major intermediates in the oxidation of gasoline/ethanol fuel mixtures. A rise in the ambient concentration of aldehydes due to transport emissions can affect atmospheric chemistry, contributing to ozone and secondary pollutant formation. The International Agency for Research on Cancer (IARC) classifies formaldehyde as carcinogenic and acetaldehyde as probably carcinogenic. While most research primarily associates these emissions with the ethanol content in fuel, investigations into other components have yielded inconsistent results. There is a gap in thoroughly understanding the effect of fuel composition on aldehyde emissions.

Therefore, this work considers aldehyde emissions from commonly used gasoline surrogate components, including ethanol, iso-octane, n-heptane, and toluene, which are representative of different fuel classification groups. They were evaluated in their pure forms and in binary, ternary, and quaternary blends to investigate how ethanol's interaction with each component influences aldehyde emissions. Additionally, two market-representative fuels, E0 (no ethanol) and E10 (10 %v/v ethanol in gasoline), were formulated from refinery streams.

Formaldehyde and acetaldehyde emissions were assessed from a single-cylinder gasoline direct injection engine, operated under conditions of low speeds and loads. These operating conditions have been reported as being conducive to increased aldehyde production. The impact of varying the fuel-air equivalence ratio (ϕ) from lean to rich conditions was also evaluated. The aldehydes were measured at 5 Hz using the Fourier Transform Infrared (FTIR) spectroscopy method.

These experimental investigations were supported with chemical kinetics analyses, which examined formaldehyde and acetaldehyde across several reactor models, including plug flow reactor (PFR), perfectly-stirred reactor (PSR), spherical constant volume combustion vessel, and one-dimensional single-cylinder engine models.

Additionally, the market-representative fuels (E0 and E10) were investigated on four light-duty gasoline vehicles. Real-driving emissions (RDE) of formaldehyde and acetaldehyde were measured using a volatile organic compounds (VOCs) system which could segregate the emissions based on driving phase.

Aldehyde emissions from pure ethanol were ten-fold and five-fold greater than pure toluene and iso-octane, respectively. Greater formaldehyde than acetaldehyde was found for iso-octane and toluene, while the opposite was true for ethanol. Pure toluene produced negligible quantities (10 to 30 ppm) of aldehydes. The addition of iso-octane, toluene, and n-heptane to ethanol inhibited aldehyde formation. Specifically, toluene was more effective in reducing formaldehyde emissions, whereas n-heptane showed a stronger effect on acetaldehyde suppression.

Chemical kinetics analyses indicated that at low temperatures, ethanol's oxidation directly produced acetaldehyde. Adding other fuel components creates competition among H, OH, and HO_2 radicals, leading ethanol to favour chain-propagating reactions over chain-terminating ones, thus reducing stable intermediate aldehyde formation. These processes, influenced by temperature, pressure, and fuel-air ratio, vary within the combustion chamber, affecting aldehyde formation.

RDE tests showed aldehyde emissions were greatest at cold-start and lowest under motorway conditions. A 30 % increase in tailpipe formaldehyde emissions for E10 compared to E0 for 3 out of the 4 cars tested. Acetaldehyde emissions were below the detectable threshold for both E0 and E10 fuels, likely removed by the after-treatment system. However, in the single-cylinder engine (with no after-treatment system), the acetaldehyde emissions were detected for both E0 and E10, with the latter producing higher quantities.

This study showed that components other than ethanol in a gasoline surrogate can generate aldehyde emissions. When blended, the interaction between these components can result in reduced aldehyde emissions. However, the extent of suppression and their specific impacts on formaldehyde and/or acetaldehyde vary based on the composition of the blend. Further studies on a broader range of engine operating conditions, coupled with enhancements in chemical kinetic mechanisms and reactor models for accurately predicting aldehyde formation, consumption, and emissions, would be beneficial for developing strategies to mitigate these emissions.

Contents

List of Figures

List of Tables

List of Abbreviations

General

0-D . . . . . Zero-dimensional

1-D . . . . . One-dimensional

2,4-DNPH 2,4-Dinitrophenylhydrazine

°CA . . . . . Crank angle degrees

AA . . . . . Acetaldehyde

AFR . . . . . Air-fuel equivalence ratio

AHRR . . . . . Apparent heat release rate

ASME . . . . . American Society of Mechanical Engineers

BDC . . . . . Bottom dead centre

BEV . . . . . Battery electric vehicle

BNC . . . . . Berkeley Nucleonics Corporation

CARB . . . . . California air resources board

CC . . . . . Carbonyl compound

CD . . . . . Chassis dynamometer

CF . . . . . Counter flow

CNRS . . . . . Centre National de la Researche Scientifique

CoV . . . . . Coefficient of variation

CS . . . . . Cold-start

DIDS . . . . . Direct injection driver system

DVPE . . . . . Dry vapour pressure equivalent

ECD . . . . . Electron capture detector

EPA . . . . . Environmental protection agency

EPRF . . . . . PRF with ethanol

ETPRF . . . . . TPRF with ethanol

EU . . . . . European Union

EUDC . . . . . Extra urban drive cycle

EVC . . . . . Exhaust valve closing

EVO . . . . . Exhaust valve opening

FA . . . . . Formaldehyde

FA:AA . . . . . Formaldehyde-to-acetaldehyde ratio

FID . . . . . Flame ionisation detector

FTP . . . . . Federal test procedure

FTIR . . . . . Fourier transform infrared spectroscopy

GC . . . . . Gas chromatography

GCxGC . . . . . Two-dimensional gas chromatography

GDI . . . . . Gasoline direct injection

GHG . . . . . Greenhouse gas

GPF . . . . . Gasoline particulate filter

GPS . . . . . Global positioning system

GT . . . . . Gamma technologies

GTR . . . . . Global technical regulations

HAP . . . . . Hazardous air pollutant

HC . . . . . Hydrocarbon

HF . . . . . Heat flux

HiQAQ . . . . . High-speed data acquisition

HPLC . . . . . High performance liquid chromatography

Hz . . . . . Hertz

IARC . . . . . International agency for research on cancer

ICE . . . . . Internal combustion engine

IDT . . . . . Ignition delay time

IEA . . . . . International energy agency

IVO . . . . . Intake valve opening

IVC . . . . . Intake valve closing

JSAE . . . . . Japan Society of Automotive Engineers

JSR . . . . . Jet-stirred reactor

KAUST . . . . . King Abdullah University of Science and Technology

LBV . . . . . Laminar burning velocity

LDV . . . . . Light-duty vehicle

LHV . . . . . Lower heating value

LLNL . . . . . Lawrence Livermore National Laboratories

M . . . . . Motorway

M1 . . . . . Mechanism M1

M2 . . . . . Mechanism M2

MCM . . . . . Master chemical mechanism

MON . . . . . Motor octane number

NASA . . . . . National Aeronautics and Space Administration

NEDC . . . . . New European drive cycle

NI . . . . . National Instruments

nIMEP . . . . . Net indicated mean effective pressure

NMHC . . . . . Non-methane hydrocarbons

NMOG . . . . . Non-methane organic gases

NTC . . . . . Negative temperature coefficient

PAN . . . . . Peroxy acetyl nitrate

PAH . . . . . Polycyclic aromatic hydrocarbon

PC . . . . . Personal computer

PEMS . . . . . Portable emissions measurement system

PF . . . . . Plug flow reactor

PFI . . . . . Port fuel injection

PM . . . . . Particulate matter

PSR . . . . . Perfectly-stirred reactor

R . . . . . Rural

RFNBO . . . . . Renewable fuel of non-biological origin

RFS . . . . . Renewable fuel standard

RDE . . . . . Real-driving emissions

RFNBO . . . . . Renewable fuel of non-biological origin

RON . . . . . Research octane number

RfC . . . . . Reference concentration

SF . . . . . Spherical flame

SI . . . . . Spark ignition

T10 . . . . . 10 %v/v distillation

T50 . . . . . 50 %v/v distillation

TDC . . . . . Top dead centre

TDCf . . . . . Top dead centre firing

THC . . . . . Total hydrocarbons

TOF-MS . . . . . Time-of-flight mass spectroscopy

TWC . . . . . Three-way catalyst

UNECE . . . . . United Nations Economic Commission for Europe

U.S. . . . . . United States

U . . . . . Urban

UDC . . . . . Urban drive cycle

UHC . . . . . Unburned hydrocarbons

UV . . . . . Ultraviolet

VOC . . . . . Volatile organic compound

WLTC . . . . . Worldwide harmonised light duty test cycle

Mathematical nomenclature

ϕ	Fuel-air equivalence ratio
λ	Air-fuel equivalence ratio
τ	Residence time
P	Pressure
T	Temperature
t	Time
i	Reaction number
$m_{reactions}$	Set of reactions
$n_{species}$	Number of species
v_{ki}	Stoichiometric coefficient
k	Species
q_i	Rate of progress of reaction i
$K_i^{reverse}$	Reverse rate constant
$K_i^{forward}$	Forward rate constant
$[X_k]$	Molar concentration of species k
ω_k	Rate of production of species, k
χ_k	chemical symbol for the kth species
A	Pre-exponential factor
E_a	Reaction activation energy
n	Temperature exponent
R	Gas constant
$\Delta H^{\ddagger}$	Enthalpy of activation of each reaction
$\Delta S^{\ddagger}$	Entropy of activation of each reaction
$C_{p,k}^{\ominus}$	Constant pressure specific heat capacity
p	Constant pressure
$H_k^{\ominus}$	Enthalpy of species, k

$S_k^{\ominus}$ . . . . . Entropy of species, k

a_d . . . . . NASA polynomial coefficients (d = 1 to 7)

Fuels in this study

E . . . . . Ethanol

E100 . . . . . Pure ethanol

EH . . . . . Ethanol and n-heptane

EO . . . . . Ethanol and iso-octane

ET . . . . . Ethanol and toluene

H . . . . . N-heptane

HE65 . . . . . N-heptane and 65 %v/v ethanol

HE85 . . . . . N-heptane and 85 %v/v ethanol

HO95 . . . . . N-heptane and 95 %v/v iso-octane

HT . . . . . N-heptane and toluene

O . . . . . Iso-octane

O100 . . . . . Pure iso-octane

OE20 . . . . . Iso-octane and 20 %v/v ethanol

OE50 . . . . . Iso-octane and 50 %v/v ethanol

OE85 . . . . . Iso-octane and 85 %v/v ethanol

OH . . . . . Iso-octane and n-heptane

OHE . . . . . Iso-octane, n-heptane, and ethanol

OHE20 . . . . . Iso-octane, n-heptane, and 20 %v/v ethanol

OHE85 . . . . . Iso-octane, n-heptane, and 85 %v/v ethanol

OHT . . . . . Iso-octane, n-heptane, and toluene

OT . . . . . Iso-octane and toluene

PRF . . . . . Primary reference fuel

PRF-E . . . . . PRF with ethanol

PRF-E20 . . . . . PRF with 20 %v/v ethanol

PRF-E85 . . . . . PRF with 85 %v/v ethanol

T . . . . . Toluene

T100 . . . . . Pure toluene

TE25 . . . . . Toluene and 25 %v/v ethanol

TE50 . . . . . Toluene and 50 %v/v ethanol

TE75 . . . . . Toluene and 75 %v/v ethanol

THEO . . . . . Toluene, n-heptane, ethanol, and iso-octane

THOE20 . . . . . Toluene, n-heptane, iso-octane, and 20 %v/v ethanol

THOE85 . . . . . Toluene, n-heptane, iso-octane, and 85 %v/v ethanol

TO25 . . . . . Toluene and 25 %v/v iso-octane

TO50 . . . . . Toluene and 50 %v/v iso-octane

TO75 . . . . . Toluene and 75 %v/v iso-octane

TPRF . . . . . Toluene-based primary reference fuel

TPRF-E . . . . . TPRF with ethanol

TPRF-E20 . . . . TPRF with 20 %v/v ethanol

TPRF-E85 . . . . TPRF with 85 %v/v ethanol

OHT_HighT . . . Iso-octane, n-heptane, and high toluene

OHT_LowT . . . Iso-octane, n-heptane, and low toluene

OTE25_HighT . . Iso-octane, 25 %v/v ethanol, and high toluene

OTE25_LowT . . Iso-octane, 25 %v/v ethanol, and low toluene

1

Introduction

Contents

Greenhouse gas (GHG) emissions from industrialisation contribute significantly to climate change. In particular, anthropogenic emissions of greenhouse gases from the transport sector have grown in the last two decades. In 2023, this sector accounted for approximately 23 % of the global carbon dioxide (CO_2) emissions, with passenger vehicles contributing to a significant share of 33 % [1].

The path towards decarbonisation of the road transport sector is encouraging governments, car manufacturers, and energy companies to experiment with innovative fuels and powertrain technologies. By 2035, it is anticipated that there will be close to 1.5 billion vehicles on the road globally, with only a quarter of those being low emission vehicles

under the policies as of 2023 [1]. However, the primary technology considered for low emission vehicles in these policies was pure battery electric vehicles (BEVs), whose benefits depend on the decarbonisation of electricity generation and improved energy efficiency. Therefore, alternative solutions are needed to supplement the BEV growth to reduce the GHG emissions from the transport sector. Renewable fuels present an avenue for transitioning the transportation sector towards reduced lifecycle emissions with minimal adjustments to existing powertrain architectures and energy infrastructure.

1.1 Renewable fuels

Renewable fuels can be divided into three categories: standard biofuels, advanced biofuels, and renewable fuels of non-biological origin (RFNBO). Standard biofuels are usually derived from biomass feedstocks, such as biodegradable, agricultural, or forestry products, or biodegradable industrial and municipal wastes or residues. Advanced biofuels are made from non-edible feedstocks and by-products. RFNBOs are primarily synthetic fuels obtained through the combination of captured CO_2 and green hydrogen (H_2), which could be obtained from electrolysis of water powered by renewable electricity, though there can be other ways to produce green hydrogen too. The International Energy Agency (IEA) state that ramping up biofuels as a supplement to electrification will play a major role in decarbonising road transport to 2030 [2]. Consequently, the well-established biofuel sector production is forecasted to expand by 38 billion litres over 2023-2028, a near 30 % increase from the last five-year period, to meet the total global biofuel demand [2]. On the other hand, RFNBOs are still nascent and their growth is dependent on excess renewable electricity.

The most common biofuel is ethanol as it can easily be produced through fermentation of sugars. Ethanol can also be produced as an advanced biofuel from lignocellulosic biomass and algae. The European Union (EU) has set a minimum target of 3.5 % advanced biofuel use by 2030 [3]. In the United States (U.S.), the renewable fuel standard (RFS) and the California low-carbon fuel standard both encourage the use of biofuels. Major Asian

countries, including India and China, also support the development of bio-refineries with a mandated focus on advanced biofuel production for use in the transport sector [4].

These initiatives are driven by the observation that blending increasing proportions of renewable fuels with conventional fuel can lead to a reduction in life-cycle GHG emissions. However, there is a need for more stringent vehicle tailpipe emissions regulations to address the currently unregulated toxic pollutants generated by the combustion of renewable fuels. It is important to test renewable fuels, such as ethanol, and their interactions with conventional fuels to assess their impact on exhaust emissions and ensure that any harmful pollutants are adequately regulated.

1.2 Emissions

Ethanol-blended gasoline has been recognised as a promising strategy for the reduction in regulated emissions of carbon monoxide (CO), CO_2, tailpipe particulate matter (PM), and unburned hydrocarbons (UHC) [5]. In spark ignition (SI) engines, there has been an observed reduction in soot and polycyclic aromatic hydrocarbons (PAH), which are a major precursor to soot [6]. The impact of ethanol on nitrogen oxides (NO_x) emissions is still inconclusive with some studies that show a reduction, whilst others show a promotion [5].

However, a disadvantage of these fuels is the significant increase in aldehyde emissions, which have a deteriorating impact on air quality, as detailed in Section 1.3.1. Aldehydes contribute to the formation of secondary pollutants like peroxyacetyl nitrate (PAN) and play a role in ozone formation. Aldehyde emissions also pose a health risk, as detailed in Section 1.3.2. Continuous exposure to aldehydes can affect the respiratory system.

1.3 Aldehydes

Aldehydes are classified as carbonyl compounds (CCs) as they contain the carbonyl functional group composed of a carbon atom double-bonded to an oxygen atom (C=O). Specifically, aldehydes have the structure $-$CHO consisting of a carbonyl centre with a hydrogen, H, bonded to one side and an alkyl group, R, on the other side. The other CC

type is a ketone, where the C=O is in between two alkyl groups, R and R'. An alkyl group represents an alkane with a missing hydrogen atom, hence its attachment to the carbonyl function group. Both are illustrated in Figure 1.1.

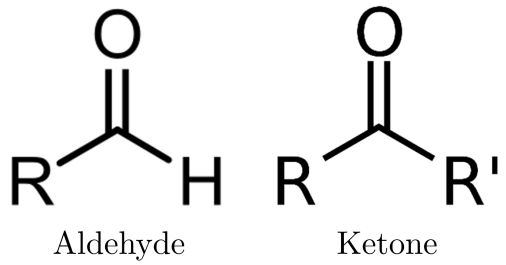

Figure 1.1: Generic aldehyde and ketone structures

Aldehydes are emitted through anthropogenic sources, including paint fumes and combustion of fuels, and natural sources such as vegetation [7]. Formaldehyde (CH_2O) and acetaldehyde (CH_3CHO) are the two most abundant aldehydes in ambient air. During combustion, the quantity of the aldehyde emissions depend on a multitude of factors including fuel composition, combustion temperature, engine operating conditions, age of catalytic converter, and traffic conditions [8]. One of the primary pathways for aldehyde formation is the partial oxidation of unburned fuel hydrocarbons. Therefore, when considering fuel composition, the presence of oxygenated fuels, such as ethanol, may contribute to increased acetaldehyde emissions due to the partial oxidation of these fuel molecules. Aldehydes can also be formed as intermediate products when the decomposition of unburned fuel hydrocarbons is interrupted due to reduced temperature and oxygen concentration in the exhaust. Therefore, during cold-start, the incomplete combustion and lower exhaust temperatures favour the formation of aldehydes, especially acetaldehyde when ethanol is present in the fuel. Each of these factors will be reviewed in detail in Chapter 2.

1.3.1 Air quality impact

Aldehydes may also be considered secondary pollutants because they can form indirectly from unburned renewable fuel emissions, as shown by the atmospheric conversion of unburned ethanol to formaldehyde, acetaldehyde, and PAN in Figure 1.2 [9]. This is a

representation of the Master Chemical Mechanism (MCM) degradation scheme for the reaction of ethanol with the hydroxyl (OH) radical in the presence of NO_x adapted from Dunmore *et al.* [10]. Due to the high volatility of aldehydes, they are categorised as oxygenated volatile organic compounds (VOCs).

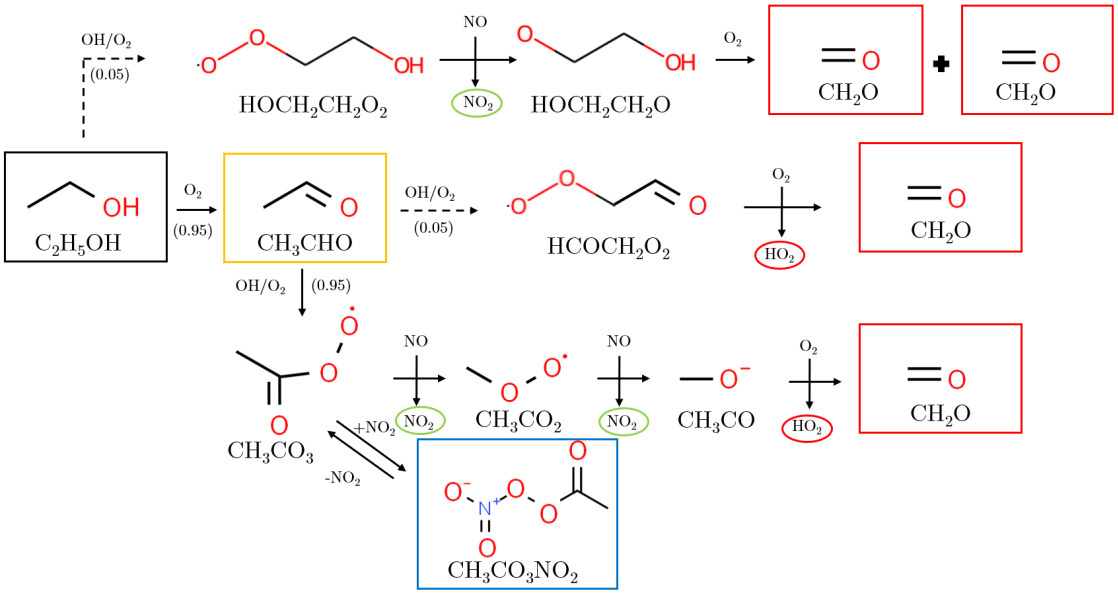

Figure 1.2: Simplified schematic mechanism for the photo-oxidation of ethanol initiated by the OH radical in the atmosphere. Reproduced (adapted) from Dunmore *et al.* [10] with permission from the Royal Society of Chemistry. Ethanol, formaldehyde, acetaldehyde, and PAN are boxed in black, red, orange, and blue, respectively. The NO to NO_2 conversions and HO_2 formation are highlighted by green and red circles, respectively.

A rise in the ambient concentration of aldehydes can affect atmospheric chemistry, leading to increased formation of ozone and secondary pollutants [7, 11]. The ozone (O_3) is formed through a chain of photochemical reactions dependent on solar radiation, high temperatures, and concentrations of aldehydes and nitrogen oxides (NO_x) [7]. Higher ozone levels have direct impacts on climate change by acting as a potent GHG, therefore contributing to global warming. Additionally, increased ozone concentrations can damage vegetation and reduce agricultural productivity, while also playing a significant role in the formation of photochemical smog, further deteriorating local air quality.

Aldehydes can also act as a GHG in both the vapour and the aerosol phases as they are strong infrared absorbers, and can contribute to local heating of the atmosphere [12].

It should be noted that the concentration of these species depends on meteorological conditions including temperature, humidity, and wind speed [13].

The increase in ambient concentrations of aldehydes has been studied around the world, particularly in areas with increased uptake of ethanol, such as Brazil [7, 8, 14, 15], Mexico [16], parts of the U.S. [17, 18], and China [19].

1.3.2 Health impacts

Direct inhalation of formaldehyde and acetaldehyde can be detrimental to human and animal health in numerous ways. The International Agency for Research on Cancer (IARC) and the U.S. Environmental Protection Agency (EPA) have extensively studied the effect of each of these CCs [20, 21]. Based on these investigations, they classify the pollutants into groups that define their carcinogenicity and outline any other effects as shown in Table 1.1. The reference inhalation concentration (RfC) represents an estimate of continuous inhalation exposure to the human population that is likely to be without an appreciable risk of deleterious effects during a lifetime [22].

Given the link between CC exposure and respiratory impairment, Petroni *et al.* [23] showed that chronic exposure to these pollutants even at very low levels, reduces the ability of the body to recover from COVID-19 in the United States of America. Similar effects have been observed in other studies which show coughing, burning sensation in the nose and throat, and asthma-like symptoms due to inhaling these pollutants [24, 25].

Jacobson *et al.* [17] were able to associate the increased usage of high ethanol content fuels with cancer and mortality in the United States of America. There is also an increasing focus placed on higher carbon number alcohol components in a fuel blend, such as incorporating butanol [26]. Therefore, longer carbon chain aldehydes including propionaldehyde, butyraldehyde, and crotonaldehyde would also need to be reviewed as they form part of the emissions from longer chain alcohols [27–29]. Currently, the concentrations of these pollutants are significantly less and their primary effects include irritation to the skin and eye [30].

Table 1.1: Health effect of most dominant aldehydes

Name	IARC Group*	Health effect	RfC (μg/m^3)	Ref
Formaldehyde	1	nasopharyngeal cancer; eye irritation, dry and/or sore throats, inflammation, bronchial asthma-like symptoms, childhood asthma, and upper respiratory tract infections; potentially leukemia; pregnancy problems and menstrual disorders	9.8	[24, 31–34]
Acetaldehyde	2A	Eye and respiratory tract irritant. At higher concentrations, can cause damage to respiratory and cardiovascular systems in humans	9	[35–37]

* Group 1 and 2A refer to carcinogenic and probably carcinogenic to humans, respectively.

1.3.3 Current emissions legislation

Given the significant health and air quality concerns associated with aldehyde emissions, including formaldehyde and acetaldehyde, it is crucial to regulate these hazardous air pollutants (HAPs). Beyond standard pollutants, regulations often focus on total hydrocarbons (THC) and a subset known as non-methane hydrocarbons (NMHC), which excludes methane. More specific legislation considers the sum of non-methane and oxygenated (NMOG) hydrocarbons (HCs) present in a gas sample, encompassing all oxygenated organic gases with up to five carbon atoms. Therefore, aldehydes are often accounted for in either the THC, NMHC, and/or NMOG categories.

Flame ionisation detector (FID) is the standard instrument for THC measurement and is calibrated using propane. However, its response to aldehydes is inconsistent due to a reduced sensitivity to oxygenated compounds. Wallner *et al.* [38] highlighted this issue, showing that alcohol addition in fuel also leads to significant under-reporting of THC emissions by FID, due to a reduced response to oxygenated emissions (unburned alcohols and carbonyls) in the exhaust. To rectify this, they developed a methodology using response factors to accurately quantify the levels of THC and oxygenated emissions, including aldehydes, in the exhaust, especially for alcohol-based fuels. Nonetheless, Suarez-Bertoa *et al.* [39] reported that aldehyde emissions are still significantly under-

predicted when measured using FID, with discrepancies up to 74 % for fuels with high ethanol content.

To overcome these measurement challenges, alternative techniques such as impingers, 2,4-Dinitrophenylhydrazine (2,4-DNPH) cartridges coupled with gas chromatography (GC) and/or high performance liquid chromatography (HPLC), and Fourier Transform Infrared (FTIR) spectroscopy are employed. These methods provide a more accurate and specific assessment of NMOG and particularly aldehyde emissions as further elaborated in Section 2.6.

Currently, three major markets have established aldehyde emission limits. The U.S. Tier 3 standards set a formaldehyde limit of 2.5 mg/km [40, 41] and Brazil has the PROCONVE L7 regulations, which set a limit of 15 mg/km for the combined emissions of formaldehyde and acetaldehyde [42, 43]. The Republic of Korea has a formaldehyde limit of 7 mg/km in the K-LEVIII standards [44]. Future regulations in these areas are looking at stricter rules for aldehyde emissions. The European standards set limits for hydrocarbon emissions quantified using FID [45]. This methodology is also adopted in India and China [4]. However, this technique does not individually consider the emissions of standard and oxygenated VOCs. Even with the response factors, there may be inaccuracies in estimating actual aldehyde emissions from vehicles fuelled with ethanol blends, as discussed earlier [38]. With the growing adoption of renewable fuels, particularly methanol and ethanol, in these regions, implementing a uniform limit on aldehyde emissions could mitigate the potential rise in ambient levels of these compounds.

1.4 Objectives

In countries where the transition to electrified road transportation remains challenging for the foreseeable future, the integration of ethanol into gasoline presents a viable alternative for achieving low-carbon mobility. However, existing literature has highlighted that the blending of ethanol has been associated with increased aldehyde emissions.

This research systematically aims to identify and quantify the impact of gasoline fuel composition, with a particular emphasis on ethanol, on the generation of toxic and currently

unregulated aldehyde emissions. Aldehydes such as formaldehyde and acetaldehyde, are not only classified as carcinogenic, but also play a significant role in atmospheric chemistry, rapidly converting into greenhouse gases.

1.5 Thesis outline

The thesis is structured into nine chapters. Chapter 2 presents a comprehensive review of the existing literature, identifying the gaps and objectives for the subsequent experimental and theoretical investigations.

Chapters 3 and 4 delve into the methodologies used in this study. Chapter 3 details the experimental setup, discussing the selection of research and surrogate fuels, the configuration of the single-cylinder engine test cell, and the real-driving emissions equipment. It also outlines the general procedures followed in each test. Chapter 4 provides an in-depth look at the numerical modelling tools used, focusing on their application in understanding the chemical kinetics behind aldehyde formation under a range of operating conditions. This chapter also includes a thorough validation of two gasoline surrogate chemical kinetic mechanisms, to enable their application in later chapters.

The primary experimental results are presented in Chapters 5 and 6, which focus on the research and surrogate fuels, respectively. These chapters explore the aldehyde emissions observed under a range of operating conditions. Each test run comprised data from 300 engine cycles and was repeated three times to ensure accuracy and repeatability.

In Chapter 7, the fuel matrix from Chapters 5 and 6 was simulated in a series of reactor models, including a single-cylinder engine model. These simulations aim to provide deeper insights into the chemical kinetics, complementing the experimental findings.

Chapter 8 shifts the focus to real-driving aldehyde emissions, featuring results from four modern passenger vehicles fuelled with two specially formulated fuels, both with and without ethanol. These fuels were designed to have similar physical and chemical

properties, allowing for a direct comparison. This chapter also integrates data from the single-cylinder engine to support the real-driving test results.

The thesis ends with Chapter 9, which synthesises the main conclusions drawn from the research. It recaps the key findings and provides areas for future research to further enhance the understanding of aldehyde emissions from gasoline SI engines.

1.6 List of Publications

A part of the content presented in **Chapter 4** has been peer-reviewed and published in the papers enlisted below with the respective contributions.

The contribution of V. Shankar to the following paper includes: Data curation, and Writing - original draft.

- Sekularac N., Fang X., Shankar V., Baker S.J., Leach F.C.P., and Davy M.H., "Development of a Laminar Burning Velocity Empirical Correlation for Combustion of iso-octane/ethanol Blends in Air". *Fuel*, Vol 307, 121880, 2022. doi.org/10.1016/j.fuel.2021.121880

The contribution of V. Shankar to the following paper includes: Investigation, Formal analysis, and Writing original draft.

- Shankar V., Fang X., Hinton N.I.D., Davy M.H., and Leach F.C.P., Effect of Ethanol Addition on the Laminar Burning Velocities of Gasoline Surrogates. *Fuel*, Vol 327, 125186, 2022. doi:10.1016/j.fuel.2022.125186

The contribution of V. Shankar to the following paper includes: Conceptualisation, Investigation, Data curation, Formal analysis, Visualisation, and Writing - original draft. Additionally, the paper was presented at a conference.

- Shankar V., Fang X., Hinton N.I.D., Davy M.H., and Leach F.C.P., Effect of Ethanol Addition on the Laminar Burning Velocity of Gasoline Surrogates with Toluene". *American Society of Mechanical Engineers (ASME), ICE Division Fall Technical*

Conference, Vol. 86540, ICEF2022-90452, 2022. doi.org/10.1115/ICEF2022-90452

A part of the content presented in **Chapter 5** has been peer-reviewed, published, and presented at a conference. The contribution of V. Shankar to the following paper includes: Conceptualisation, Methodology, Investigation, Data curation, Formal analysis, Validation, Visualisation, and Writing - original draft.

- Shankar V., and Leach F.C.P., "Effects of Oxygenate and Aromatic Content on Engine-out Aldehyde Emissions from Pure, Binary, and Ternary mixtures of Ethanol, Toluene, and Iso-octane". *Society of Automotive Engineers (SAE) Technical Paper - JSAE/SAE Powertrains, Energy and Lubricants International Meeting*, 2023-32-0029, 2023. doi.org/10.4271/2023-32-0029

A part of the content presented in **Chapter 8** has been peer-reviewed, published, and presented at a conference. The contribution of V. Shankar to the following paper includes: Conceptualisation, Methodology, Investigation, Formal analysis, Visualisation, and Writing - original draft.

- Shankar V., Usen I., Molden N., Willman C., and Leach F.C.P., "Comparing Real Driving Emissions from Euro 6d-TEMP Vehicles running on E0 and E10 Gasoline Blends". *SAE Technical Paper - Energy & Propulsion Conference & Exhibition*, 2023-01-1662, 2023. doi.org/10.4271/2023-01-1662

A part of the content presented in **Appendix A** has been peer-reviewed, published, and presented at a conference. The contribution of V. Shankar to the following paper includes: Investigation, Data curation, and Writing - original draft.

- Bajwa A.U., Shankar V., and Leach F.C.P., "Engine-out Ammonia Emissions from a Gasoline Direct Injection Engine". *SAE Technical Paper - Energy & Propulsion Conference & Exhibition*, 2023-01-1655, 2023. doi.org/10.4271/2023-01-1655

2

Literature review

Contents

2.1 Motivation

The formation, consumption, and emissions of aldehydes from SI engines are influenced by several factors. These include the composition of the fuel used, the operating conditions, and the ambient environment. This chapter firstly explores the effects of different gasoline surrogate fuel component groups on aldehydes and then reviews existing literature on aldehyde formation in a range of combustion reactors, from a plug flow reactor to engines in test cells and vehicles both on a chassis dynamometer and on the road. Finally, gaps are identified that will guide further investigation, emphasising the importance of thoroughly understanding the formation of aldehyde emissions from SI engines.

2.2 Effect of fuel components on aldehyde formation

Gasoline is a complex mixture of various types of hydrocarbon compounds. These include alkanes which can make up 4 to 8 %v/v; iso-alkanes, or branched alkanes, which can make up 25 to 40 %v/v; alkenes, or olefins, which constitute 2 to 5 %v/v; cyclo-alkanes, or naphthenes, account for 3-7 %v/v; cyclo-alkenes, or cyclic alkenes, constitute 1 to 4 %v/v; and aromatic hydrocarbons make up 20-35 %v/v [46]. Gasoline can also contain varying proportion of alcohol content, such as methanol or ethanol, dependent on the legislation. For instance, 10 %v/v of ethanol blending is typical, commonly referred to as E10. The type and quantity of fuel components blended in a fuel mixture influences the formation of aldehydes as a combustion intermediate, as observed in previous studies [47, 48]. This section delves into the impact of common fuel component classification groups on the formation of aldehydes.

2.2.1 Alkanes and branched alkanes

Alkanes and branched (iso-) alkanes constitute a significant portion of gasoline fuels and also referred to as paraffins and iso-paraffins, respectively. The thermal cracking and β-scission of these hydrocarbons, whether straight-chained or branched, lead to the formation of methyl and ethyl radicals [49]. β-scission is a chemical reaction in which a bond adjacent to a radical centre breaks, leading to the formation of two separate molecules, which are often radicals [50]. In this case, these radicals can react with oxygen to form formaldehyde and acetaldehyde, respectively, with the former, which is more commonly formed, shown at the top of Figure 2.1.

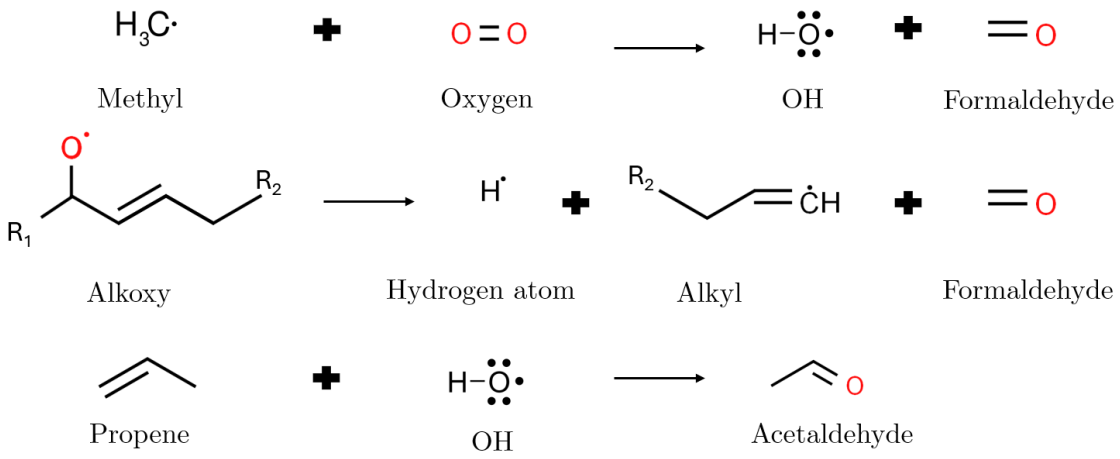

Figure 2.1: Decomposition pathways leading to aldehyde formation, originating from various radicals generated during the oxidation of branched alkanes.

Additionally, the low-temperature oxidation of alkanes, as shown by the Waddington mechanism, is also known to primarily yield carbonyls, especially formaldehyde [51]. Specifically, for branched alkanes such as iso-octane, Curran *et al.* [49] demonstrated that their low-temperature oxidation results in the formation of large alkoxy ($RO^{\bullet}$) radicals. These radicals can undergo β-scission, leading to the generation of stable aldehydes, primarily formaldehyde, alongside a hydrogen atom and an alkyl radical, as seen in the middle of Figure 2.1. Broustail *et al.* [52] also reported that for iso-octane, another pathway to produce formaldehyde is through acetaldehyde.

Furthermore, as larger alkanes are fragmented into smaller, more reactive molecules through β-scission, these can combine with hydroxyl ($HO^{\bullet}$) radicals, producing formaldehyde or acetaldehyde [53]. For instance, propene (C_3H_6), formed due to the decomposition of iso-octane, can react with hydroxyl ($HO^{\bullet}$) radicals to form acetaldehyde, as highlighted in studies by Ray *et al.* and Sway *et al.* [54, 55], and also shown in the bottom of Figure 2.1. However, when Barraza-Botet *et al.* [56] studied the combustion chemistry of iso-octane in a rapid compression machine, they reported that there are no significant pathways for formation of acetaldehyde from iso-octane. Nevertheless, Seidel *et al.* [57] found that acetaldehyde can be formed via various pathways by C_2 to C_7 species, of which about 11 % through low-temperature pathways, when studying n-heptane oxidation.

Whilst most of these studies indicate a link between alkanes and aldehyde formation, particularly formaldehyde, the majority of these studies were conducted in fundamental reactors that attempt to isolate the chemical kinetics by developing well-defined physical conditions. According to the author's knowledge, no engine or vehicle level based studies, where both physical and chemical factors play a role were conducted to solely examine the effects of alkanes, such as iso-octane, on engine-out or exhaust aldehyde emissions.

2.2.2 Alkenes

Alkenes, also referred to as olefins, are frequently found in fuel compositions and can also be produced alongside an alkyl radical during the decomposition of an alkane, particularly at high temperatures [58]. Alkenes primarily decompose into allylic radicals through hydrogen atom abstraction, which is a chemical process where a hydrogen atom is removed from a molecule by a radical, leading to the formation of new radicals. This process plays a critical role in combustion reactions. These allylic radicals can either undergo β-scission or react with hydroperoxyl ($HO_2^{\bullet}$) radicals, forming allyloxy radicals [58]. Subsequently, the allyloxy radicals break down via β-scission, generating an aldehyde and a vinylic radical. This potential reaction pathway for alkenes leading to aldehyde formation is shown in Figure 2.2 [58].

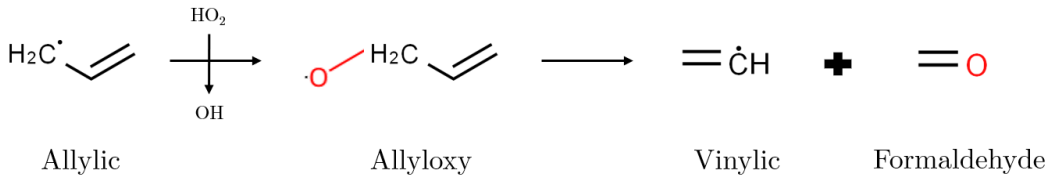

Figure 2.2: Allylic radical decomposition to aldehydes.

While earlier research by Grosjean *et al.* [59] identified a correlation between olefin content in a gasoline fuel composition and aldehyde emissions, more recent studies have not found a significant statistical trend [60–62].

2.2.3 Aromatics

Aromatics are incorporated into fuel compositions to enhance octane characteristics, which define the fuel's capability to resist knocking or premature combustion in an engine, thereby improving efficiency and performance. Karavalakis *et al.* [63] investigated the effects of increasing aromatic content from 15 %v/v to 35 %v/v while maintaining all other properties of an E10 (10 %v/v ethanol and 90 %v/v gasoline) market fuel on five gasoline direct injection (GDI) vehicles. They found no statistically significant effect on formaldehyde and acetaldehyde emissions. However, Goodfellow *et al.* [64] and Zervas *et al.* [65] reported that the lower carbon number aldehydes (formaldehyde and acetaldehyde) decreased with increasing aromatic content.

In contrast, when Yang *et al.* [61, 66] investigated the relationship between ethanol and aromatic content in fuels on aldehyde emissions, they observed that higher aromatic content fuels resulted in increased formaldehyde emissions. Shuetzle *et al.* [47] and Zhang et al. [67] also found significant impacts of aromatic contents on aldehyde emissions, similar to Yang *et al.* [61]. They suggest that formaldehyde and acetaldehyde are primarily generated by the methyl and ethyl radicals from the partial combustion of iso-paraffins and alkyl aromatics [47, 61]. In particular, Zhang *et al.* [67] reported that C8 and C9 aromatics strongly favoured aldehyde formation. He *et al.* [68] also found a link between aromatic content and aldehyde emissions from an engine test cell study and attributed the aldehydes' source to be incomplete oxidation of the aromatics.

Another pathway for aldehyde formation, specifically acetaldehyde, involves the decomposition of benzaldehyde, an inherent intermediate formed during toluene's oxidation [69, 70]. On the other hand, Reaction R1 illustrates the benzyl radical, produced via toluene's hydrogen abstraction, reacting with atomic oxygen to yield the phenyl radical and formaldehyde.

$$C_6H_5C^{\bullet}H_2 + O_2 \rightleftharpoons C_6H_5^{\bullet} + CH_2O \quad \{1\}$$

Not only do these studies show varied outcomes, but the complex oxidation process of toluene also complicates the identification of specific chemical reactions responsible for aldehyde formation. Additionally, these studies typically involve toluene as part of a broader fuel composition, including other components that may produce radicals influencing aldehyde formation and consumption.

To the best of the author's knowledge, the impact of toluene individually on aldehyde formation, consumption, and emissions in the context of an engine has not been studied. A focused investigation on toluene's independent effects would be beneficial before examining its interactions with other fuel components and the subsequent influence on aldehyde emissions.

2.2.4 Alcohols

Low carbon chain length alcohols, such as ethanol, are increasingly added to fuels due to their renewable origins and their ability to enhance the efficiency of spark ignition engines. The combustion characteristics of these alcohols and their emission profiles have been investigated in the literature [5]. Emissions from the combustion of such alcohols include formaldehyde, acetaldehyde, acetone, and acrolein. These oxygenated emissions can be associated with the combustion chemistry of alcohols, particularly taking into account the role of fuel-bound oxygen during combustion [5]. At high temperatures, hydrogen atom abstraction and β-scission of parent alcohols can lead to the formation of aldehydes, a process shown at the top part of Figure 2.3. Conversely, at lower temperatures, the

oxidation of α-hydroxyalkyl radicals results in the direct formation of carbonyls, as demonstrated in the bottom part of Figure 2.3 [71].

In alcohols, the hydrogen atom bonded to the carbon atom adjacent (α-position) to the $-$OH functional group is weaker due to electron delocalisation. Consequently, as identified by Sarathy *et al.* [5] and supported by Curran *et al.* [72], abstraction from this site occurs more readily, leading to a relatively higher formation of α-hydroxyalkyl radicals in alcohols compared to other sites. Furthermore, reactions occurring at the α-site are inhibiting, therefore resulting in the formation of stable aldehyde intermediates that are not further consumed and are subsequently emitted, as indicated in the studies by Mittal *et al.* [73] and Saggese *et al.* [74].

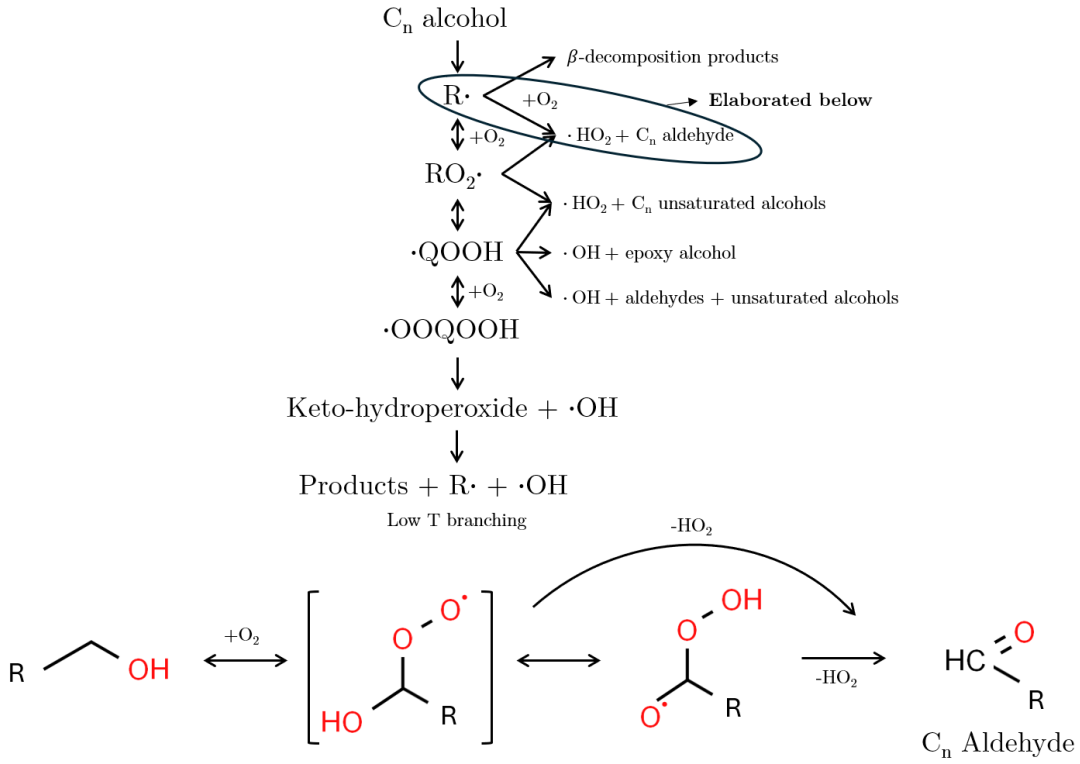

Figure 2.3: (Top) Schematic representation of alcohol's low-temperature oxidation mechanism. Reproduced (adapted) from Pelucchi *et al.* [75] with permission from the SAE International. **(Bottom)** generic α-hydroxyalkyl radical reaction with O_2 for any alcohol. Reproduced (adapted) from Da Silva *et al.* [71], Copyright 2009, with permission from American Chemical Society.

Ethanol, the most commonly used alcohol in gasoline, displays these trends as well, attributable to its $-$OH functional group [5]. In comparison to conventional low-temperature chain branching pathways, ethanol favours OH radical scavenging pathways

[76]. The breakdown of ethanol begins with the abstraction of a hydrogen atom, followed by β-scission, primarily yielding acetaldehyde as a stable intermediate. The reaction pathways of ethylhydroxy and α-hydroxyethyl radicals, originating from the hydrogen atom abstraction in ethanol, lead to the production of formaldehyde and acetaldehyde. These processes are detailed in Reactions R2 and R3, respectively [71, 77]. Similar to the general alcohol oxidation, the reaction at the α site is more common, thus leading to ethanol being a key precursor to acetaldehyde emissions.

$$CH_3CH_2O^{\bullet} \rightleftharpoons CH_2O + CH_3^{\bullet} \quad \{2\}$$

$$CH_3C^{\bullet}H_2O \rightleftharpoons CH_3CHO + H^{\bullet} \quad \{3\}$$

As alcohols, in particular ethanol, have shown a distinct relationship with aldehyde formation, they have also been investigated in engine test cells and vehicles, as further elaborated in Section 2.5. Nevertheless, for the majority of these studies, either ethanol was tested individually, or as part of gasoline composition. Fewer studies explored ethanol's interactions with individual fuel components that would commonly be found in a gasoline fuel.

2.2.5 Summary

The review of the literature indicates that various fuel component classification groups influence aldehyde generation and consumption, each exhibiting distinct underlying oxidation chemistries. Oxygenated fuel components have been shown to have specific oxidation pathways leading to aldehyde formation. In particular, ethanol has been directly associated with acetaldehyde generation. In contrast, groups such as aromatics, alkanes, and alkenes follow less direct pathways to aldehyde emissions. Many of these studies were conducted at a fundamental level, focusing on isolated chemical kinetic processes.

Additionally, engine-based studies have primarily examined the effect of varying a single component in a gasoline composition on aldehyde formation, consumption, and emissions.

Given the complexity of gasoline, which comprises a wide range of hydrocarbons with carbon chain lengths from 2 to 13, direct analysis of such mixtures is challenging. Consequently, the results have been inconsistent as the complex interactions among different fuel components can either enhance or inhibit aldehyde formation and thus affect emissions.

This review also highlighted the pivotal role of temperature in determining oxidation chemistry and the resultant aldehyde production from each of the fuel component groups. To further explore the impact of various operating conditions, these dynamics have been investigated across different reactors and engine types, as detailed in subsequent sections.

2.3 Fundamental reactors

Leveraging studies conducted in fundamental reactors can be beneficial for understanding how operating conditions influence the chemical kinetics of aldehyde generation. These reactors are able to separate physical and chemical processes, providing valuable data such as speciation measurements, ignition delay times, and flame speed metrics under controlled conditions. Therefore, this approach can offer a comprehensive understanding of the reaction dynamics involved.

2.3.1 Speciation studies

In a plug flow reactor (PFR) at the University of Melbourne, Lu *et al.* [78] examined the effects of adding ethanol to gasoline surrogates. In this reactor type, a diluted fuel, thoroughly mixed with an oxidiser, flows through a tube or pipe, reacting as it progresses. Each segment of the flow, or 'plug', is designed to maintain uniformity without axial mixing, ensuring perfect mixing only in the transverse direction. The reactor tube is maintained at a specific pressure and temperature, enabling detailed observation of reaction progression and species evolution at these conditions. An example of a variable pressure PFR from the Princeton University by Li *et al.* [79] is shown in Figure 2.4. From this, a simple one-dimensional model can be developed, as further elaborated in Section 4.5.2.

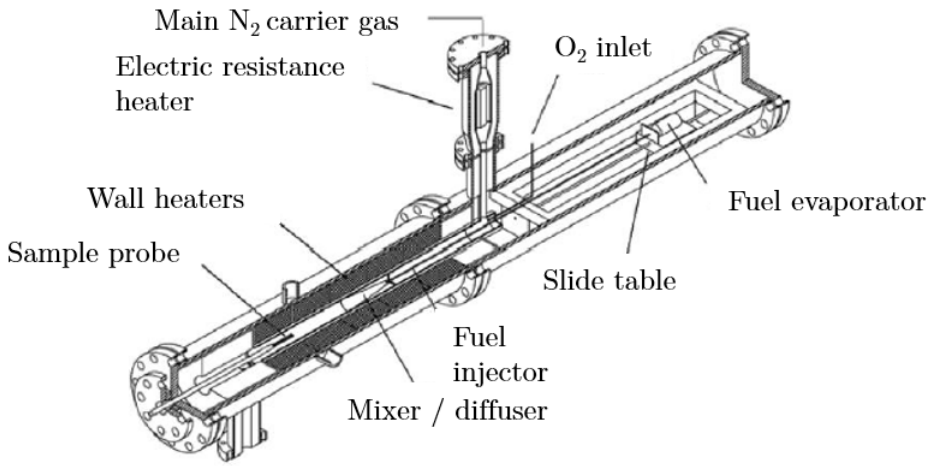

Figure 2.4: An experimental setup of the plug flow reactor (PFR). Reproduced (adapted) from Li *et al.* [79].

In the PFR, the group at University of Melbourne examined the effects of adding ethanol to iso-octane [78], a primary reference fuel (PRF) composed of iso-octane, and n-heptane [80], and a toluene-based primary reference fuel (TPRF) composed of toluene, iso-octane, and n-heptane [81]. The respective findings are shown in Figures 2.5 (a), (b), and (c).

For the iso-octane and ethanol (OE) blends, various mixtures with increasing ethanol content were analysed by Lu *et al.* [78], indicated by the number following the fuel name. For instance, OE20 consists of 20 %v/v ethanol, with the remainder being iso-octane.

The experimental data by the group at University of Melbourne [78, 80, 81] showed that reaction progression in the OE blends was slower compared to the ethanol and PRF (EPRF) or ethanol and TPRF (ETPRF) blends under similar conditions. A 4-fold increase in peak acetaldehyde concentration was observed at the end of the reactor with the addition of just 10 %v/v ethanol to iso-octane. In comparisons of blends containing 50 %v/v ethanol, the ETPRF blend exhibited a 45 % higher peak acetaldehyde concentration than the OE50 blend. Although the reactions in the OE blends appeared to still be in progress, this data suggests that additional components like n-heptane and toluene in the fuel mix accelerate the pathways leading to acetaldehyde formation. Additionally, the study indicated that the introduction of toluene to the ETPRF mixture resulted in a 3 % increase in peak acetaldehyde concentration compared to the EPRF blend. Conversely,

the incorporation of toluene into the PRF blend appeared to reduce and delay the peak acetaldehyde concentration, indicating a later onset of its formation.

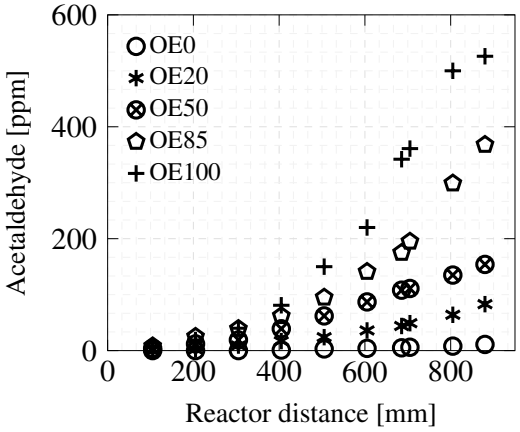

(a) Iso-octane and ethanol (OE) in PFR

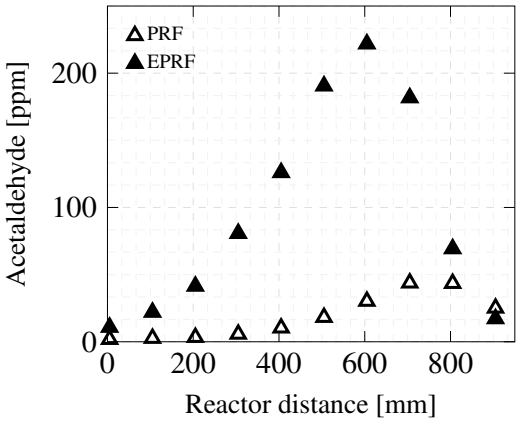

(b) PRF and EPRF blends in PFR

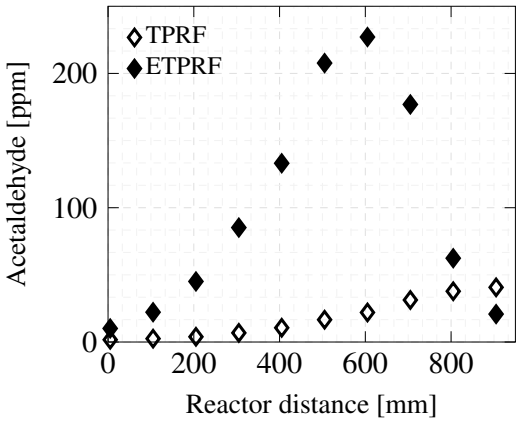

(c) TPRF and ETPRF blends in PFR

Figure 2.5: All percentages are %v/v; Acetaldehyde species concentration for **(a)** varying ethanol percentage volume addition to iso-octane; **(b)** PRF (iso-octane: 91 % / n-heptane: 9 %) and EPRF (iso-octane: 45.5 % / n-heptane: 4.5 % / ethanol: 50.0 %); and **(c)** TPRF (iso-octane: 53.2 % / n-heptane: 17 % / toluene: 29.8 %) and ETPRF (iso-octane: 26.6 % / n-heptane: 8.5 % / toluene: 14.9 % / ethanol: 50.0 %). All data is from the University of Melbourne PFR at 10 bar, air-fuel equivalence ratio (λ) = 0.058, and 875 K for **(a)** as well as 900 K for **(b)** and **(c)**. Figures **(a), (b),** and **(c)** are reproduced (adapted) from Combustion and Flame, Lu *et al.* [78], Copyright 2020, Proceedings of the Combustion Institute, Lu *et al.* [80], Copyright 2018, and Combustion and Flame, Yuan *et al.* [81], Copyright 2018, respectively, with permission from Elsevier.

In further analysis of the PFR data by Lu *et al.* [78], when comparing iso-octane with a PRF blend containing 9 %v/v n-heptane, it was observed that the addition of n-heptane not only accelerated the reaction progress and subsequent aldehyde formation, but also resulted in an increased peak acetaldehyde concentration, though the overall quantities

were still low. This finding emphasises the importance of studying the interactions between fuel components on aldehyde formation, beyond analysing pure components in isolation. Supporting this, Haas *et al.* [76] demonstrated that n-heptane's low-temperature reactions produce $HO_2^{\bullet}$ radicals, which can interact with ethanol to form $C_2H_5O^{\bullet}$ radicals. These radicals rapidly react with oxygen (O_2), leading to the production of acetaldehyde, as detailed in Section 2.2, while simultaneously regenerating $HO_2^{\bullet}$ radicals. This set of reactions contribute to the stable and high concentrations of acetaldehyde observed in the EPRF mixture. Conversely, the addition of ethanol into either iso-octane or n-heptane mixtures is shown to reduce formaldehyde concentrations, as shown in Figures 2.6 (a) and (b) for iso-octane and n-heptane, respectively.

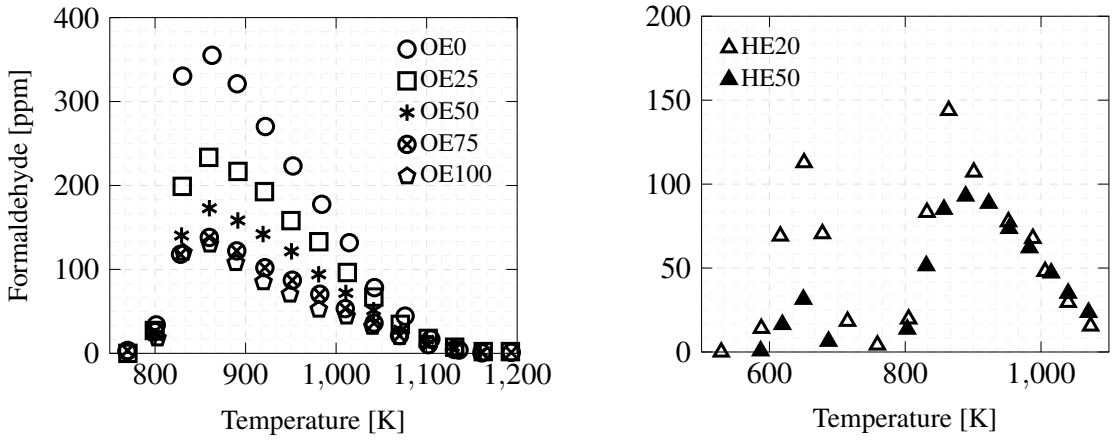

(a) Iso-octane and ethanol in JSR **(b)** N-heptane and ethanol in JSR

Figure 2.6: Formaldehyde species concentration across a temperature range at 10 bar and air-fuel equivalence ratio (λ) = 1 in the University of Orleans JSR with: **(a)** varying iso-octane and ethanol (OE) mixtures; and **(b)** varying n-heptane and ethanol. Figure **(a)** and **(b)** are reproduced (adapted) from Combustion Science and Technology, Dagaut *et al.* [82], Copyright 2012, and Fuel, Dagaut *et al.* [83], Copyright 2009, with permission from Informa UK Limited, trading as Taylor & Taylor & Francis Group and from Elsevier, respectively.

The data presented in Figure 2.6 was obtained by Dagaut *et al.* [82, 83] using a jet-stirred reactor (JSR), also known as a perfectly-stirred reactor (PSR). In a JSR, reactants are continuously introduced and products are constantly removed from a reactor that maintains a constant volume, ensuring homogeneous mixing and uniform conditions, thus providing an ideal setting for investigating steady-state chemical kinetics. The reactor pressure is held constant, and species concentrations are measured at specific residence

times, over a range of temperatures. This methodology allows for an understanding of how species concentrations vary with temperature under set pressure and initial equivalence ratio conditions.

A schematic of the experimental setup at University of Orleans [84] is shown in Figure 2.7. This can also be modelled as a zero-dimensional constant volume reactor, as further elaborated in Section 4.5.1.

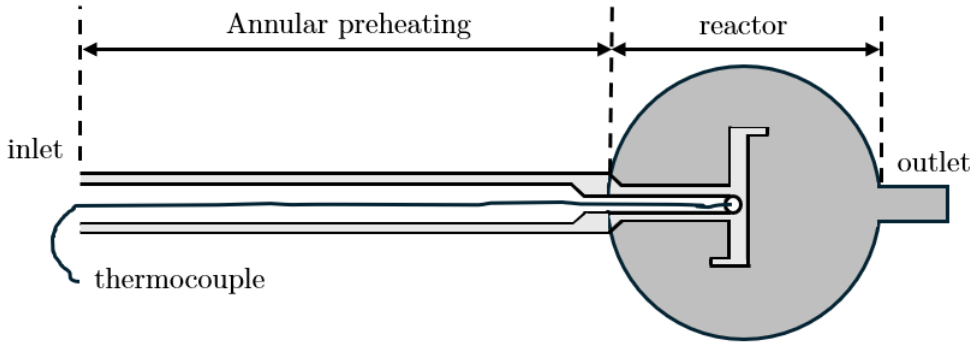

Figure 2.7: Schematic of an experimental setup of the JSR based on the equipment from the University of Orleans [84]. Reproduced (adapted) from Battin-Leclerc *et al.* [85] with permission from Springer Nature.

Dagaut *et al.* [83] and Li *et al.* [79] explored the influence of pressure and equivalence ratio on the formation and consumption of acetaldehyde (CH_3CHO), with results presented in Figure 2.8. The former collected data in a JSR whereas the latter used a PFR.

As the pressure increases, a decrease in peak acetaldehyde concentration was observed, along with a reduction in the temperature range where acetaldehyde was both formed and consumed. Consequently, this leads to a longer residence time for acetaldehyde within the reactor. These trends are illustrated in Figures 2.8 (a) and (b). In the case of richer fuel-air equivalence ratios (ϕ), which have more fuel than air relative to stoichiometric conditions, there is an increase in both the peak concentration of acetaldehyde and its residence time, as shown in Figures 2.8 (c) and (d). However, the temperature at which acetaldehyde forms is independent of the equivalence ratio for a given pressure and residence time.

This part of the literature offers additional insights into how operating conditions, such as pressure, temperature, and equivalence ratio, influence the subsequent production

and consumption of aldehydes in fuels. It highlights the importance of examining fuel components in fundamental reactors or their models, which can complement findings from engine-based studies.

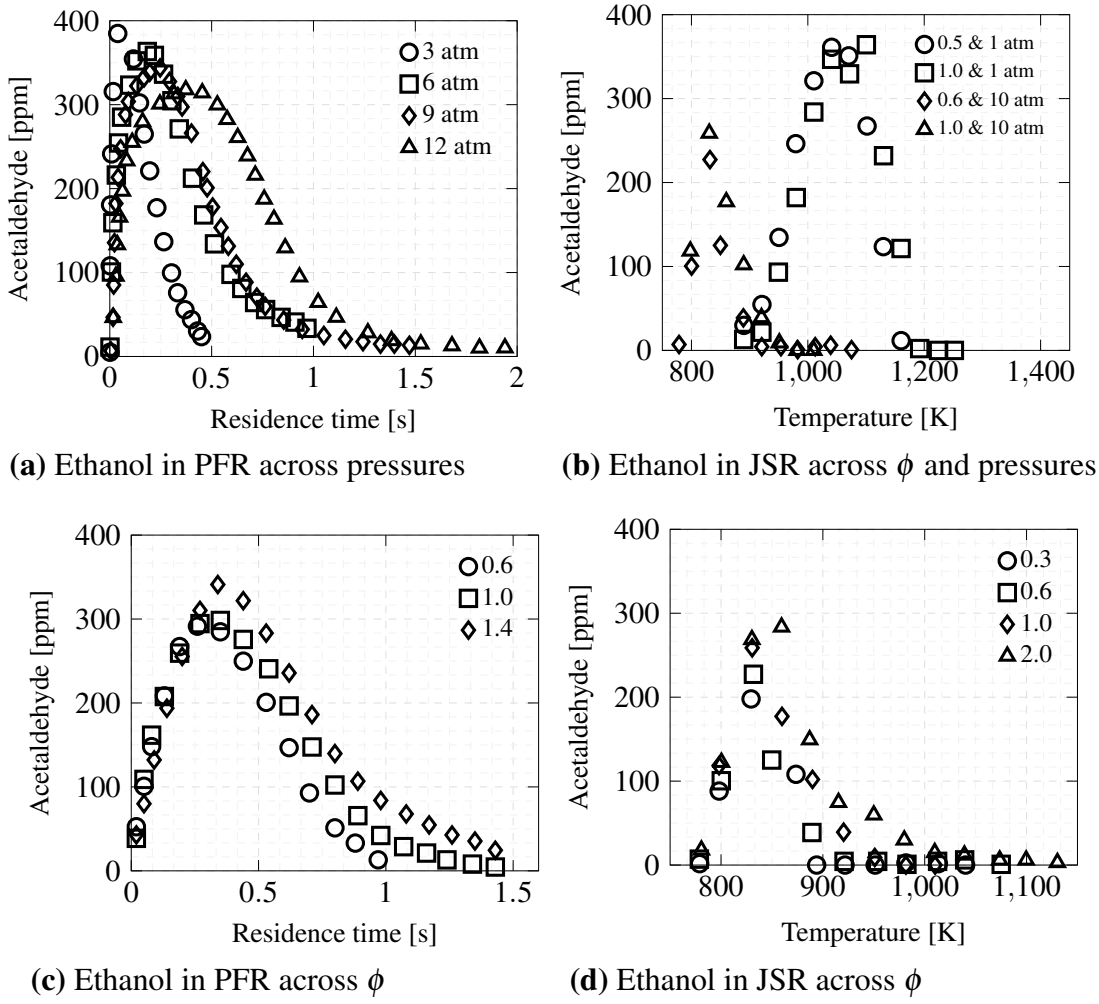

(a) Ethanol in PFR across pressures

(b) Ethanol in JSR across ϕ and pressures

(c) Ethanol in PFR across ϕ

(d) Ethanol in JSR across ϕ

Figure 2.8: Acetaldehyde species concentration from ethanol at: **(a)** $\phi = 0.6$ with varying pressures on time-history profile; **(b)** two fuel-air equivalence ratios and pressures across a temperature range; **(c)** 9 atm and 830 K with three different fuel-air equivalence ratios on time-history profile; and **(d)** 10 atm and residence time $\tau = 0.7$ s across a temperature range. **(a)** and **(c)** are from the data obtained in the Princeton University PFR. Reproduced (adapted) from Li *et al.* [79]. Whereas, **(b)** and **(d)** are from the data obtained in the University of Orleans JSR. Reproduced (adapted) from Fuel, Dagaut *et al.* [83], Copyright 2009, with permission from Elsevier.

2.3.2 Effect of aldehyde reactions on combustion parameters

The reaction pathways that lead to aldehyde formation can also affect the combustion properties of the fuel composition.

Ignition delay time

Adding ethanol to conventional gasoline components modifies ignition behaviour, as observed by changes in the ignition delay time (IDT). IDT is the time interval between fuel injection and the start of combustion and can be crucial in understanding a fuel's ignition characteristics. Specifically, the addition of ethanol leads to the disappearance of the negative temperature coefficient (NTC) region in the IDT, thus enhancing ignition propensity in the intermediate temperature range (900 K to 1050 K). In contrast, in the low-temperature region (below approximately 900 K), where engine knock, ethanol increases resistance to ignition. At these lower temperatures, ethanol promotes chain-terminating reactions that effectively scavenge OH radicals, leading to the production of stable intermediate aldehydes. These OH radicals are fundamental to the auto-ignition process, especially in the OH recombination reaction that forms H_2O_2. Therefore, the generation of aldehydes through alternative pathways consuming the OH radicals illustrates the intrinsic link between aldehyde formation and the characteristics of IDT. This highlights the complex combination effects of fuel composition, ignition behaviour, and emission formation.

Flame speed

The rate at which a flame front moves through a fuel mixture, known as flame speed, is a critical parameter characterising flame propagation inside a combustion chamber. This propagation can vary significantly, influenced by both fuel composition and operating conditions. Hinton [86] conducted studies on ethanol and its binary, tertiary, and quaternary blends with gasoline surrogate components like iso-octane, n-heptane, and toluene. Hinton [86] utilised a spherical constant volume combustion vessel for the experiments, the schematic of which is shown in Figure 2.9. In this setup, fuel is injected into a heated air stream using a syringe and actuator, with a pair of electrodes forming the spark gap at the centre of the vessel. Ignition is driven by a conventional automotive inductive ignition system. The approach used by Hinton [86] was versatile, allowing for two distinct methods of determining laminar burning velocities (LBV): through imaging of flame front propagation under constant pressure conditions, and by measuring the pressure

rise in conjunction with a constant volume combustion model. LBV is the measure of flame speed in a steady, unidirectional flow and is an essential metric for understanding how quickly and efficiently the fuel burns, directly impacting the combustion process and emissions.

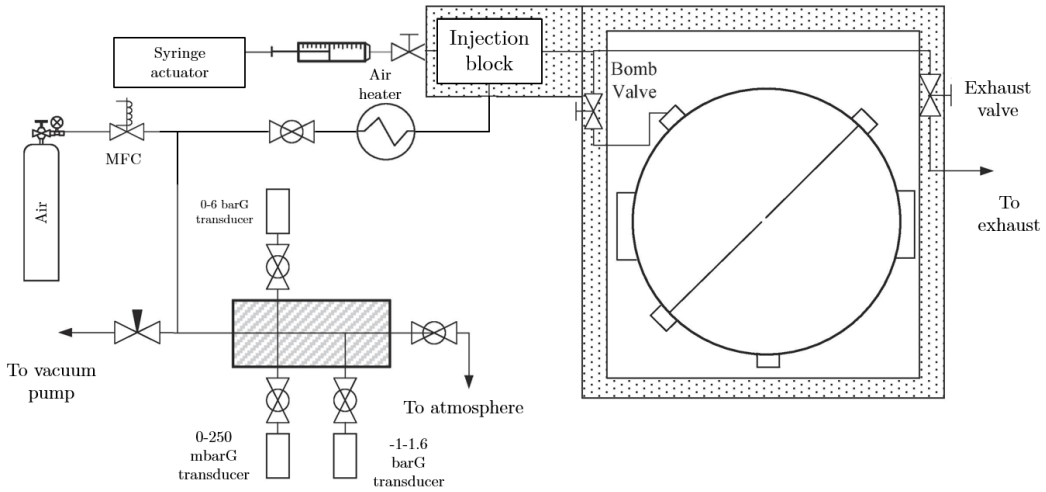

Figure 2.9: Schematic of an experimental setup for the spherical constant volume combustion vessel. Reproduced (adapted) from Fuel, Hinton *et al.* [87], Copyright 2018, with permission from Elsevier.

Studies by Hinton [86, 87], and supported by several others in literature [88, 89], consistently indicate that ethanol exhibits a higher LBV compared to many common gasoline surrogate fuel components. When added to fuel mixtures, ethanol enhances the overall blend's reactivity, thus increasing its LBV. The greater reactivity can be attributed to the chain-terminating reactions promoted by ethanol, which are also integral in the formation of acetaldehyde. These reactions effectively consume the OH radical pool, as highlighted by Lu *et al.* [78], leading to the generation of stable aldehyde intermediates. Consequently, the formation and consumption of aldehydes during ethanol's oxidation process is also shown to directly influence the LBV.

2.3.3 Summary

Research in fundamental reactors showcase how operating conditions and fuel composition impact aldehyde formation and consumption. Studies show that with pure ethanol, increased pressure leads to lower and earlier peak acetaldehyde concentrations. Richer

ethanol mixtures result in higher acetaldehyde levels over longer durations and broader temperature ranges. Blending ethanol with gasoline surrogates like PRFs and TPRFs, or components such as iso-octane and n-heptane, significantly increases acetaldehyde formation, with other components accelerating this process. These reactor studies can also provide critical insights into how different fuels influence combustion parameters, thereby highlighting their relationship with aldehyde formation and behaviour.

2.4 Effect of engine and fuel parameters

Beyond the scope of fundamental reactor studies, which allow for the isolation of physical and chemical processes, engine environments are more complex by the fact that both factors play an interdependent role. Given that this work will conduct experimental investigations of aldehyde emissions from a single-cylinder engine, this section presents a thorough review of engine-based studies from existing literature. It concentrates on examining the impact of standard engine parameters including engine speed, load, injection and ignition timing, as well as fuel parameters such as fuel-air equivalence ratio and volatility, on aldehyde emissions, as reported in previous studies. The common operating conditions at which aldehydes are formed and the gaps in literature are also identified to guide the experimental test matrix configuration.

2.4.1 Engine speed and load

The studies referenced investigate the impact of varying ethanol concentrations in fuel composition on aldehyde emissions, across different engine speeds and load conditions. These operating conditions present a complex interaction with aldehyde emissions. For instance, Gailis *et al.* [90] observed an increase in acetaldehyde emissions with engine load at higher speeds (2000 rpm), whereas the opposite trend at a lower speed of 1500 rpm.

However, Wallner *et al.* [91] observed higher emissions of formaldehyde and acetaldehyde at low speeds (1500 to 2000 rpm) and low loads (2 to 2.62 bar brake mean effective pressure (BMEP)), with emissions decreasing as speed and load increased. Similarly, Golke *et al.* [92], at a fixed engine speed of 1500 rpm, found that higher engine loads

resulted in lower aldehyde emissions, attributing this reduction to thermal oxidation mechanisms. Qian *et al.* [93] also reported a decrease in formaldehyde emissions with an increased load due to increased in-cylinder temperatures with higher loads. Furthermore, at an engine speed of 2800 rpm, Pang *et al.* [94] identified maximum engine-out aldehyde emissions under low load conditions, associating this with incomplete fuel combustion and reduced cylinder temperatures at low loads. Broustail *et al.* [52] highlighted the influence of fuel composition, reporting lower acetaldehyde emissions at increased ethanol concentrations and elevated loads (6 bar BMEP), due to the higher in-cylinder temperatures suppressing acetaldehyde formation at these higher loads.

On the other hand, Zarante *et al.* [95] found increased concentrations of aldehydes, particularly formaldehyde and acetaldehyde, with rising engine speed. Interestingly, they attribute this to the increase of exhaust gas temperature with engine speed due to the shorter time for the engine cycle to be completed, therefore delaying the combustion in the cycle. This in conjunction with increased concentrations of methane, ethane, and unburned ethanol oxidises in the exhaust to form the aldehydes [95]. However, this is highly dependent on the fuel composition.

These studies generally suggest that lower speeds and loads tend to increase aldehyde emissions. Consequently, further research focusing on the specific effects of varying ethanol concentrations in fuel on engine-out aldehyde emissions under these operating conditions would contribute to the existing literature.

2.4.2 Equivalence ratio

With conventional gasoline surrogates, Amaral *et al.* [96, 97] observed that enriching the fuel-air (ϕ) ratio (greater fuel than air relative to stoichiometric) resulted in reduced aldehyde emissions. Zervas *et al.* [65] demonstrated that acetaldehyde exhaust concentration peaks at stoichiometric conditions for iso-octane, as seen in Figure 2.10 (a). For these fuels, they found that under rich conditions, the acetaldehyde precursors are preferably transformed to CO, rather than to acetaldehyde due to the lack of oxygen. In lean

conditions, the reduction is acetaldehyde is observed as its precursors and acetaldehyde itself are rapidly oxidised. Similar behaviour was observed for formaldehyde.

However, when considering ethanol-blended fuels, Zervas *et al.* [65] noted that the peak concentration of acetaldehyde occurs under rich conditions ($\phi > 1$), as a result of the enhanced oxidation of unburned ethanol to acetaldehyde. This trend is illustrated Figure 2.10 (a) for E20 (20 %v/v ethanol in conventional fuel). On the other hand, Golke *et al.* [92] reported an increase in both formaldehyde and acetaldehyde emissions with mixture enleanment, attributed to the increased availability of oxygen. This was different to he findings of Zervas *et al.* at lean conditions. However, Oliveira *et al.* [98] reported that lean combustion reduces aldehydes emission for a fuel with high ethanol content (i.e., E95) but the contrary for a fuel with lower ethanol content (i.e., E27).

Therefore, aldehyde emissions demonstrate varied responses across different equivalence ratios, with the addition of ethanol playing a significant role in this behaviour. This highlights the need for additional research into the effects of gasoline surrogate components on aldehyde emissions at varying equivalence ratios, especially considering the implications of ethanol addition.

2.4.3 Fuel volatility

Qian *et al.* [93] conducted a study on the effects of five fuels, each with T50 (50 %v/v distillation temperature) values around 90 °C, 95 °C, 100 °C, 110 °C, and 120 °C. The variation in aldehyde emissions from this study are presented in Figure 2.10 (b).

Notably, fuel G5 exhibited higher acetaldehyde emissions compared to the others. This was linked to G5's lower volatility, resulting in an increased presence of unburned hydrocarbons, including ethylene. The higher levels of ethylene in G5 consequently led to its oxidation in the exhaust, further contributing to the raised acetaldehyde emissions. The study also highlighted the significance of T10 (10 %v/v distillation temperature) for cold-start conditions. Adding ethanol to gasoline typically reduces T10 and T50 values, influencing the fuel's cold-start performance.

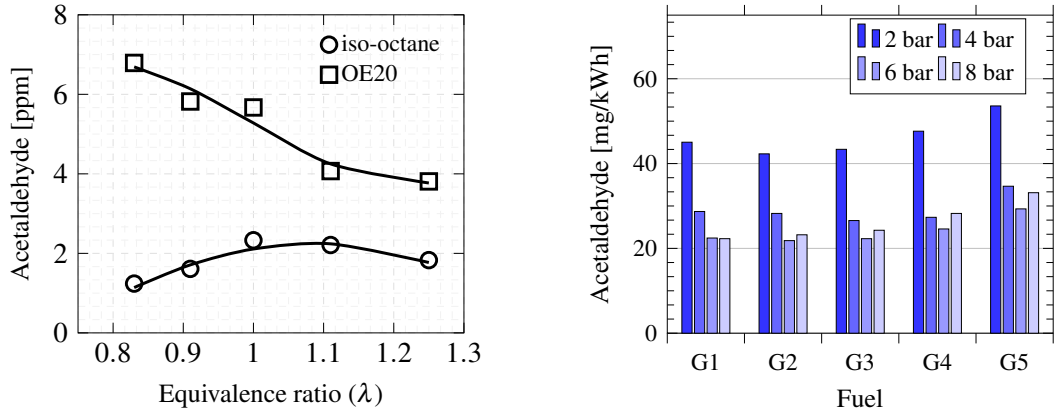

(a) Iso-octane & OE20 in engine **(b)** Five fuels in engine

Figure 2.10: **(a)** Acetaldehyde concentration based on varying the fuel-air equivalence ratio for pure iso-octane against OE20 blend. Reproduced (adapted) from Zervas *et al.* [65]. **(b)** Acetaldehyde concentration based on varying the fuel volatility of five different fuels with similar oxygen content. Reproduced (adapted) from Fuel, Qian *et al.* [93], Copyright 2020, with permission from Elsevier.

Thus, ethanol's role extends beyond directly impacting aldehyde emissions through combustion chemistry; it also modifies physical properties of the fuel, therefore influencing conditions that affect aldehyde emissions.

2.4.4 Injection and ignition timing

Considering the distinctive physical and combustion properties of alcohols compared to standard gasoline components, the influence of injection and ignition timings on aldehyde emissions has been reviewed in the literature. The majority of existing research focuses on methanol-based fuels in SI engines, specifically targeting formaldehyde emissions, while studies addressing ethanol fuels and consequent aldehyde emissions are relatively less. Daniel [99] reported that GDI engines generally emit a higher quantity of carbonyl compounds than their port fuel injection (PFI) counterparts, a phenomenon attributed to the lower operating temperatures in GDI engines, which favour the formation of such aldehydes.

Qian *et al.* [100] highlight that the integration of alcohols with fuels would require an advancement in the knock limit ignition timing. This is because retarding the ignition timing is linked with increased emissions of both formaldehyde and unburned methanol

due to delayed and less efficient combustion, leading to non-optimal cylinder temperatures, despite potentially elevated cylinder pressures [101–105]. This observation is consistent across various engine configurations, including PFI and GDI, both naturally-aspirated and turbocharged, as well as in a stratified direct injection spark ignition (DISI) engine under lean conditions as studied by Gong *et al.* [103]. Nonetheless, it is noted that higher exhaust temperatures, as a result of retarded ignition timing, may lead to the oxidation of formaldehyde if they exceed its critical temperature [106].

On the other hand, advancing the injection timing is associated with a more homogeneous mixture, improved combustion, and an increase in maximum in-cylinder pressure. This adjustment lowers unburned methanol emissions but results in higher formaldehyde emissions [102]. Sahu *et al.* [107] also observed a trade-off between unburned methanol and formaldehyde emissions, implying that formaldehyde is predominantly a product of methanol oxidation.

Although these studies focus on methanol and resultant formaldehyde emissions, it is anticipated that ethanol would exhibit similar behaviour. This would occur at lower temperatures of formation and consumption. Therefore, both the injection and ignition timing needs to be suitably advanced to reduce unburned fuel emissions but also optimised to reduce the aldehyde emissions.

2.4.5 Summary

Engine-based studies show that low speed and load conditions are favourable for aldehyde formation. During ethanol-blended fuel combustion, the aldehyde emissions can decrease when not run on stoichiometry and this phenomenon needs to be explored further. The formaldehyde emissions for methanol were predicted to decrease with retarded injection timing and advanced ignition timing, though this behaviour would vary dependent on the fuel mixture.

2.5 Chassis dynamometer and drive cycle studies

The examination of aldehyde emissions has also been covered globally in commercially available multi-cylinder engines, with studies conducted in various settings ranging from test cells to chassis dynamometer (CD) assessments, focusing on both engine-out and tailpipe emissions [108, 109]. The most prominent blend investigated, primarily due to fuel legislation limits, is E10 (10 %v/v ethanol and 90 %v/v gasoline). However, research has also investigated fuels with higher ethanol content, providing insights valuable for forthcoming legislation [110]. Additionally, studies have been conducted on flexible-fuel vehicles (FFV), capable of running on E85 (85 %v/v ethanol and 15 %v/v gasoline) or higher ethanol content blends. The key findings from geographically diverse literature in these areas are presented in this section.

Over the past decade, the University of California, Riverside in the U.S. have conducted studies on the impacts of ethanol concentration variations in gasoline on emissions, including aldehydes, in light-duty vehicles. These investigations were conducted post a three-way catalyst (TWC) using a CD with the Federal Test Procedure (FTP) and Unified Cycle (UC) drive cycles. Karavalakis *et al.* [111, 112] conducted analyses on emissions from a diverse fleet of gasoline vehicles, including a FFV, with fuel blends ranging from E10 to E85. The findings consistently indicated an increase in acetaldehyde emissions corresponding with increased ethanol content, with E85 being particularly notable for the significant formaldehyde and acetaldehyde emissions [111]. This is similar to other studies on this drive cycle in literature [113–115]. They have also investigated the impacts of other fuel components, as discussed in Section 2.2. Further investigations into SI vehicles with different fuel injection systems, including PFI, spray-guided and wall-guided GDI, and different ethanol blends (E10, E15, E20) identified that while aldehyde emissions generally increased with ethanol content, the trends were more pronounced in PFI than in GDI vehicles [116, 117]. Complementing these findings, Broustail *et al.* [52] observed similar trends in a PFI vehicle. Both studies attribute the acetaldehyde formation through the partial oxidation of ethanol, particularly during the cold-start phase of the drive cycle, and that formaldehyde is generally produced from oxygenated fuels.

In South Korea, Jin *et al.* [118] evaluated the impact of ethanol blends (E0, E10, E30, E50, and E85) on unregulated emissions post the TWC in a GDI SI passenger vehicle on the CD over the FTP cycle. They showed that acetaldehyde was essentially zero when normal gasoline was used, however, the E85 fuel exhibited a relatively high acetaldehyde level of 5.87 mg/km. This affirms that ethanol is one of the major contributors to these unregulated emissions. Meanwhile, in China, Wang *et al.* [119] tested vehicles ranging from China-3 to China-5 compliance (similar to Euro 3 to Euro 5) with methanol-based (up to M15) fuels and ethanol-based (E10) fuels. They observed more formaldehyde emissions with M15 fuel compared to E10 and gasoline, attributing this to formaldehyde being the primary by-product of methanol oxidation, and reported more acetaldehyde emissions with E10 fuel. Nevertheless, Wang *et al.* suggested that the newer vehicles with improved calibration and catalysts showed a reduction in aldehyde emissions [119]. However, further studies by Zhang *et al.* [67, 120] identified that the addition of ethanol (10 %v/v) to commercial gasoline through match blending in China-6 vehicles significantly increased aldehyde emissions. This shows that impact of the catalytic conversion can be variable and this is further explored in Section 2.5.1.

In the European context, at the Joint Research Centre, Clairotte and Suarez-Bertoa *et al.* [121–123] looked at the effects of oxygenated fuel on unregulated emissions from European vehicles. Their studies on Euro 4, 5a, and 6a emission standard gasoline vehicles and FFVs, performed over the Euro-certified New European Drive Cycle (NEDC) and Worldwide Harmonised Light Vehicles Test Cycle (WLTC), demonstrated a 2- to 4-fold rise in formaldehyde, acetaldehyde, and unburned ethanol emissions when using E85 compared to E5. Two primary findings include; significant emissions at ambient conditions of -7 °C compared to 23 °C, further discussed in Section 2.5.2, and majority (>95 %) of the unregulated emissions produced at the start of the cycle. Despite the test cycle, the emissions primarily occurred at the start of the cycle when the engine is cold. Moreover, they found that aldehyde emissions from conventional Euro 5 compliant internal combustion engine (ICE) vehicles and hybrid electric vehicles using E5 and E10 fuels were comparable [124].

Building on these insights, Kolbeck *et al.* [110] investigated the effects of increasing ethanol content in fuel from 10 %v/v to 20 %v/v / 25 %v/v while maintaining European Standard EN228 specifications on vehicles with Euro 6c technology. Their data indicated a consistent rise in aldehyde emissions across varying vehicle and weather conditions on the WLTC [110].

In more recent investigations, Anselmi *et al.* [125] and Fortune *et al.* [126] studied three vehicles that were either Euro 6d-temp or Euro 6c compliant and were adapted to variable ethanol concentrations, either through flex-fuel or E85 conversion kit so that they could run on fuels from E10 to E85. They reported that emission levels of ethanol and aldehydes for E10 and E20 were comparable, whereas a significant increase was noted for E50 and E85 [126]. Interestingly, they reported that the Euro 6c FFV running on E85 resulted in substantial aldehyde emissions, with formaldehyde levels even surpassing the U.S. regulatory limits of 2.5 mg/km [126].

2.5.1 Catalytic conversion

A TWC is recognised as an effective method to mitigate aldehyde emissions. Schifter *et al.* [16] demonstrated that advancements in TWC technology have resulted in a significant reduction, up to 50 %, in aldehyde emissions, attributed to enhanced oxidising efficiencies. Bielaczyc *et al.* [127] compared engine-out (pre-cat) and tailpipe (post-cat) emissions, identifying that formaldehyde and acetaldehyde were eliminated with approximately equal efficacy during both the urban drive cycle (UDC) and extra urban drive cycle (EUDC), which are components of the NEDC. This is shown in Figure 2.11. Their tests, conducted on SI engines certified to Euro 5 emission standards and fuelled with E5, E10, E25, and E50, indicated that the effectiveness of the TWC was more visible during the EUDC than the UDC [127]. This is to be expected, as the EUDC segment accounts for more aggressive and high-speed driving modes, leading to higher catalyst and exhaust temperatures thus increased oxidation efficiency for aldehydes.

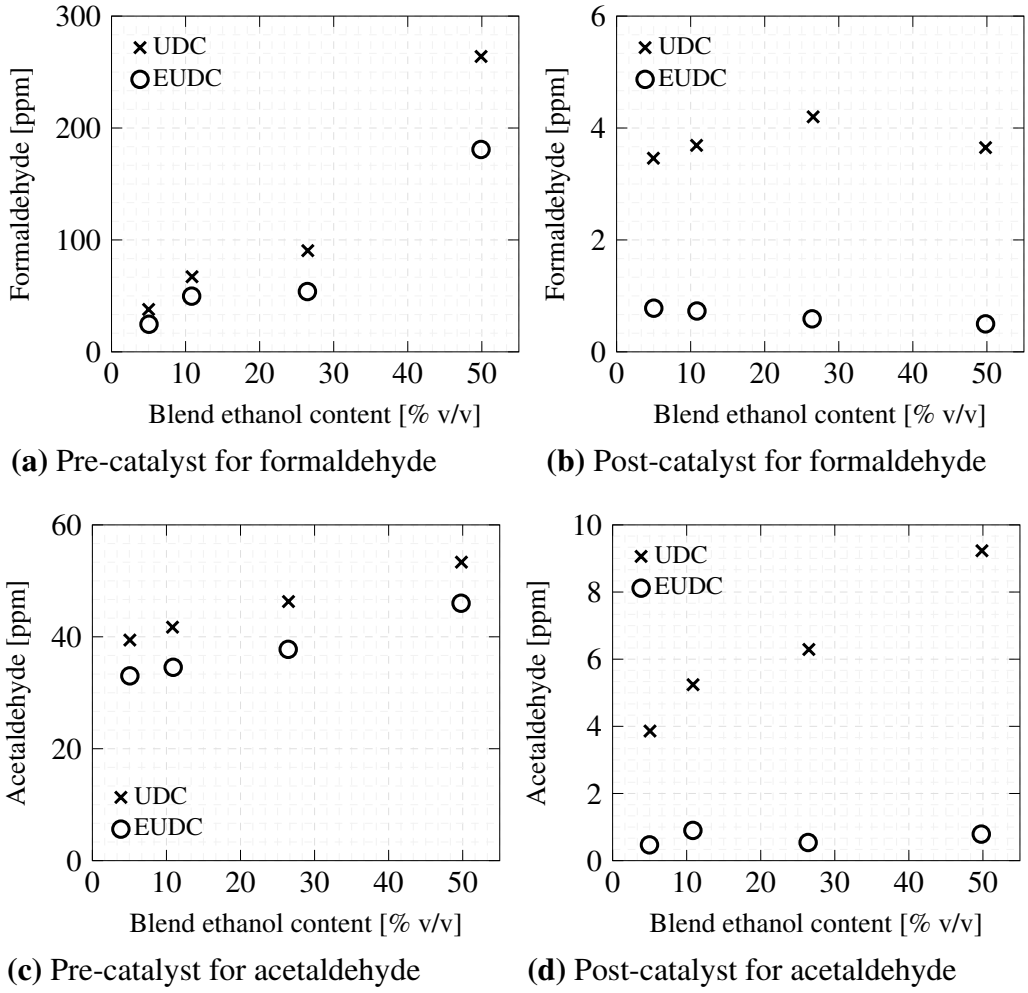

(a) Pre-catalyst for formaldehyde **(b)** Post-catalyst for formaldehyde

(c) Pre-catalyst for acetaldehyde **(d)** Post-catalyst for acetaldehyde

Figure 2.11: Formaldehyde ((**a**) and (**b**)) and acetaldehyde ((**c**) and (**d**)) measurements pre- and post-catalytic converter from a vehicle on chassis dynamometer on the UDC and EUDC. Reproduced (adapted) from Fuel Processing Technology, Bielaczyc *et al.* [127], Copyright 2013, with permission from Elsevier.

However, the oxidation process of aldehydes can also be inhibited by strongly adsorbing alkene intermediates, which are products of alkane decomposition, and these intermediates occupy the active sites of the TWC. This interaction can result in a distinct double-peak feature in the post-TWC aldehyde concentration profiles, as observed by Hasan *et al.* [128] and Sinha Majumdar *et al.* [48]. This trend can be observed in some of the modelling studies detailed in Section 2.3.1. Furthermore, ethene, which can be generated from the oxidation of ethanol or short alkane chains, may undergo oxidation over the catalyst, leading to the formation of ethanol, which then oxidises to acetaldehyde [129].

In more recent investigations, Suarez-Bertoa *et al.* [130] examined emissions from vehicles equipped with a gasoline particulate filter (GPF) in conjunction with a TWC. Their findings indicated no difference in formaldehyde and acetaldehyde emissions compared to prior studies involving only a TWC.

While the TWC represents a viable solution for mitigating aldehyde emissions, its efficiency depends on reaching the light-off temperature for complete conversion. Additionally, catalyst aging, a consequence of vehicle usage, can affect its efficacy. West *et al.* [113] observed that approximately two-thirds of vehicles fuelled with ethanol blends exhibited increased emissions due to catalyst degradation. Hence, exploring additional measures to curb aldehyde emissions prior to the TWC is a crucial avenue for further research.

2.5.2 Cold start

A common finding across these studies so far is that the majority of aldehyde emissions predominantly occur during the cold-start phase of the drive cycle [111, 116, 120, 123]. Further elaborating on this, Suarez-Bertoa *et al.* [123] highlighted the disparity in emissions at two ambient temperatures of 23 °C and -7 °C, reporting a more pronounced increase in aldehyde emissions under colder conditions. This increase is attributed to two factors: the extended duration required for the in-cylinder temperature to rise, leading to more prevalent partial oxidation, and at -7 °C, the delayed activation and light-off of the TWC, consequently prolonging the period at which emissions including acetaldehyde, ethanol, and other VOCs are emitted.

Supporting these observations, Aakko-Saksa *et al.* [108, 131] conducted tests exclusively at -7 °C and reported that acetaldehyde emissions increased with ethanol content and were particularly high for FFVs using E85. However, they also observed a decrease in formaldehyde emissions transitioning from Euro $2-5$ to Euro 6a vehicles. Although predominantly observed during the cold-start phase, Mehsein *et al.* [132] detected formaldehyde emissions consistently throughout the cycle at the tailpipe. Despite these findings strongly linking aldehyde emissions with temperature conditions, Sales *et al.*

[133] found that replacing the conventional cold-start system with a system featuring heated intake air and ethanol did not alter the post-catalytic concentration of aldehydes.

2.5.3 Summary

In Section 2.5, a comprehensive review of aldehyde emissions from light-duty SI vehicles across diverse regions is presented, focusing on various vehicle classifications, emission standards, environmental conditions, and driving cycles. These studies primarily focus on emissions from E10 fuel (comprising 10 %v/v ethanol and 90 %v/v gasoline), in comparison to pure gasoline. The literature research also extends to higher ethanol blends, offering insights relevant to evolving fuel regulations. In general, all studies unanimously agree that increasing ethanol content in a gasoline fuel would lead to greater aldehyde, specifically acetaldehyde emissions. These findings are clearer for fuels with ethanol concentrations above 50 %v/v.

The majority of these studies also found whilst the TWC can play a crucial role in reducing aldehyde emissions, its effectiveness is influenced by a range of factors and shows variability. Furthermore, across the range of drive cycles investigated, the greatest proportion of aldehyde emissions are affiliated with the cold-start phase, supporting the role of temperature in the chemistry of aldehyde formation as outlined in Section 2.2 and delved deeper in Section 2.3.

Nevertheless, all the studies focus on ethanol addition to a gasoline composition, which, as identified in Section 2.2 can contain hundreds of different hydrocarbon molecules that have a carbon chain length range from 2 to 13. This complexity makes it challenging to attribute specific emission behaviours to particular fuel compositions or operating conditions. Additionally, the range of methodologies used for measuring aldehyde emissions, each with unique capabilities, can further complicate the interpretation of results. Therefore, an in-depth understanding of these measurement techniques, as discussed in Section 2.6, can be beneficial for improved emission data analysis.

2.6 Measurement techniques

Aldehydes are difficult to measure as they are VOCs and the conventional emissions measurement equipment is not capable of distinctively measuring these emissions. Therefore, a brief assessment of suitable techniques to measure aldehyde emissions was made to aid the understanding and subsequent approach for the experimental investigations of this study. The three common analytical methods include impinger sampling or 2,4-DNPH cartridges with HPLC, FID, and high resolution FTIR are presented. Sandstroem-Dahl *et al.* [134] and Suarez-Bertoa *et al.* [39] have presented comparative reviews on these techniques and this section summarises the findings.

2.6.1 Impinger sampling and 2,4-DNPH cartridge

In the United States, as part of the California Air Resources Board (CARB), the impinger sampling (Method 1001) is recognised for alcohols, such as ethanol, and the 2,4-DNPH cartridges sampling (Method 1004) is a standard for aldehydes during automotive homologation tests. In Method 1001, the exhaust is sampled through two impingers, placed in series, containing 15 ml of deionised water. It is then cooled using a cryogenic bath at 0 °C. From each impinger, sealed samples are stored at 4 °C in duplicated vials and the ethanol in aqueous solution is determined through GC and flame ionisation detection [39]. Method 1004 is used to monitor a range of up to 14 carbonyl compounds in engine exhaust, including formaldehyde, acetaldehyde, and acrolein. The exhaust is drawn through cartridges impregnated with 2,4-DNPH at a sampling rate of 100-2000 mL/min for an appropriate period of time depending on carbonyl concentration. The cartridges are then immediately washed by gravity feed elution with 5 mL of acetonitrile. The eluate solution is then examined using an isocratic reverse phase HPLC with an ultraviolet (UV) absorption detector to determine the aldehydes, as illustrated in Figure 2.12 [135].

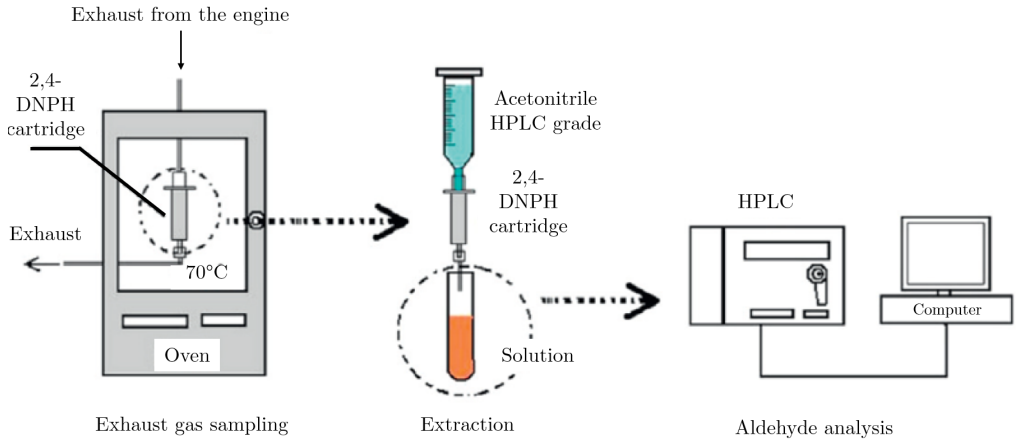

Figure 2.12: Schematic showing the process using 2,4-DNPH with HPLC method; adapted from the U.S. Environmental Protection Agency (EPA) [135].

2.6.2 FID

The FID is a standardised method for UHC measurement in the United States and European Union. However, as total hydrocarbons are measured, this method is insensitive to alcohols and aldehydes. Therefore, Wallner *et al.* [91] attempted to empirically determine FID correction factors for oxygenate fuels through comparison with other measurement methods. However, both Sandstroem-Dahl *et al.* [134] and Suarez-Bertoa *et al.* [39] show that even with the correlation factors, the FID under-predicts the oxygenate emissions, particularly with vehicles powered with higher concentrations of ethanol.

2.6.3 FTIR

The FTIR is not yet a recognised method for standardised emissions testing, nevertheless, it has recently been prescribed in the United Nations Economic Commission for Europe (UNECE) light-duty vehicles Global Technical Regulation 15 (GTR-15) for ethanol, formaldehyde, and acetaldehyde from the dilution tunnel [136]. The FTIR is heavily used for research purposes as it enables close to real-time (up to 5 Hz) emissions measurement of unburned ethanol, formaldehyde, and acetaldehyde among over 30 other gases from the exhaust [134].

The FTIR involves the collection of an interferogram, which is a unique pattern that results from the interaction of infrared (IR) radiation with a sample. The fundamental

component in the FTIR is the Michelson Interferometer, which consists of a beamsplitter, a fixed mirror, and a moveable mirror. These are shown in Figure 2.13.

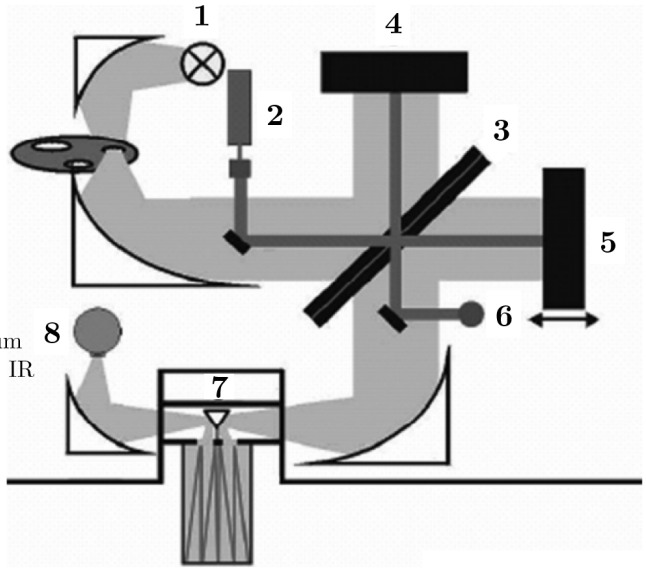

Figure 2.13: Schematic of the FTIR operation setup; adapted from AVL [137]

In operation, IR radiation from a light source is split into two beams by a beamsplitter. About half of the light beam reflects off the fixed mirror, whilst the other half reflects off the movable mirror. When these beams recombine at the beamsplitter, they create interference patterns that vary depending on the movable mirror's position [137]. This interference creates a unique pattern of light intensity over time, known as an interferogram.

The interferogram captures information about all the infrared frequencies emitted from the source. The Fourier Transform mathematical technique is applied to transform the time-based interferogram into a frequency-based spectrum. Each gas in the sample absorbs IR radiation at specific frequencies, leaving characteristic peaks in the spectrum. These are compared against a calibration spectrum to identify the gases being analysed and determine their concentrations [137]. The mercury cadmium telluride (MCT) detector is a critical component for this process as it enables detecting these specific frequencies with high precision and sensitivity. Therefore, it can help identify the unique frequency features of different gases, making it possible to measure multiple gas concentrations simultaneously and almost at real time (5 Hz). However, it should be noted that it is

necessary to cool the MCT detectors to suppress thermally induced noise and liquid nitrogen is often used for this.

In addition to producing real-time data which can be useful to gain further insights into the conditions that lead to aldehyde emissions, the accuracy of the FTIR is comparable to the standardised CARB Methods 1001 and 1004 [39, 95, 134].

2.6.4 Summary

Three different methods for measuring aldehydes, frequently used in literature, have been presented with their capabilities and limitations. FID and the use of 2,4-DNPH coupled with HPLC are recognised methodologies for emissions regulations. However, FTIR spectroscopy, commonly used in research, not only offers comparable accuracy but also provides near real-time measurement (at 5 Hz) of formaldehyde, acetaldehyde, and other exhaust gases. As highlighted in Section 2.5, the ability of FTIR to rapidly detect changes in aldehyde concentrations is particularly valuable, given that a substantial portion of these emissions occurs during the cold-start phase of an engine. This capability facilitates a more detailed analysis of the specific operating conditions that lead to increased aldehyde emissions.

Nevertheless, it is important to note that these three methods are only applicable for stationary settings, such as engine test cells or vehicles on chassis dynamometers. With the growing emphasis on assessing real-driving emissions, there is a need for more compact, on-board technologies capable of detecting aldehydes during actual vehicle operation. A brief review of these emerging technologies in real-world scenarios is further detailed in Section 2.7.

2.7 Real-driving emissions

Whilst conventional portable emissions measurement systems (PEMS) can be used to detect emissions instantaneously during real-driving conditions, the system is limited to certain pollutants such as NO, NO_2, CO, CO_2, and THC. The latter encompasses hundreds of hydrocarbons without speciation and identification of VOCs, such as aldehydes. Most

studies that examine these emissions are collected over a period of time or drive cycle and then post-processed. A detailed understanding of the proportion of the emissions based on driving segmentation is essential as an increasingly high proportion of emissions are produced during cold-start conditions, which may otherwise be under-represented if it forms a small share of the official test cycle [138].

To address these limitations, Zhu *et al.* [139] developed a portable system capable of measuring formaldehyde with a low detection threshold and a time resolution of around 100 seconds, suitable for up to 10 minutes of continuous sampling. Building on this, Suarez-Bertoa *et al.* [140] implemented the Quantum Cascade Laser Infrared Spectrometer (QCL-IR) for direct, real-time exhaust sampling from Euro 6 compliant gasoline and diesel vehicles. Their research, with equipment from Horiba [141, 142], demonstrated strong correlations between QCL-IR and FTIR measurements in vehicles tested on a chassis dynamometer (CD), suggesting the feasibility of real-world aldehyde emissions monitoring [140].

However, these studies primarily focus on formaldehyde and not acetaldehyde or other VOCs. Emissions Analytics developed a proprietary method to segregate the VOCs and N_2O emissions based on driving phases [138]. Through this approach, not only can aldehydes be studied, but also alcohol emissions which are precursors to aldehydes, and other toxic unregulated hydrocarbon emissions can be individually evaluated. Some of these include acetone, acetic acid, benzaldehyde, and toluene, which have been associated with ethanol content in the fuel.

2.8 Literature gap and objectives

The literature review covers a wide range of studies, from basic chemical reactions to real-world driving emissions, focusing on aldehyde generation, consumption, and emissions. These studies consistently show that ethanol is a key precursor of aldehydes, particularly acetaldehyde. However, data for other types of fuel components are inconsistent as they are usually studied as part of a more complex gasoline mixture. A gap in the literature is to further understand how each of the common gasoline surrogate fuel components affects

aldehydes on their own, and subsequently how their interactions in a range of multi-component fuels of known composition in increasing complexity can affect aldehydes.

Fundamental reactors can be beneficial to enhance the understanding of engine-based experimental results. Developing models of these reactors can provide the ability to study a wide range of fuel compositions. Though these models and the chemical kinetic mechanisms they use need to be validated against existing research first. The literature indicates that investigating the same fuel composition from the engine experiments in fundamental reactor models can help understand the underlying chemistry and link the fuel component effects to the aldehyde emissions.

Engine-based investigations highlight the role of operating conditions, particularly temperature, in influencing aldehyde production. Operating engines under conditions that promote lower combustion temperatures, such as lower speed and load, is anticipated to increase aldehyde emissions, thus facilitating an enhanced examination of fuel composition effects. Changing the fuel-air mixture ratio can also show how both the fuel composition and operating conditions impact aldehyde emissions.

The vehicle exhaust studies show that the TWC can play a major role in the outcomes of aldehyde emissions, therefore linking the findings back to fuel composition can be challenging. This suggests that when studying the impact of fuel compositions, engine-out emissions can be advantageous as they are not altered by TWC behaviour. Furthermore, it would be beneficial to use the FTIR to measure the aldehyde emissions as it can provide instantaneous measurements at 5 Hz and simultaneously measure formaldehyde and acetaldehyde.

Real-driving measurements of aldehydes are still in their nascent stages and primarily focus on formaldehyde. There is a gap in the literature to examine real-driving acetaldehyde measurements in conjunction with formaldehyde.

Therefore, taking the suggestions and gaps in literature, this study will:

- Evaluate the effect of gasoline surrogate fuel component interaction at varying complexities on engine-out aldehyde emissions under conditions conducive to higher aldehyde production.
- Complement the experimental findings with simulations on a range of fundamental reactor models to understand the underlying chemistry impacts of the aldehyde formation.
- Investigate and report the impact of ethanol-blended gasoline on real-driving formaldehyde and acetaldehyde emissions using the Emission Analytics VOCs system.

3

Experimental setup

Contents

3.1 Motivation

To achieve the objectives outlined in Section 2.8, this study examined fuels designed specifically for research purposes, along with gasoline surrogates and market-representative fuels, both with and without ethanol content. The studies were conducted through experiments and supplemented with simulations for which the setup can be found in Chapter 4.

A comprehensive fuel matrix, aimed at investigating the influence of these fuels on aldehyde emissions, was formulated, as detailed in Section 3.2. For the experiments, a single-cylinder engine, described in Section 3.3, was assembled. This engine was beneficial for its capability to operate with a wide range of fuels and its ability to precisely control and measure various parameters. Engine-out emissions were measured. This setup and approach enabled a focused analysis on the relationship between fuel composition, engine operating conditions, and resultant measured emissions.

To broaden the scope of this work's findings beyond the laboratory-based engine test cell experiments, the ability to measure aldehyde emissions in real-driving conditions was evaluated. This part of the study involved market representative fuels tested on four passenger light-duty vehicles with an advanced portable emissions measuring equipment, for which the details can be found in Section 3.4. This would help determine the impact of gasoline composition with and without ethanol on real-driving aldehyde emissions.

3.2 Fuel compositions

The fuels compositions for this work were split in three categories, with the aim to better understand fuel impact on aldehyde emissions:

1. Research fuels formulated to understand the impact of conventional gasoline surrogate fuel components in their pure form and specially designed binary and ternary combinations.

2. Surrogate fuels with incremental additions of ethanol were used to assess the influence of ethanol content.

3. Market representative E0 (0 %v/v ethanol in gasoline) and E10 (10 %v/v ethanol in gasoline) fuels were evaluated for their real-world relevance.

For the first two categories, the fuels were composed of mixtures of ethanol (E), iso-octane (O), n-heptane (H), and toluene (T). These blends were tailored to facilitate focused investigations, as detailed in Sections 3.2.1 and 3.2.2, respectively. The pure components of these fuels, sourced from Thermo Fisher Scientific, had high purity levels of 99.8 %, 99.9 %, 99.5 %, and 99.5 %, respectively, as stated by the supplier.

In the third category, fuels derived from refinery streams, as elaborated in Section 3.2.3, were used. These market representative fuels were tested in both the single-cylinder engine, to measure engine-out emissions, and in four passenger light-duty vehicles, to evaluate real-driving emissions.

3.2.1 Research fuels

The research fuels, shown in Table 3.1, were specifically designed to examine how ethanol interacts with conventional components of gasoline surrogates and its resultant impact on aldehyde emissions. Firstly, an investigation of each individual component was conducted. The pure components tested were ethanol, iso-octane, and toluene, whereas n-heptane was not tested. This was followed by a systematic study of binary and ternary mixtures to examine the effects of varying their proportions within the blends on aldehyde emissions.

The binary fuel mixtures were examined in three sets: 1) Iso-octane, a simple gasoline representative, with ethanol in two concentrations, 20 %v/v and 85 %v/v, reflecting the quantities at which they are used in a global context. 2) Mixtures of toluene with ethanol in increments of 25 %v/v, which are combinations not previously tested in engines, aimed at examining the effects of combining aromatic (toluene) and oxygenated (ethanol) components on aldehyde emissions. 3) Mixtures of n-heptane with ethanol in two quantities, 65 %v/v and 85 %v/v, which are not typical pairings for engine tests due to n-heptane's low octane rating, were analysed to assess the impact of their interaction on aldehyde emissions.

The ternary mixtures investigated the impact of aromatic content, as represented by toluene, on aldehyde emissions from multi-component fuels. This exploration was conducted in two sets: 1) Mixtures of iso-octane and n-heptane combined with varying levels of toluene, referred as "LowT" for low toluene content and "HighT" for high toluene content. 2) Mixtures involving a constant 25 %v/v concentration of ethanol and iso-octane, with toluene varying between low and high levels, using the same "LowT" and "HighT" designations as in the first set.

Table 3.1: The volumetric and molar fractions of the research fuels tested.

Fuel	Ethanol		Toluene		Iso-octane		N-heptane	
	mol	vol	mol	vol	mol	vol	mol	vol
E100	1.00	1.00	-	-	-	-	-	-
O100	-	-	-	-	1.00	1.00	-	-
T100	-	-	1.00	1.00	-	-	-	-
OE20	0.42	0.20	-	-	0.58	0.80	-	-
OE85	0.94	0.85	-	-	0.06	0.20	-	-
HE65	0.82	0.65	-	-	-	-	0.18	0.35
HE85	0.935	0.85	-	-	-	-	0.065	0.15
TE25	0.38	0.25	0.62	0.75	-	-	-	-
TE50	0.65	0.50	0.35	0.50	-	-	-	-
TE75	0.85	0.75	0.15	0.25	-	-	-	-
OTE25_LowT	0.48	0.25	0.05	0.05	0.47	0.70	-	-
OTE25_HighT	0.44	0.25	0.29	0.35	0.28	0.40	-	-
OHT_LowT	-	-	0.08	0.05	0.84	0.875	0.08	0.075
OHT_HighT	-	-	0.45	0.35	0.41	0.50	0.14	0.15

All fuels tested in this section had physical and combustion properties that varied significantly, as shown in Table 3.2. The research and motor octane number (RON and MON) were estimated using linear-by-mole approach incorporating ethanol as per the methodology outlined by Knop *et al.* [143, 144]. The density at room temperature of each fuel blend was determined by multiplying the volume fraction of each component with its respective density, derived from literature. Therefore, the density was linearly associated with the volume. The lower heating value (LHV) at 15 °C was calculated by subtracting the heat of vaporisation from the heat of combustion (as a gas). The air-to-fuel ratio (AFR) was determined by formulating the balanced chemical reaction for complete combustion, calculating the molar masses, and subsequently deriving the ratio with the mass of fuel and air.

Table 3.2: The physical and combustion properties of the research fuels tested.

	RON	MON	LHV	Density	AFR
	-	-	MJ/kg	kg/m^3	-
E100	108	90	26.8	789	9.00
O100	100	100	44.4	692	15.1
T100	116	102	1.00	867	13.5
OE20	103	93	40.5	716	13.7
OE85	107	95	29.2	779	9.67
HE65	91	79	32.5	767	10.9
HE85	102	87	29.2	782	9.75
TE25	114	94	37.3	852	12.3
TE50	112	91	33.9	832	11.2
TE75	109	90	30.5	813	10.1
OTE25_LowT	106	104	39.3	730	13.2
OTE25_HighT	110	98	38.4	782	12.8
OHT_LowT	94	91	44.1	710	14.9
OHT_HighT	94	84	42.9	761	14.4

The analysis of these mixtures aims to highlight the influence of each gasoline surrogate fuel constituent on aldehyde emissions. This includes understanding their effects both as pure fuels and when integrated in different proportions within a fuel mixture. The insights from this research are expected to significantly support the existing body of literature that primarily focuses on aldehyde emissions originating from ethanol and ethanol-blended gasoline.

3.2.2 Surrogate fuels

This study focused on two types of gasoline surrogates: standard and toluene-based primary reference fuels (PRF and TPRF, respectively). Both were developed in accordance with the European Commission's EN228 fuel specification, as close as possible [145]. For PRF, key properties such as the RON were taken into consideration. The TPRF's properties included both RON, MON, and density. The maximum aromatic content, which, in this study, is represented by toluene. The primary objective was to investigate engine-out aldehyde emissions from these surrogates to gain insights into the contributions of conventional surrogates to these emissions. Additionally, the study evaluated the impact of increasing ethanol addition to these surrogate fuels and the resulting effects on aldehyde emissions.

Details regarding the volumetric and molar fractions of these fuel blends are presented in Table 3.3 and the properties of the fuels are shown in Table 3.4. It should be noted that OHT_HighT was designed to also be a TPRF representative, therefore is investigated in this section as well. Two specific ethanol concentrations were examined: 20 %v/v, which is becoming increasingly mandated in countries like India [146], and 85 %v/v, a common blend in U.S. flex-fuel vehicles [147]. These concentrations were chosen to represent the range of ethanol use in different global contexts.

Table 3.3: The volumetric and molar fractions of the surrogate fuels tested.

Fuel	**Ethanol**		**Toluene**		**Iso-octane**		**N-heptane**	
	mol	**vol**	**mol**	**vol**	**mol**	**vol**	**mol**	**vol**
HO95	-	-	-	-	0.94	0.95	0.06	0.05
OHE20	0.41	0.20	-	-	0.47	0.65	0.12	0.15
OHE85	0.94	0.85	-	-	0.04	0.10	0.02	0.05
OHT_HighT	-	-	0.45	0.35	0.41	0.50	0.14	0.15
THOE20	0.35	0.20	0.36	0.375	0.08	0.125	0.21	0.30
THOE85	0.94	0.85	0.01	0.02	0.03	0.075	0.02	0.055

Table 3.4: The physical and combustion properties of the surrogate tested.

	RON	**MON**	**LHV**	**Density**	**AFR**
	-	**-**	**MJ/kg**	**kg/m^3**	**-**
HO95	95	95	44.4	698	15.0
OHE20	96	94	40.5	719	13.7
OHE85	106	92	29.2	780	9.75
OHT_HighT	94	84	42.9	761	14.4
THOE20	101	90	39.5	771	13.2
THOE85	107	90	27.9	784	9.72

3.2.3 Market representative fuels

Two bespoke fuels, E0 and E10, designed to be representative of market standards and compliant to EN228 specifications, were formulated [145]. They were made from refinery streams blended together by Coryton Fuels [148]. The physical and chemical properties of both fuels were examined and are reported in Table 3.5.

Table 3.5: E0 and E10 common fuel properties and composition specification.

Property	Unit	E0	E10
RON	-	95.5	95.7
MON	-	85.6	85.2
Density at 15° C	kg/L	0.7429	0.7497
DVPE at 38° C	kPa	67.6	60.6
E70	%v/v	27.5	46.5
E100	%v/v	49.8	62.1
E150	%v/v	86.7	93.8
Net calorific value	MJ/kg	42.83	40.82
n-paraffins	%v/v	9.3	11.8
iso-paraffins	%v/v	43.0	34.2
olefins	%v/v	10.8	8.1
naphthenes	%v/v	4.1	2.3
aromatics	%v/v	32.1	33.3
Oxygenates (ethanol)	%v/v	0.03	10.2

The aim was to ensure that both fuels had similar characteristics, including research and motor octane numbers, densities, and volumetric aromatic content. However, due to the differing physical properties of ethanol, such as distillation and vapour pressure, compared to conventional gasoline components, exact matching was not feasible. This influenced the composition of the fuel, as each classification group (e.g., n-paraffins, olefins, aromatics, etc) had different properties. These fuels were tested in two environments: a laboratory-based engine (as described in Section 3.3) and onboard passenger vehicles (detailed in Section 3.4).

3.2.4 Overview

The comprehensive analysis presented in this work includes both experimental and simulation-based investigations. The experimental results are categorised into different chapters, based on the purpose of each fuel blend studied, as detailed in Table 3.6. Chapter 5 is dedicated to examining research fuels, while surrogate fuels are investigated in Chapter 6. To complement the experimental data, Chapter 7 presents simulations of fuel behaviour using various reactor models. Market representative fuels are evaluated in Chapter 8. Each chapter provides in-depth results about the fuels it covers. This structured approach allows for a thorough understanding of how each fuel type contributes to aldehyde emissions.

Table 3.6: Categories and purpose of the fuels investigated in this work.

Category	Purpose	Fuels
Research fuels	Pure fuels	E, T, O, and H
	Alcohol and branched alkane	OE20 and OE85
	Alcohol and straight chain alkane	HE65 and HE85
	Alcohol and aromatic	TE25, TE50, TE75, OTE25_LowT, OTE25_HighT, OHT_LowT, and OHT_HighT
Surrogate fuels	Primary reference fuel (PRF)	HO95, OHE20, OHE85
	Toluene primary reference fuels (TPRF)	OHT_HighT, THOE20, and THOE85
Real-driving emissions	Market fuels	E0 and E10

3.3 Single-cylinder engine

An overview of the single-cylinder engine configuration used for experiments is provided in this section. A photo of the engine test cell is presented in Figure 3.1.

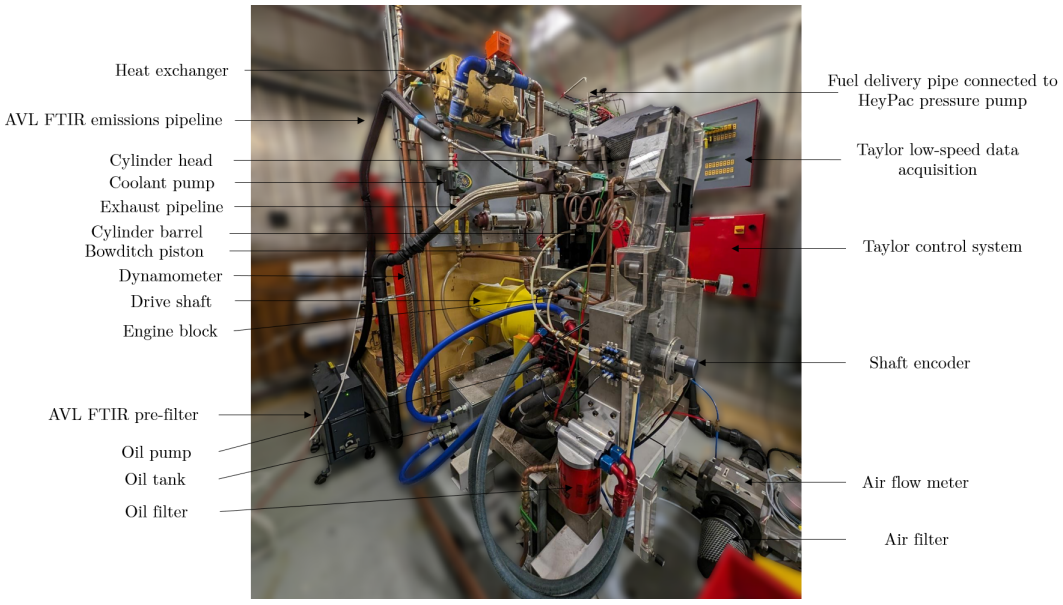

Figure 3.1: Photo of the single-cylinder engine.

Whilst this engine is equipped for optical access and allows for combustion and fuel spray imaging, these features were not utilised for this study's experiments. The engine was run in a non-optical configuration with a steel blank insert in the piston. The setup has a Bowditch piston assembly, where the extended piston adds significant mass to the crank and slider mechanism. The pent roof of the combustion chamber

contains a fused quartz window. Therefore, these factors limit the engine speed to a maximum of 2400 rpm and the engine can only be run at low loads to prevent fracture of the fused quartz window. Furthermore, it should be noted that quartz material has a significantly lower thermal conductivity compared to metals such as aluminium or iron used in conventional engines. This low thermal conductivity could lead to higher combustion chamber surface temperatures and reduced heat flux through the quartz windows (higher bulk gas temperatures). The higher surface temperatures of quartz windows can influence the formation and destruction pathways of aldehydes near the walls as the aldehydes are formed through partial oxidation reactions, which are sensitive to temperature. Additionally, as an optical access engine was used, the location of the piston ring pack in the combustion chambers differs from a conventional engine leading to larger crevices in which intermediate aldehydes could be formed.

The combustion system consists of a centrally mounted spark plug and conventional gasoline fuel injector, which operates at fuel pressures of up to 150 bar, provided by a Heypac hydraulic pressure pump, and is capable of multiple injections per cycle. As the same gasoline injector was used across the fuel matrix in this study, it should be noted that fuels with higher density and viscosity, such as ethanol, can affect the injector flow characteristics and spray patterns, potentially impacting combustion and emissions. Differences in surface tension between fuels can influence the atomisation and spray formation processes, affecting fuel-air mixing and combustion efficiency.

3.3.1 Overall setup

The bottom end of the engine has a crank angle marked flywheel which is mounted on a DC Control Techniques dynamometer for torque and speed control. This dynamometer can be controlled remotely from outside the engine bay using the Taylor DynPro$_2$ system. A shaft encoder mounted onto the crankshaft at the front of the engine with a resolution of 0.1°CA provides 720 pulses per revolution for data acquisition using the AVL X-ion high-speed modular data acquisition (HiDAQ) platform. A Kistler Type 6041A high-speed pressure transducer was used to measure the cylinder pressure data. The net indicated mean effective pressure (nIMEP) was calculated using the cylinder pressure. The engine

operates in a GDI mode where the fuel is injected directly into the combustion chamber. The injection and ignition timings and duration are controlled by Berkeley Nucleonics Corporation's (BNC's) model 725 multi-trigger digital delay generator using signals from the shaft encoder. A schematic of the configuration is shown in Figure 3.2.

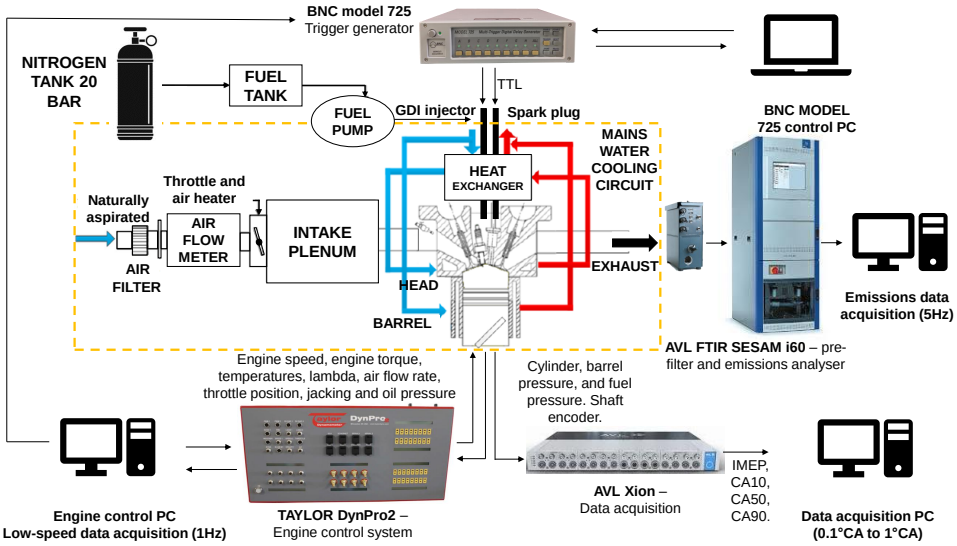

Figure 3.2: Schematic of the single-cylinder engine and auxiliary equipment configuration.

The support structure for the cylinder head permits easy access to the piston. This is achieved by a drop-down cylinder system [149] which facilitates interchangeable pistons and annuli depending on experimental requirements. Nevertheless, this functionality was not used for this work. During engine operation, nitrogen at a pressure of 20 bar was used to lift the piston and seal the liner to the cylinder head. The main engine parameters are shown in Table 3.7.

Table 3.7: Summary of various reaction mechanisms used in the present work

Parameter	Unit	Value
Bore	mm	89.0
Stroke	mm	90.3
Displacement	cm^3	561.9
Compression ratio	-	11:1
Fuel pressure	bar	150
Valves per cylinder	-	2 intake; 2 exhaust
IVO	°CA aTDC	-336
IVC	°CA aTDC	-86
EVO	°CA aTDC	116
EVC	°CA aTDC	366
Inlet valve lift	mm	10.5
Exhaust valve lift	mm	9.8

3.3.2 Control system

The Taylor DynPro$_2$ system is used for the majority of the engine control. The system is composed of three boxes. Firstly, the Sensor Enclosure box which houses the main circuit boards for the data acquisition and control system, as shown in Figure 3.2. This box is capable of taking in pressure, K-type temperature, analogue, and frequency inputs. Secondly, the Connections Enclosure box is where the dynamometer connections, control valves (e.g. throttle, coolant), and selected accessories are terminated. Finally, the Operations Enclosure box provides control of the emergency stop, power to the Sensor and Connections Enclosure boxes, and engine dynamometer system starter control. This box is placed outside the engine bay and is connected to a PC for full control and visualisation. This box is also used for slow speed (i.e., 1 Hz) data logging. Therefore, the input signals in the Sensor Enclosure box are used for closed-loop control, e.g. pre- and post-heat exchanger temperature readings for controlling the coolant circuit, and safety measures, e.g. winding down the dynamometer drive if the oil pressure drops below a set threshold.

The engine has an oil-free combustion system, so that the emission impacts can be attributed directly to the fuel and operating conditions. Polyamide-imide piston rings were used and the engine coolant was maintained at 45 °C to reduce the risk of melting the rings. K-type thermocouples were used to measure all temperatures.

Injection and ignition timing

The injection and ignition timing and injection duration are controlled by the BNC model 725 based on the signals it receives from the shaft encoder. The injection trigger is sent to a National Instruments (NI) Direct Injection Drive System (DIDS) which controls the current sent to the injector and is capable of being modified to perform multiple injections. The spark timing is controlled by the BNC model 725, similarly.

Two signals, the 0.5 °CA and 0 °CA flag, the latter describing when the engine is at bottom dead centre (BDC), were used to ensure the injection and ignition timings are performed at the end of the compression stroke. The BNC model 725 provides eight

functioning channels, each with an input and output. Two input channels are taken by the shaft encoder signals. For each timing control parameter, the setup requires an intermediate and output channel. Therefore, the BNC model 725 is capable of providing timing control for three devices. The timerPRO software that comes with the BNC is set up on a laptop to write the control logic for the timing device and was configured for the experiments to be run in this study.

3.3.3 Data acquisition system

The AVL X-ion is a compact system with 16 input channels which is mounted on a rack outside the engine bay. The signals are acquired with 18-bit resolution at a sampling rate of 2 MHz per channel. The module provides an input voltage range of +/-10 V. The AVL X-ion allows time and crank angle based sampling at the same time. The signals from the shaft encoder, cylinder, barrel, and fuel line pressure transducers, and BNC are connected to this for data acquisition. These are logged at a resolution of 0.1 °CA.

Depending on investigation requirements, there are additional channels available for data input. The device is connected to a PC which runs the AVL IndiCOM software which provides live visualisation of all signals registered. These measurements are saved as cycle-based and post-processed on AVL Concerto software.

3.3.4 Equivalence ratio

The air-fuel equivalence ratio (λ) was measured using a Bosch wide-band oxygen (O_2) sensor which has a planar zirconia (ZrO_2) dual cell limiting current sensor and integrated heater. The sensor was calibrated with free air. The Innovate Motorsport LM-1 digital air-fuel ratio (λ) meter was used to modify the stoichiometric fuel-air ratio (ϕ) appropriate to the fuel mixture tested.

3.3.5 Emissions analysis

A FTIR was procured to enable accurate measurement and analysis of aldehyde and alcohol engine-out emissions.

The AVL SESAM FTIR i-60 was used to measure real-time engine-out emissions. The FTIR analyser operates at a sampling rate of 5 Hz. With a gas cell capacity of 200 mL, the FTIR analyser operates with a sample flow rate of 8 L/min maintaining 191 °C and 800 hPa to achieve effective gas exchange at this rate. Prior to each fuel test, the background spectrum used to determine absorbance was collected and normalised by purging the gas cell with nitrogen gas. Through operating at 191 °C, the FTIR analyser samples the raw exhaust without contaminating the optics with water vapour and emission constituents. Upstream, the FTIR analyser sample line is also heated to 191 °C thus preventing losses from adsorption and condensation. Between the engine-out exhaust and the heated line, a heated filter removes particulate matter to prevent optical cell contamination. This filter was replaced with a new filter for each fuel tested.

The specifications of the relevant measured emissions can be found in Table 3.8. For the NMHC emissions, the FTIR identifies a group of hydrocarbons, including oxygenated species and excluding methane, that are present in the exhaust above pre-determined threshold levels. The analysis of infrared spectra works best for HCs with low carbon numbers as they have strong and sharp absorbance bands [150]. As the top ten compounds account for 80 % of the HCs in the exhaust, Gierczak *et al.* [151] found that the FTIR method yielded NMHC measurements within 5% of the regulatory FID method for fuel blends ranging from gasoline to E85 (85 %v/v ethanol and 15 %v/v gasoline). The total nitrogen oxides (NO_x) were calculated as a sum of nitrogen monoxide (NO) and dioxide (NO_2).

Table 3.8: FTIR emissions specifications relevant to this study.

Emission component	Formula	Unit	Range	Accuracy
Formaldehyde	HCHO	ppm	0-1000	± 0.15
Acetaldehyde	CH_3CHO	ppm	0 - 3000	± 0.35
Nitrogen monoxide	NO	ppm	0 - 10000	± 0.15
Nitrogen dioxide	NO_2	ppm	0 - 1000	± 0.06
Nitrous oxide	N_2O	ppm	0 - 1000	± 0.05
Carbon monoxide	CO	ppm	0 - 100000	± 0.1
Carbon dioxide	CO_2	ppm	0 - 200000	± 10.0
Ethanol	C_2H_5OH	ppm	0 - 1000	± 0.30
Non-methane hydrocarbons	NMHC	ppm	0 - 10000	± 2.50

3.4 RDE equipment

On-road tailpipe exhaust emissions were measured by Emissions Analytics using SEMTECH-LDV PEMS developed by Sensors Inc [152]. The measurement accuracy and linearity of the SEMTECH-LDV PEMS satisfy the European Union and the United States of America emissions testing requirements and are within the range of laboratory testing [153, 154].

The SEMTECH-LDV PEMS unit (Figure 3.3) was equipped with a tailpipe attachment, heated exhaust lines, a range of gas analysers, a global positioning system (GPS) receiver, a weather station for ambient measurement, and an interface with the vehicle's onboard diagnostics [154]. A non-dispersive infrared sensor was used to measure the carbon monoxide (CO) and carbon dioxide (CO_2), whereas a non-dispersive ultraviolet sensor was used for nitrogen monoxide and dioxide which were summed to calculate the nitrogen oxides (NOx) concentration [152]. All the gaseous emissions were recorded at 1 Hz. The GPS receiver recorded vehicle speed, longitude, latitude, and altitude [155]. The engine operation was not affected by the PEMS as it was powered by batteries and the additional weight of the PEMS was uniform for each test. This additional weight, approximately 20 kilograms according to SEMTECH [152], may have affected the test vehicle's power-to-mass ratio and previous results have found a potential increase in CO_2 emissions by up to 3 % [153]. Further detail on the PEMS installation and SEMTECH-LDV operation can be found in the literature [154, 156].

Figure 3.3: SEMTECH-LDV portable emissions measuring system (PEMS) (left) and an example vehicle with the PEMS experimental measurement set-up (right) adapted from [196] with permission from SAE International.

The concentrations of VOCs, semi-VOCs, hydrocarbons with two carbon atoms up to at least forty-four carbon atoms (C_2 to C_{44}), formaldehyde (CH_2O), nitrous oxide (N_2O), and many others were measured using an innovate patent-pending system by Emissions Analytics [138, 157]. This VOCs system sampled real-driving exhaust emissions onto tubes (Figure 3.4) which were subsequently analysed using gas chromatography in a laboratory. A two-dimensional gas chromatography (GCxGC) system coupled with a time-of-flight mass spectrometer (TOF-MS) from SepSolve Analytical and Markes International was used [158, 159]. The identification and quantification of the compounds were enabled by the TOF-MS and supported by other detectors such as FID and electron capture detector (ECD) for nitrous oxide (N_2O). Formaldehyde (CH_2O) was analysed by the 1220 Infinity II HPLC technique provided by Agilent [160].

Figure 3.4: Thermal desorption tube from Markes International (left) and two-dimensional gas chromatography (GCxGC) system coupled with a time-of-flight mass spectrometer (TOF-MS) from SepSolve Analytical (right).

The system could simultaneously sample onto multiple tubes with distinct characteristics. For formaldehyde (CH_2O), the tubes contained a 2,4-DNPH cartridge which transformed CH_2O into hydrazones, which are immobilised on the cartridge. These compounds can be easily eluted from the cartridge with acetonitrile and analysed by HPLC with UV detection. For N_2O, the tubes had a molecular sieve. This approach enabled the identification and collection of a wide spectrum of measured compounds with a high degree of sensitivity thus picking up species with low concentrations.

Coupled with the PEMS unit that had exhaust flow rate and GPS data, the concentration of the measured VOCs was converted to mass values, and subsequently, distance-specific emission rates were calculated and presented as milligrams per kilometre.

With this approach, the sample collection on tubes would be cumulative meaning that the real-time (second-by-second) data was not obtained. Therefore, the average concentrations determined may be unrepresentative of the conditions during which greater VOC emissions were formed. To address this, a proprietary onboard constant volume sampling and proportional flow dilution system together with a geofencing system, that automatically switched between different sample tubes at pre-set geographical points on the test cycle, enabled an understanding of the breakdown of emissions between different driving modes [138]. For this work, the driving modes and respective geofences were cold-start (CS), urban (U), rural (R), and motorway (M). An example of test route geofencing is shown on the right of Figure 3.5. The array of tubes, with rows for geofenced segments, and columns for different sample tubes (VOCs, CH_2O, N_2O, etc) are shown on the left of Figure 3.5 [138].

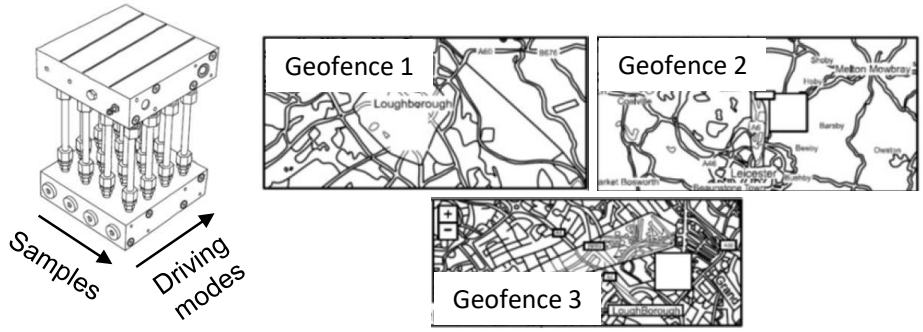

Figure 3.5: Sampling tube array for the VOCs system (left) and an example geofencing of the test routes (right); adapted from Molden *et al.* [138].

3.5 Procedure

The section provides insight into the fuel mixing and process followed single-cylinder engine and real-driving emissions studies.

3.5.1 Fuels

The fuel compositions were blended by carefully mixing volumetric proportions of the pure fuels in a fume cupboard, and the resultant mixtures were stored at the University, as shown in Figure 3.6.

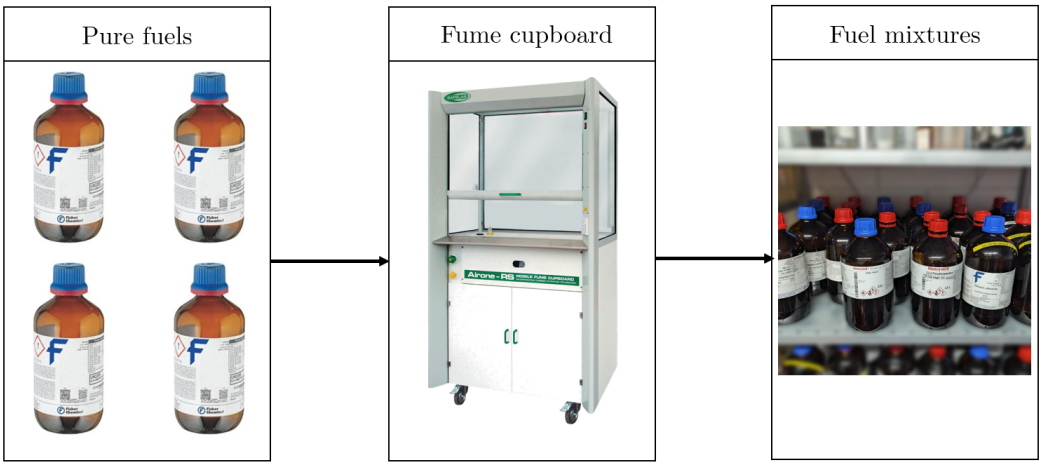

Figure 3.6: Process followed to mix the wide range fuels tested in this work.

3.5.2 Single-cylinder engine

The engine was first warmed up until the coolant temperatures had stabilised at a setpoint of 45 °C. All the tests were carried out at ambient conditions of 298 K and atmospheric pressure. The operating conditions were controlled using the throttle setting and fuel injection quantity. This facilitated operation between two loads of 1.95 ±0.15 and 3 ±0.10 bar (nIMEP) and two engine speeds of 1100 and 1500 rpm (± 10 rpm) whilst the air-fuel ratio was stoichiometric. These low speed and load conditions were selected as the literature in Section 2.4 reports greater aldehyde formation at these settings. Additionally, as stated in Section 3.3, the engine has optical access facilities and is thus limited by a relatively low maximum cylinder pressure. At the lower engine speed and load conditions, the fuel-air equivalence ratio (ϕ) was investigated between 0.90 and 1.20 for the majority of fuels tested. Across all tests, the median coefficient of variation (CoV) of nIMEP was 3 %. The fuel-air equivalence ratio (ϕ) and nIMEP were controlled by adjusting the throttle position and injection duration. The ignition and injection timing were fixed across all tested fuel compositions and operating conditions as shown in Table 3.9. While this study holds the ignition timing constant to isolate the effects of fuel properties, it should be noted that another approach could be to optimise the ignition timing by holding a different parameter, such as the crank angle at 50 % mass fraction burn for each fuel, to enable a comparison and assessment of emissions characteristics. However, due to the limitations of the experimental setup in study, the ignition timing was fixed.

Table 3.9: Summary of various reaction mechanisms used in the present work

Engine parameter	Unit	Value
Injection timing	°CA aTDCf	-270
Ignition timing	°CA aTDCf	-46.3
Air intake temperature	K	298 ± 5
Air intake pressure	kPa	101.325

For each test run, the high-speed data acquisition system was complemented by the low-speed data acquisition recording at 1 Hz, and the FTIR measuring the engine-out emissions at 5 Hz. All data collection was done simultaneously. To ensure the results are replicable, three repeats of each test run were conducted. To ensure any repeats of the same operating condition were not consecutive, a range of conditions were conducted as a block and then repeated, as the example with equivalence ratio variation is shown in Table 3.10. It should be noted that Table 3.10 only shows a partial extract from the test matrix for one of the fuels (OE20) to represent the test block based on the operating conditions whilst also ensuring each condition was repeated three times.

Table 3.10: Engine test set example with equivalence ratio range

Block	**Ref**	**Speed** **rpm**	**Load** **bar**	**Equivalence ratio** λ	**Fuel**
1	VS_16_06_22_OE20.001	1100	1.95	1.00	OE20
	VS_16_06_22_OE20.002	1100	1.95	0.83	OE20
	VS_16_06_22_OE20.003	1100	1.95	0.91	OE20
	VS_16_06_22_OE20.004	1100	1.95	1.05	OE20
	VS_16_06_22_OE20.005	1100	1.95	1.10	OE20
2	VS_16_06_22_OE20.006	1100	1.95	1.00	OE20
	VS_16_06_22_OE20.007	etc	etc	etc	etc

The air-fuel equivalence ratio (λ) was configured for each fuel. The fuel tank was fully emptied prior to each fuel change. Furthermore, the engine was run for a period of time to ensure the fuel line was filled with the new fuel before any tests. For the pure ethanol, the FTIR default setting was changed to adapt the measurement range for the fuels. The filter in the FTIR was replaced for each fuel so no residues in the pre-filtering process would affect the measured emissions. A typical process followed for a fuel is shown in Figure 3.7.

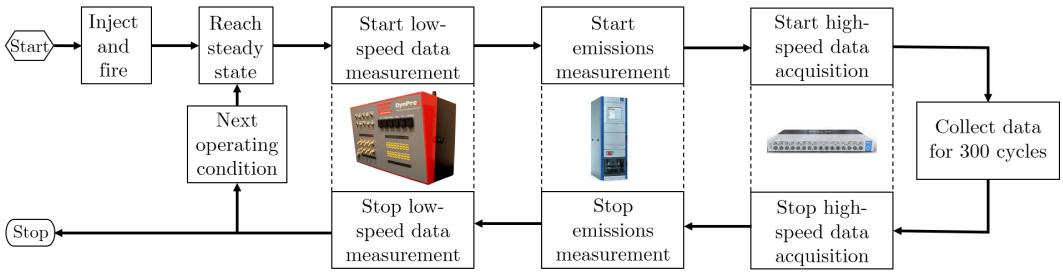

Figure 3.7: Flowchart to show procedure followed to collect experimental data.

3.5.3 RDE drive cycle

Four small to medium-sized vehicles with Euro 6d-TEMP emissions regulation standards were used in this study, as described in Table 3.11.

Table 3.11: Specification of the four cars used in this study.

	Car 1	**Car 2**	**Car 3**	**Car 4**
Model year	2020	2022		
Regulatory stage	Euro 6d-Temp (WLTP)	Euro 6d-Temp-EVAP-ISC (WLTP)		
Vehicle Segment	Medium Car (C)	Multi-purpose Car (M)	Small Car (B)	
Make	Kia	Peugeot	Citroen	Renault
Model	Sportage	2008	C3	Clio
Power (bhp)	174	129	82	90
Engine capacity (cc)	1591	1199	1199	999

All vehicles were solely powered with a gasoline ICE and none of the vehicles were hybrid with electric drive functionality. The vehicles were selected from four different manufacturers. Three out of the four cars tested had manual gearboxes and the default driver selectable mode was engaged, as detailed in Appendix B. The vehicles had similar after-treatment system architecture composed of a TWC and a gasoline particulate filter (GPF). Car 1 was an older model vehicle than Cars 2 to 4 and had a greater mileage than the other vehicles which may impact the condition of the after-treatment systems. The mileages of the vehicles are presented in Appendix B. All vehicles were tested in October 2022. Both fuels were tested in each vehicle and the entire fuel system was flushed before running the tests. The emissions for each vehicle were measured at the tailpipe using both the SEMTECH-LDV PEMS and the VOCs system.

The vehicle and fuel combinations were tested on Emissions Analytics' standard EQUA™ Index test cycle which was twice as long and has a wider range of dynamic driving modes compared to the certification real-driving emissions (RDE) test [138]. Furthermore, the EQUA™ route was used as it contained boundary conditions of speed, acceleration, idling, and gradients, therefore providing good repeatability.

A cold-start phase was included whilst the urban, rural, and motorway driving modes were conducted with a warm engine. The cold-start phase was conducted in urban-like conditions but with no stop/start scenarios. The end of the cold-start driving condition was determined at a point when the engine temperature reached between 80 - 84 °C and this approach was maintained across all vehicle and fuel combinations. The distances for the cold-start, urban, rural, and motorway conditions were 4.0 miles, 26.6 miles, 11.3 miles, and 38.7 miles, respectively, totaling approximately 80.8 miles on average across all vehicle and fuel combinations. Furthermore, the mean speeds of the cold-start, urban, rural, and motorway conditions were 28 mph, 19 mph, 29 mph, and 65 mph on average across all vehicle and fuel combinations, respectively. The test route in this study was aimed to replicate real-driving conditions in the United Kingdom. The higher speeds on the test were achieved during the motorway condition where the speed limit is 70 mph (112 km/h). The average fuel consumption of the vehicles during the test route with each of the fuels is detailed in Appendix B.

A single test was performed for each vehicle-fuel combination. Before commencing each test, the fuel was drained from the tank by pumping it completely out and the new fuel was pumped in. Once the new fuel was put in the vehicle, it was run for 100 miles to be pre-conditioned and exposed to the new fuel. Additionally, for all cars in the study, the vehicles were first run on the E0 and subsequently the E10 fuel. It should be noted that there would be variability in driving conditions, traffic patterns, and environmental factors during each of the tests coupled with technical challenges such as sensor accuracy, measurement precision, and data processing complexities which can affect the reliability of RDE measurements.

3.6 Data processing

This section provides insight into the processing of raw data collected from the single-cylinder engine test cell setup and real-driving emissions measurements, explaining how the findings presented in the results chapters were extracted.

3.6.1 Single-cylinder engine

For the engine test cell, the data collection involved three different pieces of equipment, each operating at varying frequencies. Figure 3.8 shows the procedure used to process this data. To ensure accuracy in integrating data from each equipment, timestamps were cross-referenced prior to merging the datasets.

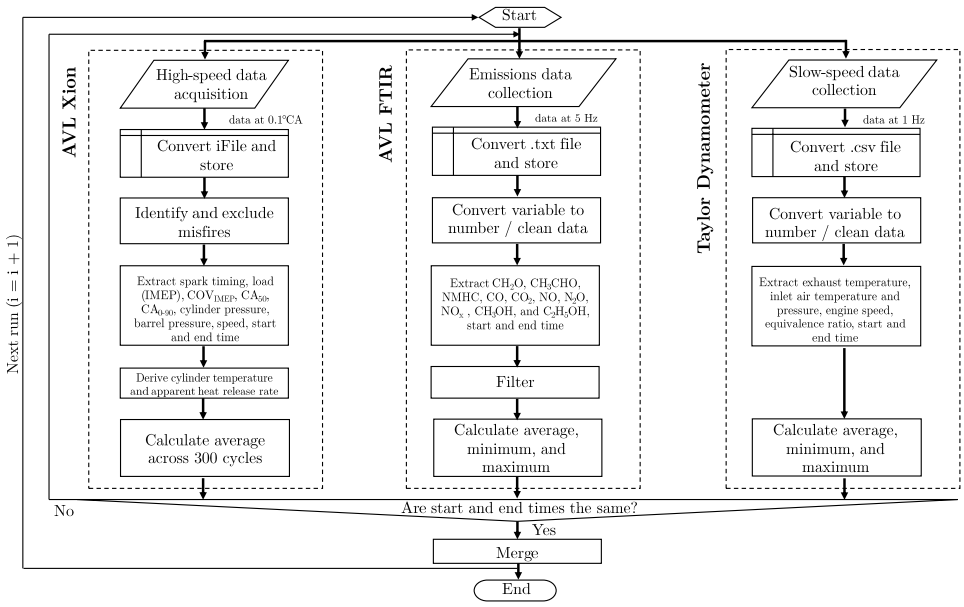

Figure 3.8: Flowchart followed to process experimental data from the single-cylinder engine.

In the emissions measurement process, instances of anomalous data were observed due to misfires during the 300 consecutive cycles. An example with the THOE20 surrogate fuel is shown in Figure 3.9. The raw and filtered data is shown for all three repeats.

These misfires resulted in time-delayed spikes in all measured emissions. To ensure the accuracy of the analysis, spikes caused by misfires were excluded from the dataset for each repeat before calculating the average emissions per repeat, as well as the minimum and maximum errors. For certain runs, emissions spikes were detected at the beginning

of the measurements, as was the case for the second repeat (r2). This was attributed to a misfire occurring just prior to data collection for the 300 cycles. Such data were also identified and excluded to prevent distortion of the findings.

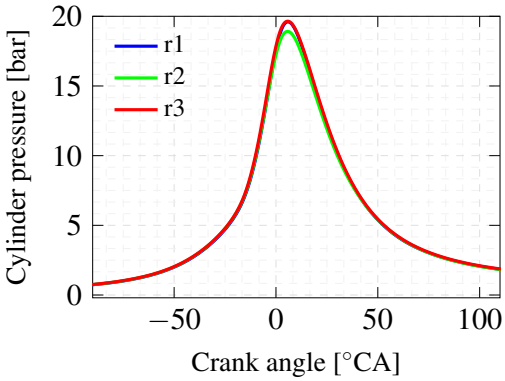

(a) Cylinder pressure

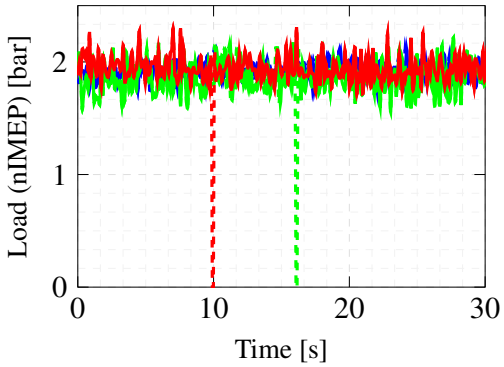

(b) Load (nIMEP)

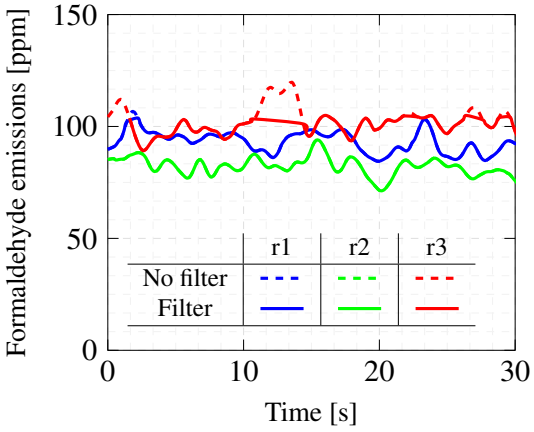

(c) Engine-out formaldehyde emissions

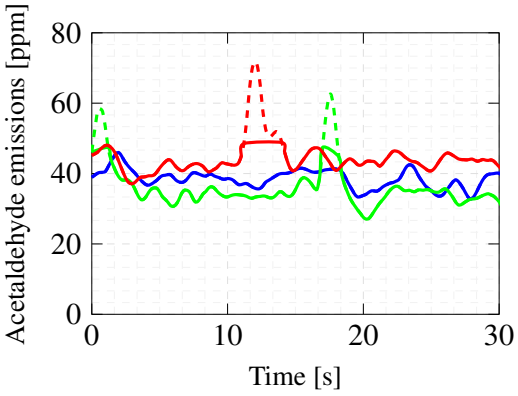

(d) Engine-out acetaldehyde emissions

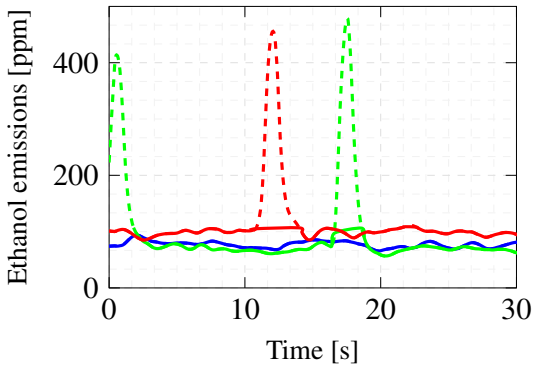

(e) Engine-out ethanol emissions

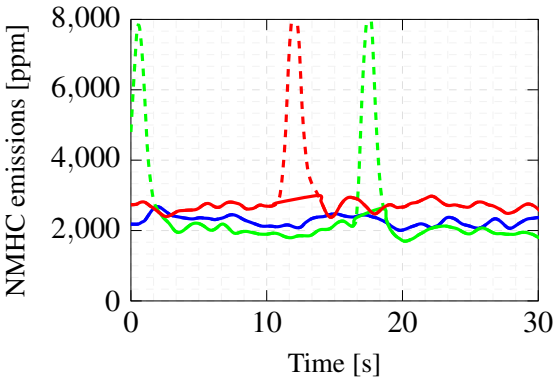

(f) Engine-out NMHC emissions

Figure 3.9: THOE20 combustion at 1100 rpm and 1.95 ±0.15 bar nIMEP under stoichiometry in the single-cylinder engine. **(a)** Cylinder pressure, **(b)** load nIMEP, and engine-out **(c)** formaldehyde, **(d)** acetaldehyde, **(e)** ethanol, and **(f)** NMHC emissions raw data for each of the 3 repeats. Non-filtered data with dashed lines and filtered data with solid lines.

3.6.2 RDE

As the tailpipe exhaust emissions collected through the SEMTECH-LDV PEMS unit were recorded in real-time (1 Hz), the data was divided into respective driving modes based on the geofences. An example with Car 2 using the E0 fuel is shown in Figure 3.10. This enabled comparison with the other emissions data collected through the VOCs system. The vehicles had an active start/stop system during the testing.

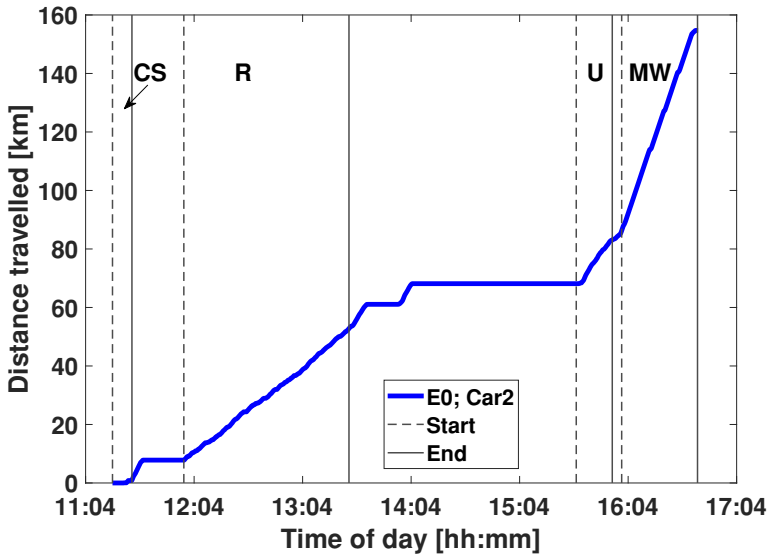

Figure 3.10: Driving segmentation for sample Car 2 with E0 fuel.

3.7 Summary

For this study, three distinct categories of fuels were formulated:

- Fuels explicitly formulated to assess the influence of fuel composition on aldehyde emissions.
- Gasoline surrogate fuels, complying with EN228 standards where possible, evaluated for their aldehyde emissions both in their original form and with incremental additions of ethanol.
- Two market-representative fuels, one with and the other without ethanol, derived from refinery streams to investigate their impact on aldehyde emissions.

Each of these fuels were tested in a single-cylinder engine modified for this research. The engine was operated under low speed and load conditions, with the fuel-air equivalence ratio (ϕ) adjusted between 0.90 and 1.20. Engine-out emissions were measured in real-time (5 Hz) using the AVL FTIR system. Three runs for each condition was conducted to ensure repeatability in the results. This work particularly focused on the analysis of formaldehyde, acetaldehyde, ethanol, and NMHC engine-out emissions. Additionally, the last category of fuels was evaluated in four passenger vehicles to assess real-driving VOC emissions in conjunction with the conventional emissions measured using the PEMS.

4

Modelling setup

Contents

4.1 Motivation

While it is important to study aldehyde emissions through experimental investigations, obtaining data of sufficient quality and consistency can be challenging due to the wide range of factors influencing the outcomes. Therefore, isolating the fundamental kinetic process from other physical effects can be beneficial in understanding the underlying

conditions which lead to aldehyde formation and consumption. To enable this, detailed combustion reactor models are useful. These models can provide key insights into the complex chemical processes that occur during combustion. They can identify reaction pathways and conditions that lead to the formation of pollutants like aldehydes, emphasising key reaction steps. Furthermore, they provide important insights on the combustion properties of a fuel composition.

To achieve this, chemical kinetic mechanisms are required. They comprise of a comprehensive list of reactions for a defined group of species, with the mechanism's complexity dependent on the number of species. These mechanisms are employed to simulate combustion in reactors designed to emphasise reaction kinetics under controlled flow conditions. This approach allows for a precise investigation of combustion chemistry, identifying fuel reactions responsible for aldehyde formation and degradation.

This chapter explores the fundamental principles of chemical kinetics in combustion modelling, and the selection of chemical kinetic mechanisms and reactor models to be used in this study. These selections aim to enhance understanding of aldehyde formation and consumption from a chemical perspective. The chosen mechanisms will undergo validation against literature data within the reactor models, specifically using the fuel components that are to be investigated in this study.

4.2 Fundamental principles

At the simplest level, three sets of information are provided within the mechanism formulation. This includes thermodynamic information represented by the thermochemical quantities associated with each species, kinetic information associated with a set of reactions detailing how each of the species reacts with each other, and collision dynamics information identifying the colliding species and their frequency and energies under an extensive range of operating conditions.

Therefore, each reaction in a chemical kinetic mechanism for combustion describes the transformation of reactants to products at a molecular level. For example, a broad reaction such as the oxidation of methane, represented as $CH_4 + 2\,O_2 <=> CO_2 + 2\,H_2O$, actually

involves approximately 30 species and 200 elementary reactions to accurately depict its oxidation process [72]. Chemical kinetics is key to predicting the rate of a reaction, where the nature and speed of each reaction are fundamentally governed by factors such as temperature, pressure, and the concentration of reactants and products. This helps understand the elementary steps of the reaction mechanism, the intermediate species produced, the reaction pathways, and the factors influencing the chemical composition of the products.

Ultimately, the reactant-to-product chemical kinetics is transformed into numerical combustion models, which solve the mass and energy conservation equations, dependent on the type of reactor. Software such as ChemkinPro 19.0 have preset libraries with these reactor models [161]. An essential component of the numerical form describing chemistry is the chemical source term, which defines the rate of change of concentration of the reacting species, which is extensively described in textbooks [85, 162]. For example, reaction i in the set of $m_{reactions}$ in a mechanism including $n_{species}$ can be generally written as shown in Equation 4.2.0.1.

$$\sum_{k=1}^{n_{species}} v_{ki}^{forward} \chi_k <=> \sum_{k=1}^{n_{species}} v_{ki}^{reverse} \chi_k \quad (i = 1, \ldots, m_{reactions}) \tag{4.2.0.1}$$

where v_{ki} are integer numbers and represent the stoichiometric coefficients and χ_k is the chemical symbol for the kth species in reaction i. The rate-of-progress, q_i, of the reaction i can then be expressed as shown in Equation 4.2.0.2.

$$q_i = K_i^{forward} \prod_{k=1}^{n_{species}} [X_k]^{v_{ki}^{forward}} - K_i^{reverse} \prod_{k=1}^{n_{species}} [X_k]^{v_{ki}^{reverse}} \tag{4.2.0.2}$$

where $[X_k]$ is the molar concentration of the kth species and $K_i^{forward}$ and $K_i^{reverse}$ are the forward and reverse rate constants of reaction i. The rate of production, ω_k, of the kth species can written as a summation of the rate-of-progress variables for all reactions involving the kth species, as shown in Equation 4.2.0.3. This is the chemical source term.

$$\omega_k = \prod_{i=1}^{m_{reactions}} (v_{ki}^{reverse} - v_{ki}^{forward}) q_i \quad (k = 1, \ldots, n_{species}) \tag{4.2.0.3}$$

The rate constants, $K_i^{forward}$ and $K_i^{reverse}$, are usually expressed using the modified Arrhenius form, as shown in Equation 4.2.0.4. The Arrhenius equation explains how the rate of a chemical reaction depends on temperature. The modified Arrhenius equation extends this concept by incorporating an additional parameter to account for variations in reaction rate due to changes in temperature, therefore providing a more accurate description of the temperature dependence of reaction rates in chemical kinetics.

$$K = AT^n e \frac{-E_a}{RT} \tag{4.2.0.4}$$

where A is the pre-exponential factor, T is the temperature, n is the temperature exponent, E_a is the activation energy, and R is the gas constant in J.K^{-1}. The rate constant is exponentially dependent on the activation energy for low to medium temperatures, but the pre-exponential factor is important at high temperatures. This rate constant describes the overall rate of reaction, however, there are several elementary reactions and intermediate species in a combustion mechanism. Direct experimental determination of the rate constant for each elementary reaction over a wide range of temperatures and pressures is often difficult and limited to light species. Therefore, estimation methods including collision theory and correlations of structure and reactivity are used [72]. These values have also been stored in online databases.

For each species, the temperature-dependent thermochemical data includes enthalpy, entropy, and heat capacities. This data can also be linked to the Arrhenius equation as shown in Equation 4.2.0.5.

$$\ln K = -\frac{\Delta G^{\ddagger}}{RT} = -\frac{\Delta H^{\ddagger} - T\Delta S^{\ddagger}}{RT} \tag{4.2.0.5}$$

where $\Delta G^{\ddagger}$ is Gibbs free energy of activation and $\Delta H^{\ddagger}$, and $\Delta S^{\ddagger}$ are the enthalpy and entropy of activation of each reaction, respectively. These are calculated using entropy and enthalpy of the product species minus the reactant species.

The enthalpy, $H^{\ominus}$, and the entropy, $S^{\ominus}$, along with the specific heat capacity at constant pressure, $C_p^{\ominus}$, for a species k, can be accurately determined using the National Aeronautics and Space Administration (NASA) polynomials. These polynomial fits are applied to $C_p^{\ominus}$ data of species k over specific temperature ranges. The calculations for $C_p^{\ominus}$, $H^{\ominus}$, and $S^{\ominus}$ of species k are outlined in Equations 4.2.0.6 to 4.2.0.8, respectively, using the NASA polynomials [163]. The NASA polynomials are obtained through a process that involves fitting experimental and theoretical data of thermodynamic properties of chemical species. There are seven for each designated temperature range. These include the low (around 300 K) to medium (approximately 1000 K), and medium (approximately 1000 K) to high (up to 5000 K) ranges. They enable the calculation of these thermodynamic properties at any given temperature, T, within these ranges. The use of polynomials of arbitrary order in this methodology ensures the accurate and flexible determination of thermodynamic properties for each species across a wide range of temperatures.

$$\frac{C_{p,k}^{\ominus}}{R} = a_1 + a_2 T + a_3 T^2 + a_4 T^3 + a_5 T^4 \tag{4.2.0.6}$$

$$\frac{H_k^{\ominus}}{RT} = a_1 + \frac{a_2}{2} T + \frac{a_3}{3} T^2 + \frac{a_4}{4} T^3 + \frac{a_5}{5} T^4 + \frac{a_6}{T} \tag{4.2.0.7}$$

$$\frac{S_k^{\ominus}}{R} = a_1 \ln T + a_2 T + \frac{a_3}{2} T^2 + \frac{a_4}{3} T^3 + \frac{a_5}{4} T^4 + a_7 \tag{4.2.0.8}$$

It should be noted that for each species, the associated transport properties are also provided in the chemical kinetic mechanism. This information is used for the evaluation of gas-phase multi-component viscosities, thermal conductivities, diffusion coefficients, and thermal diffusion coefficients.

4.3 Sensitivity analysis

Sensitivity analyses are used to evaluate how variations in input parameters affect the output of a model [164]. This methodology quantifies the impact of input changes on outputs like species concentration, temperature, IDT, or LBV. This resultant impact is quantified as the relative sensitivity coefficient S_i^{rel} [165]. The sensitivity coefficient is normalised so it can be compared across a range of conditions.

In this study, sensitivity analysis was used to evaluate the impact of each reaction on the LBV. As described in Section 4.2, each reaction has a unique reaction rate expression and pre-exponential factor, A. Therefore, by individually perturbing each pre-exponential factor in the reaction rate expression in the mechanism by a factor, the resultant impact on the model output, specifically the LBV, was observed. The sensitivity coefficients were then calculated to quantify the effect of each reaction on the predicted LBV. The details of the process can be found in the ChemkinPro 19.0 manual [165]. The reactions that affect the flame speed the most are identified and compared for different fuels compositions, initial operating conditions, and chemical kinetic mechanisms.

4.4 Chemical kinetics mechanisms

It is important to select suitable chemical kinetic mechanisms that are designed for the potential compositions examined and with recently updated species information. While it is possible to use large chemical mechanisms for the simulation of fundamental reactors, for high-fidelity or full-cycle engine simulations, reduced/skeletal mechanisms are most often adopted [166]. Therefore, for this work, two commercially available chemical mechanisms with different origins and reduction methods were considered (see Table 4.1).

Table 4.1: Summary of reaction mechanisms used in this work

Ref	Reduced mechanism	Fuels	Species-Reactions	Origin mechanism
M1	Li *et al.*[167]	ETPRF	59-270	Sarathy *et al.* [168]
M2	Wu *et al.*[169]	ETPRF	165-839	Mehl *et al.* [170]

The first mechanism, referred to as M1, is a reduced four-component, toluene / n-heptane / ethanol / iso-octane (THEO), gasoline surrogate kinetics mechanism developed by Li *et al.*[167]. The model was validated against various experimental data (IDTs and LBVs) for different ethanol concentrations. The results obtained with THEO mixtures containing 27.5 % / 20.0 % / 8.20 % / 44.3 % by liquid volume, respectively, suggested that the model can qualitatively predict the experimental trends.

The second mechanism, M2, is based on the work of Wu *et al.* where three different reduction techniques including isomer lumping were employed under a wide range of temperature, pressure, and equivalence ratio conditions relevant to modern internal combustion engines [169]. For THEO mixtures, experimental data for IDT by Cancino *et al.* and LBV by Dirrenberger *et al.* was employed for validation [88, 171]. This skeletal mechanism was shown to be within the error limits in comparison to experimental data and the detailed mechanism on which it is based.

4.5 Reactor models

Chemical kinetic mechanisms rely on experimental data obtained over a large range of conditions. As combustion strongly couples chemical and physical processes, to better assess the kinetics accuracy of these mechanisms, reactors with simple physical processes are modelled. Three reactor models were considered in this work. The perfectly-stirred reactor (PSR) model enables the study of chemical species concentrations across range of temperatures at a constant pressure, whereas the plug flow reactor (PFR) model allows for the analysis of intermediate aldehydes at specific reaction stages. The 1-Dimension (1-D) premixed laminar flame model was used to calculate the laminar burning velocity which aids in understanding the combustion behaviour of the range of fuel mixtures. Each of these models will be described in detail in this Section. By combining the different reactor facilities, a broad range of operating conditions relevant to engines and aldehyde formation and consumption can be reviewed. The fundamental modelling assumptions used in comparing the kinetic calculations to experiments are detailed as follows.

The PSR, PFR, and premixed laminar flame models were simulated on ChemkinPro 19.0 [165]. In these models, convergence can be challenging due to the highly non-linear and coupled nature of the governing equations. ChemkinPro 19.0 provides various options and settings to aid convergence, such as specifying initial estimates, adjusting tolerances and damping factors, and incorporating time integration methods. For each of the models, the solver properties and initial operating conditions that were modified in this study to aid convergence are detailed.

4.5.1 PSR

Description and assumptions

The JSR enables the understanding of the concentration of species formation, specifically aldehydes, across a range of temperatures for a specific pressure. Through this approach, for combustion pressures, the temperature region at which the greatest aldehyde concentration can be identified.

This reactor, referred to as the PSR model in ChemkinPro 19.0 [165], is simulated as a homogeneous constant volume reactor with contents assumed to be spatially uniform due to high diffusion rates and forced turbulent mixing. Therefore the conversion rate from reactants to intermediate and product species is controlled by chemical reaction rates and not by mixing processes. A schematic of the PSR is shown in Figure 4.1.

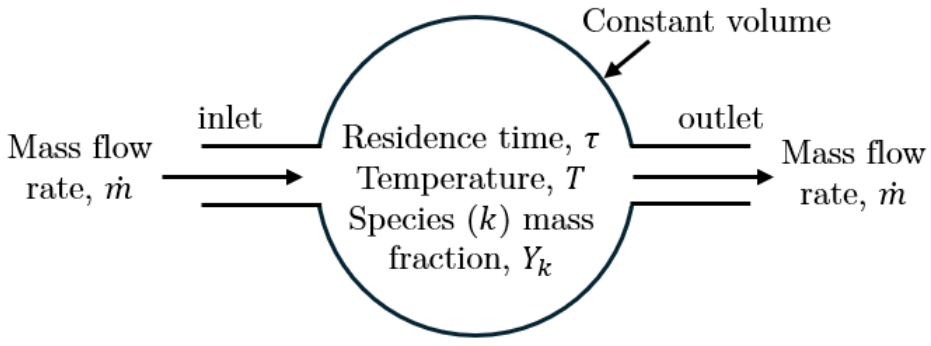

Figure 4.1: Schematic of the perfectly-stirred reactor model adapted from ChemkinPro 19.0 Manual [165].

The mass transport to the reactor walls is assumed to be infinitely fast, and the flow through the reactor is characterised by a nominal residence time, τ, which can be deduced

from the mass flow rate and reactor volume. The residence time measures the duration for which the reactants undergo chemical processes inside the reactor at a specific temperature and pressure. Solutions were iterated until a convergence point at which no change in species concentration occurred. At a specific pressure and residence time, this model can be simulated at varying temperatures to understand how reactant, intermediate, and product species concentrations vary with operating conditions.

Validation settings

To validate the chemical mechanism's capability in a PSR, the predictions of the model were compared against experimental data from the JSR at the Centre National de la Researche Scientifique (CNRS) in the University of Orleans by Dagaut *et al.* [172]. The property settings are shown in Table 4.2. The residence time was based on the fuel.

Table 4.2: PSR properties for the fuels tested in this study.

Property	Unit	Value(s)
Reactor physical properties		
Volume	cm^3	33.5
Inlet temperature	K	298
Problem type		Fixed gas temperature; steady-state solver
Solver properties		
Absolute tolerance		1.0E-09
Relative tolerance		1.0E-08
Operating conditions		
Temperature range	K	600 - 1100
Pressure	atm	10
Reactant mol fraction		0.002
N2 mol fraction		0.992
O2 mol fraction		0.006

Fuel experiment settings

For the modelling results based on the fuel tested in this study, the same properties as shown in Table 4.2 were used. The residence time for all experimented fuels was fixed at 0.7 s, similar to that of ethanol in the validation settings. For multi-component fuels, the proportions of each component were subdivided to sum up to the same reactant molar fraction of 0.2 %.

4.5.2 PFR

Description and assumption

The PFR enables the understanding of reactant, intermediate, and final product species concentration profiles along a spatial dimension. The reacting mixtures are highly diluted, so the kinetics are slow and the reaction zone is long. Through this approach, the unique effect of each of the fuel components on intermediate aldehyde formation can be identified and also their impact in multi-component mixtures can be studied.

This reactor is modelled in ChemkinPro 19.0 [165]. As the reactant mixtures are very dilute, the reaction temperature minimally deviates from the initial temperature (<50 K) and the reactor wall temperature is closely maintained to the initial reactor temperature. Consequently, the changes in chemical enthalpy closely follow adiabatic reaction conditions. Furthermore, as the core reacting flow is assumed to be radially uniform, the plug flow conditions can be modelled. Therefore, the experiment is modelled as a zero-dimensional system with isobaric and adiabatic approximations. The steady-state plug flow considers that the fluid is perfectly mixed in the radial direction; consequently, each reactor cross-section has uniform fluid properties including velocity, composition, temperature, and pressure. The change in these parameters along the distance of the reactor can be modelled and used to compare the effect of different fuel compositions and reactor conditions.

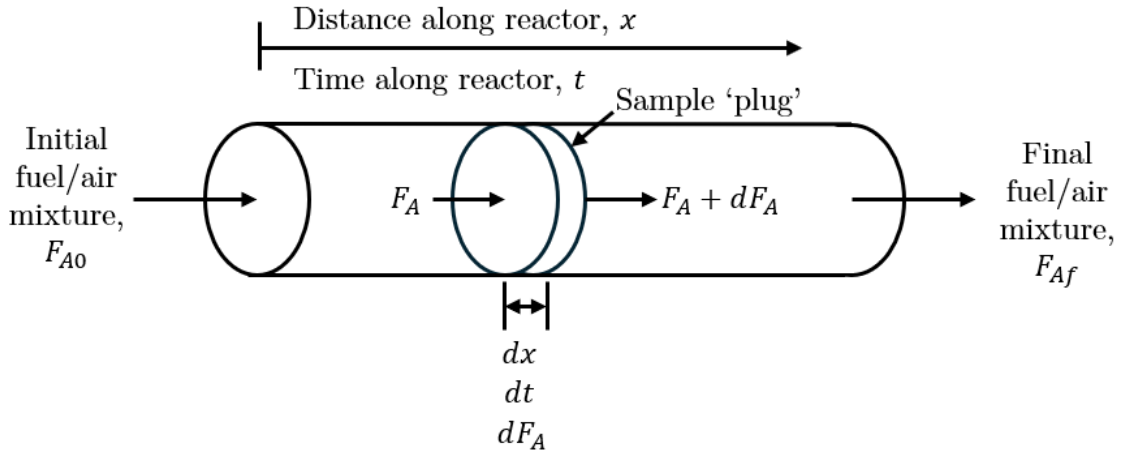

Figure 4.2: Schematic of the perfectly-stirred reactor model. Reproduced (adapted) from Battin-Leclerc *et al.* [85] with permission from Springer Nature.

Validation settings

To validate the chemical mechanism's capability in a PFR, the predictions of the model were compared against experimental data from the PFR at the University of Melbourne by Lu *et al.* [173]. The property settings are shown in Table 4.3.

Fuel experiment settings

For the modelling results based on the fuel tested in this study, the same properties as shown in Table 4.3 were used. The equivalence ratio for all pure and multi-component fuels was set at 0.058.

Table 4.3: PFR properties for the fuels tested in this study.

Property	Unit	Value(s)
Reactor physical properties		
Diameter	mm	25
Start axial position	mm	0
End axial position	mm	905
Axial velocity	m/s	3.34
Problem type		Fixed gas temperature; momentum equation - on
Solver properties		
Absolute tolerance		1.0E-13
Relative tolerance		1.0E-10
Solver integration steps		20
Operating conditions		
Temperature	K	875 - 900
Pressure	bar	10
Equivalence ratio		0.058

4.5.3 Spherical constant volume combustion vessel

Description and assumptions

The laminar burning velocity is the velocity of an unstretched adiabatic 1-D flame propagating towards the unburned gas. It is dependent on the mixture conditions, i.e. pressure, temperature, and equivalence ratio and its correlation with burn duration influences the power output and efficiency [174]. Therefore, it is key to ensure the chemical kinetic mechanisms not only predict the species concentrations but the combustion properties too.

The LBVs were computed using the 1-D laminar premix model in ChemkinPro 19.0 [165]. Computationally, flame instabilities are usually avoided by the assumption of a one-dimensional, planar flame. The equations governing the steady, isobaric, quasi-one-dimensional flame propagation can be found in the manual [165]. The burning velocity model involves a freely propagating flame. This configuration is used to determine the LBV of the gas mixture at a specified pressure and inlet unburned temperature. An assumption is made that there are no heat losses and the temperatures are computed from the energy equation. The model also assumes steady-state conditions with one-dimensional flow and uniform inlet conditions when determining the transport of heat.

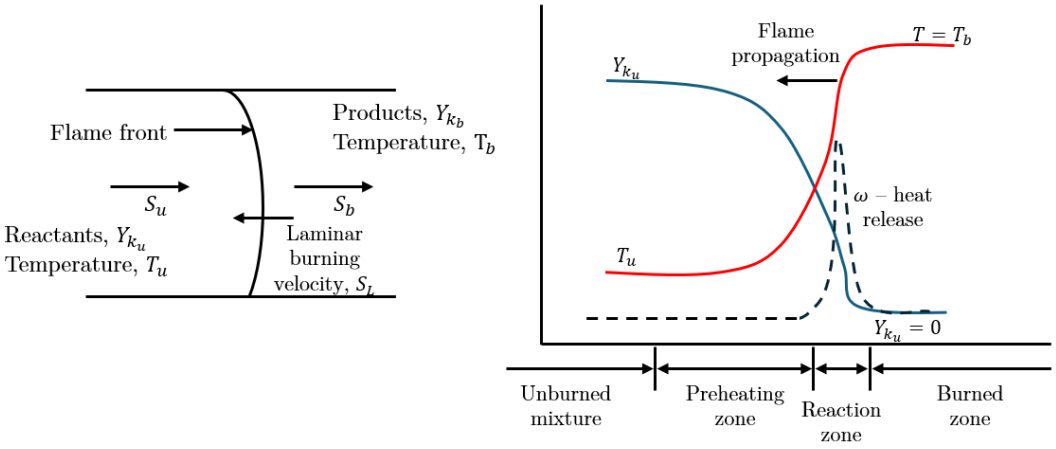

Figure 4.3: Schematic of the laminar burning velocity model. Reprinted (adapted) with permission from Liu *et al.* [175]. Copyright 2002, American Chemical Society.

Validation settings

To validate the chemical mechanism's capability for the prediction of combustion properties, the model was compared against experimental data from literature. This includes the data from the spherical constant volume combustion vessel from the University of Oxford by Hinton *et al.* [86] at elevated pressures and temperatures. The property settings are shown in Table 4.4. To ensure grid convergence, the grid parameters and solver properties shown in Table 4.4 were adopted.

Table 4.4: LBV properties for the fuels tested in this study.

Property	Unit	Value(s)
Reactor physical properties		
Start axial position	mm	0
End axial position	mm	100
Inlet velocity	cm/s	30
Inlet temperature	K	298
Solver properties		
Maximum grid points		6000
Adaptive grid points		1200
Gradiant		0.01
Curvature		0.05
Absolute tolerance		1.0E-09
Relative tolerance		0.001
Operating conditions		
Unburnt gas temperature	K	353 - 450
Pressure	bar	1 - 4
Equivalence ratio ϕ		0.70 - 1.20

Fuel experiment settings

The laminar burning velocity of the fuels tested in this study were not simulated. Modelling the laminar burning velocity in a vessel at these low pressure and temperature conditions aids the validation and development of chemical kinetic mechanisms that can accurately predict combustion behaviour over a wide range of conditions, including the high pressures relevant to engine combustion.

4.5.4 Single-cylinder engine model

Description and assumptions

A single-cylinder engine model was set up on GT-Power. The model is based on one-dimensional fluid dynamics, representing the flow and heat transfer in the piping and other flow components of an engine system as seen in Figure 4.4. At the start of combustion (spark in the SI engine), the cylinder is divided into two zones: an unburned zone and a burned zone. All the cylinder contents at the beginning are in the unburned zone. At each time step, a mixture of fuel and air is transferred from the unburned zone to the burned zone. The amount of fuel-air mixture that is transferred to the burned zone is defined by

the burn rate. For this a non-predictive combustion model is used. The 'EngSIWiebe' model imposes the burn rate for SI engines using a Wiebe function, which approximates the typical shape of an SI burn rate. When investigating different fuels, the relevant fuel properties, combustion initiation, and combustion duration can be entered in the simulation based on experimental data as detailed later in this Section. Subsequently, GT-Power's 'EngSIWiebe' model would then calculate the appropriate Wiebe function parameters for that fuel without the need for direct calibration.

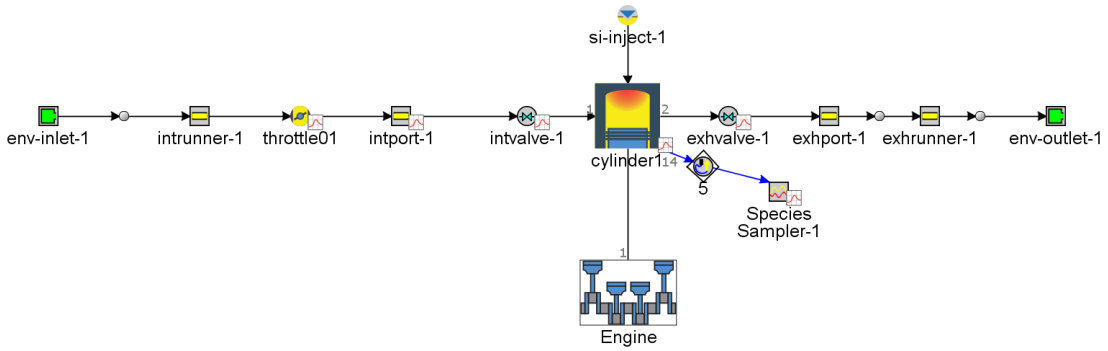

Figure 4.4: Schematic of the single-cylinder engine model developed to replicate the engine test cell in this work.

In the burned zoned, detailed chemistry was used to predict the heat release rates and emissions concentrations. The species quantities are calculated by accounting for the time required for the species to combine and react. Mechanism M2 was used for this as it has shown to closely predict species concentration profiles in the PFR and PSR for a wide range of fuel combinations.

Validation settings

The model was designed to match the experimental test cell setup in this work, where possible. Some of the model parameters are shown in Table 4.5 and the rest of properties were derived from Chapter 3 Section 3.3. This includes the cylinder geometry, the valve timings, and an average valve lift. The compression ratio was lowered to 10:1 as the experimental setup is an oil-free optical access engine which has additional pressure losses due to the higher levels of leakage past the piston rings. As the cylinder barrel was

externally cooled in the experiment, the head, piston, and cylinder temperatures were set at low values as shown in Table 4.5.

Table 4.5: Single-cylinder engine properties for the fuels tested in this study.

Property	Unit	Value(s)
Reactor physical properties		
Inlet pressure	atm	1
Inlet temperature	K	293.15
Throttle diameter	mm	35
Inlet valve diameter	mm	39
Exhaust valve diameter	mm	36
TDC clearance	mm	1.5
Compression ratio		10:1
Head temperature	K	333
Piston temperature	K	343
Cylinder temperature	K	308

Fuel experiment settings

For the engine model, only one set of operating conditions was tested across the comprehensive fuel matrix. This approach was adopted to assess the model's capability to follow the experimental data collected under simple stoichiometric conditions, before exploring a wider range of conditions. The operating conditions are detailed in Table 4.6. Given that these conditions include low engine speed and load, which typically result in lower combustion temperatures, it is expected to lead to the formation of aldehyde emissions across the various fuels in the matrix.

Table 4.6: Operating conditions in the single-cylinder engine model for the fuels tested in this study.

Operating conditions		
nIMEP	bar	2.00
Speed	bar	1100
Equivalence ratio [ϕ]		1.00

The model is basic and makes several assumptions, including a simple two-zone approach and non-predictive combustion. The burn rate parameters, such as the crank angle at 50 % mass fraction burned (CA_{50}) and the burn duration (CA_{10-90}), were individually modified for each fuel to closely match the experimental data. These parameters were

derived using AVL Indicom and subsequently used to inform the model. Additionally, the throttle opening was varied to match the desired load (nIMEP) and air-fuel ratio based on the fuel.

4.6 Modelling validation

This section presents a detailed validation of mechanisms and models with a range of fuels from literature that closely represent the fuels that will be investigated in this study. The two reduced and skeletal mechanisms introduced in this chapter, M1 and M2, were evaluated and the predicted outputs were compared to the experimental data from literature to assess their validity. This includes both global data, such as LBV, and detailed data, such as intermediate species concentration.

Through assessing the validity of the mechanisms, they can be used two-fold; to explore the operating conditions that lead to aldehyde formation and better understand the experimental emissions output from testing different fuels in the single-cylinder engine. This is a critical step before their application with novel fuel compositions studied in this work that do not have experimental data from fundamental reactors to compare against.

4.6.1 Pure fuels

Ethanol was simulated using both mechanisms at 875 K and 10 bar in a PFR and compared against the experimental data by Lu *et al.* [173]. The reactor and model properties can be found in Section 4.5.2.

For all figures in this section, the results from the simulations using the mechanisms are presented as lines and the experimental data from literature used for validation are presented as marker points. Figure 4.5 shows the comparison of the experimental and simulation data. As the ethanol decomposes, the intermediate acetaldehyde concentration increases [176]. Due to the low-temperature operating condition, the production of CO is greater than CO_2. The simulation output using M1 (dashed) predicts ethanol's decomposition is quicker than that of the measured data, therefore, the respective intermediate and product species form and decompose quicker than experimental data.

Whilst the simulation outputs of M1 in the reactor model show a discrepancy to the literature experimental data, the predictions using M2 (solid) present a closer match to the measured data.

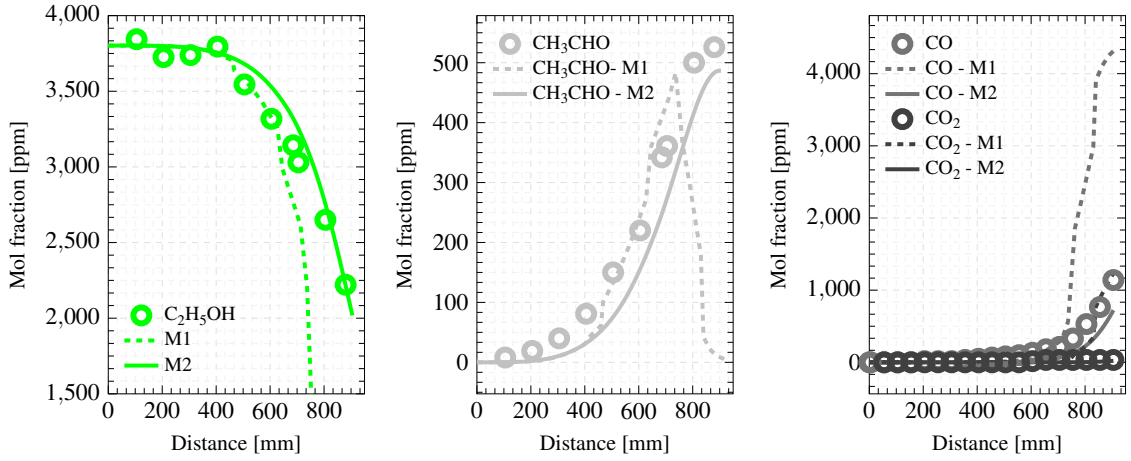

(a) Reactants **(b)** Intermediates **(c)** Products

Figure 4.5: Species concentration profiles of: **(a)** reactant (ethanol (C_2H_5OH)); **(b)** intermediate acetaldehyde (CH_3CHO)); and **(c)** product (carbon monoxide (CO), carbon dioxide (CO_2)) at 875 K, 10 bar, and $\phi = 0.058$ from the University of Melbourne PFR [176]. Mechanism M1 [167] (dashed lines) and M2 [169] (solid lines) predictions are presented.

The difference between the two predictions could be attributed to the relative size of each of the mechanisms. M2 has more species and associated reactions which were derived from the extensive Lawrence Livermore National Laboratories (LLNL) mechanism. This mechanism was specifically designed with an emphasis on an ethanol sub-model and its interactions with gasoline surrogates. On the other hand, M1, with fewer elementary reactions, might not fully capture the wide range of reactions that could lead to the formation and consumption of aldehydes. Additionally, while M1 successfully predicts the general trends of the various species concentrations examined, it seems to simulate reactions occurring more rapidly than what is observed experimentally. Therefore, for reactor models that study species concentration profiles under varying operating conditions, such as the PFR and PSR, further validation will be performed exclusively with the M2 mechanism due to its more comprehensive set of elementary reactions.

In addition to understanding ethanol's reaction progression at a specific pressure and temperature, its oxidation across a wide temperature range was evaluated with experimental

data from the University of Orleans JSR at a pressure of 10 atm [172]. Figure 4.6 shows the M2 mechanism's prediction capabilities compared to the experimental JSR data.

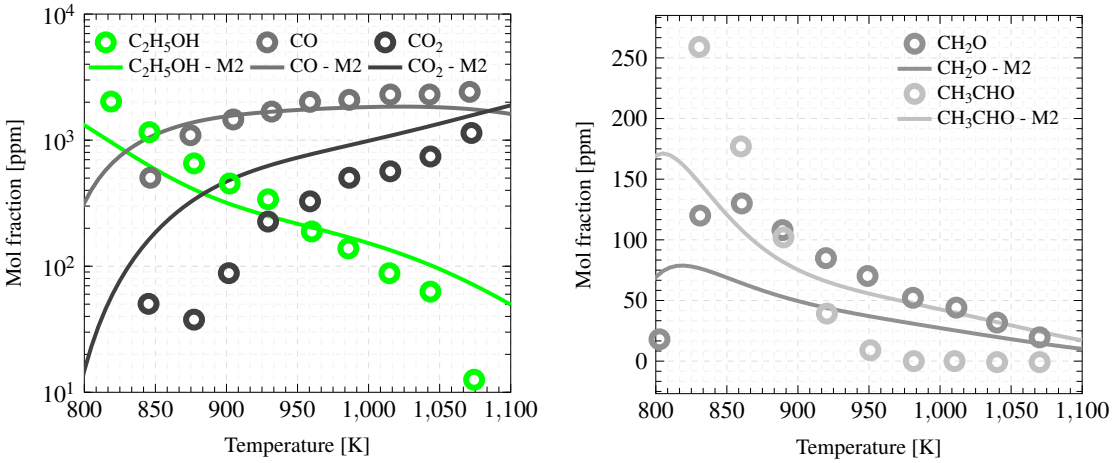

(a) Reactants and products **(b)** Intermediates

Figure 4.6: Data obtained from the reaction of 0.2% ethanol (C_2H_5OH), 0.6% oxygen (O_2), and 99.2% nitrogen (N_2) in the University of Orleans JSR (τ = 0.7 s, ϕ = 1.0, P = 10 atm) [172]. **(a)** Reactant (ethanol (C_2H_5OH)) and product species (carbon monoxide (CO) and carbon dioxide (CO_2)) and **(b)** intermediate species (formaldehyde (CH_2O), and acetaldehyde (CH_3CHO). Mechanism M2 [169] (solid lines) predictions are presented.

The ethanol oxidation and the CO production were well simulated by M2, however, there was an over-prediction of complete combustion at the lower temperatures, as shown by the greater estimation of CO_2. The model followed the experimental data trend and highlighted that the acetaldehyde concentration was greater than the formaldehyde for ethanol. However, the experimental data show this to be primarily true at low temperatures (< 900 K), whereas at higher temperatures, there was greater formaldehyde than acetaldehyde. This phenomena was not well captured by the M2 mechanism. Furthermore, there was an under-prediction of acetaldehyde and formaldehyde, particularly at low temperatures.

The oxidation of iso-octane, a fundamental gasoline surrogate component, was tested in similar operating conditions as ethanol in the University of Melbourne PFR by Lu *et al.* [176]. This data was used for M2's validation as shown in the reactant, intermediate, and product species concentration profiles in Figure 4.7.

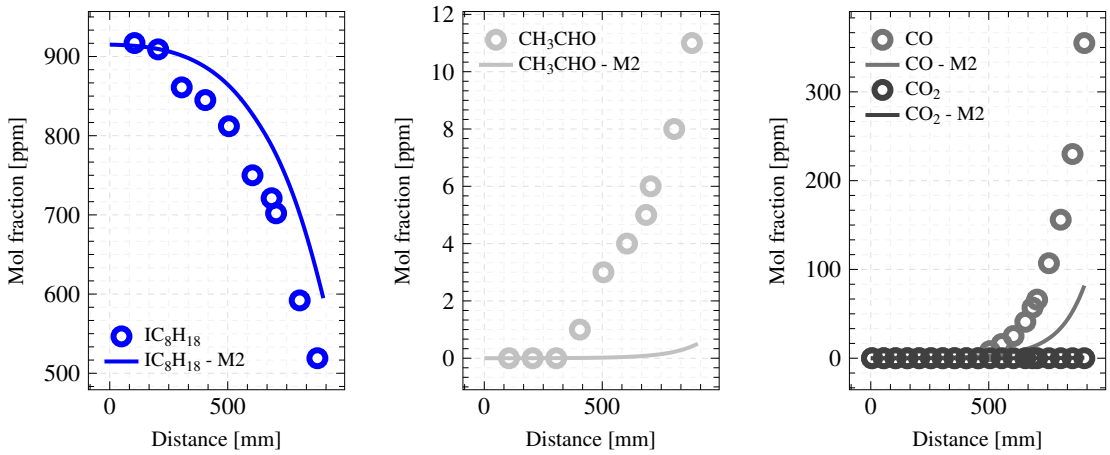

(a) Reactants **(b)** Intermediates **(c)** Products

Figure 4.7: Species concentration profiles of **(a)** reactants (iso-octane (IC_8H_{18})), **(b)** intermediates (acetaldehyde (CH_3CHO)), and **(c)** products (carbon monoxide (CO), carbon dioxide (CO_2)) at 875 K and 10 bar from the University of Melbourne PFR [176]. Mechanism M2 [169] (solid lines) predictions are presented.

The results show that the oxidation of iso-octane was well-predicted by M2, albeit an under-prediction of acetaldehyde (CH_3CHO) and carbon monoxide (CO). Despite the low measured values, it is key to note that M2 may not thoroughly account for the reaction pathways that lead to intermediate aldehyde formation in iso-octane's oxidation.

To validate M2's capability in predicting n-heptane's characteristics, experimental data from the University of Orleans JSR by Dagaut *et al.* [177] was used for validation as shown in Figure 4.8. Across the temperature range, M2 was able to capture the n-heptane consumption and the production of CO and CO_2. The model also accounted for the unique low-temperature (< 700 K) reactivity of n-heptane.

However, for the intermediate formaldehyde and acetaldehyde concentrations, a discrepancy due to under-prediction was observed at lower temperatures. Despite the model's capability to capture the behavioural trends of aldehyde formation, the simulated quantities were significantly different to the experimental data. Both the experimental and simulated data show that there is greater formaldehyde than acetaldehyde for n-heptane at the test conditions and beyond 750 K, there is no acetaldehyde concentration.

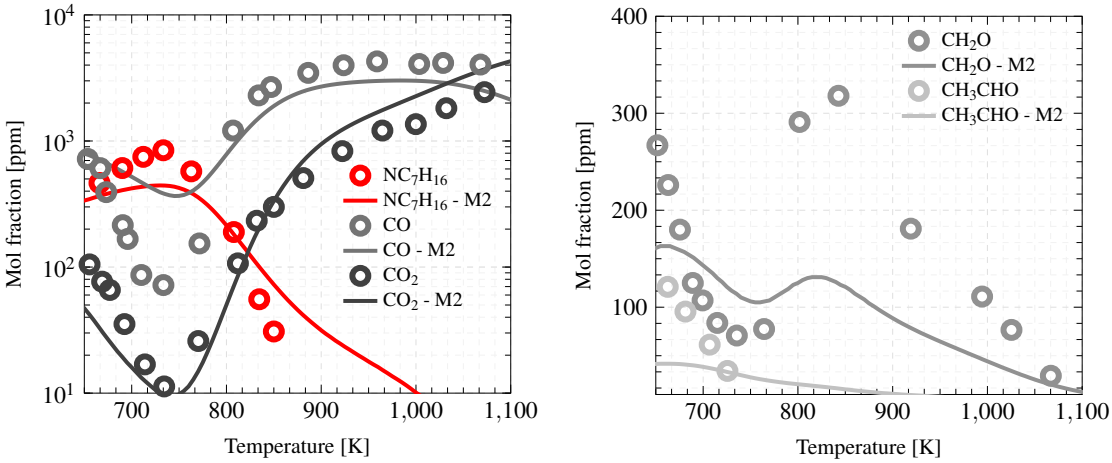

(a) Reactants and products **(b)** Intermediates

Figure 4.8: Data obtained from the reaction of 0.1% n-heptane (NC_7H_{16}), 1.1% oxygen (O_2), and 98.8% nitrogen (N_2) in a jet-stirred reactor (τ = 1 s, ϕ = 1.0, P = 10 atm) by Dagaut *et al.* [177]. **(a)** Reactant (n-heptane (NC_7H_{16})) and product species (carbon monoxide (CO) and carbon dioxide (CO_2)) and **(b)** intermediate species (formaldehyde (CH_2O), and acetaldehyde (CH_3CHO). Mechanism M2 [169] (solid lines) predictions are presented.

In addition to simulating the fuel oxidation pathways and conditions which favour increased concentrations of aldehyde species, the prediction of key combustion characteristics for the pure fuels was also assessed. Figure 4.9 shows the capabilities of mechanisms M1 and M2 for each of the pure components (iso-octane, n-heptane, ethanol, and toluene) at different initial conditions derived from literature.

For iso-octane, it is seen that the simulation results from both mechanisms closely follow the experimental data at the higher pressure conditions across the equivalence ratio range. A systematic over-prediction at lower pressure, however, is shown for both mechanisms. This is likely due to the over-prediction of the original mechanism's temperature exponents as detailed by Konnov *et al* [89].

For n-heptane, it can be seen that the predictions at lower pressure and higher temperature illustrate a significant discrepancy in M2's capability. This may be because the original detailed mechanism used to reduce to form M2 was not validated for propagating flames due to the mechanism's large size as observed by Jerzembeck *et al.* [178] However, at

higher pressures, more towards engine-like conditions, both mechanisms present similar predictions that match the experimental data.

For ethanol, both mechanisms under-predict at the lower pressure, however, they closely match the experimental data at the higher pressure, except at the leaner conditions. M1 and M2 present similar predictions of the ethanol LBV data.

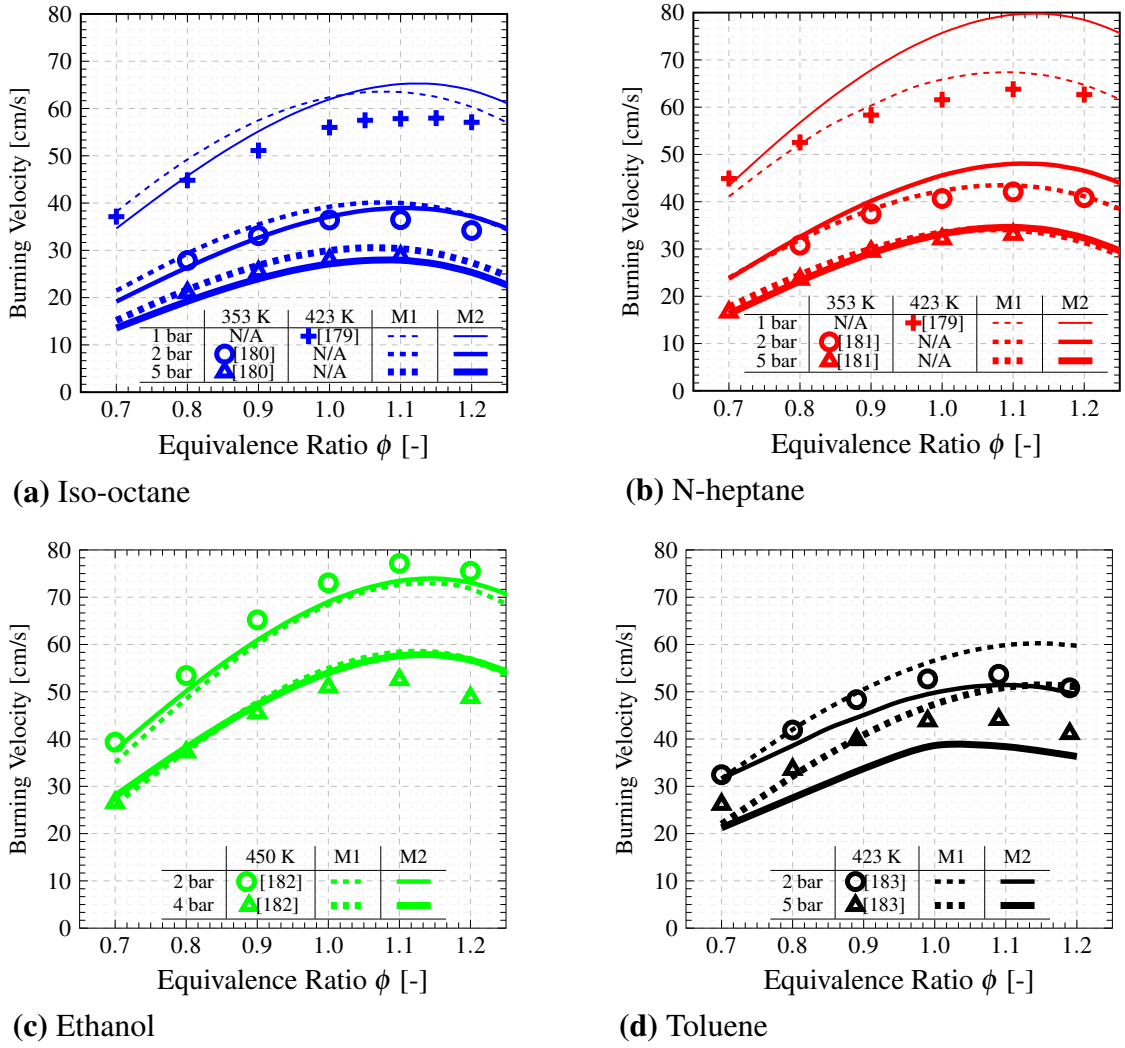

(a) Iso-octane **(b)** N-heptane

(c) Ethanol **(d)** Toluene

Figure 4.9: Comparison of mechanisms M1 [167] (dashed) and M2 [169] (solid) across equivalence ratio range for pure components. **(a)** iso-octane at 2 and 5 bar at 353 K [180] and at 1 bar and 423 K [179],**(b)** n-heptane at 2 and 5 bar at 353 K [181] and at 1 bar and 423 K [179], **(c)** ethanol at 2 and 4 bar at 450 K [86], and **(d)** toluene at 2 and 5 bar at 423 K [183]

On the other hand, for pure toluene, the prediction from the two mechanisms diverges across the equivalence ratio range from rich to lean. At stoichiometric conditions,

mechanism M2 over-predicts and the opposite is observed with M1. The difference is accentuated the higher pressure condition.

The experimental data were determined through a range of techniques, including spherical flame (SF), counter flow (CF), and heat flux (HF) methods, which can assume the flame front to be planar and adiabatic but it may be wrinkled, unsteady, and exist in flow fields that are themselves non uniform and unsteady [184]. Hinton *et al.* [185] collected stretch corrected experimental data using the spherical constant volume combustion vessel facility with both flame front imaging and pressure rise techniques. In addition to the pure fuels, Hinton *et al.* [185] tested equal volume binary, ternary, and quaternary mixtures with the same facility. This experimental data is ideal for further validation of the two mechanisms. Figure 4.10 shows the comparison of simulation and experimental data for the pure fuels across a pressure range of 1 - 4 bar at 380 K and 450 K. These results are at stoichiometric conditions.

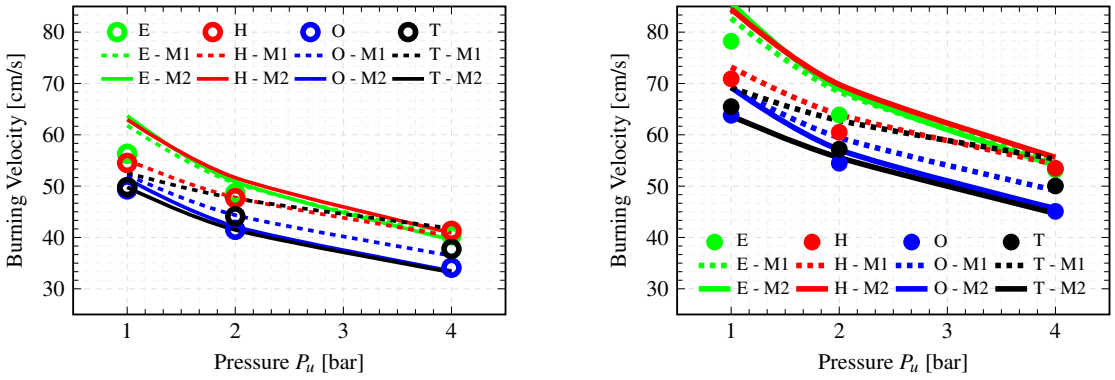

(a) LBV at 380 K **(b)** LBV at 450 K

Figure 4.10: LBVs at 1, 2, and 4 bar at **(a)** 380 K (hollow) and **(b)** 450 K (filled) for ethanol (E), n-heptane (H), iso-octane (O), and toluene (T) with data obtained from the University of Oxford spherical constant volume combustion vessel [86]. Mechanism M1 [167] (dashed) and M2 [169] (solid) are presented.

The results show ethanol and n-heptane have a greater LBV than iso-octane and toluene. The difference in the experimental data amongst the fuels is greater at the higher temperature condition. At lower pressures, M1 captures the difference between ethanol and n-heptane, however, at higher pressures, the two mechanisms have similar predictions that match the experimental data. Ethanol and iso-octane display stronger pressure

dependency and both mechanisms were able to capture this. In particular, M2 is better able to predict this for iso-octane. Similar to the behaviour in Figure 4.9, M1 over-predicts for toluene and the opposite for M2. This behaviour is likely due to the complex molecular structure and reaction process of toluene involving significant number of elementary reactions, which is difficult to synthesise in a reduced mechanism.

To explore this further, the two mechanisms' capabilities were examined through sensitivity analyses as shown in Figure 4.11 for all fours pure fuels at 2 bar and 450 K which is one of the operating conditions from Hinton's experimental data [86].

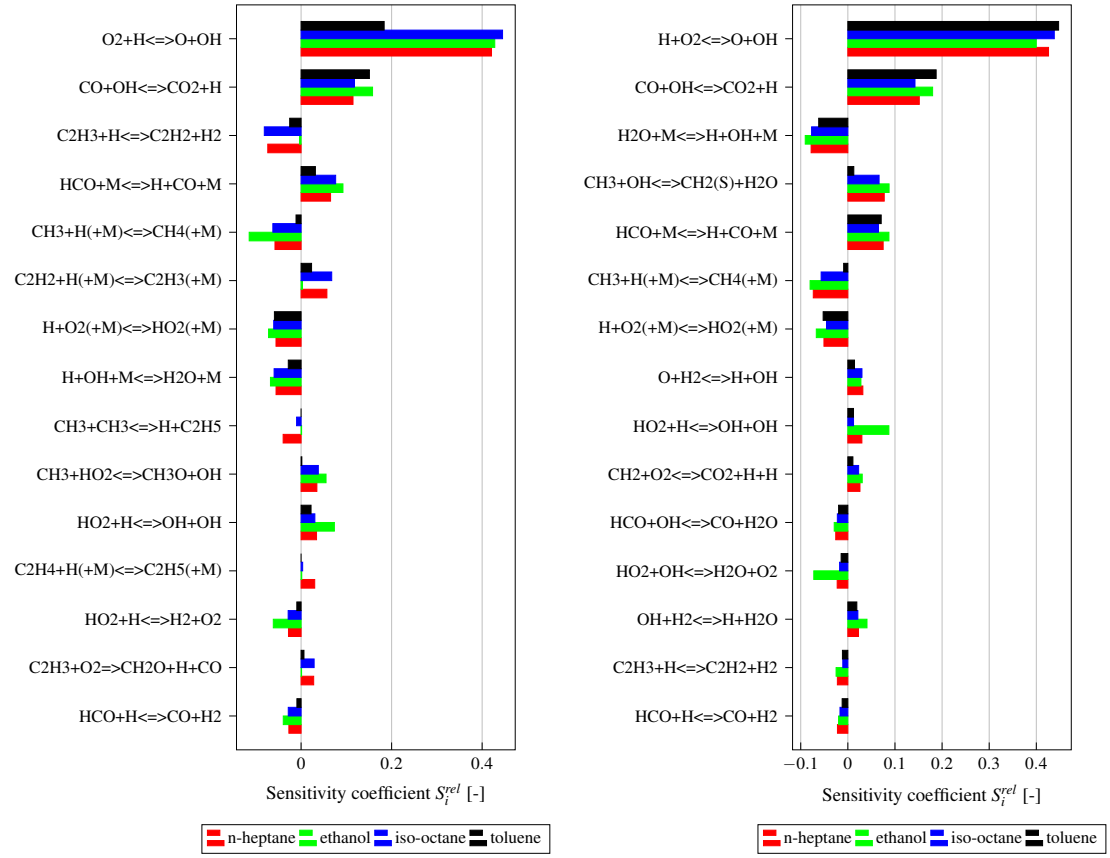

(a) Mechanism M1 **(b)** Mechanism M2

Figure 4.11: LBV sensitivity analysis of the pure fuels (ethanol, n-heptane, iso-octane, and toluene) at 2 bar and 450 K. Top 15 (absolute) sensitivity coefficients S_l of **(a)** Mechanism M1 [167] and **(b)** M2 [169] are presented.

The sensitivity coefficient S_i^{rel} quantifies the relative change in the laminar burning velocity for a relative change in the pre-exponential factor in the reaction rate expression. A small positive sensitivity coefficient (e.g., 0.1) indicates that a 10 % increase in the

pre-exponential factor (and subsequently reaction rate expression) will result in a 1 % increase in the laminar burning velocity, whereas a negative sensitivity coefficient of -0.3 means that a 10 % increase in the pre-exponential factor will result in a 3 % decrease in the laminar burning velocity. Therefore, a positive sensitivity coefficient shows the reactions influence in increasing the LBV and a negative sensitivity coefficient shows the opposite. This work has also been published in the journal Fuel [184].

While fuel-specific reactions can directly affect the LBV to some extent, based on the sensitivity analysis for each of the pure fuels, reactions related to H radical is found to have the largest impact on LBV [186]. The key chain branching reaction in any hydrogen containing system is Reaction 4:

$$H + O_2 \rightleftharpoons O + OH \qquad \{4\}$$

Any reaction that produces the H radicals needed by Reaction 4 can increase the overall fuel oxidation rate and thereby promote the combustion process. This was true across all pure fuels. These reactions are better emphasised in M2 than M1 for toluene. M2 retains both the high and low-temperature chemistry, which are extremely different in the case of large molecules such as n-heptane and iso-octane and important for engine-relevant simulations. However, for the study of propagating flame, additional adjustment might be needed.

The indirect effect of the fuel-specific reactions on the LBV can be analysed by examining how they influence the presence of small molecule H and OH radicals. These reactions can also be linked to the pathways that subsequently promote or inhibit aldehyde formation.

For ethanol, these reactions can stem from the decomposition of acetaldehyde. Initially, acetaldehyde breaks down into methyl (CH_3) and formyl (HCO) radicals as shown in Reaction 5. The formyl radical can undergo a chain-carrying process, Reaction 6, to form carbon monoxide (CO). Subsequently, the reaction of CO with OH radicals, shown in Reaction 7, increases the H radical concentration. This increase promotes the chain-branching reaction (Reaction 4) and consequently influencing the LBV.

$$CH_3CHO \rightleftharpoons CH_3 + HCO \quad \{5\}$$

$$HCO(+ M) \rightleftharpoons H + CO(+ M) \quad \{6\}$$

$$CO + OH \rightleftharpoons CO_2 + H \quad \{7\}$$

As previously discussed in the literature review (Chapter 2), acetaldehyde primarily originates from the H-atom abstraction of ethanol. This process leads to the formation of one of three isomeric C_2H_5O radicals, that undergoes secondary H-atom abstraction to form ethylhydroxy and α-hydroxyethyl radicals. These decompose to yield formaldehyde and acetaldehyde, as shown in Reactions 8 and 9 respectively, with a radical. The latter reaction produces H radicals which can influence the LBV. Additionally, as mentioned earlier, the acetaldehyde can further break down, potentially influencing the LBV. This observation suggests that for ethanol, there may be an inverse relationship between the conditions that favour acetaldehyde formation and those that promote combustion properties such as the LBV.

$$CH_3CH_2O^{\bullet} \rightleftharpoons CH_2O + CH_3 \quad \{8\}$$

$$CH_3C^{\bullet}H_2O \rightleftharpoons CH_3CHO + H \quad \{9\}$$

For the study of iso-octane's LBV, the primary intermediates include iso-butene and propene. Iso-butene further decompose to allyl (CH_2CHCH_2) and methyl (CH_3) radicals. Propene can react with OH radicals to form acetaldehyde. Under radical rich conditions, methyl (CH_3) and alkoxyl (RO) radicals can react with O_2 forming formaldehyde. The appropriate reaction pathways depend on the operating condition, however, highlight potential links between the combustion properties and aldehyde formation.

The oxidation of a linear alkanes, such as n-heptane, results in a higher production of ethylene (C_2H_4), which can oxidise to form vinyl radicals (C_2H_3), which are more reactive. This leads to a comparatively faster LBV for n-heptane than iso-octane. These reaction can produce or consume H and OH radicals, influencing the LBV and potentially reacting with stable aldehyde intermediates to decompose them.

For toluene, given its aromatic structure, reactions associated with the phenyl radical (C_6H_5), affect both the production and consumption of H and OH radicals. They can have a fuel-specific influence on the LBV, as will be illustrated in Figure 4.20 later in this Chapter. The phenyl radical can be formed through the reaction of the benzyl radical ($C_6H_5C^{\bullet}H_2$) with atomic oxygen as shown in Reaction 10. Benzaldehyde, an intermediate in toluene's oxidation, can undergo H-atom abstraction to form the benzyl radical, but it can also decompose to produce acetaldehyde, further demonstrating the link between aldehyde formation pathways and combustion properties.

$$C_6H_5C^{\bullet}H_2 + O \rightleftharpoons C_6H_5 + CH_2O \quad \{10\}$$

For the following section covering multi-component fuels, M2's predictions will be validated against experimental data for zero-dimensional reactor models with a wide temperature range, whereas both mechanisms will be explored for one-dimensional LBV validation.

4.6.2 Multi-component fuels

Varying binary, ternary, and quaternary compositions of the pure fuels were validated against experimental data to ensure the mechanisms were capable of predicting the behaviour accounting for the component interactions. Intermediate aldehyde species concentrations, where available, were evaluated.

Binary

Mechanism M2 was validated for a primary reference fuel with PFR experimental data by Yuan *et al.* [81]. This data was also collected in the University of Melbourne PFR. The

composition was 91 % vol iso-octane and 9 % vol n-heptane. As M2 was developed for gasoline surrogates, the M2 predictions closely follow the species concentration profiles of the experimental data as shown in Figure 4.12.

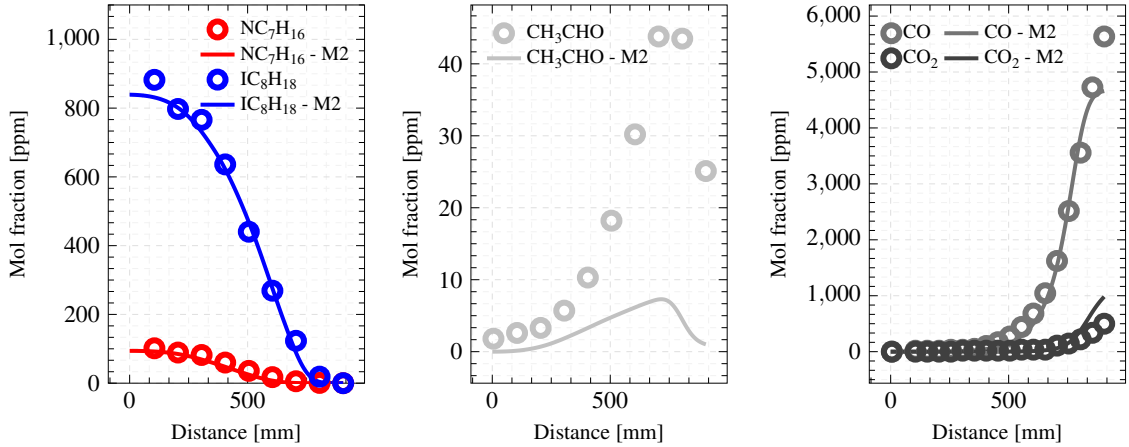

(a) Reactants **(b)** Intermediates **(c)** Products

Figure 4.12: Species concentration profiles of **(a)** reactant (iso-octane (IC_8H_{18}) and n-heptane (NC_7H_{16})), **(b)** intermediate (acetaldehyde (CH_3CHO)), and **(c)** product (carbon monoxide (CO), carbon dioxide (CO_2)) at 900 K, 10 bar, and ϕ = 0.058 from the University of Melbourne PFR [81]. Mechanism M2 [169] (solid lines) predictions are presented.

Similar to the behaviour of iso-octane and n-heptane pure fuels, M2 under-predicts the acetaldehyde (CH_3CHO) concentration of the PRF blend. By accurately simulating the behaviour of a gasoline surrogate, the impact on the aldehyde formation and consumption by adding other components such as ethanol can be evaluated.

The addition of 20 %v/v ethanol to pure iso-octane was simulated and compared to experimental data. This was collected in the University of Melbourne PFR by Lu *et al.* [176]. The model predictions closely follow the literature data with improved accuracy for acetaldehyde estimation except for an under-prediction of carbon monoxide (CO) as shown in Figure 4.13. With the ethanol addition to iso-octane, a 7-fold increase in acetaldehyde concentration is observed compared to pure iso-octane.

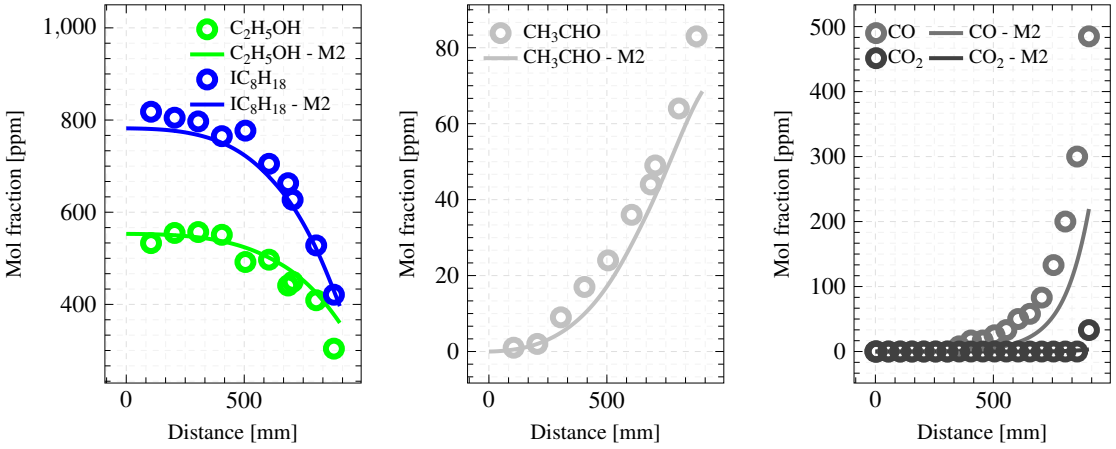

(a) Reactants **(b)** Intermediates **(c)** Products

Figure 4.13: Species concentration profiles of **(a)** reactant (iso-octane (IC_8H_{18}) and ethanol (C_2H_5OH)), **(b)** intermediate (acetaldehyde (CH_3CHO)), and **(c)** product (carbon monoxide (CO), carbon dioxide (CO_2)) at 875 K, 10 bar, and $\phi = 0.058$ from the University of Melbourne PFR [176]. Mechanism M2 [169] (solid lines) predictions are represented.

Additional to conventional gasoline surrogate blends, literature data on less conventional binary compositions with varying blending ratios of ethanol and toluene (ET) and iso-octane and toluene (OT) were also used to validate the model and M2 predictions. Only the CO data were measured for these mixtures at 900 K and 10 bar [81]. The results can be seen in Figure 4.14.

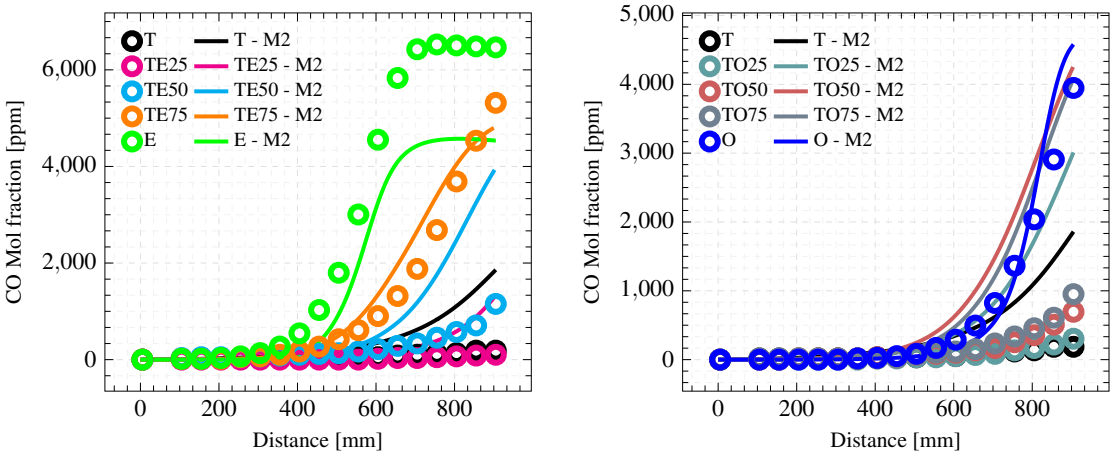

(a) Toluene and ethanol (TE) blends **(b)** Toluene and iso-octane (TO) blends

Figure 4.14: Species concentration of carbon monoxide (CO) for **(a)** pure toluene (T), ethanol (E), and mixtures of ethanol and toluene (TE) with increasing ethanol fraction of 0.25 (TE25), 0.50 (TE50), and 0.75 (TE75) and **(b)** for pure toluene (T), iso-octane (O), and mixtures of ethanol and iso-octane (TO) with increasing iso-octane fraction of 0.25 (TO25), 0.50 (TO50), and 0.75 (TO75). Data from the University of Melbourne PFR at 900 K, 10 bar, and $\phi = 0.058$ [81]. Mechanism M2 [169] (solid lines) are presented.

At the experimental operating conditions of 900 K and 10 bar, toluene is less reactive than both ethanol and iso-octane. Therefore, increasing the addition of ethanol (0.25 (ET25), 0.50 (ET50), and 0.75 (ET75) molar fraction of ethanol) accelerates the reactivity of the mixture. Similar behaviour is noticed with iso-octane addition to toluene, although with a lower rate of reactivity as iso-octane is less reactive than ethanol. The mechanism is expected to have difficulty reproducing toluene-containing mixtures as it over-predicts the oxidation of neat toluene, similar to the original LLNL mechanism [81].

In addition to species profiles, the LBV was also evaluated for binary mixtures. A comparison of three equal volume binary mixtures (ethanol and iso-octane (EO), ethanol and n-heptane (EH), and iso-octane and n-heptane (OH)) is shown in Figure 4.15. The experimental data was collected by Hinton *et al.* [86] using the spherical constant volume combustion vessel in the same conditions as the pure fuels.

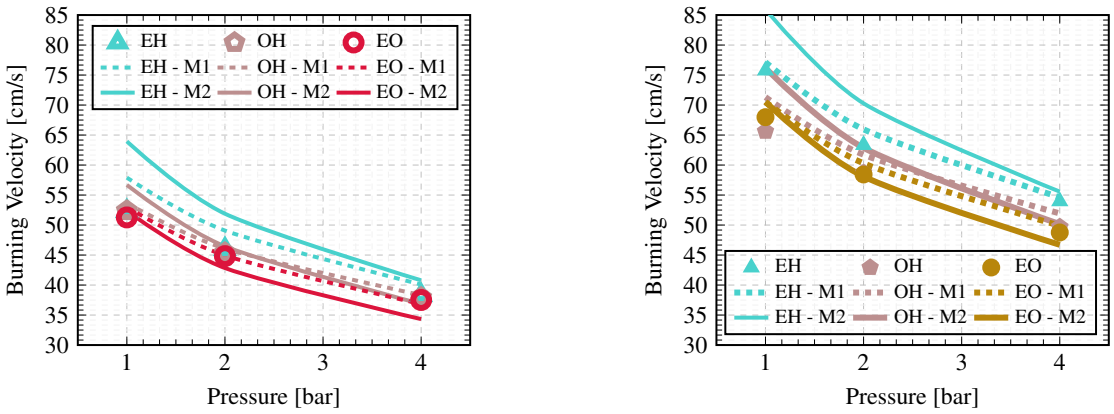

(a) LBV at 380 K **(b)** LBV at 450 K

Figure 4.15: LBV data comparing equal volume binary (EH, OH, EO) mixtures from University of Oxford spherical constant volume combustion vessel [86]. Conditions are at **(a)** 380 K (hollow) and **(b)** 450 K (filled) at pressures of 1, 2, and 4 bar under stoichiometry. Mechanisms M1 [167] (dashed lines) and M2 [169] (solid lines) are presented.

For the EO mixtures, due to the presence of both iso-octane and ethanol, the mixture illustrated strong pressure dependency. At lower pressures, the LBV of EO was greater than OH but the opposite was observed at higher pressures. This phenomena was better captured with M1. The EH mixture has a greater LBV than the other two mixtures and this is to be expected as both ethanol and n-heptane have high LBVs. Both mechanisms were

able to predict this and M2 presented a closer match to the experimental data, particularly at the higher temperature condition.

While the binary mixtures' LBVs are expected to be bounded by the pure component constituents, this was not the case for the EH mixture. The LBV of the EH mixture was lower than the pure ethanol and n-heptane fuels and this was observed both experimental and predicted by the mechanisms. The findings showed that peak in the H radical concentration decreases at higher pressure and temperature conditions as ethanol suppresses n-heptane's low temperature reactivity. This leads to the mixture having a lower LBV than the pure fuel components. This shows the importance of the H radical distribution and the role of the chemical kinetic mechanisms in helping understand the experimental data.

The LBV of less conventional equal-volume binary compositions (ethanol and toluene (ET), n-heptane and toluene (HT), iso-octane and toluene (OT)) were also used to validate the two mechanisms. As toluene has shown contrasting effects on aldehyde emissions, it will be investigated in this study. Therefore, this validation is key to understand the mechanisms's capability in replicating combustion data of toluene-based binary mixtures. This is shown in Figure 4.16.

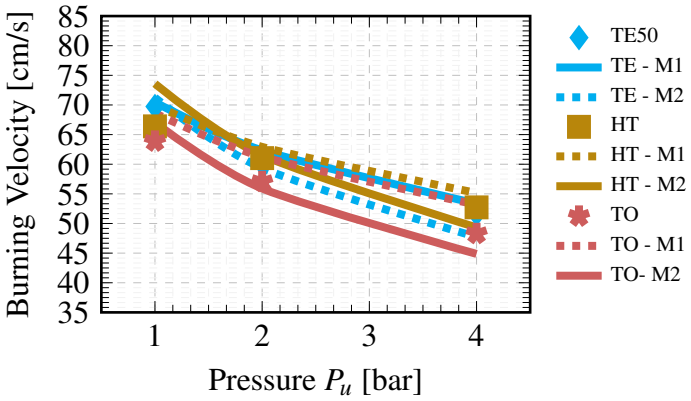

Figure 4.16: LBV data comparing equal volume binary (TE, HT, TO) mixtures from University of Oxford spherical constant volume combustion vessel [86]. Conditions are 450 K (filled) at pressures of 1, 2, and 4 bar under stoichiometry. Mechanisms M1 [167] (dashed lines) and M2 [169] (solid lines) are presented.

Ethanol's pressure dependency significantly affects the ET mixtures' LBV at 4 bar. This

behaviour is over-emphasised with M2 than M1. Similar to the pure fuels, M1 over-predicts and the opposite is observed for M2. However, the over-arching trends are captured by both mechanisms.

Surrogate fuels

Following the validation of the binary PRFs, the addition of 50 % of ethanol to the PRF to form a ternary mixture, referred to as EPRF, was also evaluated as the M2 mechanism will be used in engine models with market representative fuels. At 900 K and 10 bar, the reactant concentration profiles replicated the experimental data from the University of Melbourne PFR by Yuan *et al.* [81] as seen in Figure 4.17. The acetaldehyde (CH_3CHO) concentrations were predicted well.

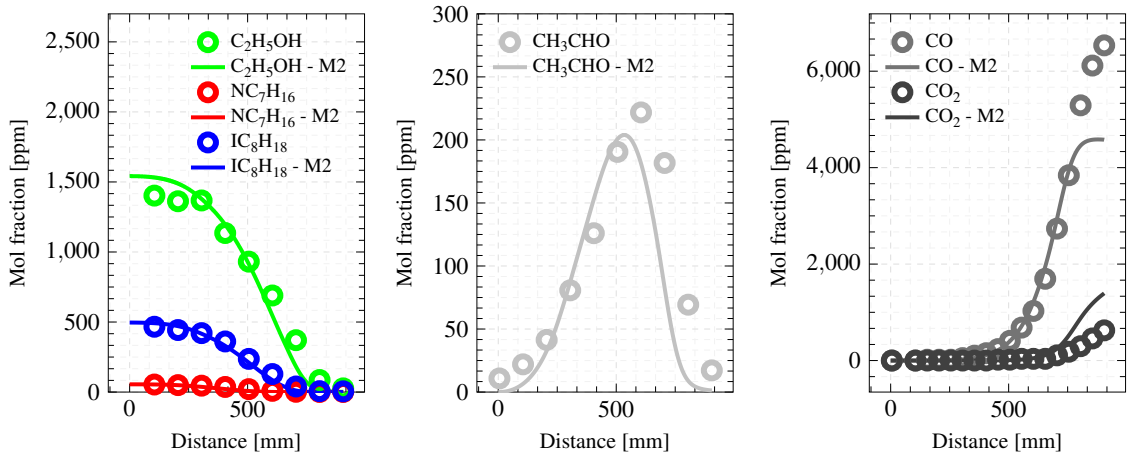

(a) Reactants **(b)** Intermediates **(c)** Products

Figure 4.17: Species concentration profiles of **(a)** reactant (iso-octane (IC_8H_{18}), n-heptane (NC_7H_{16}), and ethanol (C_2H_5OH)), **(b)** intermediate acetaldehyde (CH_3CHO)), and **(c)** product (carbon monoxide (CO), carbon dioxide (CO_2)) at 900 K, 10 bar, and $\phi = 0.058$ from the University of Melbourne PFR [81]. Mechanism M2 [169] (solid lines) predictions are presented.

As commercial gasoline contains aromatics, toluene can be included to form a gasoline surrogate mixture of iso-octane, n-heptane, and toluene, referred to as TPRF. The M2 mechanism's ability to predict TPRF mixture with 50 %v/v addition of ethanol, referred to as ETPRF, was evaluated against experimental data from the Melbourne PFR at 900 K and 10 bar collected by Yuan *et al.* [81]. The results are shown in Figure 4.18.

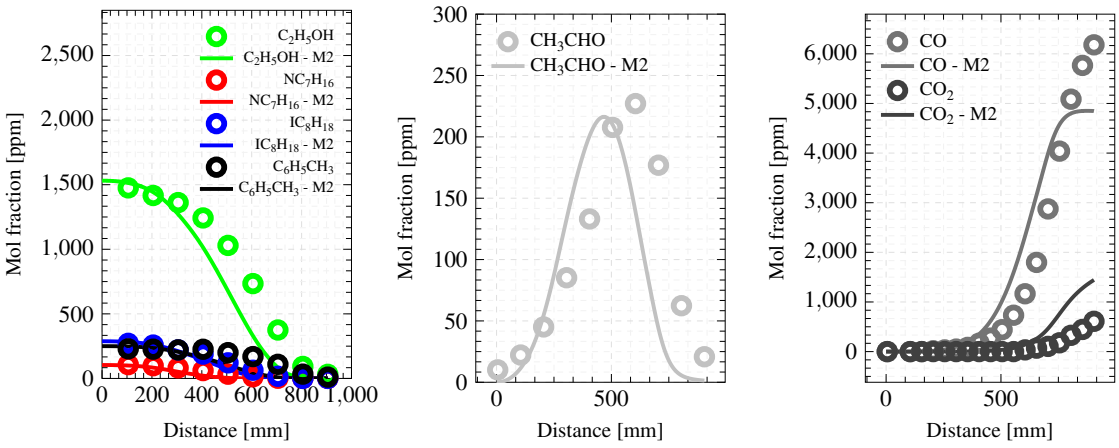

(a) Reactants **(b)** Intermediates **(c)** Products

Figure 4.18: Species concentration profiles of **(a)** reactant (iso-octane (IC_8H_{18}), n-heptane (NC_7H_{16}), toluene ($C_6H_5CH_3$), and ethanol (C_2H_5OH)), **(b)** intermediate acetaldehyde (CH_3CHO)), and **(c)** product (carbon monoxide (CO), carbon dioxide (CO_2)) at 900 K, 10 bar, and $\phi = 0.058$ from the University of Melbourne PFR [81]. Mechanism M2 [169] (solid lines) predictions are presented.

The reaction rate of the model is faster than the experimental data and this may be due to the assumptions made by the model. The peak acetaldehyde concentration was similar to EPRF and the mechanism was able to predict this trend, albeit lower than the measured values.

The LBV of the OH and OHT mixtures without and with ethanol is presented in Figure 4.19. All mixtures are equal-volume (letters representing composition) and the experimental data is from Hinton *et al.* [86] using the spherical constant volume combustion vessel. Both mechanisms were assessed against this data.

At the lower pressure conditions, both mechanisms over-predict the LBVs, however, at 4 bar, they display a close match to the experimental data. The pressure dependency of ethanol is displayed as it slows down the LBV of the OHE and THEO mixtures to be similar to the OH and OHT mixtures at the higher pressure condition. The mechanisms are able to predict this better for the OH and OHE mixtures than the OHT and THEO mixtures. This stems from the difficulty in accurately simulating the behaviour of toluene. Therefore, the impact on the LBV due to ethanol addition amongst other toluene-specific

binary and ternary compositions was further studied and published as a conference proceedings paper [187].

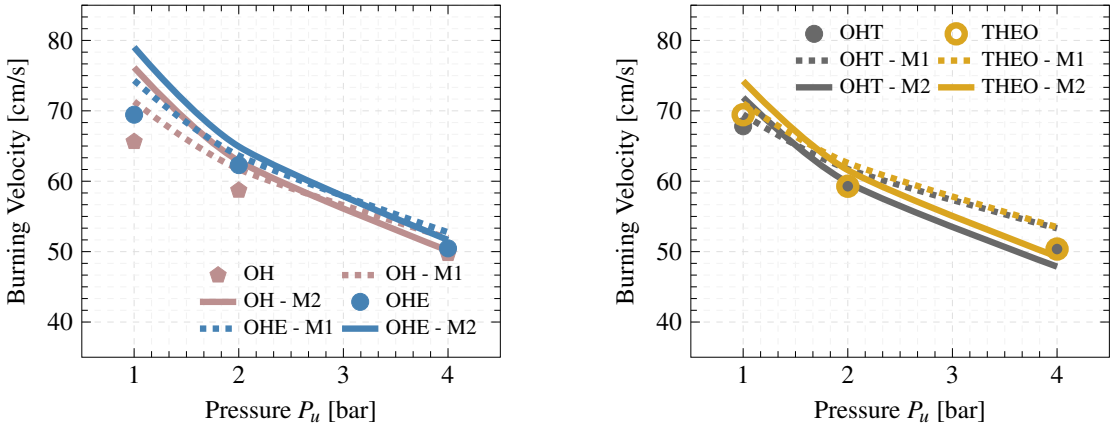

(a) OH and OHE blends at 450 K **(b)** OHT and THEO blends at 450 K

Figure 4.19: LBV data comparing **(a)** equal volume OH and OHE mixtures and **(b)** equal volume OHT and THEO mixtures from University of Oxford spherical constant volume combustion vessel [86]. Conditions are 450 K at pressures of 1, 2, and 4 bar under stoichiometry. Mechanisms M1 [167] (dashed lines) and M2 [169] (solid lines) are presented.

Figure 4.20 shows the sensitivity analysis using both mechanisms to highlight the top 11 reactions for the OHT and THEO mixtures at 1 and 4 bar and 450 K.

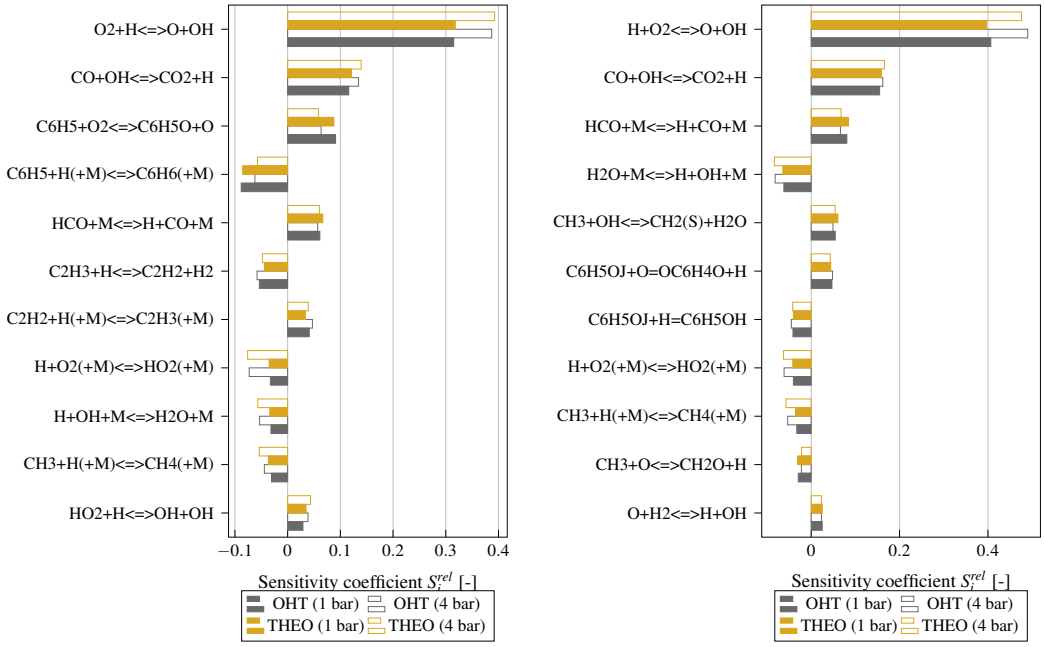

(a) Mechanism M1 **(b)** Mechanism M2

Figure 4.20: LBV sensitivity analysis of the equal volume OHT and THEO mixtures at 450 K and pressures of 1 and 2 bar and 450 K. Top 11 (absolute) sensitivity coefficients S_l of **(a)** Mechanism M1 [167] and **(b)** M2 [169] are presented.

The difference in sensitivity coefficients for the THEO mixture between 1 and 4 bar demonstrates the pressure dependency of ethanol more effectively in M1 than in M2. Both M1 and M2 mechanisms illustrate the influence of fuel-specific reactions. However, M2 presents a more comprehensive set of detailed elementary reactions compared to M1, which could be advantageous in identifying the range of reaction pathways potentially leading to aldehyde formation.

4.6.3 Single-cylinder engine model

A single-cylinder engine model, as described in Section 4.5.4 is validated against the experimental data measured in the laboratory test cell. Firstly, the motoring traces, representing the engine behaviour when it was driven by the dynamometer without fuelling, were used to validate the model. In this case, there is no influence of combustion. Through using these traces, the engine characteristics, including pumping losses, compression, and the efficiency of the intake and exhaust systems, can be evaluated. Subsequently, they can be used to amend the model to match the experimental setup. The results comparing the simulated and experimental cylinder pressure profiles for a motored case are shown in Figure 4.21. The experimental data is an average of 300 consecutive cycles.

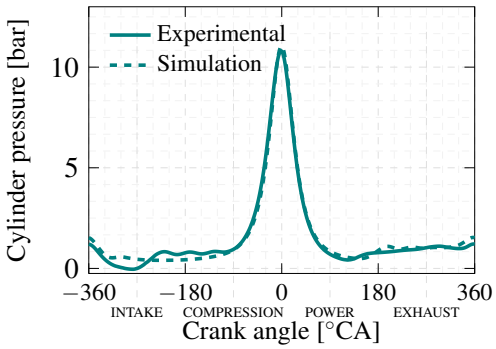

Figure 4.21: Motoring cylinder pressure trace from this work in the single-cylinder engine test cell. Conditions of 1100 rpm, ambient intake pressure, and temperature, and throttle opening at 10°. Mechanism M2 [169] (dashed lines) simulation on GT-Power is presented.

In addition to validating the motored test case, for each of the fuels, the model's cylinder pressure and apparent heat release rate (AHRR) was evaluated against the experimental data. This accounts for the influence of combustion. Figure 4.22 presents an example with the average cylinder pressure trace from one of the repeats for pure ethanol.

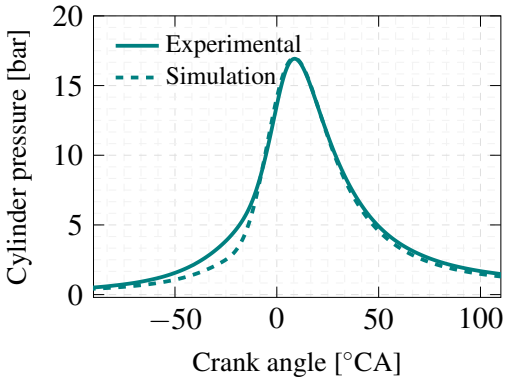

(a) Cylinder pressure of ethanol

Figure 4.22: Ethanol combustion cylinder pressure trace averaged over 300 cycles from this work in the single-cylinder engine test cell. Conditions of 1100 rpm, load of 2 bar nIMEP, ambient intake pressure, and temperature, and throttle opening at 2°. Mechanism M2 [169] (dashed lines) simulation on GT-Power is presented.

Despite these efforts, the engine model predicted significantly lower quantities of both formaldehyde and acetaldehyde compared to the experimental analyses. It underestimates the quantity of aldehydes and fails to replicate the observed emissions trends for these fuels under the same operating conditions. The model suggests that any formaldehyde or acetaldehyde generated is quickly consumed within the power stroke, potentially due to in-cylinder temperatures exceeding the oxidation temperatures of intermediate aldehydes. This rapid consumption might be an oversimplification, as it may not fully capture real-world complexities, such as combustion chamber crevices, which can contribute to engine-out aldehyde emissions. These crevices would be larger in an optical-access engine than a conventional thermal engine.

4.7 Summary

Fundamental combustion modelling can play a vital role in identifying the key reaction pathways responsible for the formation and consumption of aldehydes during the oxidation of gasoline surrogate fuels, both with and without ethanol.

The reactor models require the selection of appropriate chemical kinetics mechanisms that not only align with experimental data but also facilitate the exploration of reaction behaviours over a wide range of operating conditions. To enable this, two mechanisms

have been selected for evaluation: the reduced mechanism M1 by Li *et al.* [167], and the skeletal mechanism M2 by Wu *et al.* [169]. These mechanisms will be applied across various model setups, including the PSR, PFR, LBV, and the single-cylinder engine models.

Firstly, it is important to validate both the mechanisms and the model configurations. Therefore, the species concentration profiles from the PFR and PSR models, laminar burning velocity data from literature, and single-cylinder engine data were utilised to validate two mechanisms in well-defined reactor models. Mechanism M2 showed good agreement with experimental results in the PSR and PFR models, likely due to its comprehensive set of elementary reactions that more accurately interpret species formation and consumption. While both mechanisms matched the laminar burning velocity at higher pressures and temperatures, mechanism M1 was more accurate under lower pressure conditions.

For the single-cylinder engine model, mechanism M2 was exclusively evaluated, given its detailed species and reactions, which are crucial for understanding aldehyde behaviour. The model's performance during motoring and combustion closely aligned with the experimental engine data. However, the engine model's predictions of engine-out aldehyde emissions were several orders of magnitude lower than expected, indicating a need for refinement to align with observed real-world data. Improved modelling of the heat losses and creating multiple zones in the combustion chamber can help identify regions where stable aldehydes would be formed. Therefore, for the rest of this study, no engine model results will be presented.

The novel fuel compositions introduced in this study are further investigated using the PFR and PSR models with mechanism M2. This approach aims to deepen the understanding of aldehyde formation and consumption. The findings from these investigations are presented in Chapter 7.

5

Results: Research fuels

Contents

5.1 Motivation

This chapter presents the findings on research fuels described in Section 3.2, focusing on how fuel compositions affect aldehyde formation. The selected components, representing common elements of a gasoline surrogate, include ethanol, iso-octane, toluene, and n-heptane. Experiments were conducted using these fuels in their pure forms, as well as in binary and ternary mixtures. These compositions are generally unsuitable for engine use, as their physical and combustion characteristics fall outside the standard specifications of

conventional gasoline. The rationale behind each tested fuel composition is detailed in Chapter 3 Section 3.2.1.

Due to their deviation from standard gasoline specifications, these fuels provide unique insights into the effects of combustion on aldehyde emissions. Tests were conducted at low engine speeds and loads to assess engine-out emissions of aldehydes, NMHC, and ethanol. Additionally, the impact of altering the fuel-air equivalence ratio (ϕ) and the effects of increased loads and speeds on aldehyde emissions were evaluated. Richer fuel-air mixtures ($\phi > 1$) lead to incomplete combustion due to insufficient oxygen, favouring the formation of partially oxidised species like aldehydes. Higher temperatures associated with richer mixtures could also promote aldehyde formation through thermal decomposition of fuel molecules. However, the additional oxygen content in ethanol can influence this behaviour. Therefore, this chapter also examines the effects of increasing ethanol blending with conventional gasoline surrogate components in binary and ternary mixtures.

5.2 Pure fuels

Ethanol, toluene, and iso-octane were first considered separately. N-heptane was excluded from this analysis because of its low RON and MON. The low octane rating implies a reduced resistance to knocking, a problem characterised by premature detonation of the air-fuel mixture which could lead to engine damage. Figure 5.1 shows the engine-out formaldehyde and acetaldehyde emissions for the pure fuels tested. Ethanol exhibited substantially greater formaldehyde and acetaldehyde emissions than both toluene and iso-octane. Ethanol produced an average increase in engine-out aldehyde emissions that was 14-fold and 5-fold higher than toluene and iso-octane, respectively. Specifically, this difference was driven by the significantly higher acetaldehyde emissions by ethanol, which were observed to be 32-fold and 12-fold greater than those from toluene and iso-octane, respectively. While the relationship between ethanol combustion and engine-out aldehyde emissions has been previously explored in literature, this research presents

the first comparative analysis of the engine-out emissions impact of pure iso-octane and toluene under the same operating conditions.

In addition to examining the relative quantities of aldehyde emissions amongst the fuels tested, the formaldehyde-to-acetaldehyde (FA:AA) ratio is an important indicator of the fuel decomposition pathways. Different fuels and operating conditions can result in varying ratios of these aldehydes, offering insights into the impacts of each of the fuel components on the aldehyde emissions. Figure 5.1 shows the FA:AA for ethanol to be approximately 0.76, in contrast to a ratio of around 3.00 for both toluene and iso-octane. The higher acetaldehyde formation in ethanol can be attributed to the greater probability of the α-hydroxyethyl reaction pathway as discussed in Section 2.2.4.

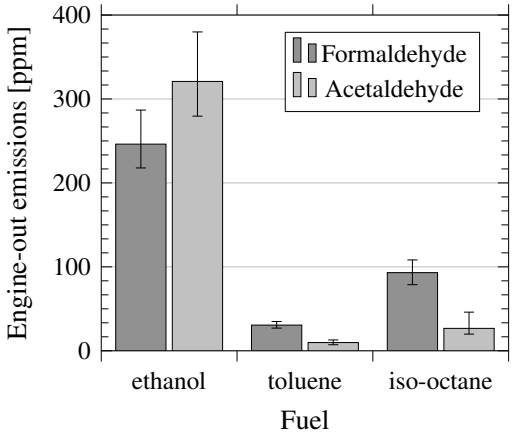

Figure 5.1: Engine-out formaldehyde and acetaldehyde emissions for ethanol, toluene, and iso-octane at 1.95 $\pm$0.15 bar nIMEP, 1100 rpm, and stoichiometric conditions. Ignition timing was fixed for all fuels at -46.3 °CA aTDCf. Throttle position and fuel injection quantity were varied to maintain similar load (nIMEP). Error bars represent minimum and maximum emissions over three repeats.

This study on pure fuels demonstrates that engine-out aldehyde emissions are generated even from non-oxygenated fuel components under similar operating conditions using the same experimental setup. Specifically, the preferential formation of formaldehyde over acetaldehyde from iso-octane combustion can be directly linked to the reaction pathways detailed in Section 2.2.1. This work presents them in the context of engine-out emissions attributed to iso-octane.

Regarding toluene, this study finds that its combustion within an engine directly results in aldehyde emissions, though in relatively small quantities (10 to 30 ppm). The observed

trend of higher formaldehyde emissions is consistent with the pathways described in Section 2.2.3. However, these pathways were identified through fundamental processes, and this study extends these findings to an engine context, where various factors may influence the formation of aldehydes. To investigate this behaviour further, the pure fuels were simulated in both PFR and PSR models, as discussed in Section 7.2.

Building on the literature in Section 2.4.2, where Zervas *et al.* [65] reported the engine-out concentration of acetaldehyde to increase in rich conditions and Golke *et al.* [92] found the acetaldehyde emissions to increase in lean conditions when ethanol is blended in a fuel, this study further investigates this phenomenon. Firstly, just the pure fuels were considered. The engine-out formaldehyde and acetaldehyde emissions for the different pure fuels are compared across the equivalence ratio range, as illustrated in Figures 5.2 (a) and (b), respectively.

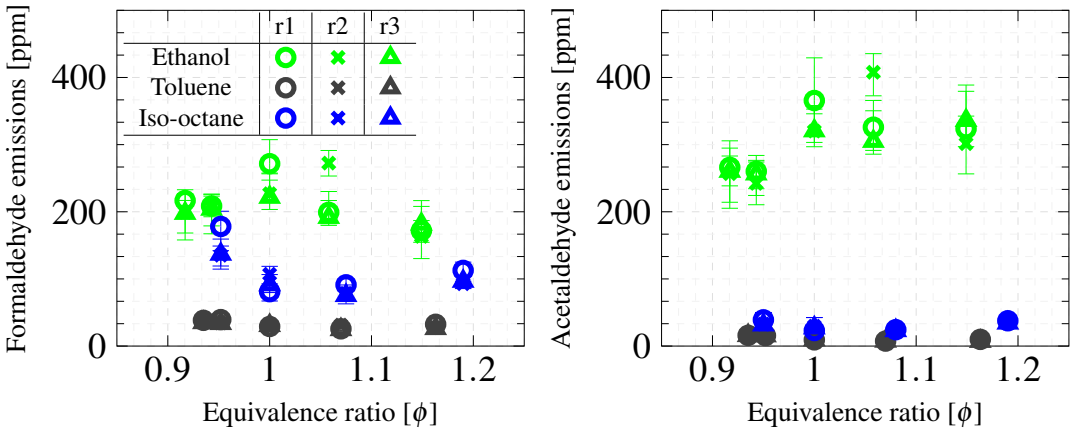

(a) Formaldehyde engine-out emissions **(b)** Acetaldehyde engine-out emissions

Figure 5.2: Engine-out **(a)** formaldehyde emissions and **(b)** acetaldehyde emissions for ethanol, toluene, and iso-octane fuels across fuel-air equivalence ratio (ϕ) range at 1.95 $\pm$0.15 bar nIMEP and 1100 rpm. Ignition timing was fixed for all fuels at -46.3 °CA aTDCf across the ϕ range. Throttle position and fuel injection quantity were varied to maintain similar load (nIMEP). Error bars represent minimum and maximum emissions for each repeat.

At each of the fuel-air equivalence ratios (ϕ) tested, ethanol produced greater engine-out aldehyde emissions than iso-octane and toluene. For ethanol, the formaldehyde and acetaldehyde engine-out emissions peak at stoichiometric ($\phi = 1$) and decrease at lean ($\phi < 1$) and rich ($\phi > 1$) conditions, contrary to the findings of Zervas *et al.* [65],

though they did not test pure ethanol. This could be due to additional presence of oxygen in ethanol, relative to other fuels tested, which could contribute to the oxidation and consumption of intermediate aldehydes under rich conditions. Furthermore, under lean operating conditions, a general decrease in aldehyde emissions would be expected as there is surplus oxygen to consume the intermediate aldehydes. Additionally, the ignition timing was fixed for all the tests at -46.3 °CA aTDCf. This may be favourable for ethanol as it has a faster flame propagation speed, as highlighted in Section 4.6.1.

At rich conditions, an increase in aldehyde emissions was observed for both iso-octane and toluene. This rise in emissions could be due to the increased presence of unburned fuels. During lean operating conditions, there was a relative increase in engine-out aldehyde emissions for these fuels when compared to stoichiometric conditions. This could be due to the unfavourable combustion conditions for iso-octane and toluene. For these fuels, the ignition timing was also fixed at -46.3 °CA aTDCf. However, iso-octane and toluene have slower flame speeds than ethanol, as highlighted in Section 4.6.1. Therefore, the ignition timing may have been too late for these fuels with slower flame speeds, thus increasing the amount of unburned intermediates.

The increase in aldehyde emissions at lean conditions compared to stoichiometric was greater for iso-octane in comparison to toluene. This could be because toluene burns at a slightly higher temperature than iso-octane, due to its aromatic structure which has a higher energy content per unit mass compared to the aliphatic structure of iso-octane, therefore leading to higher in-cylinder combustion temperatures which can consume the aldehydes. To determine whether this behaviour was specific to aldehydes or also affected other hydrocarbon emissions, the NMHC emissions were examined across the equivalence ratio range for all three pure fuels. The findings of this investigation are presented in Figure 5.3.

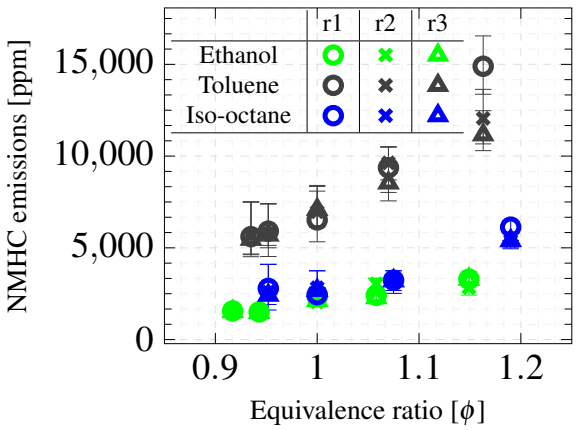

Figure 5.3: Engine-out NMHC emissions presented for ethanol, toluene, and iso-octane fuels across fuel-air equivalence ratio (ϕ) range at 1.95 $\pm$0.15 bar nIMEP and 1100 rpm. Ignition timing was fixed for all fuels at -46.3 °CA aTDCf across the ϕ range. Throttle position and fuel injection quantity were varied to maintain similar load (nIMEP). Error bars represent minimum and maximum emissions for each repeat.

For all the pure fuels tested, a trend opposite to the aldehydes was observed for NMHC emissions. Therefore, the behaviour seen for the aldehydes may not be directly attributable to the increased temperature conditions with toluene. To understand the temperature effects of toluene, the pure fuels were studied in the PSR model across a temperature range, as discussed in Section 7.2.

Ethanol emitted the lowest concentration of NMHC, whereas toluene emitted the highest among the fuels tested across the range of equivalence ratios. As the fuel-air mixture became leaner, a decreasing trend in NMHC emissions was identified. Conversely, between stoichiometric and lean conditions, there was an increase in aldehyde emissions. This divergence in trends suggests that the formation of aldehydes in these cases could be attributed to their stability as intermediates, rather than arising from partial or incomplete combustion.

The pure fuels were not tested under higher speed and load conditions due to an issue with the throttle setup, which limited the range of operating conditions.

The insights gained from these experiments with pure fuels in the single-cylinder engine contributed to a study examining the relationship between aromatic and oxygenate content on aldehyde emissions. The key findings were published in a conference paper and

presented at the 2023 Japan Society of Automotive Engineers (JSAE) International Meeting [188].

5.3 Binary fuels

Binary combinations of ethanol with each of the gasoline surrogate components were individually tested. The effect of increasing the concentration of ethanol content was studied. This was the first set of dedicated engine-out emissions experiments for binary compositions of ethanol with n-heptane and with toluene. Whereas, ethanol and iso-octane blends have been previously studied as iso-octane is considered a simple gasoline surrogate. Nevertheless, they were never specifically studied in a single-cylinder engine with a focus on engine-out aldehyde emissions. All binary mixtures were tested at similar operating conditions to the pure fuels, with a load of 1.95 $\pm$0.15 bar nIMEP, engine speed of 1100 rpm, and range of fuel-air equivalence ratios (ϕ).

5.3.1 Ethanol and iso-octane

The first set of binary results focuses on iso-octane and ethanol (OE) blends. The study examines the impacts of varying proportions of ethanol in iso-octane, comparing these to the emissions of the pure components, as shown in Figure 5.4. The engine-out formaldehyde and acetaldehyde emissions, measured under stoichiometric conditions at low speed and load, are presented.

Despite only 15 %v/v addition of iso-octane to ethanol, the OE85 mixture nearly halves the acetaldehyde emissions. On the other hand, between OE20 and OE85, the acetaldehyde emissions increase 4-fold, while formaldehyde emissions increase only by 1.5-fold. This rise in acetaldehyde emissions can be directly linked to the increased proportion of its precursor, ethanol. Regarding the formaldehyde emissions, the lower rate of increase might be due to the higher reactivity from the vinyl and allyl radicals from iso-octane's decomposition, introduced in Section 2.2.1, potentially leading to the consumption of formaldehyde. This difference in behaviour between formaldehyde and acetaldehyde emissions from the OE blends was further explored in the PFR and PSR models, as

discussed in Section 7.3.1. Additionally, the results demonstrate a shift in the FA:AA in favour of acetaldehyde as the ethanol content increased. For the OE mixtures, this ratio shifts from 2.40 for OE20 to 0.91 for OE85.

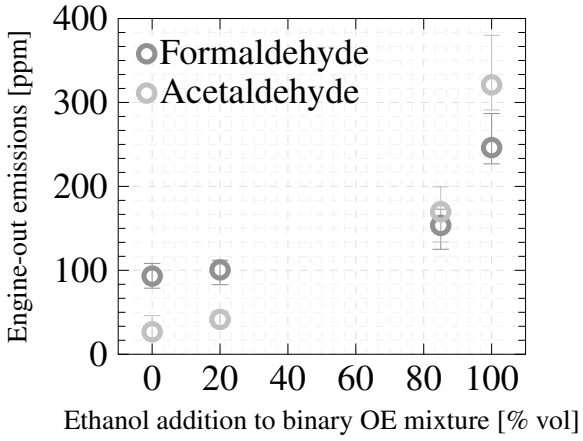

Figure 5.4: Engine-out formaldehyde and acetaldehyde emissions for OE fuel mixtures with increasing ethanol addition at 1.95 ±0.15 bar nIMEP, 1100 rpm, and stoichiometric conditions. Ignition timing was fixed for all fuels at -46.3 °CA aTDCf. Throttle position and fuel injection quantity were varied to maintain similar load (nIMEP). Error bars represent minimum and maximum emissions over three repeats.

To gain a deeper understanding of this behaviour and assess whether the observed differences between the fuels persist under varied operating conditions, an investigation was conducted on the effects of altering the equivalence ratio with the binary OE mixtures. The results of this study are presented in Figure 5.5.

For the OE85 fuel, formaldehyde emissions from the engine remained to be approximately 1.5 times higher than those for OE20, as seen at the stoichiometric conditions. This was consistent across various equivalence ratios. The formaldehyde emission levels for both fuels were around 140 ± 50 ppm. However, a significant difference was observed in acetaldehyde emissions between the two fuels. Similar to the stoichiometric conditions, an increase ranging between 3- to 4-fold between OE20 and OE85 was observed, with this discrepancy becoming more visible at the very rich conditions.

As the fuel-air mixture became leaner, towards stoichiometry, a reduction in acetaldehyde emissions was observed for both fuels. When the mixture became leaner (i.e., ϕ <1)

beyond stoichiometry, the acetaldehyde emissions for both fuels remained similar to those observed at stoichiometric conditions.

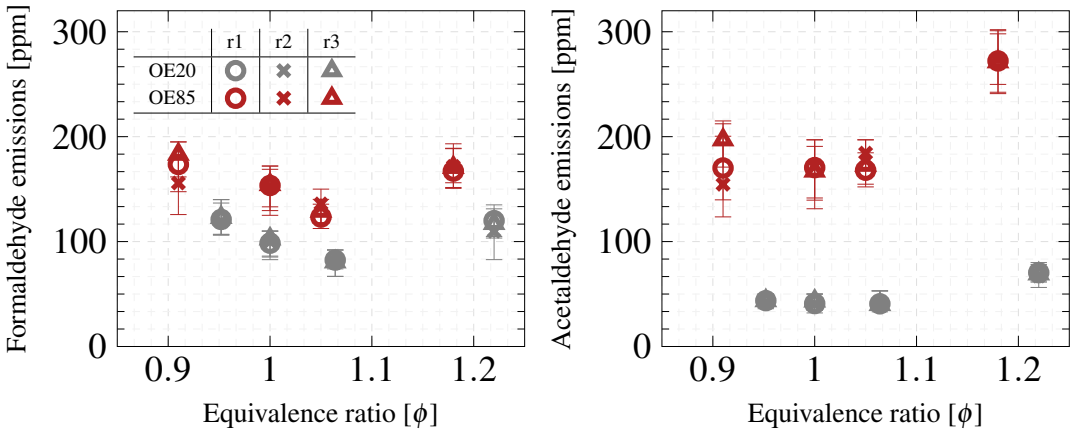

(a) Formaldehyde engine-out emissions **(b)** Acetaldehyde engine-out emissions

Figure 5.5: Engine-out **(a)** formaldehyde emissions and **(b)** acetaldehyde emissions for OE20 and OE85 fuels across fuel-air equivalence ratio (ϕ) range at 1.95 $\pm$0.15 bar nIMEP and 1100 rpm. Ignition timing was fixed for all fuels at -46.3 °CA aTDCf across the ϕ range. Throttle position and fuel injection quantity were varied to maintain similar load (nIMEP). Error bars represent minimum and maximum emissions for each repeat.

Conversely, under these lean conditions, an increase in formaldehyde emissions was observed compared to stoichiometric levels for both fuels. Additionally, formaldehyde emissions were higher at stoichiometry than under richer conditions (ϕ= 1.08) for both fuels. This behaviour could be attributed to engine instability during lean operation, as seen with pure iso-octane in Section 5.2, which also showed an increase in formaldehyde emissions at lean conditions. To further understand if this impact of the OE mixtures was also observed on other hydrocarbon emissions, the engine-out NMHC emissions, detailed in Figure 5.6, were also examined.

In the analysis of NMHC engine-out emissions, the OE85 blend consistently demonstrated lower emissions across all tested equivalence ratios. This could be attributed to its higher ethanol content, which as shown in Section 5.2 results in significantly reduced NMHC emissions. Across the three repeated measurements for each operating condition tested, the consistency in results for the OE85 blend exhibited less variability compared to that observed in the OE20 blend. Nevertheless, it should be noted that absolute maximum

and minimum deviations in the measurements are reported as the error margins in this study. The higher ethanol presence in OE85 may have accelerated the mixture's flame propagation speed, similar to the observations in Section 4.6.1, rendering it suitable for the combustion conditions in this engine.

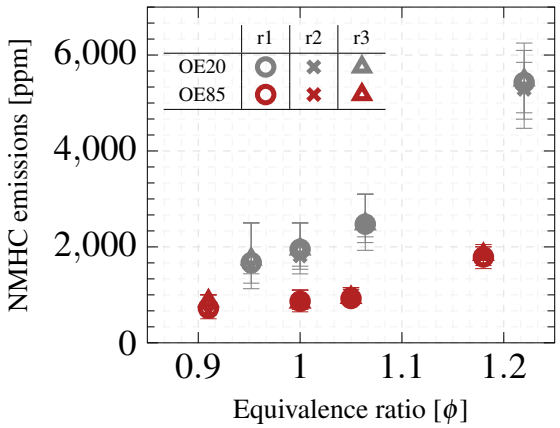

Figure 5.6: Engine-out NMHC emissions for OE20 and OE85 fuels across fuel-air equivalence ratio (ϕ) range at 1.95 $\pm$0.15 bar nIMEP and 1100 rpm. Ignition timing was fixed for all fuels at -46.3 °CA aTDCf across the ϕ range. Throttle position and fuel injection quantity were varied to maintain similar load (nIMEP). Error bars represent minimum and maximum emissions for each repeat.

Similar to previous observations with the pure fuels, richer conditions ($\phi > 1$) were associated with increased NMHC emissions. In contrast to the trends observed with formaldehyde and acetaldehyde, the additional oxygen in the ethanol, along with leaner mixture conditions, reduces the NMHC emissions. This observation emphasises the distinct behaviour of aldehyde emissions when compared to NMHC emissions, highlighting the importance of considering them separately when analysing the impacts of fuel composition on engine-out emissions.

The impacts of increasing load and speed on aldehyde emissions were investigated using binary OE blends, with the results shown in Figure 5.7. The higher load conditions were generally more stable, though for OE20 at 3.00 bar, closer examination at the raw exhaust data for one of the repeats shows that there may have been residual formaldehyde from a major misfire just prior to the measurement. As the error bars represent the maximum and minimum values recorded from the raw data, this behaviour can be considered anomalous. For OE20 blend, aldehyde emissions increased by a factor of 1.50, whereas emissions

from OE85 remained relatively constant. This links back to the literature (Section 2.4), identifying that the fuel composition has an effect on how the aldehydes are formed at higher loads. The FA:AA ratio stayed consistent at 2.50 for OE20 and 0.90 for OE85.

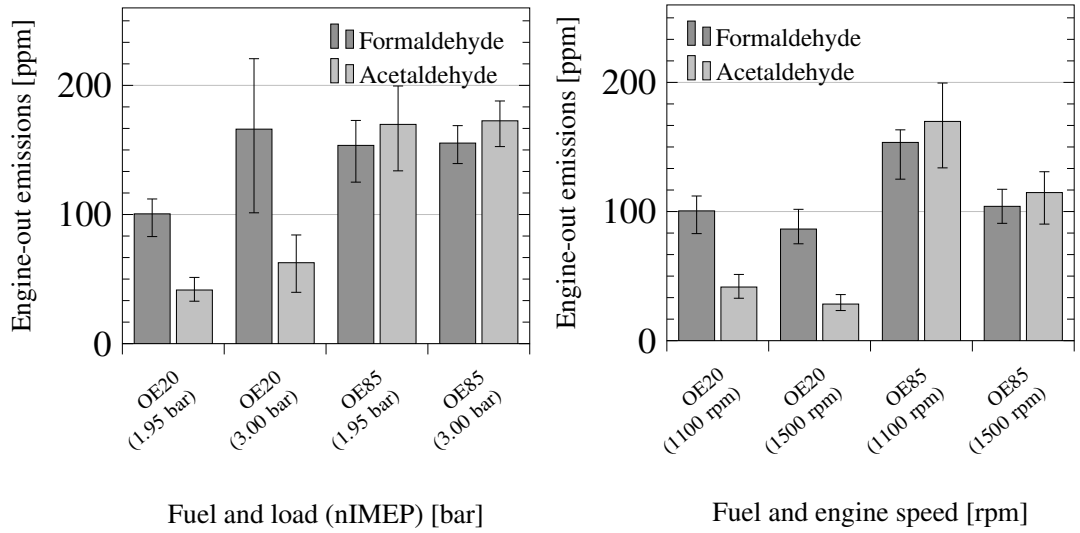

(a) Fuel and load variation **(b)** Fuel and speed variation

Figure 5.7: Engine-out formaldehyde and acetaldehyde emissions for OE20 and OE85 with: **(a)** load variation at 1.95 $\pm$0.15 bar and 3 $\pm$0.10 bar nIMEP under 1100 rpm and stoichiometric conditions; **(b)** engine speed variation at 1100 rpm and 1500 rpm under 1.95 $\pm$0.15 bar nIMEP and stoichiometric conditions. Ignition timing was fixed for all fuels at -46.3 °CA aTDCf across the speed and load range. Throttle position and fuel injection quantity were varied to maintain the expected loads (nIMEP). Error bars represent minimum and maximum emissions over three repeats.

Conversely to the observed trends with higher load, when the engine speed was increased to 1500 rpm, a reduction of approximately one third was observed for both fuels. Specifically, the reduction in acetaldehyde emissions was greater than that of formaldehyde for the OE20 fuel blend. This could be attributed to acetaldehyde's faster formation and consumption, as will be explored further in Section 7.3.1. Therefore, the higher speed created conditions favourable to acetaldehyde consumption. Nevertheless, this phenomenon seems to have a lesser impact on fuels with a high ethanol content.

5.3.2 Ethanol and toluene

The second set of binary mixtures tested on the single-cylinder engine comprised of three toluene and ethanol (TE) blends. Figure 5.8 shows the formaldehyde and acetaldehyde emissions for these mixtures in comparison to the pure constituents of ethanol and toluene.

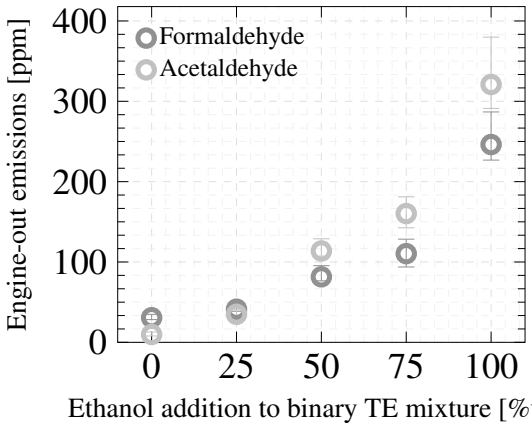

Figure 5.8: Engine-out formaldehyde and acetaldehyde emissions for increasing ethanol addition to binary TE mixtures at 1.95 ±0.15 bar nIMEP, 1100 rpm, and stoichiometric conditions. Ignition timing was fixed for all fuels at -46.3 °CA aTDCf. Throttle position and fuel injection quantity were varied to maintain similar load (nIMEP). Error bars represent minimum and maximum emissions over three repeats.

It is observed that adding 25 %v/v toluene significantly reduces aldehyde emissions, with a greater effect than iso-octane. 25 %v/v addition of toluene led to a 52 % reduction on average aldehyde emissions, whereas 15 %v/v of iso-octane led to a 43 % reduction, in their respective binary mixtures with ethanol. Specifically, while the addition of toluene and iso-octane reduced the acetaldehyde emissions by around 50 % each, for formaldehyde, the addition of toluene led to a 55 % reduction, whereas the addition of iso-octane only led to a 38 % reduction. However, it should be noted that a direct comparison is challenging due to differences in the proportions of toluene and iso-octane added to ethanol. Despite these tests using fuel compositions not typically used in engines, the findings offer valuable insights into the interactions between aromatic and oxygenate fuel components and their subsequent influence on aldehyde production.

For the TE25 blend, the FA:AA ratio was 1.20, although both emissions were similar in magnitude. However, as the proportion of ethanol in the mixture increased, this ratio shifted to approximately 0.70. This change indicates a higher concentration of acetaldehyde compared to formaldehyde, and the difference between these two aldehyde emissions became more distinct with the addition of ethanol.

The increased production of $HO_2^{\bullet}$ radicals from ethanol can accelerate the consumption of benzyl radicals derived from toluene, as reported by Fan *et al.* [189]. Therefore, while the

reactivity of ethanol was suppressed, the reactivity of toluene was enhanced, particularly during the phase of low-temperature heat release. Similar observations were made with laminar burning velocity studies as detailed in Section 4.6.1. This finding suggests that the chain termination pathways of ethanol, which lead to the formation of acetaldehyde, were inhibited due to toluene's increased reactivity. This led to a substantial decrease in engine-out aldehyde emissions. To further explore the chemical effects of toluene and ethanol interaction, these TE mixtures were simulated in the PFR and PSR models, as discussed in Section 7.3.2. Additionally, the presence of toluene in the mixture may not only mitigate the aldehyde emissions that are characteristic of pure ethanol but also raise the in-cylinder temperature or create hot spots in the cylinder, further reducing the formation of intermediate aldehydes.

Similar to the tests conducted with the pure fuels, the ethanol and toluene mixtures were evaluated across the fuel-air equivalence ratio range at the same engine speed and load conditions as shown in Figure 5.9.

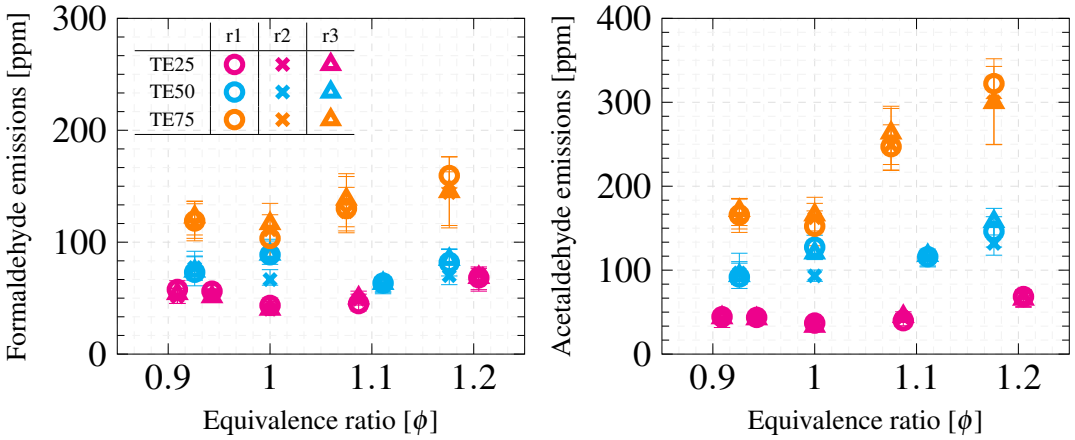

(a) Formaldehyde engine-out emissions **(b)** Acetaldehyde engine-out emissions

Figure 5.9: Engine-out **(a)** formaldehyde emissions and **(b)** acetaldehyde emissions for TE25, TE50, and TE75 fuels across fuel-air equivalence ratio (ϕ) range at 1.95 $\pm$0.15 bar nIMEP and 1100 rpm. Ignition timing was fixed for all fuels at -46.3 °CA aTDCf across the ϕ range. Throttle position and fuel injection quantity were varied to maintain similar load (nIMEP). Error bars represent minimum and maximum emissions for each repeat.

The TE75 mixture, with the highest ethanol content, exhibited two to three times greater engine-out aldehyde emissions than TE25, which had the lowest ethanol content. The increase in aldehyde emissions was greater between TE75 and TE50 compared to that

between TE50 and TE25. This finding reinforced ethanol's role as a primary precursor in aldehyde formation. However, the addition of toluene effectively reduced the oxidation of ethanol into aldehydes, particularly in mixtures with higher concentrations of toluene (TE50 and TE25).

In contrast to pure ethanol's behaviour at rich conditions, where the aldehyde emissions decreased, all tested binary TE mixtures showed an increase in aldehyde emissions under such conditions. These rich conditions were not optimal for toluene combustion, leading to less efficient combustion and a higher formation of aldehyde intermediates. Furthermore, the additional oxygen from the ethanol could be used to enhance toluene's reactivity and consume other radicals as opposed to the aldehydes. To assess this further, the NMHC emissions were also studied as shown in Figure 5.10.

For the TE mixtures, NMHC engine-out emissions were highest for TE25, which has the largest toluene concentration, and lowest for TE75, displaying the opposite trend to the aldehydes. However, this is in line with expectations based on the emissions from the pure fuels and the OE mixtures.

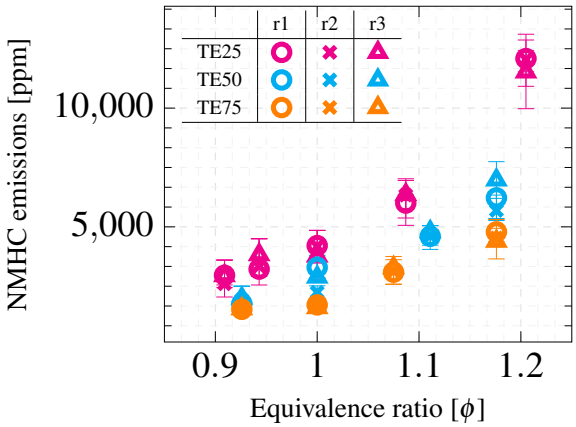

Figure 5.10: Engine-out NMHC emissions for TE25, TE50, and TE75 fuels across fuel-air equivalence ratio (ϕ) range at 1.95 $\pm$0.15 bar nIMEP and 1100 rpm. Ignition timing was fixed for all fuels at -46.3 °CA aTDCf across the ϕ range. Throttle position and fuel injection quantity were varied to maintain similar load (nIMEP). Error bars represent minimum and maximum emissions for each repeat.

Experiments of the binary TE mixtures at the higher speed and load conditions were not feasible due to constraints in the throttle setup, restricting the scope of operating conditions.

The interaction between toluene and ethanol in these mixtures yields valuable insights into their synergistic effects. Ethanol, with its fuel-bound oxygen, lowers the NMHC emissions from toluene, while toluene suppresses ethanol's aldehyde emissions by inhibiting its formation reactions. These studies conducted with binary toluene and ethanol mixtures in the single-cylinder engine provided a strong foundation for the work examining the link between aromatic and oxygenate components in influencing aldehyde emissions. The key outcomes of this research were also published in a previously mentioned conference paper and presented at the 2023 JSAE International Meeting [188].

5.3.3 Ethanol and n-heptane

Mixtures of ethanol and n-heptane are not typically run in an engine as n-heptane has a low octane rating thus poor anti-knock properties. This can lead to premature fuel ignition which can damage the engine. However, with the addition of ethanol and a robust test cell setup, two HE mixtures were tested. The engine-out formaldehyde and acetaldehyde emissions for HE65 and HE85, with addition of 65 %v/v and 85 %v/v of ethanol to n-heptane, respectively, in comparison to pure ethanol is shown in Figure 5.11. These results were obtained at stoichiometry with the low speed and load conditions.

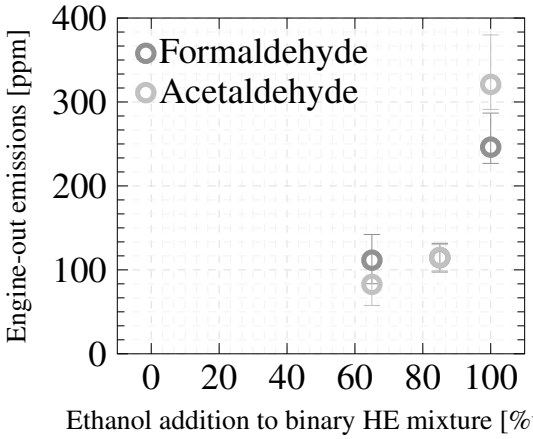

Figure 5.11: Engine-out formaldehyde and acetaldehyde emissions for increasing ethanol addition to binary HE mixtures at 1.95 ±0.15 bar nIMEP, 1100 rpm, and stoichiometric conditions. Ignition timing was fixed for all fuels at -46.3 °CA aTDCf. Throttle position and fuel injection quantity were varied to maintain similar load (nIMEP). Error bars represent minimum and maximum emissions over three repeats.

When 35 %v/v of n-heptane was added to ethanol, there was a significant decrease in emissions: formaldehyde reduced by 50 % and acetaldehyde by 75 %, compared to pure

ethanol. For the HE85 mixture, while the formaldehyde emissions remained similar to those in HE65, the acetaldehyde emissions increased. This re-iterates ethanol's role in increasing stable acetaldehyde formation.

Nevertheless, in comparison to the binary blends of iso-octane and toluene with ethanol, n-heptane demonstrates a greater suppressive effect on aldehyde emissions, particularly acetaldehyde. For example, considering HE85 and OE85 mixtures with similar ethanol content, the formaldehyde and acetaldehyde emissions were a quarter and a third lower, respectively, with HE85 compared to OE85. This could be attributed to the two-stage reactivity of n-heptane, shown in the validation (Section 4.6.1), and elaborated further in Section 7.3.3. At the low temperature region, where the aldehydes are typically formed, n-heptane's first stage increased reactivity might consume radicals that would otherwise convert into aldehydes.

In addition to stoichiometric conditions, the two HE binary mixtures were also tested across the equivalence ratio range. The results at 1100 rpm and 1.95 ±0.15 bar nIMEP load is shown in Figure 5.12.

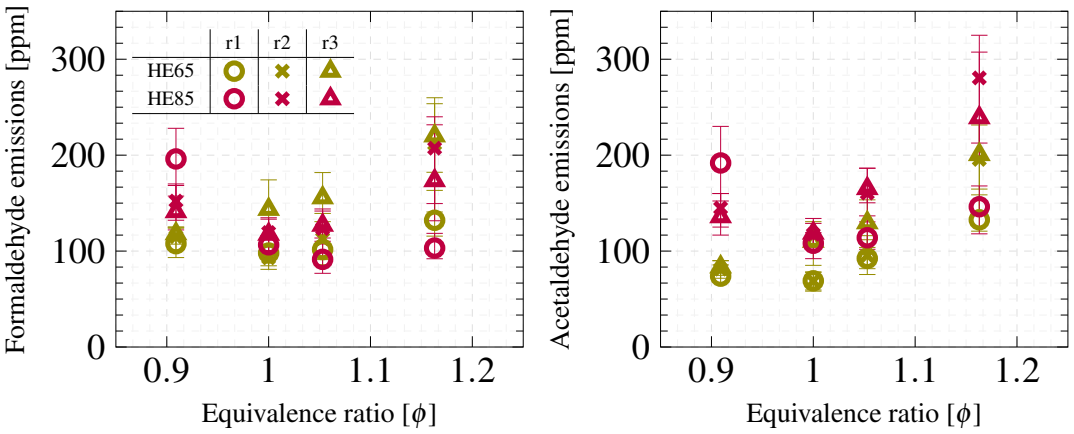

(a) Formaldehyde engine-out emissions **(b)** Acetaldehyde engine-out emissions

Figure 5.12: Engine-out **(a)** formaldehyde emissions and **(b)** acetaldehyde emissions for HE65 and HE85 fuels across fuel-air equivalence ratio (ϕ) range at 1.95 ±0.15 bar nIMEP and 1100 rpm. Ignition timing was fixed for all fuels at -46.3 °CA aTDCf across the ϕ range. Throttle position and fuel injection quantity were varied to maintain similar load (nIMEP). Error bars represent minimum and maximum emissions for each repeat.

Figure 5.12 (a) demonstrates that both fuels show similar formaldehyde emissions, ranging

approximately from 100 to 200 ppm. The acetaldehyde emissions were in a similar range, albeit lower for conditions closer to stoichiometry and higher for the lean and very rich points. Relative to other binary blends, these fuels demonstrated greater variability in repeated measurements. This inconsistency might be attributed to the knock propensity of n-heptane, which could lead to frequent misfires and/or instances of incomplete combustion, as will be discussed later. Similar behaviour was observed for acetaldehyde emissions. Except in lean conditions, where HE85 showed higher acetaldehyde emissions than HE65, the emissions for other operating conditions were comparable for both fuels, although the data showed larger error margins in repeated tests. This error represents the maximum and minimum emissions values measured across each repeat. In general, a reduction in aldehyde emissions from rich to stoichiometric conditions was observed. But, as with the other fuels tested, there was an increase under lean conditions.

For both HE mixtures, there was poor repeatability in the runs for formaldehyde and acetaldehyde emissions. Specifically, at the very rich condition (ϕ = 1.15), one repeat for HE65 showed distinctly lower emissions, likely due to a reduced exhaust temperature of around 240 °C, compared to the typical range of 280 °C to 320 °C. This discrepancy may be attributed to this being the first run during which the engine was not fully warmed up, resulting in a lower temperature, despite matching load and cylinder pressure traces. In the case of HE85 at this operating condition, achieving a stable load (which varied between 1.80 and 2.05 bar) was challenging, leading to variations in emissions. For the lean condition, one repeat with HE85 experienced two consecutive misfires and low exhaust temperatures, causing higher aldehyde emissions. Conversely, with HE65, the instances of low exhaust temperature resulted in lower aldehyde emissions.

To further explore the effects of combustion instability as a consequence of the fuel combination, the engine-out NMHC emissions were examined at same operating conditions as shown in Figure 5.13.

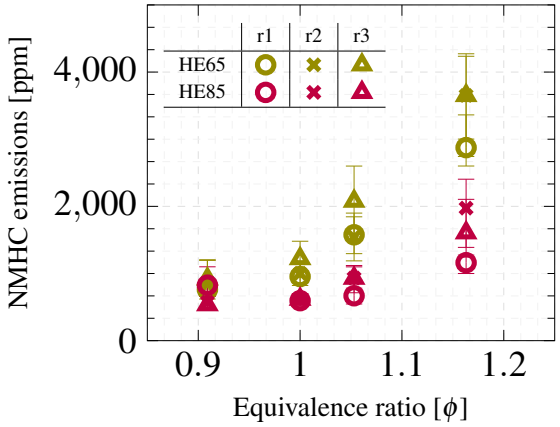

Figure 5.13: Engine-out NMHC emissions for HE65 and HE85 fuels across fuel-air equivalence ratio (ϕ) range at 1.95 $\pm$0.15 bar nIMEP and 1100 rpm. Ignition timing was fixed for all fuels at -46.3 °CA aTDCf across the ϕ range. Throttle position and fuel injection quantity were varied to maintain similar load (nIMEP). Error bars represent minimum and maximum emissions for each repeat.

Figure 5.13 shows that, similar to the aldehyde emissions, the NMHC emissions also exhibited greater variance between repeats and larger error margins. However, these errors are absolute values representing the maximum and minimum recorded emissions. The richer conditions demonstrated increased instability, similar to the behaviour seen with aldehydes. This instability could be attributed to the presence of higher amounts of n-heptane in the combustion chamber under less-than-ideal quantities and operating conditions.

The NMHC engine-out emissions for the HE blends were lower compared to the other two binary mixtures tested. The highest NMHC emissions recorded for the HE fuels were around 4000 ppm, which is a third lower than the OE20 fuel mixture and under half of what is observed with the TE25 fuel mixture under similar operating conditions. The HE65 fuel shows higher NMHC emissions than HE85 under rich conditions. However, at stoichiometry and in lean conditions, the NMHC emissions from both fuels are similar. From stoichiometry to lean conditions, NMHC emissions for HE85 remain relatively consistent, whereas a 20 % on average was noted for HE65. Overall, an expected decline in NMHC emissions is observed from rich to lean conditions across the equivalence ratio range.

The impact of increasing the load at the same speed was assessed and the results are shown in Figure 5.14. The increase in the aldehyde emissions was greater for HE65 than HE85. For HE65, the FA:AA ratio was maintained around 1.65 as the load increased, whereas for HE85, both aldehyde emissions were of similar quantities. This emphasises the impact that even 15 %v/v of n-heptane can have on the aldehyde formation in ethanol.

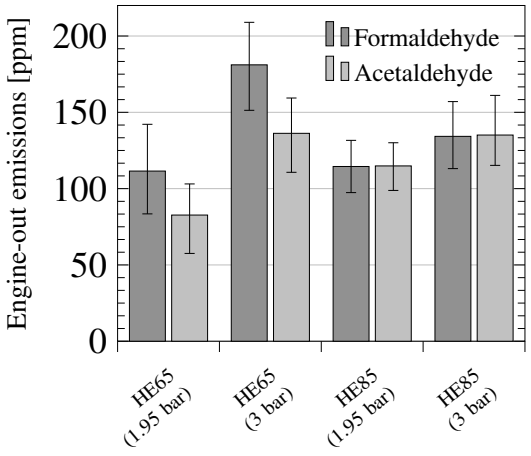

Figure 5.14: Engine-out formaldehyde and acetaldehyde emissions for HE65 and HE85 with load variation at 1.95 $\pm$0.15 bar and 3 $\pm$0.10 bar nIMEP under 1100 rpm and stoichiometric conditions. Ignition timing was fixed for all fuels at -46.3 °CA aTDCf for both loads. Throttle position and fuel injection quantity were varied to maintain the expected load (nIMEP). Error bars represent minimum and maximum emissions over three repeats.

This study finds that blending n-heptane with ethanol can reduce engine-out emissions of both aldehydes and NMHC across the range of fuel-air equivalence ratios tested. This finding is in contrast to the results observed with two other binary blends of ethanol with iso-octane and toluene, respectively. While adding iso-octane and toluene to ethanol leads to a reduction in aldehyde emissions, it also results in an increase in NMHC emissions. The distinct behaviour of n-heptane, particularly its two-stage combustion leading to low and high-temperature regimes, may account for the concurrent reduction in aldehydes and NMHC. As discussed in Section 4.6.1, n-heptane's high flame propagation speed could also contribute to the faster consumption of aldehydes before they become stable intermediates. To further understand the behaviour of these unique HE mixtures, they were explored in the PFR and PSR models in Section 7.3.3.

However, the susceptibility of n-heptane to auto-ignition in the combustion chamber prior to the spark event limits its addition to fuel blends, typically to around 20 %v/v. This constraint emphasises the importance of carefully evaluating both these properties, along with several other factors, in the development of an optimal fuel formulation.

5.4 Ternary fuels

The ternary research fuels were primarily designed to decouple the effect of ethanol and toluene. This was explored by developing two sets of ternary mixtures with and without ethanol. Each set had low and high aromatic content. The fuels without ethanol were composed of the other three common gasoline surrogate components of iso-octane, n-heptane, and toluene. The other set was composed of ethanol, toluene, and iso-octane.

Similar to the pure and binary fuels, the ternary mixtures were investigated at low engine speed (1100 rpm), low loads (≈1.95 bar and ≈3.00 bar nIMEP), and across the equivalence ratio range. For the ternary mixtures with ethanol, the unburned ethanol engine-out emissions were also examined. As ethanol concentration was constant in both fuels, this assessment is designed to showcase the influence of the other two components on the oxidation and decomposition of ethanol into aldehydes and other products. Additionally, it is important to examine the emissions of unburned ethanol, as it can rapidly transform into aldehydes in the exhaust system or in the atmosphere, depending on the conditions.

5.4.1 Iso-octane, toluene, and ethanol

The influence of low and high toluene content (referred to as LowT and HighT, respectively) with a mixture containing 25 %v/v ethanol (OTE25) was investigated in this section. Further details on their compositions are available in Section 3.2.

Figure 5.15 presents the engine-out emissions of formaldehyde, acetaldehyde, and unburned ethanol from these ternary mixtures. On average, the aldehyde emissions from the OTE25_LowT mixture were higher compared to OTE25_HighT. The reduced iso-octane content in OTE25_HighT could have resulted in the lower aldehyde emissions

for this mixture. This is because iso-octane has been shown to produce greater aldehyde emissions than toluene, as discussed in Section 5.2. Additionally, the higher concentration of toluene in OTE25_HighT appeared to suppress ethanol's reactivity, further contributing to the reduction in aldehyde emissions. To explore if the chemical kinetic mechanisms can pick up on these nuanced effects of toluene addition, the two OTE25 mixtures were further explored in the PFR and PSR models, where the chemical kinetics can be isolated, as discussed in Section 7.4.1.

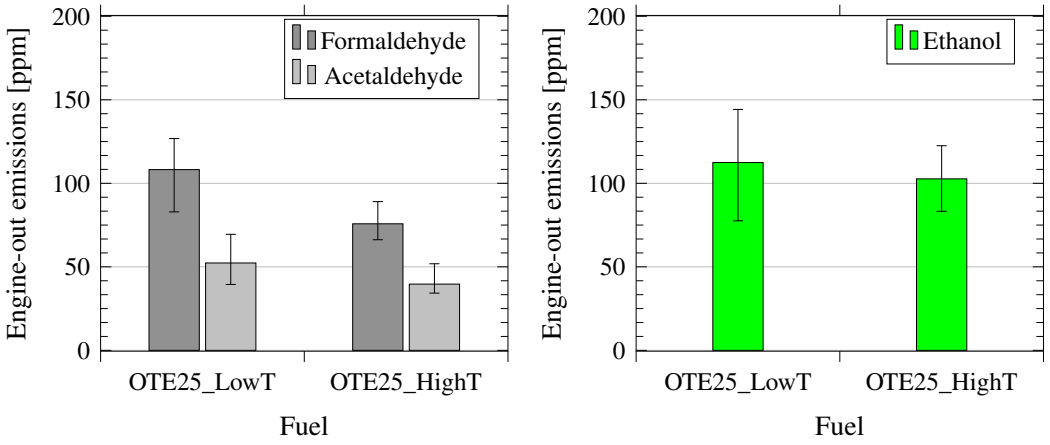

(a) Aldehyde engine-out emissions **(b)** Unburned ethanol engine-out emissions

Figure 5.15: Engine-out **(a)** formaldehyde, and acetaldehyde, and **(b)** unburned ethanol emissions for OTE25_LowT and OTE25_HighT at 1.95 ±0.15 bar nIMEP, 1100 rpm, and stoichiometric conditions. Ignition timing was fixed for all fuels at -46.3 °CA aTDCf. Throttle position and fuel injection quantity were varied to maintain similar load (nIMEP). Error bars represent minimum and maximum emissions over three repeats.

Figure 5.15 (a) shows both ternary mixtures, the FA:AA was approximately 2.00, lower than the ratio of 3.00 observed for pure iso-octane and toluene. This suggests that while ethanol's reactivity was suppressed, its presence still significantly influenced the concentration of acetaldehyde.

Figure 5.15 (b) shows the engine-out unburned ethanol emissions. For both ternary mixtures, the ethanol emissions were similar, at around 105 ppm. These experiments used a single-cylinder engine with optical access capabilities, therefore the unburned ethanol could partly originate from the combustion chamber crevices, which can be larger than production engines. Despite a change in the fuel composition, the levels of

unburned ethanol emissions remained constant for both fuels, indicating that under the tested conditions, these emissions were more influenced by the operating conditions than by the fuel composition.

However, under the same operating conditions, pure ethanol combustion led to an average of 1490 ppm of ethanol emissions, which represents a 14-fold increase in comparison to the ternary mixtures. This substantial difference could highlight the chemical kinetic impact of toluene in the fuel mixture, indicating that increased toluene presence may create localised high-temperature zones within the combustion chamber. These hot spots potentially aid in partially consuming ethanol, resultant aldehydes, and other intermediates from ethanol combustion. In addition to chemical effects outlined here, physical factors like the co-evaporative effect of toluene and ethanol within the combustion chamber also likely play a role in influencing the observed outcomes.

The ternary mixtures were evaluated across the fuel-air equivalence ratio (ϕ) range of 0.90 to 1.20 at the same low engine speed and load conditions. Figure 5.16 presents the engine-out formaldehyde and acetaldehyde emissions. The OTE25_LowT ternary mixture exhibited higher aldehyde emissions than the OTE25_HighT mixture. This is likely because of the displacement of iso-octane in the OTE25_LowT fuel, as previously discussed.

At richer conditions ($\phi > 1$), the difference in formaldehyde emissions between the fuels was greater, while variations in acetaldehyde emissions were less obvious. This difference in formaldehyde emissions might be due to the higher iso-octane content in the OTE25_LowT mixture, reinforcing the correlation between iso-octane and formaldehyde established earlier in this study. Furthermore, a decrease in engine-out emissions was noted when moving from rich to stoichiometric conditions, a trend consistent with other pure, binary, and ternary fuels tested in this study. This behaviour is expected, as moving away from rich conditions generally leads to less unburned fuel and, consequently, fewer intermediate aldehydes.

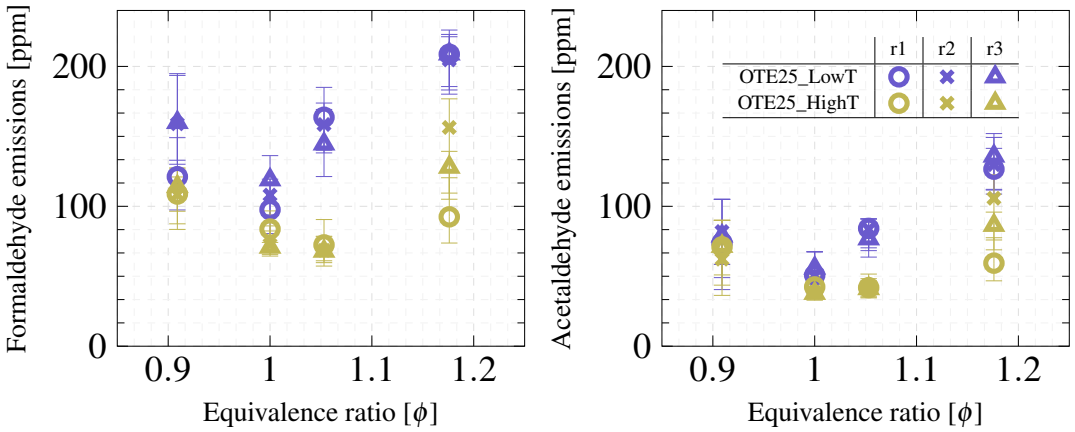

(a) Formaldehyde engine-out emissions **(b)** Acetaldehyde engine-out emissions

Figure 5.16: Engine-out **(a)** formaldehyde emissions and **(b)** acetaldehyde emissions for OTE25_LowT and OTE25_HighT fuels across fuel-air equivalence ratio (ϕ) range at 1.95 $\pm$0.15 bar nIMEP and 1100 rpm. Ignition timing was fixed for all fuels at -46.3 °CA aTDCf across the ϕ range. Throttle position and fuel injection quantity were varied to maintain similar load (nIMEP). Error bars represent minimum and maximum emissions for each repeat.

However, at lean conditions (beyond stoichiometry), engine-out emissions exceeded those at stoichiometric levels. This could be due to the slower flame propagation speeds of iso-octane and toluene, as highlighted in Section 4.6.1. To see if the chemical kinetics also played a role in this effect, the two mixtures were evaluated in the PFR and PSR models in Section 7.4.1. The significant proportion of these components in the ternary mixture, combined with the constant ignition timing applied in all tests, might have been suboptimal for these fuels, influencing the observed emissions. Furthermore, in lean conditions, advancing the ignition timing can enhance combustion efficiency and reduce emissions as this adjustment compensates for the slower burn rate of lean mixtures, ensuring complete combustion. This behaviour is similar to what was observed in tests with pure iso-octane and toluene.

To explore the extent of complete combustion, particularly at lean conditions, for the fuels tested, the other engine-out NMHC emissions were also examined as shown in Figure 5.17. Despite the higher toluene concentration in OTE25_HighT, its NMHC engine-out emissions at rich conditions were lower than those of OTE25_LowT. At stoichiometry, both mixtures showed similar levels of NMHC emissions. At leaner conditions, a shift in

trend was observed, with OTE25_HighT displaying approximately 20 % higher NMHC emissions, though these were within the error range of OTE25_LowT.

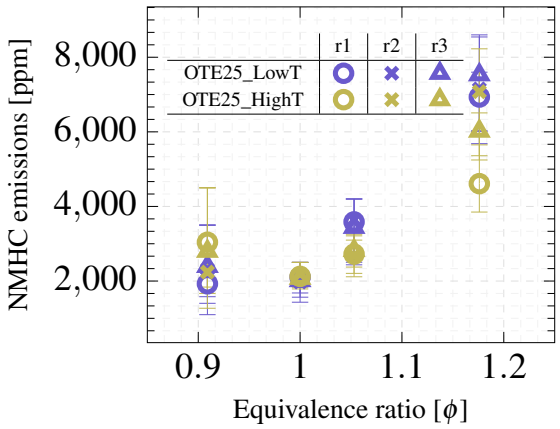

Figure 5.17: Engine-out NMHC emissions for OTE25_LowT and OTE25_HighT fuels across fuel-air equivalence ratio (ϕ) range at 1.95 $\pm$0.15 bar nIMEP and 1100 rpm. Ignition timing was fixed for all fuels at -46.3 °CA aTDCf across the ϕ range. Throttle position and fuel injection quantity were varied to maintain similar load (nIMEP). Error bars represent minimum and maximum emissions for each repeat.

Similar to the engine-out aldehyde emissions, Figure 5.17 shows that at the lean conditions, the NMHC emissions are equal to or greater than the stoichiometric conditions. Probably due to the combustion instability at the lean operating conditions, the error margins were greater but it should be noted these represent the maximum and minimum values recorded in each run.

The engine-out aldehyde emissions increased with mixtures that contained a lower concentration of toluene at low speed and load conditions. Whilst the difference between the mixtures was minimal at stoichiometric conditions, the differences disproportionately increased at rich operating conditions. To determine if this behaviour was consistent at higher load condition, the ternary mixtures were further tested at 3.00$\pm$0.1 bar nIMEP and 1100 rpm, as shown in Figure 5.18.

As the load increased, there was a corresponding rise in engine-out emissions, which can be attributed to the increased fuelling at higher loads. For both fuels, the injected quantity increased by approximately 33 %. However, Figure 5.18 shows that for OTE25_LowT, the emissions increased by approximately 60 %, whereas, for OTE25_HighT, the emissions

increased by nearly 84 % on average with the increase in load. Consistent with previous observations, the OTE25_LowT mixture produced higher engine-out aldehyde emissions than OTE25_HighT at the increased load condition. However, the rate at which both aldehyde and NMHC emissions increased was higher for OTE25_HighT compared to OTE25_LowT. The low engine speed operating conditions, which are not optimal for toluene combustion, could have contributed to this accelerated increase in the emissions for the mixture with higher toluene concentration.

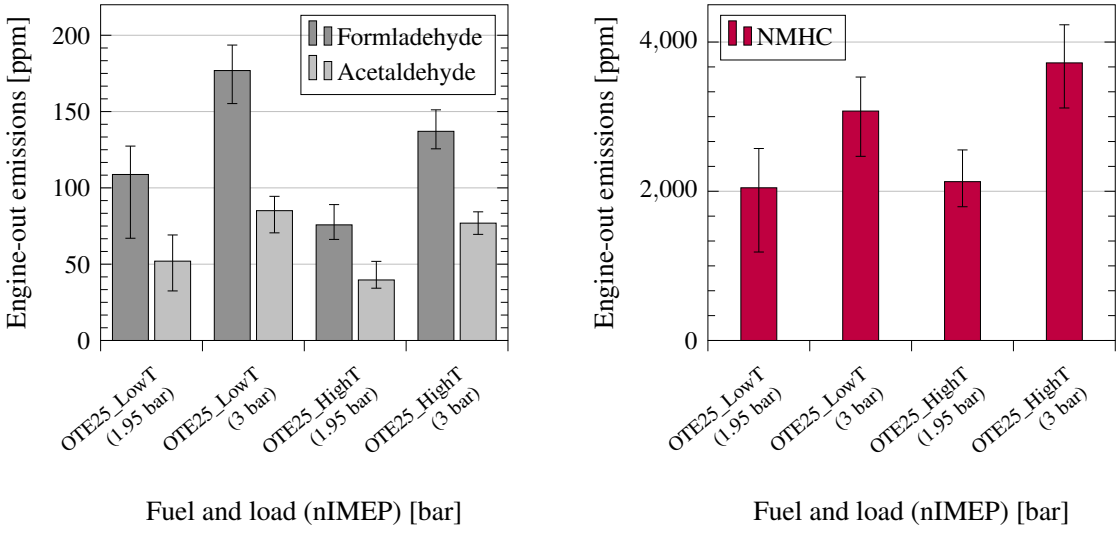

(a) Engine-out aldehyde emissions **(b)** Engine-out NMHC emissions

Figure 5.18: Engine-out **(a)** formaldehyde and acetaldehyde and **(b)** NMHC for OTE25_LowT and OTE25_HighT with load variation at 1.95 ±0.15 bar and 3 ±0.10 bar nIMEP under 1100 rpm and stoichiometric conditions. Ignition timing was fixed for all fuels at -46.3 °CA aTDCf across the two loads. Throttle position and fuel injection quantity were varied to maintain the expected loads (nIMEP). Error bars represent minimum and maximum emissions over three repeats.

For both operating loads and fuels, the FA:AA ratio emissions was approximately 2:1. Following the observations made from the binary TE mixtures, the increased presence of toluene in the latter mixture appears to suppress the formation of aldehyde emissions from ethanol.

Figure 5.18 (b) also shows that there was an observed difference in the engine-out NMHC emissions between the two ternary mixtures at the higher load condition of 3.00 ±0.1 bar, while the emissions were similar at the lower load of 1.95 ±0.15 bar. This divergence can be attributed to increased fuel injection coupled with low combustion pressures

and temperatures. These findings further affirm that these conditions were not ideal for the combustion characteristics of toluene and iso-octane, resulting in their incomplete combustion. Throughout this work, the ignition timing was fixed due to experimental constraints at the beginning of the study, however, these findings show that it would be better to adapt these timings to better match fuel composition. These observations can also explain the increased aldehyde emissions whose production is favoured by the low-temperature conditions.

This research on ternary OTE25 mixtures in the single-cylinder engine concluded the comprehensive study on the interaction between aromatic and oxygenate components, with an inclusion of iso-octane, in aldehyde emissions. The key findings were part of the conference paper presented at the 2023 JSAE International Meeting [188].

5.4.2 Iso-octane, n-heptane, and toluene

Whilst ethanol is a key precursor to engine-out aldehyde emissions, this set of fuels examine the impact of a ternary composition excluding ethanol. These ternary blends were composed of iso-octane, n-heptane, and toluene (OHT). Additionally, given that toluene has been identified as a suppressor of aldehyde emissions in ethanol-containing compositions in Sections 5.3.2 and 5.4.1, the influence of both low and high toluene concentrations in these ternary mixtures was investigated.

Figure 5.19 shows the engine-out formaldehyde and acetaldehyde emissions for OHT_LowT and OHT_HighT under stoichiometric conditions, and at low speed and load engine conditions. It is observed that both aldehyde emissions are reduced by one-third when comparing OHT_LowT to OHT_HighT. This highlights toluene's role in suppressing aldehyde emissions, irrespective of ethanol's presence. The capability of the chemical kinetic mechanism reactions to pick up on this behaviour for fuel mixtures without ethanol's presence was explored in Section 7.4.2. For both fuels, the FA:AA was around 4.10, which aligns with expectations given the lack of ethanol content in these ternary mixtures.

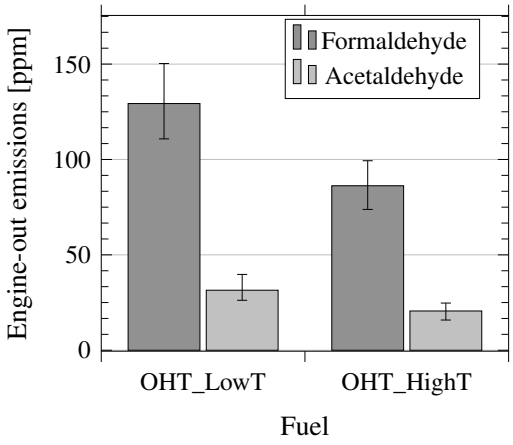

Figure 5.19: Engine-out formaldehyde and acetaldehyde emissions for OHT_LowT and OHT_HighT at 1.95 ±0.15 bar nIMEP, 1100 rpm, and stoichiometric conditions. Ignition timing was fixed for all fuels at -46.3 °CA aTDCf. Throttle position and fuel injection quantity were varied to maintain similar load (nIMEP). Error bars represent minimum and maximum emissions over three repeats.

The impact of toluene, characterised by its higher burning temperature and slower flame speed, can also be linked to increased combustion pressure, temperature, and heat release, which leads to the consumption of intermediate aldehydes. To assess if this effect is consistent across various equivalence ratios, additional experiments were conducted, with the results presented in Figure 5.20.

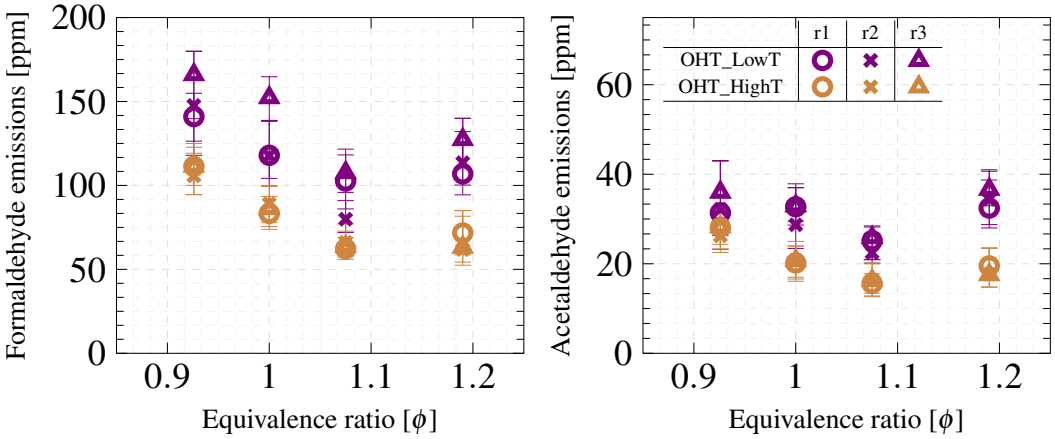

(a) Formaldehyde engine-out emissions **(b)** Acetaldehyde engine-out emissions

Figure 5.20: Engine-out **(a)** formaldehyde emissions and **(b)** acetaldehyde emissions for OHT_LowT and OHT_HighT fuels across fuel-air equivalence ratio (ϕ) range at 1.95 ±0.15 bar nIMEP and 1100 rpm. Ignition timing was fixed for all fuels at -46.3 °CA aTDCf across the ϕ range. Throttle position and fuel injection quantity were varied to maintain similar load (nIMEP). Error bars represent minimum and maximum emissions for each repeat.

The consistency in the repeatability of results for OHT_HighT is greater than that of OHT_LowT, as evidenced by the smaller error margins for OHT_HighT. These margins represent the range of maximum and minimum values recorded during the measurements. This improved consistency in OHT_HighT may be attributed to its higher octane sensitivity (OS), which is the difference between the RON and MON. A higher OS indicates that OHT_HighT exhibits enhanced knock resistance across a range of engine operating conditions, including at low speed and load conditions.

Nevertheless, the OHT_LowT mixture shows higher aldehyde emissions across the equivalence ratios, especially under richer conditions and, to a lesser extent, at lean conditions. Generally, aldehyde emissions tend to increase as the mixture becomes leaner, except in very rich conditions. The presence of excess oxygen could react with the phenyl group, originating from the oxidation of toluene, to form phenolate (C_6H_5O), which may then decompose into aldehydes. This process is further detailed in Section 7.2.

To explore the effects of excess oxygen on other hydrocarbon emissions in the absence of ethanol in the fuel composition, the NMHC emissions were also analysed across the equivalence ratio range. The findings from this analysis are presented in Figure 5.21.

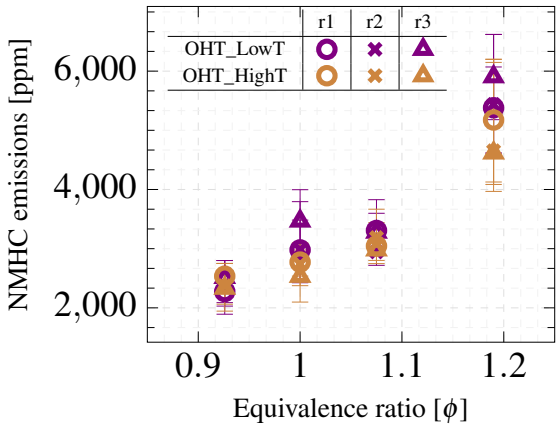

Figure 5.21: Engine-out NMHC emissions for OHT_LowT and OHT_HighT fuels across fuel-air equivalence ratio (ϕ) range at 1.95 $\pm$0.15 bar nIMEP and 1100 rpm. Ignition timing was fixed for all fuels at -46.3 °CA aTDCf across the ϕ range. Throttle position and fuel injection quantity were varied to maintain similar load (nIMEP). Error bars represent minimum and maximum emissions for each repeat.

Contrary to the trends observed for the aldehyde emissions, the NMHC levels consistently

declines as the mixture becomes leaner. This trend aligns with findings from other fuel studies. At the very rich condition (ϕ = 1.20), ternary mixtures containing ethanol (OTE25), discussed in Section 5.4.1, produced higher NMHC emissions compared to those without ethanol (OHT). This is not expected as ethanol produces low NMHC emissions, as observed in Section 5.2, and when mixed with other components, it has been shown to reduce the mixture's NMHC emissions.

Nevertheless, at the other rich and stoichiometric conditions, the OHT mixture produced greater quantities of NMHC emissions than OTE25, as anticipated. Under lean conditions, while the NMHC emissions decreased for OHT blends, they increased for OTE25 blends relative to stoichiometry, resulting in comparable engine-out NMHC emissions for both mixtures. Therefore, this finding suggests that at lean conditions, the lack of ethanol's presence leads to a consistent reduction of NMHC emissions. However, when the mixture contains ethanol, both the NMHC and aldehyde emissions increase. This could be due to the fuel-bound oxygen in ethanol which makes the overall fuel-O_2 ratio even leaner which may affect the combustion stability.

The two ternary mixtures were investigated at increased speed and load conditions too. The resulting formaldehyde and acetaldehyde emissions are presented in Figure 5.22.

At both load levels, the OHT mixture with a higher proportion of toluene resulted in lower aldehyde emissions. This is consistent with the findings from the binary TE mixtures, further reinforcing toluenes role in suppressing aldehyde emissions, independent of its interaction with ethanol. Additionally, it was observed that when the load increased from 2 to 3 bar nIMEP for both OHT ternary mixtures, the FA:AA ratio increased due to higher formaldehyde production, while acetaldehyde levels remained relatively unchanged.

An increase in speed from 1100 rpm to 1500 rpm led to a substantial 60 % reduction in aldehyde emissions for OHT_LowT, whereas OHT_HighT showed only a 25 % reduction under similar conditions. As discussed in Section 4.6.1, toluene is characterised by a slow flame propagation speed. Therefore, it is possible that an increase in speed, while maintaining constant load, does not provide sufficient time for a mixture with a higher concentration of toluene to efficiently consume the intermediate aldehydes. To investigate

this phenomenon, these ternary mixtures were analysed in a PFR model, as detailed in Section 7.4.2, examining the reaction progression along the reactor, which could be analogous to the residence time in a combustion chamber.

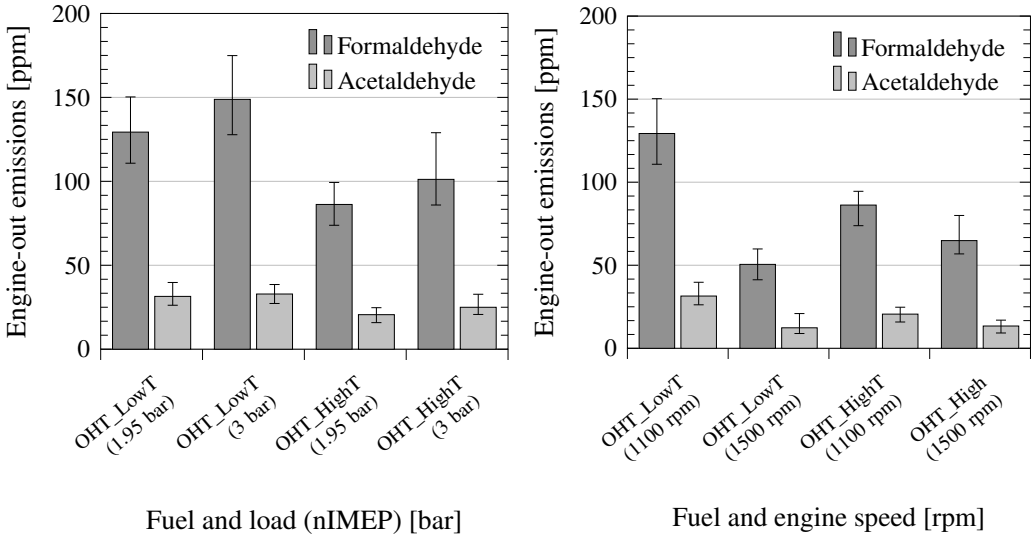

(a) Fuel and load variation

(b) Fuel and engine speed variation

Figure 5.22: Engine-out formaldehyde and acetaldehyde emissions for OHT_LowT and OHT_HighT with: **(a)** load variation at 1.95 ±0.15 bar and 3 ±0.10 bar nIMEP under 1100 rpm and stoichiometric conditions; **(b)** engine speed variation at 1100 rpm and 1500 rpm under 1.95 ±0.15 bar nIMEP and stoichiometric conditions. Ignition timing was fixed for all fuels at -46.3 °CA aTDCf across the speed and load range. Throttle position and fuel injection quantity were varied to maintain the expected loads (nIMEP). Error bars represent minimum and maximum emissions over three repeats.

5.5 Summary

Pure gasoline surrogate components, along with their novel binary and ternary mixtures, were evaluated in a single-cylinder engine under low speed and load conditions. For all the tested fuels, the ignition timing was fixed at -46.3 °CA aTDCf. This was also kept constant across the fuel-air equivalence ratio (ϕ) range. To maintain the same load (nIMEP) and account for fuel-specific behaviour when testing different fuels, the throttle position and fuel injection quantities were varied. Based on these conditions, the key findings include:

- *Pure fuels*: Ethanol's average engine-out aldehyde emissions were ten- and five-times higher than those from toluene and iso-octane, respectively. This indicates

pure toluene produces negligible (10 to 30 ppm) aldehyde emissions. Ethanol emitted lower aldehydes at lean and rich conditions compared to stoichiometric, while iso-octane and toluene showed the opposite trend. This could be due to ethanol's faster flame speed and fuel-bound oxygen facilitating more complete combustion. High NMHC emissions for iso-octane and toluene indicated they did not completely combust which could have led to intermediate aldehydes, whereas ethanol oxidation directly yielded aldehydes.

- *Iso-octane and ethanol*: Adding 15 %v/v iso-octane to ethanol (OE85) reduced average aldehyde emissions by about 43 % compared to pure ethanol. Formaldehyde emissions generally increased with leaner mixtures, except at very rich conditions. Acetaldehyde emissions displayed similar trends as pure iso-octane across the fuel-air ratio range and a larger disparity between the fuels. NMHC emissions decreased with leaner mixtures, indicating irregular formaldehyde behaviour. The FA:AA in OE mixtures varied from 2.44 for OE20 to 0.90 for OE85, highlighting iso-octane as an important contributor to formaldehyde emissions.

- *Toluene and ethanol*: Adding 25 %v/v toluene to ethanol (TE75) reduced average engine-out aldehyde emissions by half compared to pure ethanol. TE mixtures exhibited trends similar to toluene across different equivalence ratios. The FA:AA ranged from 1.20 for TE25 to 0.70 for TE75, indicating increased ethanol addition results in higher acetaldehyde production. This suggests toluene's significant suppressive effect on ethanol's aldehyde formation.

- *N-heptane and ethanol*: Adding 15 %v/v n-heptane to ethanol (HE85) reduced aldehyde emissions by 60 %, which was greater than the suppressive effects observed in OE and TE mixtures. Aldehyde and NMHC emissions across the fuel-air equivalence ratio showed no clear difference between the fuels, with larger error margins due to suboptimal combustion properties for engine operation. The FA:AA in HE mixtures ranged from 1.35 for HE65 to 1.00 for HE85, suggesting n-heptane's minimal impact on formaldehyde emissions.

- *OHT*: In OHT ternary mixtures, formaldehyde emissions were four times higher than acetaldehyde. Increasing the toluene content led to a one-third reduction in average aldehyde emissions, highlighting toluene's suppressive effect. Both OHT mixtures showed increased aldehyde emissions in leaner mixtures, except at very rich conditions, while NMHC emissions decreased with leaner mixtures. This indicates that excess oxygen may interact with intermediate fuel radicals to form aldehydes, especially as direct precursors like ethanol were absent.
- *OTE25*: In the OTE25 ternary mixtures, OTE25_HighT, with higher toluene content, had lower average engine-out aldehyde emissions than OTE25_LowT, despite equal ethanol content in both. This emphasises toluene's suppressive effect on aldehydes and iso-octane's contribution to formaldehyde emissions. The OTE25 mixtures, like iso-octane and toluene, showed increased aldehyde emissions in lean and rich conditions.
- *Speed and load*: With increased load, aldehyde emissions increased for all fuels, possibly due to higher fuel injection quantities at constant engine speeds. Conversely, higher engine speeds led to reduced aldehyde emissions across all fuels. Despite these changes in operating conditions, the FA:AA remained consistent.

6

Results: Surrogate fuels

Contents

6.1 Motivation

In addition to researching a range of specially formulated blends to understand how fuel component interactions affect aldehyde formation, it is also important to study gasoline surrogate fuels. These fuels were tested using the same single-cylinder engine with similar operating conditions to those used for the research fuels. The surrogates are of known composition and are designed to meet some physical and combustion properties, including RON, MON, and density, as defined by the European EN228 gasoline specification [145]. These factors enable the fuels to be replicated and tested in other facilities, including multi-cylinder engines. This chapter explores the impact of two types of surrogates: PRFs and TPRFs. To these, ethanol was added in increasing proportions and the resultant

impact on the aldehyde emissions was investigated. Detailed information of the fuel composition and their predicted properties can be found in Section 3.2.

6.2 PRF vs PRF-E surrogates

The first surrogate fuel analysed in this study was a PRF blend, identified as HO95 in this work, consisting of 95 %v/v iso-octane and 5 %v/v n-heptane. The study examined the effects of adding 20 %v/v and 85 %v/v ethanol to this blend, resulting in blends named OHE20 and OHE85, respectively, or alternatively referred to as PRF-E20 and PRF-E85. The choice of these ethanol concentrations reflects legislative trends, such as India's planned adoption of E20 and the existing use of E85 in some U.S. states and Brazil. Figure 6.1 presents a comparison of engine-out aldehyde emissions from these three surrogate fuels under stoichiometric conditions at low engine speed and load operating conditions.

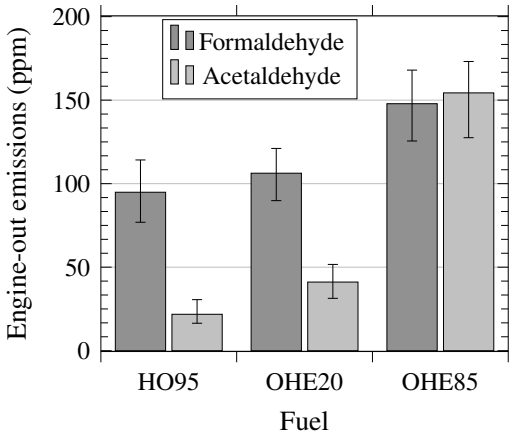

Figure 6.1: Formaldehyde and acetaldehyde engine-out emissions for HO95 (PRF), OHE20 (PRF-E20), and OHE85 (PRF-E85), at 1.95 ±0.15 bar nIMEP, 1100 rpm, and stoichiometric conditions. Ignition timing was fixed for all fuels at -46.3 °CA aTDCf. Throttle position and fuel injection quantity were varied to maintain similar load (nIMEP). Error bars represent minimum and maximum emissions over three runs.

It was observed that overall aldehyde emissions increased 2.6x between HO95 and OHE85, with formaldehyde and acetaldehyde rising by a factor of 1.6 and 7, respectively. This increase is accompanied by a change in the FA:AA ratio from 4.50 in HO95 to 0.95 in OHE85.

Compared to the binary OE blends, the addition of n-heptane to the gasoline surrogate more accurately reflects the physical and combustion properties of gasoline. Whilst OHE20 had shown a reduction of 6 % in formaldehyde and similar levels of acetaldehyde compared to OE20, OHE85 produced a 3 % increase in formaldehyde and 10 % increase in acetaldehyde compared to OE85. The 5 %v/v n-heptane addition to iso-octane in the HO95 mixture led to a 20 % reduction in acetaldehyde, though it should be noted the measured values were really low, around 20 ppm. This suggests that in multi-component fuels, the effect of n-heptane's suppression of the aldehydes is less apparent than with just the binary mixtures of n-heptane and ethanol, as the results showed in Section 5.3.3. This behaviour was further explored in the PFR and PSR models in Section 7.5.1.

The three surrogate fuels were evaluated across a range of equivalence ratios under conditions of low speed and load, with the corresponding engine-out aldehyde emissions presented in Figure 6.2.

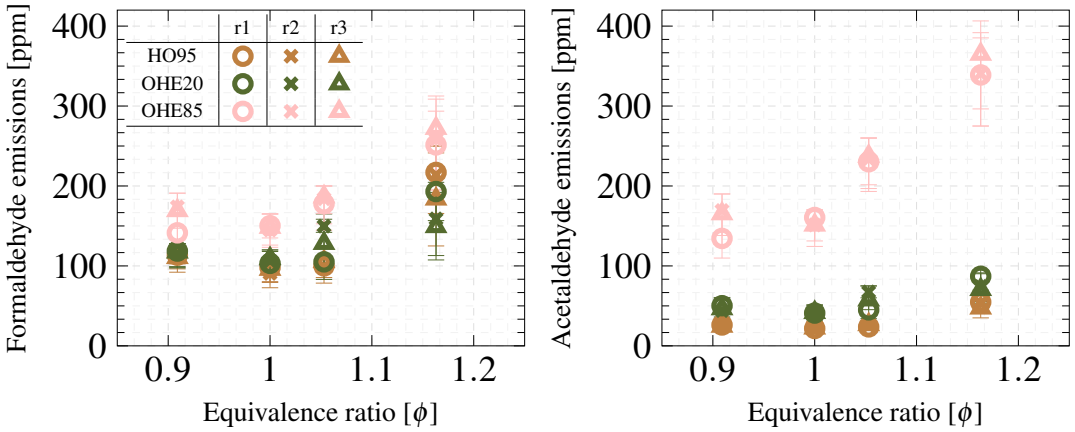

(a) Formaldehyde engine-out emissions **(b)** Acetaldehyde engine-out emissions

Figure 6.2: Engine-out **(a)** formaldehyde emissions and **(b)** acetaldehyde emissions. Fuels include HO95 (PRF), OHE20 (PRF-E20), and OHE85 (PRF-E85) across fuel-air equivalence ratio (ϕ) range at 1.95 $\pm$0.15 bar nIMEP and 1100 rpm. Ignition timing was fixed for all fuels at -46.3 °CA aTDCf across the ϕ range. Throttle position and fuel injection quantity were varied to maintain similar load (nIMEP). Error bars represent minimum and maximum emissions for each repeat.

The formaldehyde emissions were relatively consistent across different equivalence ratios, particularly between HO95 and OHE20, but moderately increased in the case of OHE85. Conversely, OHE85 exhibited significantly higher acetaldehyde emissions across the range compared to OHE20 and HO95. A decrease in acetaldehyde emissions

was observed as the fuel-air equivalence ratio shifted toward leaner conditions, especially evident in the OHE85 mixture. This trend could be linked to the presence of less unburned fuel, thereby resulting in reduced formation of intermediate aldehydes. Given ethanol's role as a precursor for acetaldehyde, this effect is more visible in OHE85.

Additionally, the difference in acetaldehyde emissions among the fuels was more significant under rich conditions compared to stoichiometric ones. The charge cooling effect of ethanol, particularly in OHE85, could contribute to lower combustion temperatures at rich conditions, creating more favourable temperature regimes for aldehyde formation. This behaviour was also observed in binary blends with high ethanol content in this study.

Within the error margin of the three repeats, the OHE20 mixtures displayed, on average, lower formaldehyde emissions than HO95 at very rich conditions (ϕ = 1.15). This reduction in emissions might be attributed to the additional oxygen content from ethanol, which, when combined with the favourable combustion properties of the OHE20 surrogate, leads to more effective consumption of intermediate aldehydes. The fixed ignition timing in this study is likely more conducive for ethanol-containing blends as ethanol has a high flame propagation speed. In contrast, iso-octane has a lower flame propagation speed and forms a major part of the HO95, therefore not effectively combusting at the set conditions. To further evaluate the combustion efficiency of the HO95 mixture, especially under rich conditions, an analysis of the NMHC emissions was conducted. The results of this analysis, including those from the mixtures with added ethanol, are presented in Figure 6.3.

In the dataset for the very rich condition (ϕ = 1.15), a distinct difference in NMHC emissions between HO95 and OHE20 was observed, indicating incomplete combustion for HO95 at this condition. This incomplete combustion could be related to lower cylinder temperatures, a consequence of the low speed and load operating points. Conversely, OHE85 demonstrated the lowest NMHC emissions, with strong repeatability and minimal error margins. Consistent with all the fuels tested in this study, a decrease in NMHC emissions was observed as the mixture became leaner. This decrease can be attributed to the increased availability of oxygen in leaner conditions, which enhances the oxidation

of unburned hydrocarbons, leading to more complete combustion and reduced NMHC emissions.

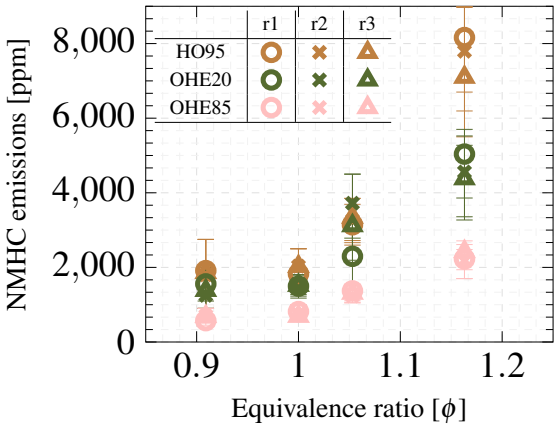

Figure 6.3: Engine-out NMHC emissions presented. Fuels include HO95 (PRF), OHE20 (PRF-E20), and OHE85 (PRF-E85) across fuel-air equivalence ratio (ϕ) range at 1.95 $\pm$0.15 bar nIMEP and 1100 rpm. Ignition timing was fixed for all fuels at -46.3 °CA aTDCf across the ϕ range. Throttle position and fuel injection quantity were varied to maintain similar load (nIMEP). Error bars represent minimum and maximum emissions for each repeat.

The effects of increasing the load to 3.00 bar for the OHE mixtures on aldehyde emissions are shown in Figure 6.4.

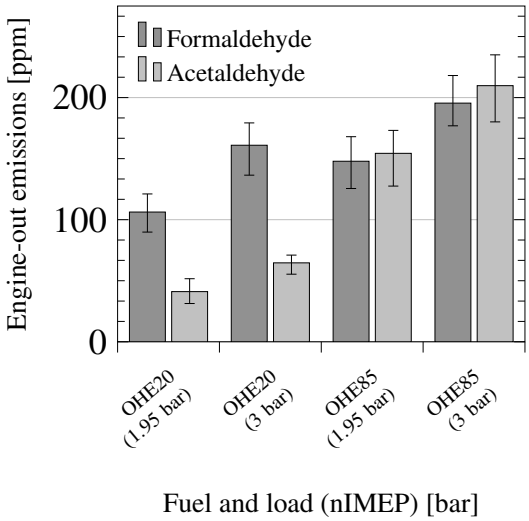

Figure 6.4: Formaldehyde and acetaldehyde engine-out emissions for OHE20 and OHE85 with load variation at 1.95 $\pm$0.15 bar and 3 $\pm$0.10 bar nIMEP under 1100 rpm and stoichiometric conditions. Ignition timing was fixed for all fuels at -46.3 °CA aTDCf for both loads. Throttle position and fuel injection quantity were varied to maintain the expected loads (nIMEP). Error bars represent minimum and maximum emissions over three repeats.

The data indicates that the FA:AA remained consistent in both fuels with the increased

load. A 1.5-fold and 1.35-fold rise in average aldehyde emissions was observed for OHE20 and OHE85, respectively. These findings are aligned with the observations from the previous fuels.

6.3 TPRF vs TPRF-E surrogates

The second surrogate evaluated was the TPRF, composed of toluene, iso-octane, and n-heptane, and referred to as OHT_HighT in this study. This fuel, previously analysed in Chapter 5, was designed to replicate the properties of a gasoline. In a similar approach to the PRFs, the impact of adding ethanol at concentrations of 20 %v/v and 85 %v/v, resulting in THOE20 and THOE85 respectively, was investigated in this section. These can also be referred to as TPRF-E20 and TPRF-E85. Figure 6.5 presents a comparison of these three surrogates under stoichiometric conditions at low speed and load.

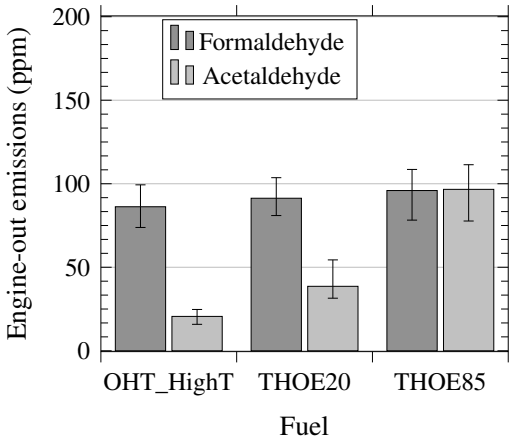

Figure 6.5: Formaldehyde and acetaldehyde engine-out emissions for OHT_HighT (TPRF), THOE20 (TPRF-E20), and THOE85 (TPRF-E85) at 1.95 ±0.15 bar nIMEP, 1100 rpm, and stoichiometric conditions. Ignition timing was fixed for all fuels at -46.3 °CA aTDCf. Throttle position and fuel injection quantity were varied to maintain similar load (nIMEP). Error bars represent minimum and maximum emissions over three repeats.

In the case of formaldehyde, the results show that on average, THOE85 produced around 10 % greater formaldehyde than OHT_HighT, however, this was only around 10 ppm. Across the three repeats at the same operating condition, the minimum and maximum values recorded for formaldehyde with both fuels were within the same range. However,

as ethanol is a key precursor for acetaldehyde, with increasing ethanol content, the acetaldehyde increased.

Nevertheless, the results indicate that the combined presence of toluene and n-heptane in the fuel mixture significantly reduced acetaldehyde formation, a trend that was most pronounced in the THOE85 blend, even though these components were present in relatively low quantities. This observation is consistent with the findings from the binary blends evaluated in this study, where toluene (Section 5.3.2) and n-heptane (Section 5.3.3), when blended with ethanol, demonstrated a substantial reduction in aldehyde emissions, particularly acetaldehyde. Similar to the results observed with PRFs, there was a shift in the FA:AA ratio, from 4.30 to 0.99. However, it is noteworthy that the total aldehyde emissions for all three surrogates, including THOE85, were lower compared to those of the PRFs. To see if the chemical kinetics depicted similar behaviour, these fuels were studied in PFR and PSR models, as detailed in Section 7.5.2.

As the OHT mixtures displayed an unusual characteristic with the aldehyde emissions increasing as the mixture became leaner, the impact of ethanol addition to this mixture was studied across the equivalence ratio range. The outcomes of this study, comparing the three TPRF surrogates under these conditions, are illustrated in Figure 6.6.

Excluding the very rich condition (ϕ = 1.18), engine-out formaldehyde emissions showed a consistent increase as the mixture became leaner. Across all three fuels, formaldehyde emissions were comparable, with the exception at ϕ = 1.18, where THOE85 produced higher levels of formaldehyde. However, the data for THOE85 at this condition demonstrated lower repeatability. In one of the repeats where higher aldehyde emissions were recorded, the exhaust temperature was observed to be elevated (over 320 °C). This could suggest that the increased exhaust temperatures may have facilitated the conversion of unburned ethanol into aldehydes under these conditions at the exhaust.

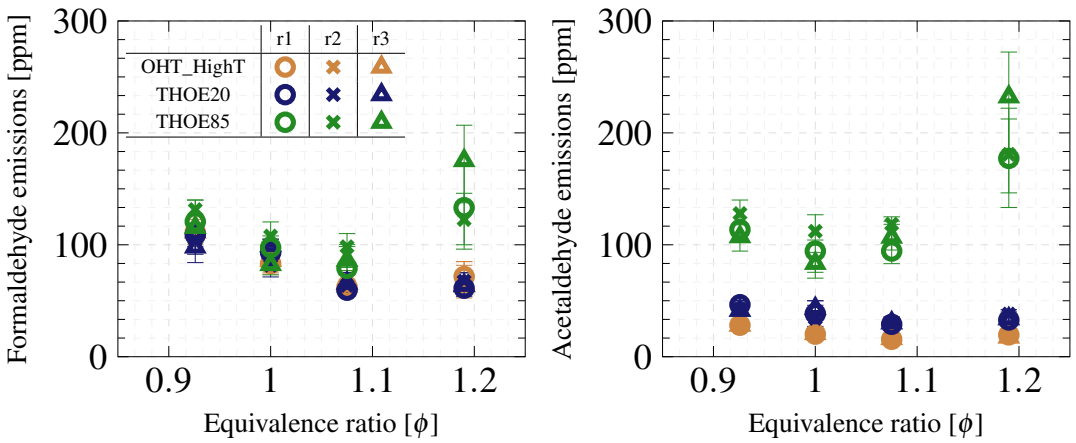

(a) Formaldehyde engine-out emissions **(b)** Acetaldehyde engine-out emissions

Figure 6.6: Engine-out **(a)** formaldehyde emissions and **(b)** acetaldehyde emissions. Fuels include OHT_HighT (TPRF), THOE20 (TPRF-E20), and THOE85 (TPRF-E85) across fuel-air equivalence ratio (ϕ) range at 1.95 $\pm$0.15 bar nIMEP and 1100 rpm. Ignition timing was fixed for all fuels at -46.3 °CA aTDCf across the ϕ range. Throttle position and fuel injection quantity were varied to maintain similar load (nIMEP). Error bars represent minimum and maximum emissions for each repeat.

For acetaldehyde emissions, the OHT_HighT (TPRF representative) and THOE20 mixtures exhibited similar levels. Furthermore, for both these fuels, despite the overall low emissions, results from the three repeats were consistent, showing minimal variation. In contrast, the THOE85 mixture led to significantly higher acetaldehyde emissions, particularly at very rich conditions. This observation aligns with previous findings in this study regarding fuels with higher ethanol content, potentially due to an increased cooling effect from a greater presence of unburned ethanol, leading to more intermediate aldehyde formation. Notably, the variability among repeats for THOE85 was more pronounced than for other surrogates, especially at very rich conditions. For OHT_HighT and THOE20, a trend of increasing acetaldehyde emissions was noted as the mixture became leaner. This was similar to the unusual behaviour noticed for the OHT fuels which contained no ethanol. However, THOE85 followed a pattern observed in previously studied fuels with ethanol, with the lowest emissions occurring at stoichiometry. To determine if these trends are consistent with other hydrocarbons, NMHC emissions were also analysed across the equivalence ratio range. The findings from this analysis are presented in Figure 6.7.

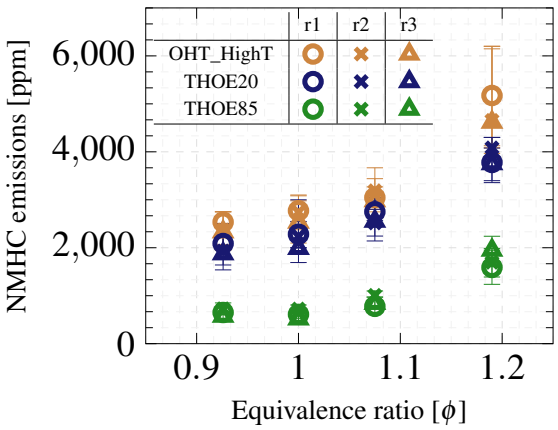

Figure 6.7: Engine-out NMHC emissions presented. Fuels include OHT_HighT (TPRF), THOE20 (TPRF-E20), and THOE85 (TPRF-E85) across fuel-air equivalence ratio (ϕ) range at 1.95 $\pm$0.15 bar nIMEP and 1100 rpm. Ignition timing was fixed for all fuels at -46.3 °CA aTDCf across the ϕ range. Throttle position and fuel injection quantity were varied to maintain similar load (nIMEP). Error bars represent minimum and maximum emissions for each repeat.

Figure 6.7 shows the NMHC decreased as the mixture became leaner. However, for THOE85, a minor increase in NMHC emissions was observed between stoichiometric and lean conditions. The NMHC emissions were similar for OHT_HighT and THOE20, with the latter moderately lower. The difference between the THOE20 and THOE85 was greater. Interestingly, the NMHC emissions were lower for the TPRF mixtures than the PRF mixtures, particularly at rich conditions. This will be further examined in Section 6.4.

The effect of increased load and speed on the two TPRF-E fuels were analysed and the results are shown in Figure 6.8. As opposed to previous findings, as the load increased for THOE20, the engine-out aldehyde emissions remained consistent despite the changes in combustion conditions. However, for THOE85, the emissions increased by 20 %. Compared to OHE85 under the load of 3 bar nIMEP, the THOE85 has a 40 % reduction in aldehyde emissions at the same conditions.

With an increase in speed, there was a decrease in the average aldehyde emissions by about one-third, consistent with the trends observed for other fuels in this study. This can be linked to enhanced air-fuel mixing and combustion efficiency, coupled with higher temperatures and pressures in the combustion chamber. These combined factors lead to more complete combustion, effectively reducing the formation and emissions of aldehydes.

In the case of THOE20, the decrease in formaldehyde emissions (27 %) was less compared to acetaldehyde (37 %). A similar trend was observed with THOE85, where the reduction in formaldehyde emissions was only 8 %, while acetaldehyde emissions decreased by 17 %. This behaviour could be attributed to the higher speed enhancing ethanol's rapid combustion characteristics, resulting in fewer intermediate aldehyde formations.

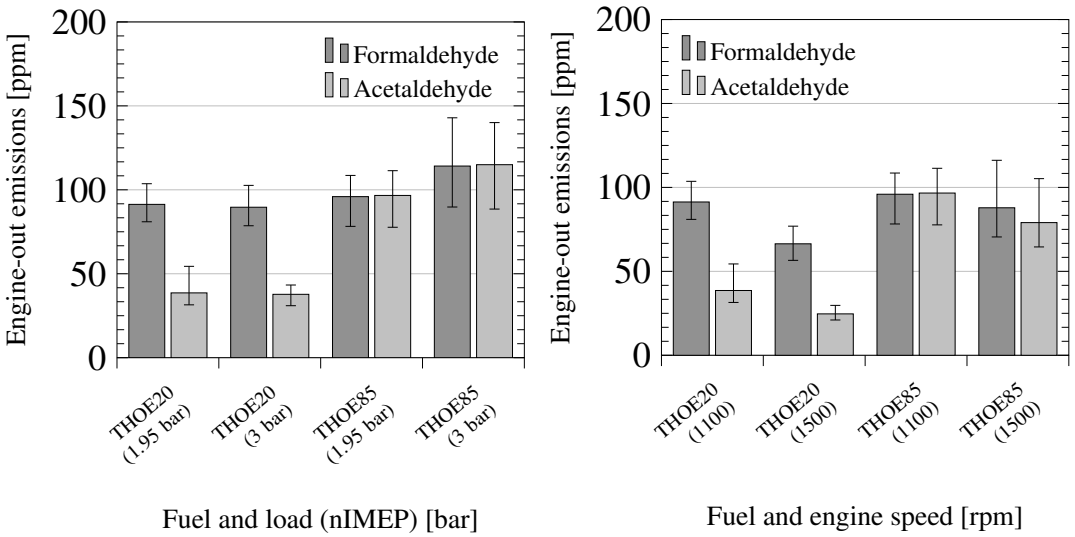

(a) Fuel and load variation

(b) Fuel and engine speed variation

Figure 6.8: Formaldehyde and acetaldehyde engine-out emissions for THOE20 (TPRF-E20) and THOE85 (TPRF-E85) with: **(a)** load variation at 1.95 ±0.15 bar and 3.00 ±0.10 bar nIMEP under 1100 rpm and stoichiometric conditions; **(b)** engine speed variation at 1100 rpm and 1500 rpm under 1.95 ±0.15 bar nIMEP and stoichiometric conditions. Ignition timing was fixed for all fuels at -46.3 °CA aTDCf for both speeds and loads. Throttle position and fuel injection quantity were varied to maintain the expected loads (nIMEP). For both, error bars represent minimum and maximum emissions over three repeats.

6.4 PRF-E85 vs TPRF-E85

The effect of aromatic content, specifically toluene, on suppressing aldehyde emissions has been extensively studied in this work. Even in fuels predominantly composed of ethanol, such as OHE85 and THOE85, the presence of toluene in THOE85 contributed to a reduction in engine-out aldehyde emissions. A detailed comparative analysis was performed on OHE85 and THOE85 to further investigate this effect.

As shown in Figure 6.9, the engine-out emissions of formaldehyde, acetaldehyde, and NMHC at stoichiometric low speed and load conditions for both OHE85 and THOE85,

were examined. The addition of just 2 %v/v of toluene led to a decrease in all three types of emissions, approximately by less than a third. Adding toluene resulted in an increased FA:AA, though this data was subject to an error margin. Interestingly, despite toluene having the highest NMHC emissions among the pure fuels, the THOE85 fuel exhibited lower NMHC emissions than OHE85.

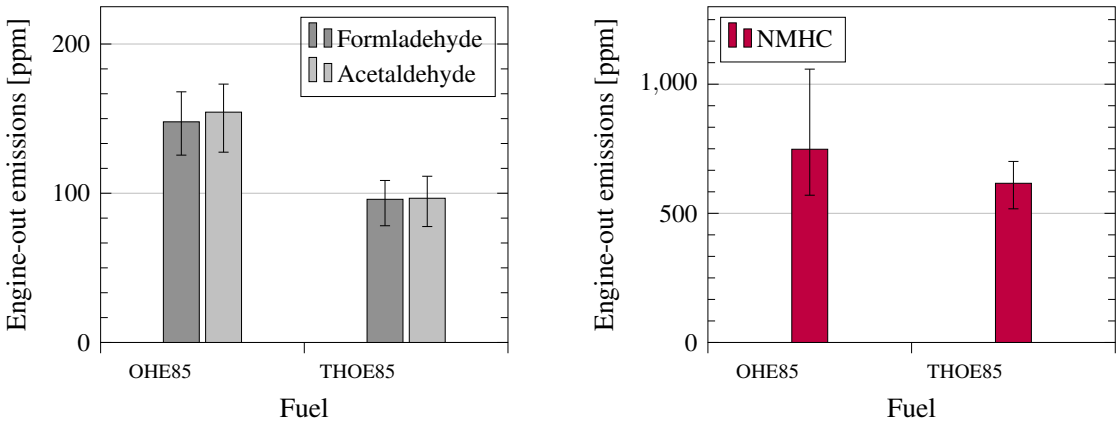

(a) Engine-out aldehyde emissions **(b)** Engine-out NMHC emissions

Figure 6.9: Engine-out **(a)** formaldehyde and acetaldehyde and **(b)** NMHC for OHE85 (PRF-E85) and THOE85 (TPRF-E85) at 1.95 ±0.15 bar nIMEP, 1100 rpm, and stoichiometric conditions. Ignition timing was fixed for all fuels at -46.3 °CA aTDCf. Throttle position and fuel injection quantity were varied to maintain similar load (nIMEP). Error bars represent minimum and maximum emissions over three repeats.

Figure 6.10 shows the formaldehyde and acetaldehyde emissions across various equivalence ratios, highlighting the impact of toluene in this range. A comparison between THOE85 and OHE85 finds that THOE85 consistently exhibits lower emissions across the entire range of fuel-air ratios. The difference in emissions between these two fuels increased as the mixture richness increased, with the smallest difference observed under lean conditions. Both fuels show good repeatability and maintain low error margins, although this consistency was not as evident at very rich conditions.

For THOE85, aldehyde emissions at operating points near stoichiometry were closer to the aldehyde emissions at stoichiometry than was the case for OHE85. This trend may be attributed to the TPRF fuel composition incorporating toluene, as indicated by the contrasting behaviours of OHT_HighT and THOE20. For these fuels, leaner mixtures resulted in higher aldehyde emissions compared to other tested fuels. Consequently, at

richer conditions, the additional ethanol might produce more intermediate aldehydes, but these are likely consumed by radicals from the other fuel components. However, it is important to note that the richest conditions resulted in the highest aldehyde emissions for both fuels.

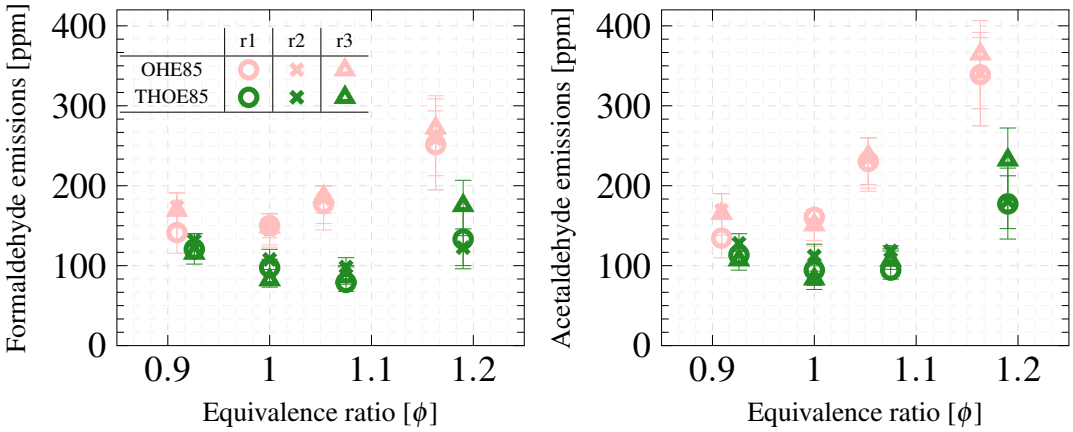

(a) Formaldehyde engine-out emissions **(b)** Acetaldehyde engine-out emissions

Figure 6.10: Engine-out **(a)** Formaldehyde emissions and **(b)** acetaldehyde emissions. Fuels include OHE85 (PRF-E85) and THOE85 (TPRF-E85) across fuel-air equivalence ratio (ϕ) range at 1.95 $\pm$0.15 bar nIMEP and 1100 rpm. Ignition timing was fixed for all fuels at -46.3 °CA aTDCf across the ϕ range. Throttle position and fuel injection quantity were varied to maintain similar load (nIMEP). Error bars represent minimum and maximum emissions for each repeat.

From the results for pure fuels in this study (Section 5.2), it was observed that toluene led to greater NMHC emissions than iso-octane and ethanol. This trend was also reflected in binary mixtures containing toluene, which exhibited higher NMHC emissions compared to the other two sets of binary blends without toluene. Consequently, even though only 2 %v/v of toluene was added to create the THOE85 blend, its impact on NMHC emissions compared to a surrogate fuel with a similar ethanol content, OHE85, was investigated. The outcomes of this comparison are presented in Figure 6.11.

As shown in Figure 6.11, this study reveals that for both fuels, NMHC emissions exhibited a similar pattern: lowest at lean and stoichiometric conditions, and increasing as the fuel-air mixture becomes richer. At richer conditions, there would typically be more unburned fuel, leading to higher hydrocarbon emissions. Despite the addition of toluene, NMHC levels were generally lower for THOE85 compared to OHE85, with the exception

of lean conditions where they were comparable. The difference in emissions between the two fuels increased with richer equivalence ratios. However, at this operating condition, there was a decrease in repeatability and larger error margins.

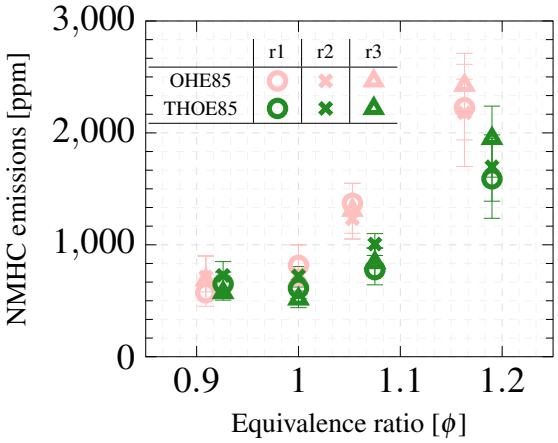

Figure 6.11: Engine-out NMHC emissions are presented. Fuels include OHE85 (PRF-E85) and THOE85 (TPRF-E85) across fuel-air equivalence ratio (ϕ) range at 1.95 $\pm$0.15 bar nIMEP and 1100 rpm. Ignition timing was fixed for all fuels at -46.3 °CA aTDCf across the ϕ range. Throttle position and fuel injection quantity were varied to maintain similar load (nIMEP). Error bars represent minimum and maximum emissions for each repeat.

6.5 Summary

PRF and TPRF fuels, both in their standard state and with 20 %v/v and 85 %v/v ethanol addition, were tested in a single-cylinder engine under low speed and load conditions. Similar to the research fuels, for all the tested fuels in this chapter, the ignition timing was fixed at -46.3 °CA aTDCf. This was also kept constant across the fuel-air equivalence ratio (ϕ) range. To maintain the same load (nIMEP) and account for fuel-specific behaviour when testing different fuels, the throttle position and fuel injection quantities were varied. Based on these conditions, the key findings include:

- *PRF and PRF-E*: Across various fuel-air ratios, formaldehyde levels in HO95 (PRF), OHE20 (PRF-E20), and OHE85 (PRF-E85) mixtures were similar, while acetaldehyde levels were higher in OHE85 (PRF-E85) compared to the other two blends, especially in richer mixtures because of higher ethanol content. The FA:AA for HO95 (PRF) was 4.50, shifting to 0.95 in OHE85 (PRF-E85), indicating n-heptane's role in suppressing acetaldehyde as the ratio is greater than it was for

OE85. NMHC emissions displayed a similar trend to previously studied fuels, being lowest at stoichiometric conditions and increasing at lean and rich conditions.

- *TPRF and TPRF-E*: The overall engine-out aldehyde emissions were lower in OHT_HighT (TPRF) mixture compared to the PRF mixture. Formaldehyde emissions across the equivalence ratio range remained consistent among the fuels, except at very rich conditions. However, acetaldehyde emissions were comparable for OHT_HighT (TPRF) and THOE20 (TPRF-E20), and higher for THOE85 (TPRF-E85). The FA:AA ratio for OHT_HighT (TPRF) was 4.30, shifting to nearly 1.00 for THOE85 (TPRF-E85). This slight ratio reduction from HO95 (PRF) to OHT_HighT (TPRF) highlights toluene's greater suppression of formaldehyde than acetaldehyde, becoming more evident as ethanol content increases, particularly as THOE85 (TPRF-E85) displayed similar levels of both aldehydes. NMHC emissions decreased in leaner mixtures, with THOE85 (TPRF-E85) showing the lowest NMHC emissions.

- *PRF-E85 and TPRF-E85*: This comparison demonstrates that even a minimal addition of toluene reduced aldehyde emissions by nearly one-third, with a subtler effect on NMHC emissions. Since aldehydes typically form at lower temperatures, this could significantly suppress aldehyde formation as it would increase the combustion temperature. With richer fuel-air mixtures, the difference in aldehyde emissions between the two fuels became more apparent, although the difference in NMHC emissions remained relatively constant.

- *Aldehyde and NMHC emissions*: NMHC emissions were relatively consistent for fuels with low or no ethanol, but decreased significantly with higher ethanol content, contrary to aldehyde emissions. Across different equivalence ratios, NMHC emissions reduced as the mixture became leaner, while aldehyde emissions generally increased, reflecting different emission behaviours. This could be linked to the additional oxygen in lean conditions and ethanol-rich fuels, which oxidises conventional hydrocarbons but also could facilitate chain-terminating reactions forming stable intermediate aldehydes, especially at lower temperatures.

7

Results: Modelling

Contents

7.1 Motivation

Simulating the fuel compositions in fundamental reactor models can be beneficial to understanding aldehyde generation and consumption as well as supporting experimental results obtained from the single-cylinder engine. The research and surrogate fuel compositions, detailed in Section 3.2, were also subjected to computational modelling. The mechanism M2, extensively validated in Chapter 4, was used in PFR and PSR. In the

PFR model, the linear flow facilitates a controlled reaction progression under consistent conditions, allowing for the analysis of intermediate aldehyde formation at specific reaction stages. On the other hand, the PSR model, characterised by its uniform mixing, enables the examination of chemical species concentrations across a range of temperatures at a constant pressure and a specific residence time. This multifaceted modelling approach aids in a comprehensive understanding of the influence of fuel composition on aldehyde emissions in combustion processes.

The PFR and PSR models were based on the University of Melbourne and University of Orleans test facilities, respectively. The physical parameters of each of the reactors are detailed in Section 4.5. No experiments on the PFR and PSR were conducted in this work. Therefore, all the results shown in this chapter are model predictions. They were analysed qualitatively and primarily used to support the experimental findings from Chapters 5 and 6. The PFR was simulated at 800 K and 15 bar, and the PSR at 18 bar with a temperature range from 650 K to 1100 K, respecting the limits of the experimental setup, chemical kinetic mechanism, and probable operating conditions for aldehyde formation. Furthermore, a pressure range of 15 to 18 bar is associated with the peak cylinder pressure observed for the single-cylinder engine experiments, given they were run at low speed and load. Additionally, the selected temperature regime covers the typical range of formation and consumption of formaldehyde and acetaldehyde, as previously defined in the literature [190].

7.2 Pure fuels

The formaldehyde and acetaldehyde formation along the PFR for the pure fuels examined is presented in Figure 7.1. Ethanol and iso-octane produced similar quantities of formaldehyde. However, ethanol displayed a faster reaction rate, as indicated by its quicker formation and consumption of formaldehyde, compared to iso-octane. This difference in reaction speed can be attributed to ethanols higher flame propagation speed, as similar reactant quantities were modelled for both fuels. The higher levels of formaldehyde from iso-octane, which is a branched alkane, are due to the ease of breaking

off the methyl group that then oxidises to form formaldehyde. Toluene demonstrated significantly lower formaldehyde formation, approximately a quarter of the other two pure fuels, and its reaction progression was significantly slower.

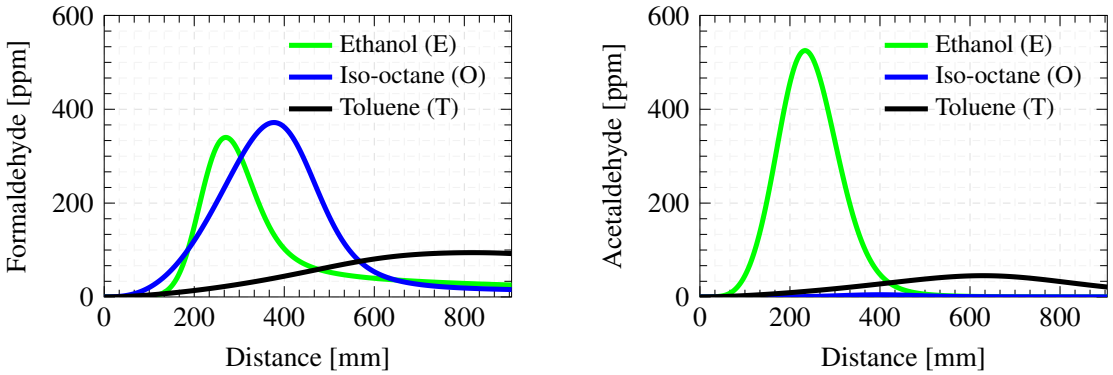

(a) Formaldehyde from PFR model **(b)** Acetaldehyde from PFR model

Figure 7.1: Species concentration profiles of intermediate **(a)** formaldehyde and **(b)** acetaldehyde at 800 K, 15 bar, and ϕ = 0.058 based on the University of Melbourne PFR [176]. Mechanism M2 [169] predictions presented for pure fuels of ethanol, iso-octane, and toluene.

With respect to acetaldehyde, the model with mechanism M2 predicts negligible quantities for iso-octane, marginally higher amounts for toluene, and a significant proportion for ethanol. However, this behaviour is contrary to the observation from the engine experimental data which shows that iso-octane produces more acetaldehyde than toluene. The model predicted acetaldehyde's formation and consumption occurred earlier as the reaction progresses. This early generation is consistent with the chemical behaviour of acetaldehyde, which forms at lower temperatures than formaldehyde [190]. Additionally, as acetaldehyde possesses a larger carbon number, it forms earlier in the fuel's oxidation reaction pathway [5].

Figure 7.2 shows the results from the PSR model for the pure fuels. Using mechanism M2, at 18 bar, the model predicts that iso-octane generates greater levels of formaldehyde compared to ethanol and toluene. This is also contrary to the experimental engine data, suggesting the mechanism may not fully capture ethanol's reaction pathways to formaldehyde. For iso-octane, formaldehyde formation appears to occur in two stages: initially between 770 K and 900 K, and subsequently at temperatures above 900 K. The first stage produced greater formaldehyde. For these conditions, it appears that

ethanol and toluene do not display the same. Ethanol shows higher emissions at the lower temperature range, while toluene's greater emissions occur at the higher temperature stage.

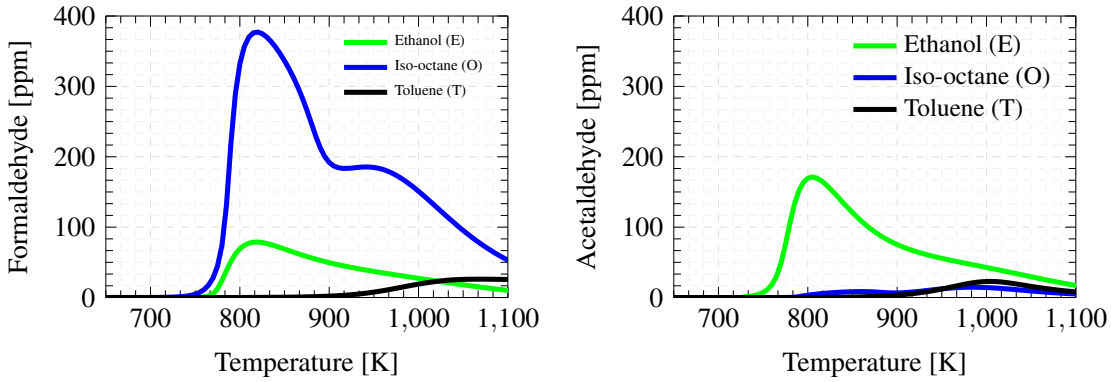

(a) Formaldehyde from PSR model **(b)** Acetaldehyde from PSR model

Figure 7.2: Species concentration profile predictions using Mechanism M2 [169] of **(a)** formaldehyde and **(b)** acetaldehyde from the pure fuels of ethanol, toluene, and iso-octane. The reactant quantity of 0.2 % with 0.6 % oxygen (O_2), and 99.2 % nitrogen (N_2) was based on the University of Orleans JSR at conditions of $\tau = 0.7$ s, $\phi = 1.0$, pressure of 18 bar, and temperature range from 650 K to 1100 K [172].

Interestingly, the PSR model suggests that, at 18 bar, the concentration of acetaldehyde formed across the temperature range is lower than that of formaldehyde. This finding contrasts with observations from the PFR, where the opposite was noted for ethanol. Nonetheless, the PSR model indicates that ethanol produces a significantly higher proportion of acetaldehyde compared to iso-octane and toluene, primarily at lower temperatures, as anticipated. For iso-octane, a two-stage behaviour in acetaldehyde formation is observed, although the predicted quantity remains significantly low. Similar to its formaldehyde generation, toluene converts to acetaldehyde at higher temperatures, albeit in low amounts. The PSR model suggests that in this temperature regime, toluene produces a higher acetaldehyde concentration than iso-octane. This was also observed with the PFR and may be attributed to factors related to the kinetic mechanism and/or operating conditions.

In this section, the effect of each of the pure fuels on formaldehyde and acetaldehyde generation and consumption in the reactor models were analysed. This approach can help

explain the subsequent effects in multi-component fuels by disseminating the role of each component. For the following multi-component fuels in this study, the analysis was also conducted on the outcomes from the PFR and PSR models.

7.3 Binary

Three sets of binary fuels, examining the interaction of ethanol with common gasoline surrogate components were investigated in the PFR and PSR models.

7.3.1 Ethanol and iso-octane

The blends of iso-octane and ethanol (OE), specifically OE20 and OE85 with 20 %v/v and 85 %v/v of ethanol, were analysed in comparison to pure ethanol and iso-octane. The concentrations of formaldehyde and acetaldehyde along the PFR for these blends are shown in Figure 7.3.

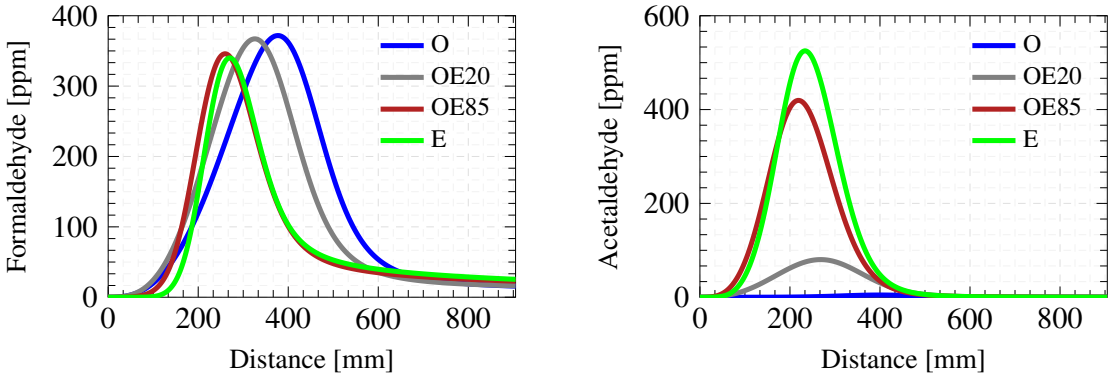

(a) Formaldehyde from PFR model **(b)** Acetaldehyde from PFR model

Figure 7.3: Species concentration profiles of intermediate **(a)** formaldehyde and **(b)** acetaldehyde at 800 K, 15 bar, and ϕ = 0.058 based on the University of Melbourne PFR [176]. Mechanism M2 [169] predictions presented for ethanol, iso-octane and binary mixtures of OE20 and OE85.

The inclusion of ethanol resulted in an earlier formation of both formaldehyde and acetaldehyde. While the model predicts similar levels of formaldehyde for all four fuels, a disparity is observed in acetaldehyde concentrations. Again, this differs from the experimental engine data for formaldehyde, in which the addition of ethanol was shown to also increase formaldehyde. Furthermore, the predicted acetaldehyde levels are greater than formaldehyde for both OE mixtures, though the experimental data only showed

this for OE85. This suggests the mechanism may over-estimate ethanol's contribution to acetaldehyde and under-estimate its contribution to formaldehyde. For the OE20 and OE85 blends in comparison to pure ethanol, there was a reduction in acetaldehyde concentration by approximately 80 % and 25 %, respectively.

In the PSR model, the OE blends were also examined alongside their pure constituents. The outcomes for formaldehyde and acetaldehyde concentrations across varying temperatures are shown in Figure 7.4.

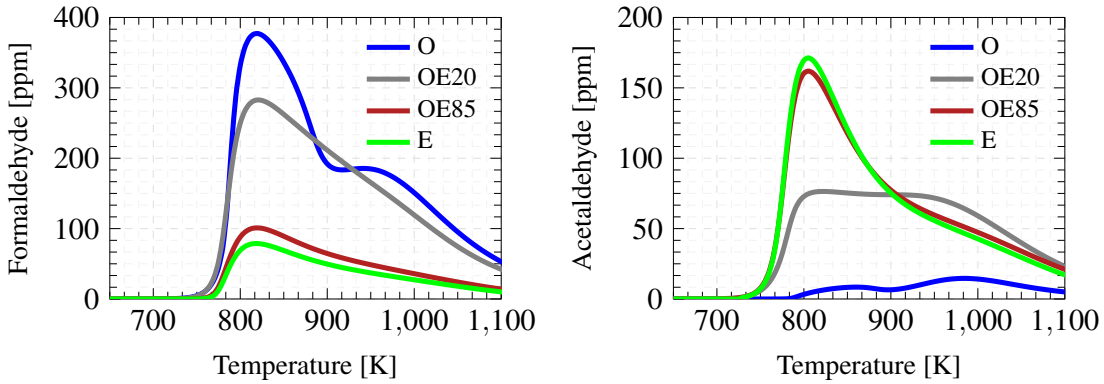

(a) Formaldehyde from PSR model **(b)** Acetaldehyde from PSR model

Figure 7.4: Species concentration profile predictions using Mechanism M2 [169] of **(a)** formaldehyde and **(b)** acetaldehyde for ethanol, iso-octane, and binary mixtures of OE20 and OE85. The reactant quantity of 0.2 % with 0.6 % oxygen (O_2), and 99.2 % nitrogen (N_2) was based on the University of Orleans JSR at conditions of τ = 0.7 s, ϕ = 1.0, pressure of 18 bar, and temperature range from 650 K to 1100 K [172].

As predicted by the PSR model, the OE20 blend, with its higher iso-octane content, exhibited an increased concentration of formaldehyde compared to other blends. This agrees with PSR model predictions for iso-octane which was also shown to produce more formaldehyde than the other components. However, as discussed in the previous section (7.2), this suggests the mechanism may over-estimate the oxidation pathways that lead to formaldehyde from iso-octane.

Interestingly, the addition of ethanol to iso-octane in OE20 appears to subdue the two stage behaviour observed for iso-octane. This could be attributed to ethanol suppressing the NTC behaviour of iso-octane, as briefly discussed in Section 2.3.2. When comparing pure ethanol and OE85, both showed similar levels and formation duration of formaldehyde and

acetaldehyde. For the OE20 blend, the presence of iso-octane extended the temperature range at which acetaldehyde was formed to higher temperatures.

7.3.2 Ethanol and toluene

This section investigates how the interaction between toluene and ethanol (TE) affects aldehyde concentrations in various reactor models. Three mixtures TE25, TE50, and TE75 with progressively increasing ethanol content (indicated by the ethanol volume percentage) were examined, similar to those previously analysed experimentally (Section 5.3.2). Figure 7.5 shows the reaction progression along the PFR for these TE mixtures, compared to their pure constituents of ethanol and toluene, from the PFR model at 800 K and 15 bar. The aldehyde generation and consumption was within the bounds of pure fuels of ethanol and toluene. Due to toluene's slower reactivity compared to ethanol, the mixtures with added ethanol displayed noticeably enhanced reactivity, as seen in Figure 7.5. All tested mixtures exhibited an increase in both formaldehyde and acetaldehyde due to the presence of ethanol.

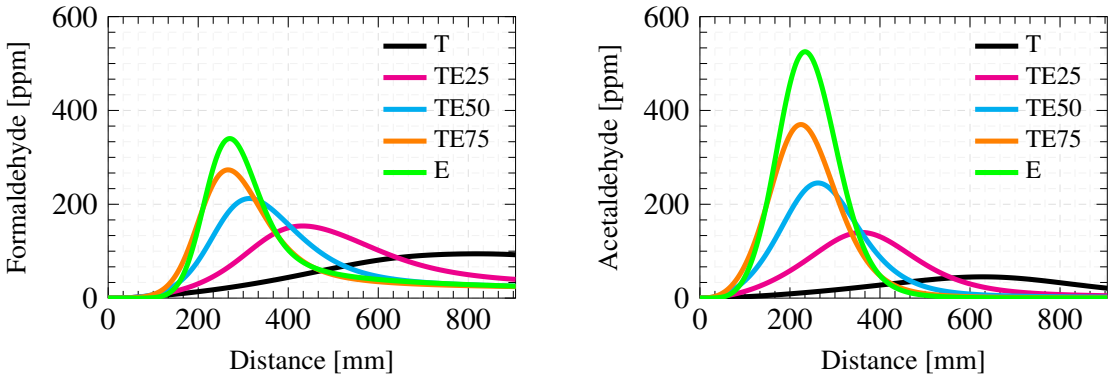

(a) Formaldehyde form PFR model **(b)** Acetaldehyde from PFR model

Figure 7.5: Species concentration profiles of intermediate **(a)** formaldehyde and **(b)** acetaldehyde at 800 K, 15 bar, and ϕ = 0.058 based on the University of Melbourne PFR [176]. Mechanism M2 [169] predictions presented for ethanol, toluene, and binary mixtures of TE25, TE50, and TE75.

Experimental findings have shown that ethanol's FA:AA ratio is less than 1, primarily because it directly leads to acetaldehyde production, while toluene produces more formaldehyde. Additionally, results from Section 5.3.2 suggest that adding ethanol to toluene alters the FA:AA ratio in TE mixtures. In line with this, the PFR model predictions

for TE mixtures with higher ethanol content, such as TE50 and TE75, demonstrated increased acetaldehyde production relative to formaldehyde. This correlation between the PFR model predictions and experimental data confirms that the observed experimental trends are supported by the underlying chemistry.

Figure 7.6 shows the formaldehyde and acetaldehyde concentrations across the temperature range as predicted by the PSR model.

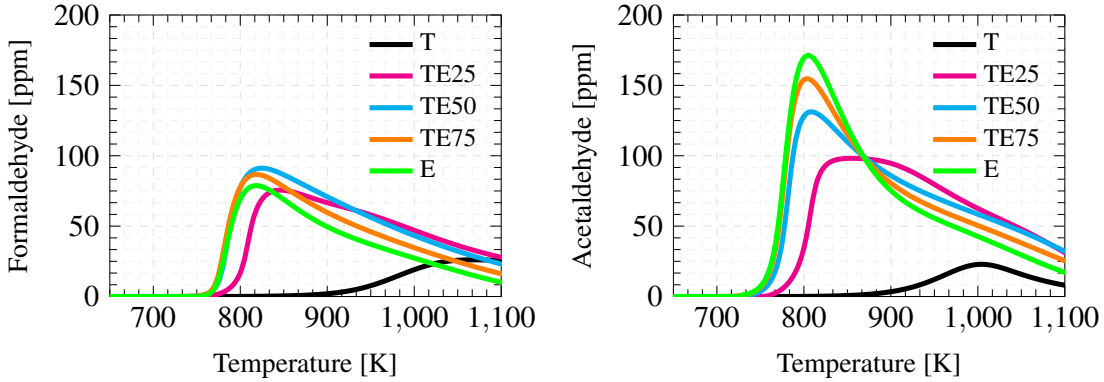

(a) Formaldehyde from PSR model **(b)** Acetaldehyde from PSR model

Figure 7.6: Species concentration profile predictions using Mechanism M2 [169] of **(a)** formaldehyde and **(b)** acetaldehyde for ethanol, toluene, and binary mixtures of TE25, TE50, and TE75 at a reactant quantity of 0.2 % with 0.6 % oxygen (O_2), and 99.2 % nitrogen (N_2). Based on the University of Orleans JSR at conditions of τ = 0.7 s, ϕ = 1.0, pressure of 18 bar, and temperature range from 650 K to 1100 K [172].

The TE mixtures generated higher levels of formaldehyde compared to their pure fuel constituents, toluene and ethanol, under these specific operating conditions. This suggests that toluene's interaction with ethanol enhances the formation of formaldehyde. This is different to the experimental observations for the TE mixtures and the PFR model predictions. This increase in formaldehyde for the TE mixtures compared to ethanol could be due to the mechanism's under-prediction of ethanol's contribution to formaldehyde formation. For acetaldehyde, similar to the OE mixtures, the mixtures with a higher proportion of toluene extended the temperature range over which acetaldehyde was formed.

In comparison to the results from the PFR model, the overall quantity of aldehydes produced in the PSR model was lower. The peak aldehyde concentrations were noted

around 800 K, consistent with the fixed temperature set in the PFR model. However, it is important to note that the PSR model simulations were conducted at a higher pressure of 18 bar, in contrast to the 15 bar setting in the PFR model.

7.3.3 Ethanol and n-heptane

As n-heptane is often used in a gasoline surrogate to optimise the octane sensitivity, this study examined the impact of ethanol and n-heptane interaction on aldehyde production and consumption across various reactor models.

The PFR results for two HE mixtures, with 65 %v/v and 85 %v/v ethanol concentrations, are shown in Figure 7.7. The concentrations of formaldehyde and acetaldehyde were analysed relative to pure ethanol. As pure n-heptane was not evaluated in the experimental analysis, it was not considered for this study too. Given n-heptane's characteristics of low-temperature ignition and fast flame propagation speed as seen in Section 4.6.1, similar to ethanol, the combined HE mixtures demonstrated both the formation and consumption of aldehydes earlier in the reactor.

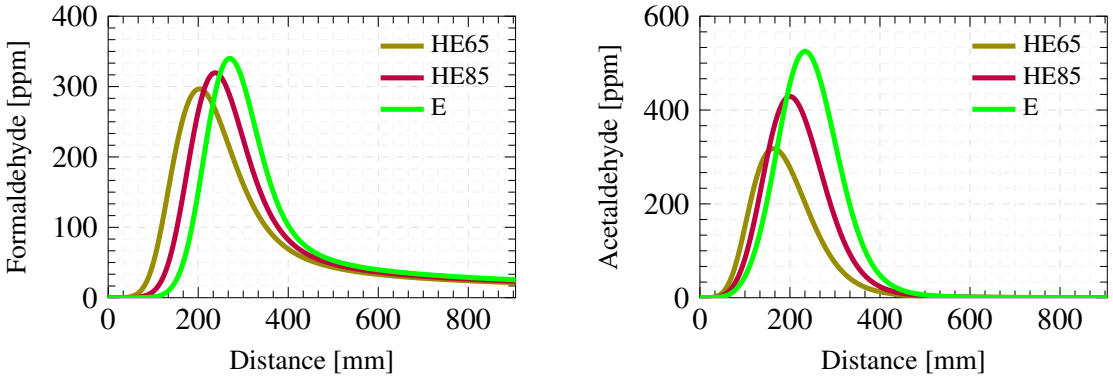

(a) Formaldehyde from PFR model **(b)** Acetaldehyde from PFR model

Figure 7.7: Species concentration profiles of intermediate **(a)** formaldehyde and **(b)** acetaldehyde at 800 K, 15 bar, and ϕ = 0.058 based on the University of Melbourne PFR [176]. Mechanism M2 [169] predictions presented for ethanol and binary mixtures of HE65 and HE85.

For both HE65 and HE85 mixtures, the generation of acetaldehyde exceeded that of formaldehyde, due to the higher ethanol content in these mixtures. However, as the proportion of n-heptane in the fuel increased, the rate of acetaldehyde reduction was greater than formaldehyde. This observation suggests that the presence of n-heptane

in the fuel mix affects the aldehyde production dynamics, particularly influencing the relative rates of acetaldehyde and formaldehyde formation supporting the experimental analyses.

The PSR model was also used to analyse the aldehyde concentrations for the HE mixtures, with results displayed across the temperature range at 18 bar in Figure 7.8. In both HE blends, the levels of formaldehyde and acetaldehyde were found to be higher than those of pure ethanol. While the presence of toluene in the TE blends showed a similar trend of increased formaldehyde formation compared to pure ethanol, an increase in acetaldehyde was unexpected, given that ethanol is its primary precursor and experimental results indicated that n-heptane significantly inhibits acetaldehyde formation.

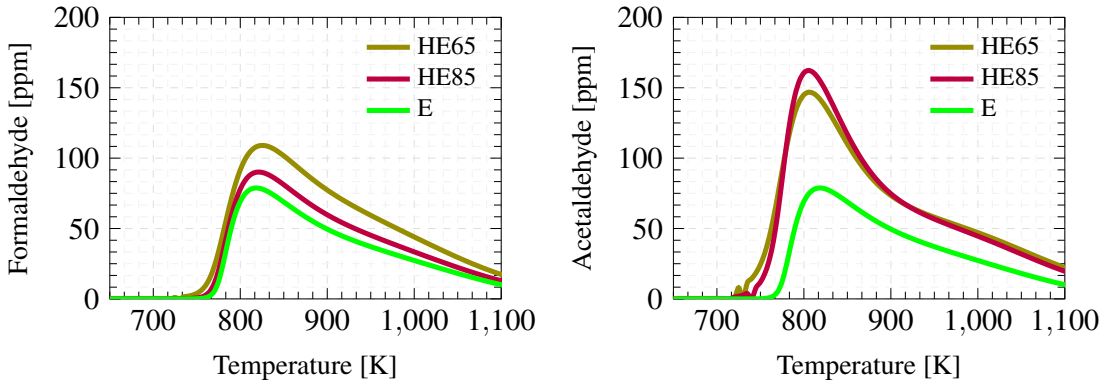

(a) Formaldehyde from PSR model **(b)** Acetaldehyde from PSR model

Figure 7.8: Species concentration profile predictions using Mechanism M2 [169] of **(a)** formaldehyde and **(b)** acetaldehyde for ethanol and binary mixtures of HE65 and HE85. The reactant quantity of 0.2 % with 0.6 % oxygen (O_2), and 99.2 % nitrogen (N_2) was based on the University of Orleans JSR at conditions of τ = 0.7 s, ϕ = 1.0, pressure of 18 bar, and temperature range from 650 K to 1100 K [172].

In both HE mixtures, acetaldehyde concentrations exceeded those of formaldehyde, with a distinct difference from pure ethanol across the temperature range. Contrary to these findings, the PFR model showed a rapid reduction in acetaldehyde with increasing n-heptane concentration in the HE mixture. Furthermore, in contrast to the PFR model and experimental findings, the PSR model predicts that HE65 leads to greater aldehyde concentration than HE85. These discrepancies highlight that the model and mechanism replicate experimental findings only under specific pressure and temperature conditions.

7.4 Ternary mixtures

The study analysed the two sets of ternary mixtures, one with ethanol (OTE) and one without (OHT), each with low and high toluene concentrations (LowT and HighT), in various reactor models to support experimental findings. As aromatic content, such as the inclusion of toluene, has been shown to present contrasting findings on their effect on aldehydes, it is key for the model and mechanisms to accurately represent this behaviour so the aromatics are proportionately added to fuels.

7.4.1 Iso-octane, toluene, and ethanol

The first set of ternary mixtures featured a constant ethanol volume of 25 %, referred to as OTE25. The variation in toluene content was analysed to assess its influence on aldehyde concentrations within a multi-component fuel.

Figure 7.9 shows the formaldehyde and acetaldehyde concentrations obtained from the PFR model at 15 bar and 800 K.

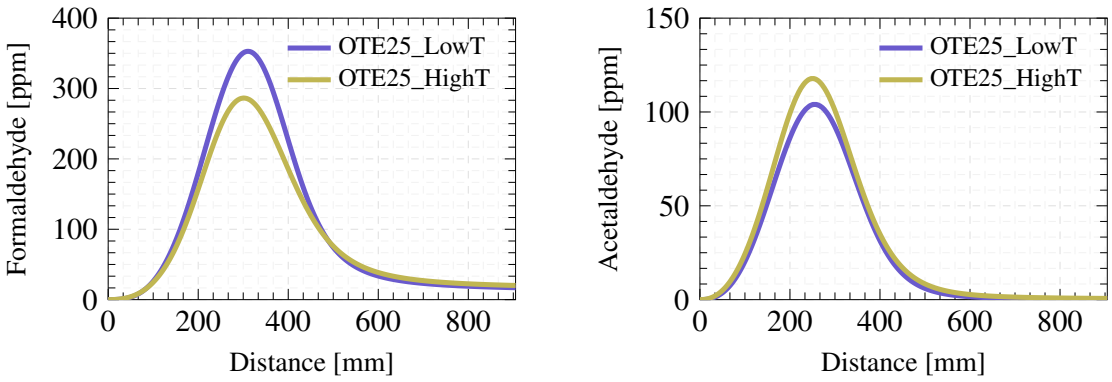

(a) Formaldehyde from PFR model

(b) Acetaldehyde from PFR model

Figure 7.9: Species concentration profiles of intermediate **(a)** formaldehyde and **(b)** acetaldehyde at 800 K, 15 bar, and ϕ = 0.058 based on the University of Melbourne PFR [176]. Mechanism M2 [169] predictions presented for ternary mixtures of OTE25_LowT and OTE25_HighT.

For these ternary mixtures, the predictions indicate formaldehyde levels to be 3 times greater compared to acetaldehyde. The higher formaldehyde can be associated with the greater proportion of iso-octane and toluene in the mixtures, both of which are precursors to formaldehyde. Furthermore, the model predicted that OTE25_LowT produced greater

formaldehyde than OTE25_HighT. This is in line with the experimental findings and can be linked to the greater proportion of iso-octane in the OTE25_LowT fuel, as detailed in Section 3.2, which has been shown to produce greater engine-out formaldehyde emissions than toluene as seen in Section 5.2. Similarly, the PFR model also predicted that iso-octane leads to greater formaldehyde than toluene as seen in Section 7.2.

The PFR model also finds OTE25_LowT produced less acetaldehyde than OTE25_HighT along the reactor, which contradicts the experimental findings. However, this difference was noted in the primarily at the peak concentration were OTE25_HighT produced 16 % less formaldehyde than acetaldehyde. This could be due to the operating conditions of the PFR. To understand if this is the case, the two ternary mixtures were studied in the PSR model too.

Figure 7.10 presents the formaldehyde and acetaldehyde levels as determined by the PSR model across a range of temperatures at 18 bar. In line with the experimental findings of this work and the PFR model predictions, the model estimates higher formaldehyde levels compared to acetaldehyde throughout the temperature range. The model indicated similar acetaldehyde quantities for both fuels, though at certain temperatures between 750 K and 850 K, the OTE25_HighT showed lower formaldehyde production than OTE25_LowT. This observation aligns with PFR model results.

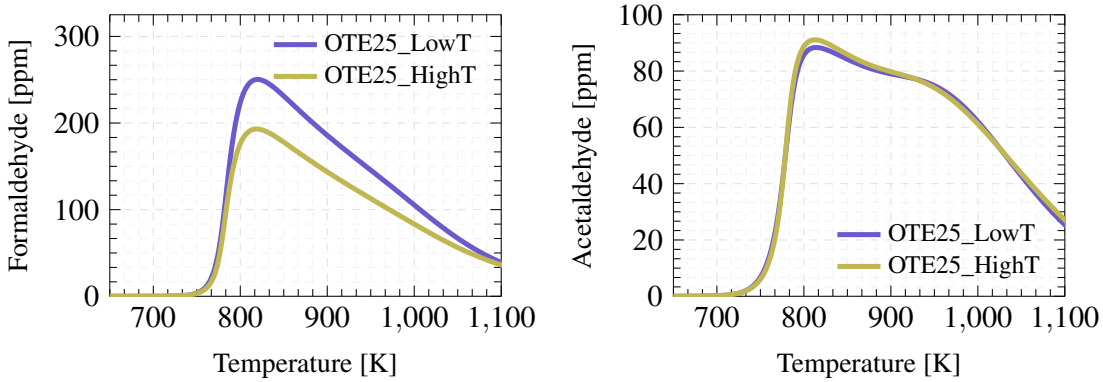

(a) Formaldehyde from PSR model **(b)** Acetaldehyde from PSR model

Figure 7.10: Species concentration profile predictions using Mechanism M2 [169] of **(a)** formaldehyde and **(b)** acetaldehyde for ternary mixtures of OTE25_LowT and OTE25_HighT. The reactant quantity of 0.2 % with 0.6 % oxygen (O_2), and 99.2 % nitrogen (N_2) was based on the University of Orleans JSR at conditions of τ = 0.7 s, ϕ = 1.0, pressure of 18 bar, and temperature range from 650 K to 1100 K [172].

In general, both the PFR and PSR model suggest that increasing the toluene concentration led to a greater increase in formaldehyde levels than the acetaldehyde levels. This agrees with the experimental findings from Section 5.4.1 which found formaldehyde to be over 30 % lower and acetaldehyde to be 25 % lower with OTE25_HighT than OTE25_LowT.

7.4.2 Iso-octane, n-heptane, and toluene

The set of ternary mixtures that contained no ethanol was referred to as OHT. Similar to OTE25, low and high concentration of toluene were assessed to further understand its impact on aldehyde emissions when ethanol is not in the blend. The ternary mixtures were simulated in the PFR model at 15 bar and 800 K. The formaldehyde and acetaldehyde levels along the reactor are shown in Figure 7.11 (a) and (b), respectively.

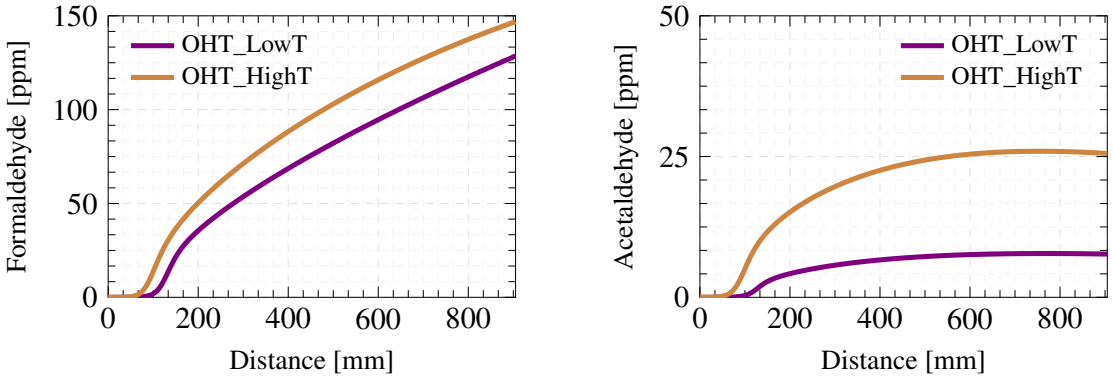

(a) Formaldehyde from PFR model **(b)** Acetaldehyde from PFR model

Figure 7.11: Species concentration profiles of intermediate **(a)** formaldehyde and **(b)** acetaldehyde at 800 K, 15 bar, and ϕ = 0.058 based on the University of Melbourne PFR [176]. Mechanism M2 [169] predictions presented for ternary mixtures of OHT_LowT and OHT_HighT.

With the lack of ethanol, the reaction progression slows down. This is evident as the formaldehyde concentration continues to increase towards the reactor end, whereas acetaldehyde levels reach a plateau. Despite n-heptane's presence, its relatively low proportion in comparison to iso-octane and toluene resulted in a slow reaction rate in both OHT mixtures. Although similar trends were observed in both OHT blends, the OHT_HighT fuel produced a larger amount of aldehydes, particularly noticeable in the case of acetaldehyde. The peak formaldehyde levels predicted were consistent with those

in previously modelled fuels, though the acetaldehyde concentrations remained below 25 ppm for both mixtures.

The two OHT mixtures were also analysed using the PSR model. Figure 7.12 shows the formaldehyde and acetaldehyde concentrations across the temperature range at 18 bar.

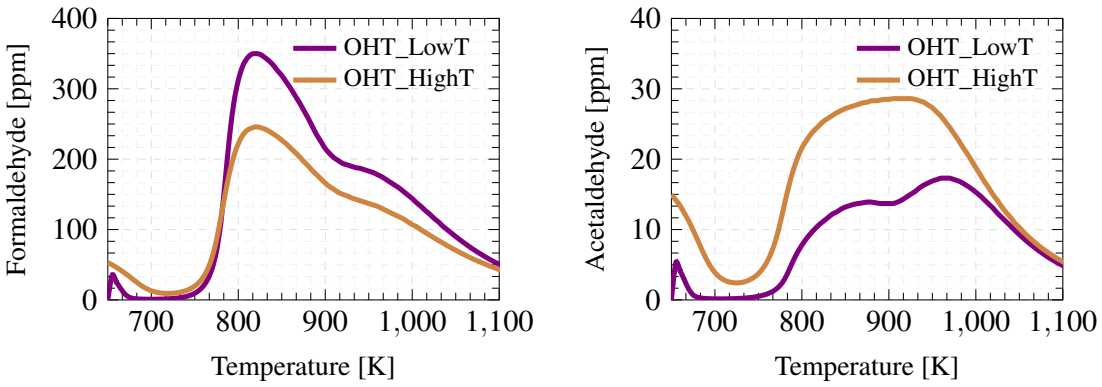

(a) Formaldehyde from PSR model **(b)** Acetaldehyde from PSR model

Figure 7.12: Species concentration profile predictions using Mechanism M2 [169] of **(a)** formaldehyde and **(b)** acetaldehyde for ternary mixtures of OHT_LowT and OHT_HighT. The reactant quantity of 0.2 % with 0.6 % oxygen (O_2), and 99.2 % nitrogen (N_2) was based on the University of Orleans JSR at conditions of τ = 0.7 s, ϕ = 1.0, pressure of 18 bar, and temperature range from 650 K to 1100 K [172].

In line with the PFR model findings, formaldehyde levels were higher than those of acetaldehyde. However, in contrast to PFR findings, the OHT_LowT led to greater acetaldehyde levels than OHT_HighT. The two stage temperature was noticeable and additionally a spike in both formaldehyde and acetaldehyde below 700 K. The latter observation was not present in the earlier PSR model tests. It is assumed that the addition of ethanol suppresses reactivity at lower temperatures (< 700 K).

7.5 Surrogate fuels

In addition to fuels designed for research purposes, surrogate fuels, with physical and combustion properties designed to match gasoline characteristics were simulated. These include PRFs and TPRFs. The effect of 20 %v/v and 85 %v/v ethanol addition on the PRFs and TPRFs on aldehyde levels in the reactor models is studied in this section.

7.5.1 PRF versus PRF-E

Figure 7.13 shows the formaldehyde and acetaldehyde concentrations along the PFR at 800 K and 15 bar for HO95 (PRF), OHE20 (PRF-E20), and OHE85 (PRF-E85). The formaldehyde levels across these fuels were comparable. However, the ethanol addition in the fuel mixture resulted in an earlier onset of formaldehyde formation and consumption. Compared to the observations with OE mixtures (Figure 7.3), the inclusion of n-heptane did not affect the formaldehyde formation. While the FA:AA exceeded 1 for HO95 and OHE20, it was lower for OHE85, aligning with the experimental findings for these fuels. The greater proportion of iso-octane in these fuels leads to the higher formaldehyde levels, as observed in the experiments (Section 5.2) and simulations (Section 7.2). The presence of both ethanol and n-heptane accelerated the reaction progress compared to their OE mixture counterparts, leading to the formation and consumption of both aldehydes within the reactor's length.

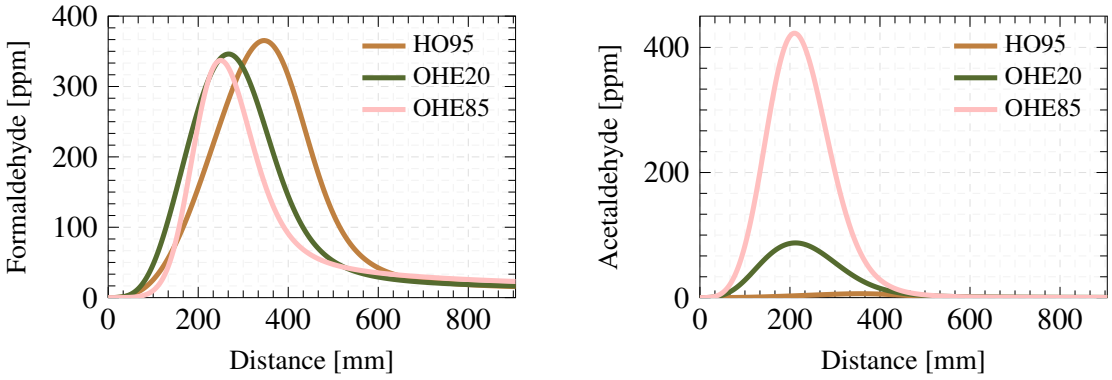

(a) Formaldehyde from PFR model **(b)** Acetaldehyde from PFR model

Figure 7.13: Species concentration profiles of intermediate **(a)** formaldehyde and **(b)** acetaldehyde at 800 K, 15 bar, and ϕ = 0.058 based on the University of Melbourne PFR [176]. Mechanism M2 [169] predictions presented for ternary mixtures of HO95 (PRF), OHE20 (PRF-E20), and OHE85 (PRF-E85)

The formaldehyde and acetaldehyde concentrations from the three PRF-based surrogate fuels were estimated using the PSR model, as shown in Figure 7.14.

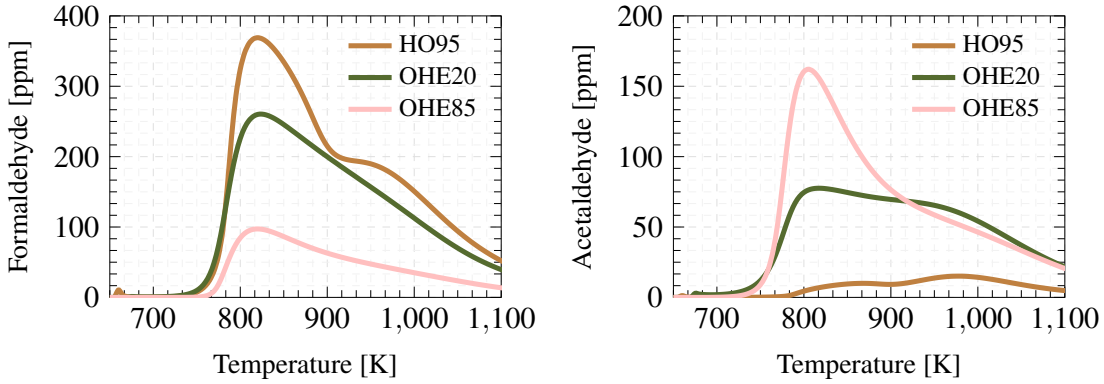

(a) Formaldehyde from PSR model **(b)** Acetaldehyde from PSR model

Figure 7.14: Species concentration profile predictions using Mechanism M2 [169] of **(a)** formaldehyde and **(b)** acetaldehyde for HO95 (PRF), OHE20 (PRF-E20), and OHE85 (PRF-E85). The reactant quantity of 0.2 % with 0.6 % oxygen (O_2), and 99.2 % nitrogen (N_2) was based on the University of Orleans JSR at conditions of τ = 0.7 s, ϕ = 1.0, pressure of 18 bar, and temperature range from 650 K to 1100 K [172].

The HO95 mixture resulted in the highest formaldehyde production, with a second stage of formation at 900 K. Consistent with the behaviour observed in OE mixtures, the OHE85 mixture, which has the highest ethanol content, produced the least formaldehyde. However, OHE85 generated the most acetaldehyde. At higher temperatures (above 900 K), OHE20 produced more acetaldehyde, due to the presence of iso-octane and n-heptane. This trend, also observed in OE mixtures, indicates that while ethanol is a primary precursor for acetaldehyde, in mixtures with a lower ethanol content, there is an increased potential for acetaldehyde formation over an extended temperature range, though at lower concentrations.

7.5.2 TPRF versus TPRF-E

This study extended to toluene inclusive PRFs, referred to as TPRFs, to analyse the effects of ethanol addition on aldehyde formation in gasoline surrogates with improved representation of commercial fuel properties. Specifically, the OHT_HighT mixture, previously evaluated in the context of ternary fuels (as discussed in Section 7.4), was also designed to serve as a TPRF. To this surrogate, ethanol was added in volumes of 20 % and 85 %, resulting in THOE20 and THOE85 blends, respectively. Figures 7.15 (a)

and (b) shows the formaldehyde and acetaldehyde concentrations, respectively, for these blends, as predicted by the PFR model at 800 K and 15 bar.

In the PFR model, THOE20 was found to produce more formaldehyde than OHT_HighT. However, the results also indicated a negligible amount of formaldehyde and a delayed onset of acetaldehyde formation in the THOE85 blend. Due to the delayed acetaldehyde formation, it is difficult to assess whether the peak concentration would be greater than the other two surrogates. If it would not be greater, then the PFR model's findings would be contrary to experimental findings, as higher ethanol content in the THOE blends should result in increased acetaldehyde production compared to THOE20.

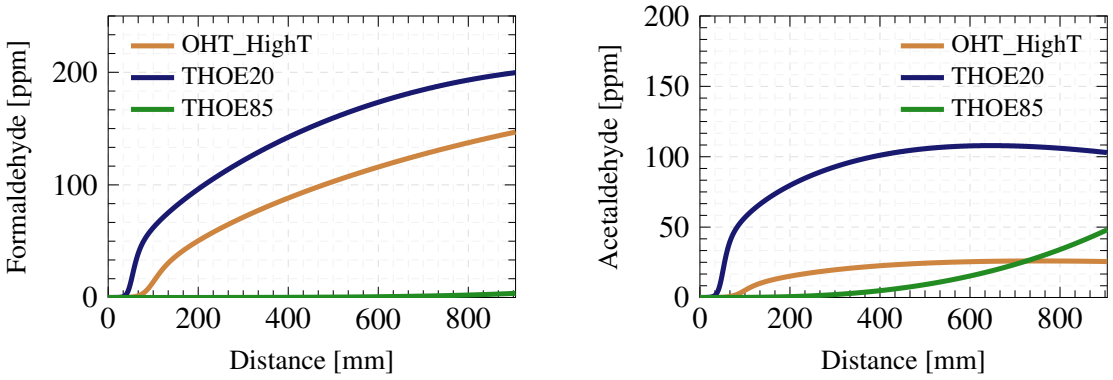

(a) Formaldehyde from PFR model **(b)** Acetaldehyde from PFR model

Figure 7.15: Species concentration profiles of intermediate **(a)** formaldehyde and **(b)** acetaldehyde at 800 K, 15 bar, and ϕ = 0.058 based on the University of Melbourne PFR [176]. Mechanism M2 [169] predictions presented for ternary mixtures of OHT_HighT (TPRF), THOE20 (TPRF-E20), and THOE85 (TPRF-E85).

Furthermore, the greater presence of ethanol in THOE85 was assumed to accelerate acetaldehyde formation, similar to the difference observed between THOE20 and OHT_HighT and previous findings throughout the modelling study. This unusual behaviour may be due to a potential modelling challenge with the THOE85 blend. To further investigate these anomalies, the three mixtures were analysed using the PSR model across the temperature range at 18 bar. The resulting formaldehyde and acetaldehyde concentrations are shown in Figures 7.16 (a) and (b), respectively.

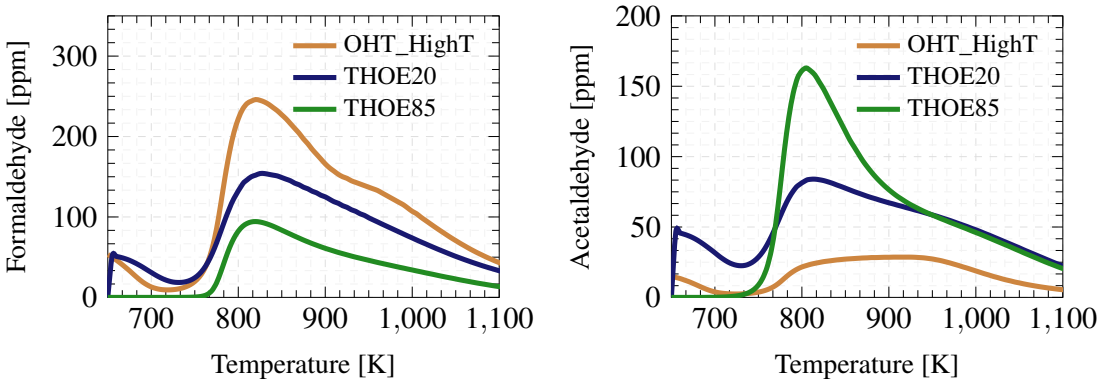

(a) Formaldehyde from PSR model **(b)** Acetaldehyde from PSR model

Figure 7.16: Species concentration profile predictions using Mechanism M2 [169] of **(a)** formaldehyde and **(b)** acetaldehyde for OHT_HighT (TPRF), THOE20 (TPRF-E20), and THOE85 (TPRF-E85). The reactant quantity of 0.2 % with 0.6 % oxygen (O_2), and 99.2 % nitrogen (N_2) was based on the University of Orleans JSR at conditions of τ = 0.7 s, ϕ = 1.0, pressure of 18 bar, and temperature range from 650 K to 1100 K [172].

At 800 K, similar to the PFR model settings, the PSR model suggests that THOE85 would lead to peak formations of formaldehyde and acetaldehyde. Therefore, the PFR model findings for THOE85 were inaccurate.

Figure 7.16 displays that OHT_HighT produced more formaldehyde compared to the other two surrogates containing ethanol. The experimental results shows that all three surrogates produced similar levels of formaldehyde. Therefore, this suggests the mechanism, when used in the PSR model, over-predicts the influence of iso-octane on formaldehyde formation and under-estimates the impact of ethanol. While iso-octane exhibits early formation of the methyl radical during oxidation, leading to formaldehyde production, the branching ratio of reactions that result in formaldehyde from ethanol is lower. However, it is important for the chemical kinetic mechanisms to account for the various pathways through which formaldehyde can be generated from ethanol across a range of temperatures. This behaviour was also noted when the pure fuels were simulated in the PSR model as seen in Section 7.2.

For acetaldehyde, however, the PSR model finds that the trend was reversed with THOE85 producing greater peak concentrations across the temperature range, similar to the behaviour observed with the other surrogates. Nevertheless, at lower temperatures

(< 750 K), the PSR model indicates that THOE20 leads to greater acetaldehyde than the other two TPRF based surrogates. When compared to the PRF surrogate, the addition of toluene resulted in higher acetaldehyde levels than predicted for the PRF surrogate under the same PSR model conditions. This suggests the mechanism predicts toluene to enhance acetaldehyde formation, whereas the experimental results shows that toluene's presence inhibits acetaldehyde formation. Improved understanding of the interactions between toluene and ethanol in the mechanism is required.

The PSR model also reports that the peak concentration observed during formaldehyde formation occurred later and spanned a wider temperature range compared to acetaldehyde. This is in line with literature which suggests formaldehyde formation occurs at higher temperatures than acetaldehyde [190].

7.6 Summary

All fuels, ranging from pure to surrogate, were simulated using tailor-made PFR and PSR reactor models in ChemkinPro 19.0 [165]. Key findings include:

- *Pure fuels*: In the PFR model, ethanol produced more acetaldehyde than iso-octane and toluene, with similar formaldehyde levels between ethanol and iso-octane but lower for toluene. Ethanol also showed faster reaction progress. In the PSR model, iso-octane had the highest formaldehyde levels, whereas ethanol produced significantly lower formaldehyde. Whilst the oxidation of iso-octane leads to methyl radicals which can oxidise to formaldehyde, ethanol also exhibits reaction pathways that can lead to formaldehyde. This behaviour was captured by the mechanism at one pressure and temperature condition in the PFR model, but not at a higher pressure across the temperature range in the PSR model. Additionally, the PSR model predicted formaldehyde exceeded acetaldehyde quantities across the temperature range, even for ethanol. This needs to be explored further. On the other hand, in comparison to other pure fuels, ethanol dominated acetaldehyde production across all reactors due to the α-hydroxyethyl reactions.

- *Iso-octane and ethanol*: Mixtures showed comparable formaldehyde levels in the PFR, but decreasing formaldehyde generation as ethanol content increased, in line with the pure fuels predictions, in the PSR model. However, the engine experimental data showed increasing formaldehyde with ethanol content. Therefore, across the temperature range, the mechanism needs to account for ethanol's oxidation pathways to formaldehyde. Nevertheless, all the reactor models showed that higher ethanol content resulted in increased acetaldehyde. Iso-octane's slower reaction rate extended the temperature range in which acetaldehyde was formed for ethanol in the OE20 mixture.

- *Toluene and ethanol*: The addition of toluene to ethanol reduces overall aldehyde generation, especially acetaldehyde, and slows reaction progress in the PFR, extending aldehyde presence. This is agreement with the experimental findings of this work and the PSR model predictions for acetaldehyde. However, the PSR model also estimates toluene increases formaldehyde. This could be attributed to Reaction 10 shown in Section 7.2, however, was not observed in the PFR model predictions or from the engine experimental results. Therefore, it is assumed for a range of temperatures at higher pressures, the mechanism may over-predict the influence of toluene on formaldehyde generation which needs to be re-evaluated.

- *N-heptane and ethanol*: Similar to TE mixtures, ethanol's higher aldehyde production was offset by n-heptane addition, reducing peak aldehyde formation, especially for acetaldehyde. N-heptane displayed faster reactivity which led to the HE mixtures to have quicker reaction progression than ethanol. This can be expected as n-heptane has a high laminar flame speed, as discussed in Section 4.6.1. Adding n-heptane increased both formaldehyde and acetaldehyde production across the temperature range, particularly for acetaldehyde. This finding is contrary to the engine experimental results where n-heptane showed the strongest ability to suppress acetaldehyde. This could be attributed to n-heptane's low temperature reactivity enhancing aldehyde generation from ethanol, though this would require further investigation as the conditions tested in this study were limited.

- *OHT*: Ternary OHT mixtures without ethanol had lower aldehyde production, especially acetaldehyde. The PFR model indicated slower reaction rates for OHT mixtures and greater aldehyde formation for the OHT blend with higher toluene. The PSR model showed higher formaldehyde but less acetaldehyde in OHT_LowT compared to OHT_HighT with a two-stage aldehyde formation process. These models showed varied results on the influence of toluene on formaldehyde generation, though they both showed acetaldehyde decreases with higher toluene content. The latter finding is in agreement with the literature (Section 2.2), pure fuel experimental (Section 5.2) and modelling (Section 7.2) results as toluene does not have explicit reaction pathways that lead to acetaldehyde. Nevertheless, toluene's impact on formaldehyde requires additional evaluation.

- *OTE25*: Ternary mixtures with ethanol showed higher aldehyde levels than OHT mixtures. This is in agreement with experimental results as ethanol would increase both formaldehyde and acetaldehyde generation. OTE25_LowT produced higher concentrations of formaldehyde than OTE25_HighT, with the opposite for acetaldehyde. The PSR model indicated higher formaldehyde but similar acetaldehyde levels for OTE25_LowT.

- *PRF and PRF-E*: The PFR model showed PRF mixtures with and without ethanol producing similar formaldehyde levels, but higher ethanol content led to increased acetaldehyde production. The PSR model agreed with this for acetaldehyde, however, mixtures with less ethanol yielded greater formaldehyde. This suggests that less ethanol in PRF increases formaldehyde, while increasing ethanol concentration shifts the ratio towards acetaldehyde. Though this is similar to previous observations from the PSR model, improved predictions of iso-octane's influence on formaldehyde generation is required.

- *TPRF and TPRF-E*: The PFR model showed unusual predictions for high ethanol TPRF blends. In the PSR model, TPRF-E85 led to lower formaldehyde but higher acetaldehyde compared to lower ethanol containing blends. This indicates that ethanol addition in surrogate fuels increases acetaldehyde emissions more

than formaldehyde. This supports the experimental findings that ethanol is a key precursor for acetaldehyde.

8

Results: Real-driving emissions

Contents

8.1 Motivation

In addition to conducting emissions testing in a laboratory-based engine test cell, it is beneficial to measure aldehyde emissions under representative real-driving conditions. Emissions Analytics has developed a practical method for measuring and speciating hydrocarbons, including formaldehyde and acetaldehyde, in real-world scenarios, as detailed in Section 3.4. To evaluate this capability, two analyses were carried out on previously collected data, with details provided in Section 8.2. Building on these preliminary studies, a comprehensive investigation was undertaken, focussing on controlled fuel and vehicle operating parameters. The methodology and results of this investigation are described in Sections 3.5.3 and 8.3.1, respectively.

8.2 Initial scoping studies

Two datasets from earlier studies were examined to assess the feasibility of measuring real-driving aldehyde emissions. The first dataset involved testing of nine vehicles. Regulated emissions from these vehicles were measured using the SEMTECH-LDV PEMS at a frequency of 1 Hz. Simultaneously, the VOCs system was used to capture unregulated emissions, categorising them based on different driving conditions. For further information on the equipment used, refer to Section 3.4. All tested vehicles were models from 2020-21, adhering to the Euro 6d-TEMP emissions standards. These were primarily small- to medium-sized vehicles powered by an ICE, using gasoline as fuel. It should be noted that these vehicles were only used for the initial scoping study. The fuel used was commercial market gasoline, probably E10, although the precise composition of the fuel was not verified. The primary aim of this initial analysis was to determine the ability of the VOCs system to detect acetaldehyde emissions from modern gasoline vehicles and to differentiate emission levels under a variety of driving conditions. Formaldehyde was not measured in this dataset.

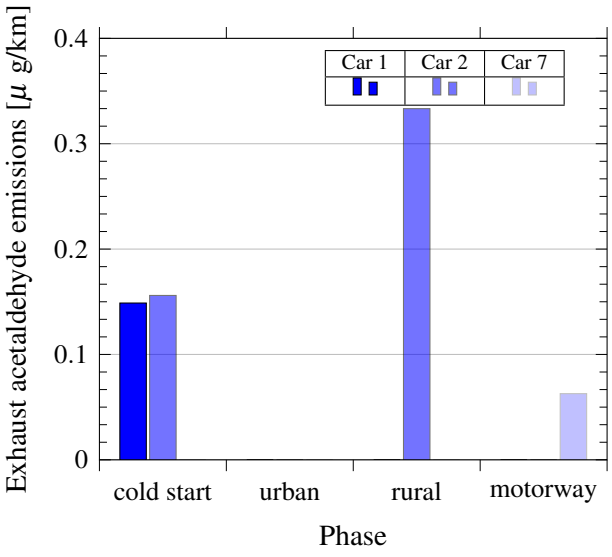

Figure 8.1: Tailpipe exhaust acetaldehyde emissions for Cars 1, 2, and 7 (represented by varying shades of blue) across four different driving modes with commercial gasoline.

The results shown in Figure 8.1 indicate that acetaldehyde emissions exceeded the measuring threshold of the equipment for only three of the nine vehicles tested. Among

these, acetaldehyde was detected in two vehicles during the cold-start condition, but not in any vehicle during urban driving conditions. For rural and motorway conditions, acetaldehyde emissions were observed in one vehicle each. Specifically, Car 2 emitted acetaldehyde during both cold-start and rural conditions, while Cars 1 and 7 emitted acetaldehyde only during cold-start and motorway conditions, respectively. Although the measured quantities were low, the VOCs measuring equipment proved capable of detecting the differences between the emission levels across different driving phases. Interestingly, the emissions recorded during cold-start were lower than those in rural conditions.

In the second dataset, a 2021 model year vehicle meeting the Euro 6d-TEMP emissions standards was examined using both E0 and E20 fuels. The aim of this second analysis was to assess the capability of the VOCs system in detecting formaldehyde emissions and in differentiating between the two fuel types. As shown in Figure 8.2, formaldehyde emissions were found to be higher with E20 fuel compared to E0 fuel.

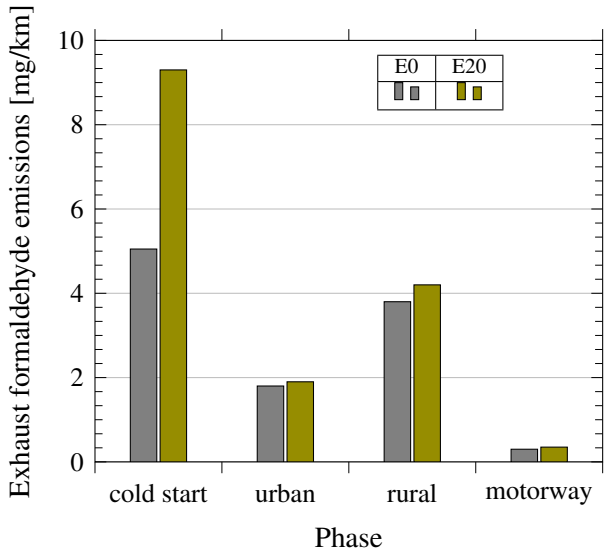

Figure 8.2: Tailpipe exhaust formaldehyde emissions for E0 (gray) and E20 (olive) fuels with one vehicle across four different driving modes.

As the Emissions Analytics equipment successfully identified formaldehyde and acetaldehyde emissions under real-driving conditions in modern gasoline vehicles, a detailed study was initiated to investigate the effects of ethanol and fuel composition on aldehyde emissions.

8.3 E0 and E10 fuels

8.3.1 Vehicle data

As aldehydes are formed during ethanol's low-temperature oxidation, this study investigated the influence of ethanol's presence in market-like gasoline on aldehyde emissions and other tailpipe outputs under real-driving conditions. Two bespoke fuels were designed and blended through refinery streams by Coryton. These were E0 (no ethanol) and E10 (10 %v/v ethanol), with their details found in Section 3.2. These fuels with known composition and properties were then individually tested across four vehicles, with the test procedure described in Section 3.5.3. The resulting aldehyde emissions were supported with data from single-cylinder engine-out measurements.

Formaldehyde

Figure 8.3 shows the tailpipe exhaust formaldehyde emissions from across all four vehicles tested. The highest levels of formaldehyde emissions were observed during the cold-start (CS) phase, while the lowest emissions occurred during the motorway (M) driving phase. This trend was consistent with both E0 and E10 fuels, as shown in Figure 8.3. These results are likely because during cold-start there could be due to lower combustion and exhaust temperatures, along with the prolonged warm-up time required for the after-treatment system.

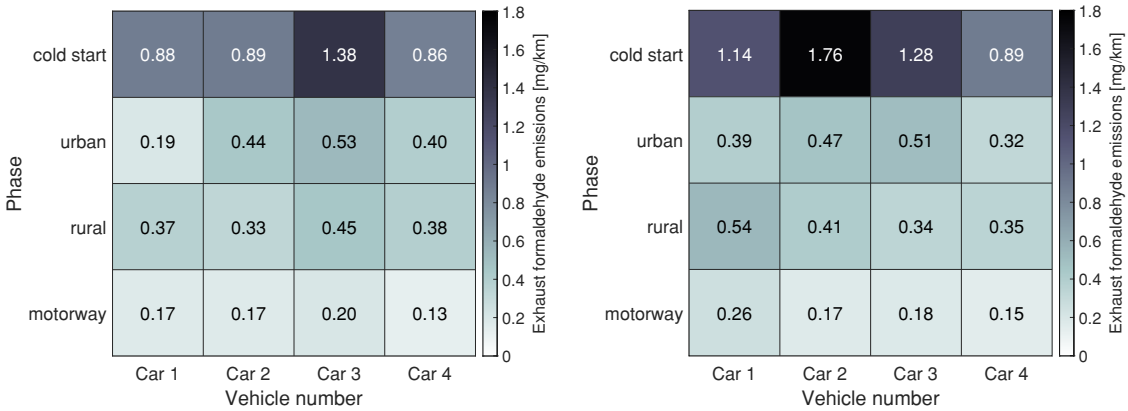

(a): Formaldehyde with E0 fuel **(b):** Formaldehyde with E10 fuel

Figure 8.3: Tailpipe exhaust formaldehyde emissions (mg/km) across the four different vehicles (columns) and driving conditions (rows) with the **(a)** E0 and **(b)** E10 fuels.

For each vehicle, the relative levels of formaldehyde emissions were comparable across the respective driving phases and fuel types. Cars 1, 2, and 4 exhibited an increase in formaldehyde emissions by about 30 % when fuelled with E10 compared to E0. The differences in emissions among the vehicles were more visible during the cold-start condition. For instance, Car 2 showed an increase by a factor of 2 for formaldehyde emissions with E10 fuel during cold-start. In contrast, Car 3 demonstrated a reduction of 12 % on average across all driving conditions in formaldehyde emissions when using E10 compared to E0.

During the motorway driving phase, high temperatures likely facilitated the combustion of formaldehyde in cylinder, while the after-treatment system would have removed any remaining emissions. However, during the rural (R) and urban (U) phases, formaldehyde emissions were comparable for both fuel types. This finding is different from the literature, which suggests that urban driving, often characterised by frequent stop-and-start scenarios, should result in lower exhaust temperatures and consequently higher formaldehyde emissions. To further investigate this, Figure 8.4 presents the percentage (%) of time the exhaust temperature, measured remained below 350 °C for each vehicle under both fuel types across various driving modes. This temperature threshold of 350 °C was chosen as the criterion because it effectively distinguishes the differences between the fuels and driving conditions, particularly in comparison with other temperatures in the range of 300°C to 400 °C that were also reviewed.

Figure 8.4 indicates that during the majority of the cold-start phase, the exhaust temperature remained below 350 °C. In contrast, during the motorway conditions, the opposite was observed, with temperatures predominantly above this threshold. In both urban and rural conditions, the exhaust temperatures fell below 350 °C for a similar duration, although variances were observed among the different vehicles. For Cars 1, 2, and 4, the exhaust temperatures were lower for a more extended period during the rural phase than in the urban phase. These observations support the hypothesis that higher formaldehyde emissions occur at lower exhaust temperatures, thus explaining the increased formaldehyde emissions observed under rural driving conditions.

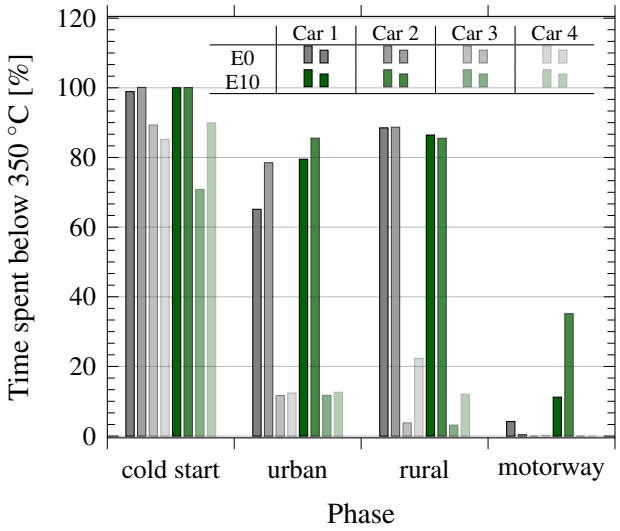

Figure 8.4: Tailpipe exhaust temperature below 350 °C represented as a percentage (%) of time in each of the driving modes for the E0 (gray) and E10 (green) fuels with the four cars (represented by varying shades of each color).

Acetaldehyde

For all four vehicles, driving segments, and both fuels, tailpipe exhaust acetaldehyde emissions were undetectable. As acetaldehyde is often present in studies involving ethanol-blended fuels, this outcome suggests that the exhaust after-treatment systems in these vehicles were effectively removing acetaldehyde. While Bielaczyc *et al.* [127] reported nearly equal efficacy in the removal of formaldehyde and acetaldehyde by the exhaust after-treatment system in Euro 5 specifications vehicles, the results from the current study present a different scenario for vehicles complying to the Euro 6d-TEMP emissions specification. In this latter case, formaldehyde emissions were detected, but acetaldehyde emissions were not, despite the equipment being able to do so as seen in Section 8.3.1.

Aldehydes and alcohols

Alcohols are commonly recognised precursors of intermediate aldehydes. The VOCs system was able to distinctively speciate alcohols and aldehydes with low carbon atom numbers. Therefore, an analysis was conducted to explore the correlation between the total tailpipe exhaust alcohols and aldehydes, each up to C_7. Although the fuel did not contain higher carbon atom number alcohols ($\geq C_3$), they can still be formed as

intermediate products during the oxidation of other fuel components. C_2 to C_7 alcohols and aldehydes were selected for analysis, as they represent a substantial portion of the total emissions in their respective categories.

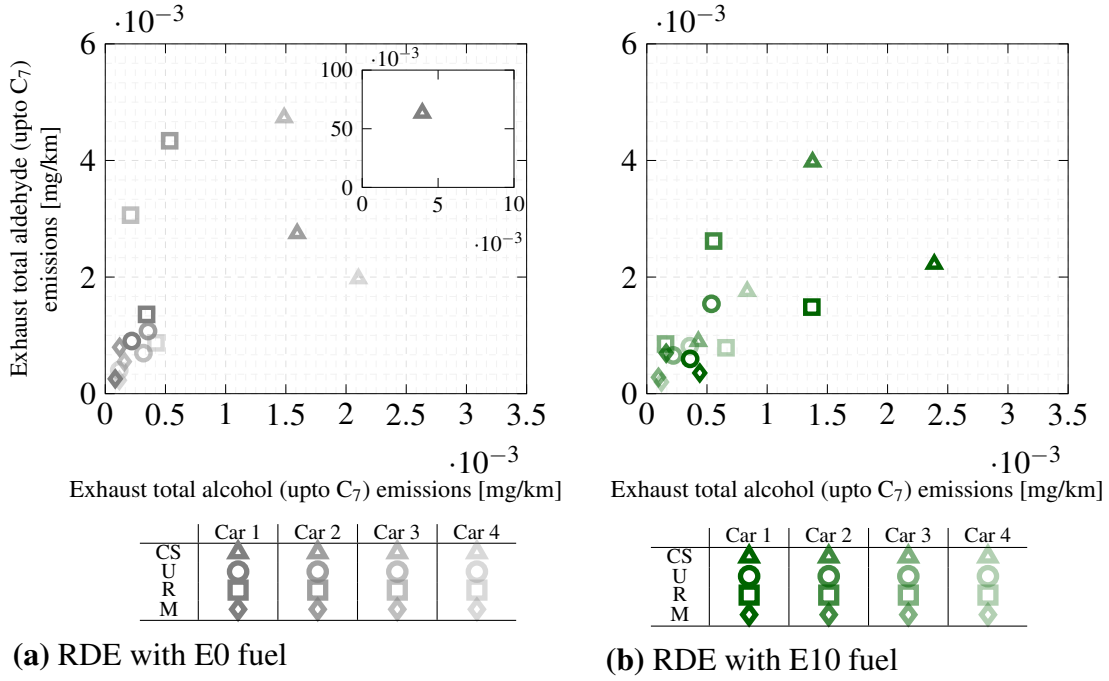

(a) RDE with E0 fuel

(b) RDE with E10 fuel

Figure 8.5: Total tailpipe exhaust aldehyde and alcohol (up to C_7) emissions (mg/km) for all four vehicles (represented by varying shades of gray) with the **(a)** E0 fuel and **(b)** E10 fuel (green). Driving phases: cold-start (CS) (triangle), urban (U) (circle), rural (R) (square), and motorway (M) (diamond). Insert plot shows anomaly data.

Figure 8.5 (a) shows that with E0 fuel, total tailpipe exhaust alcohol emissions were generally lower than aldehyde emissions, especially during motorway, rural, and urban driving conditions. In the rural phase for Cars 2 and 3, the ratio of aldehyde to alcohol emissions was approximately 9:1. Similar behaviour was observed during the cold-start condition, although the data across the four vehicles displayed greater variation compared to other driving conditions. During the cold-start phase, Car 1 exhibited anomalous behaviour with high levels of both alcohol and aldehyde emissions, potentially due to its older age, higher mileage, and consequently a more used after-treatment system. Nonetheless, the overall trend persisted, with total aldehyde emissions being about 10 times higher than the respective total alcohol emissions. These findings suggest that in

the combustion of the hydrocarbons in E0 fuel, the intermediate formation of alcohols is lower than that of aldehydes.

In Figure 8.5 (b), the data for E10 fuel shows a trend similar to that of E0, where the total tailpipe exhaust emissions of alcohol and acetaldehyde fall within the same ranges. However, when compared to E0 fuel, the ratio of aldehyde to alcohol emissions with E10 is significantly lower, particularly during the motorway, urban, and rural phases. Additionally, the correlation between alcohol and aldehyde emissions is less prominent with E10 fuel. As the E10 fuel comprises 10 %v/v ethanol, there is an inherently higher potential for increased unburned alcohol emissions compared to E0 fuel. Despite this, the total aldehyde emissions do not show a significant increase with E10 fuel.

Benzaldehyde and toluene

The VOCs system also showed its capability to detect tailpipe exhaust emissions of benzaldehyde and toluene across all driving conditions and in each of the four vehicles tested. As toluene is a known precursor for benzaldehyde, this analysis contributes to understanding how fuel composition influences tailpipe exhaust emissions of these compounds. Whilst benzaldehyde was not the primary focus of this work, it is still an aromatic aldehyde emission which has previously been linked to increased ethanol-blended gasoline [65, 191].

Figure 8.6 (a) shows that, with the exception of Car 1 during cold-start conditions, toluene emissions were significantly higher than benzaldehyde emissions. This could be due to its higher mileage and consequently more used after-treatment system, potentially leading to reduced emission reduction efficacy. On average, toluene emissions were found to be 20 times higher than those of benzaldehyde for E0. This difference could be due to toluene originating from unburned fuel components, as suggested by Zervas *et al.* [192, 193], who observed that non-aromatic fuel components do not contribute to toluene production in exhaust emissions.

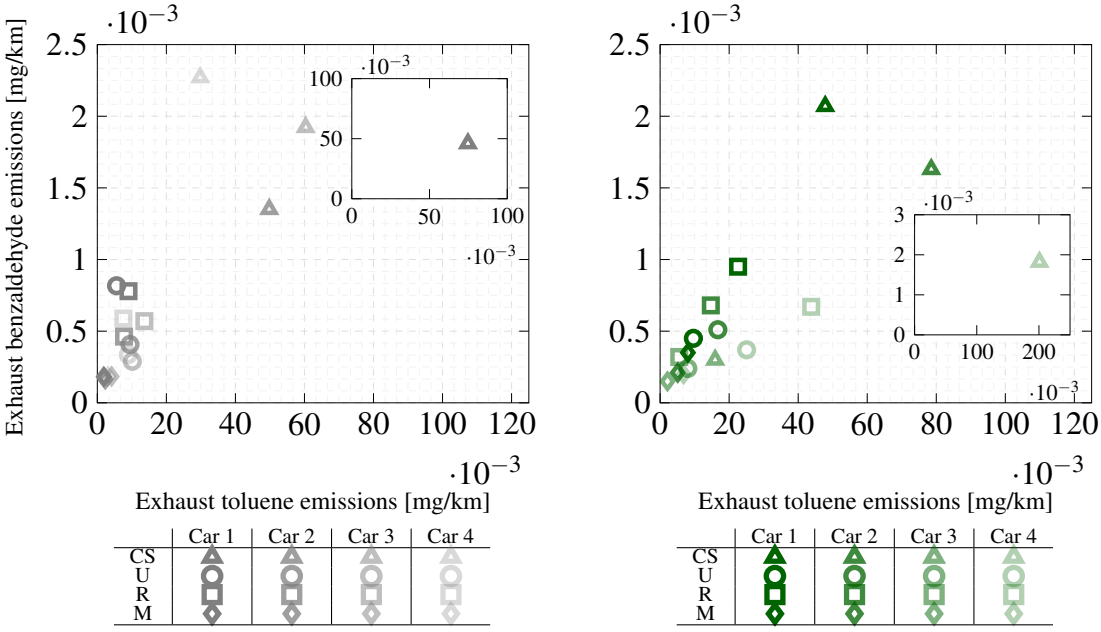

(a) RDE with E0 fuel **(b)** RDE with E10 fuel

Figure 8.6: Tailpipe exhaust benzaldehyde and toluene emissions (mg/km) for all four vehicles (represented by varying shades of gray) with the **(a)** E0 fuel and **(b)** E10 fuel (green). Driving phases: cold-start (CS) (triangle), urban (U) (circle), rural (R) (square), and motorway (M) (diamond). Insert plot top right to show anomaly data.

Similar to other emissions detected by the VOCs system, both toluene and benzaldehyde emissions were highest during cold-start and lowest during motorway conditions. Specifically, during motorway driving, emissions of toluene and benzaldehyde were about 20 and 10 times lower, respectively, than during cold-start conditions.

The levels of toluene and benzaldehyde emissions were more consistent during motorway conditions compared to the variability seen at cold-start. The latter condition, influenced by a range of factors such as engine and exhaust after-treatment temperatures, could affect the complex chemistry of toluene oxidation, leading to inconsistent results among the vehicles. Moreover, across the different driving modes, from cold-start to motorway, the toluene-to-benzaldehyde ratio decreased from 27 to 16 (with the exception of Car 1) for E0. This finding supports the conclusion that at lower temperatures, the oxidation process converting toluene to benzaldehyde is less efficient.

With the E10 fuel, the benzaldehyde to toluene ratio was lower across all driving conditions and vehicles, with this behaviour exaggerated for Car 1 at the cold-start

condition as shown in Figure 8.6 (b). Therefore, it is assumed that less of the stable intermediate benzaldehyde was formed from toluene's oxidation. For both fuels, the aromatic content was kept consistent. Therefore, this trend could be attributed to the addition of ethanol which led to lower combustion mixture temperature as the ethanol-gasoline blended fuel had a higher latent heat of vapourisation. However, the literature presents competing results as Zervas *et al.* [193] found low oxygenate content fuels to slightly enhance benzaldehyde formation, whereas Magnusson *et al.* [194] found the formation of benzaldehyde from ethanol was negligible.

For this investigation on the E10 fuel, on average, the toluene emissions were 34 times greater than the benzaldehyde emissions across the different driving phases and vehicles. Similar to the trends observed with the E0 fuel, the toluene-to-benzaldehyde ratio decreased from 42 to 24 between the cold-start and motorway driving phases. Furthermore, the relative magnitude of tailpipe benzaldehyde and toluene emissions were similar between the E0 and E10 fuels.

8.3.2 Engine data

To evaluate if the E0 and E10 fuels show similar behaviour in a controlled environment as observed in real-driving emissions, this section of the investigation focusses on analysing the engine-out formaldehyde and acetaldehyde emissions with the single-cylinder engine.

Formaldehyde

To better understand the impact of the fuel prior to the exhaust temperature effects, the engine-out formaldehyde emissions from the laboratory engine at 1100 and 1500 rpm, and 2 and 3 bar were evaluated as shown in Figure 8.7. Both fuels, E0 and E10, were tested. The error bars present the maximum and minimum readings across the 300 cycles of each of the three repeats.

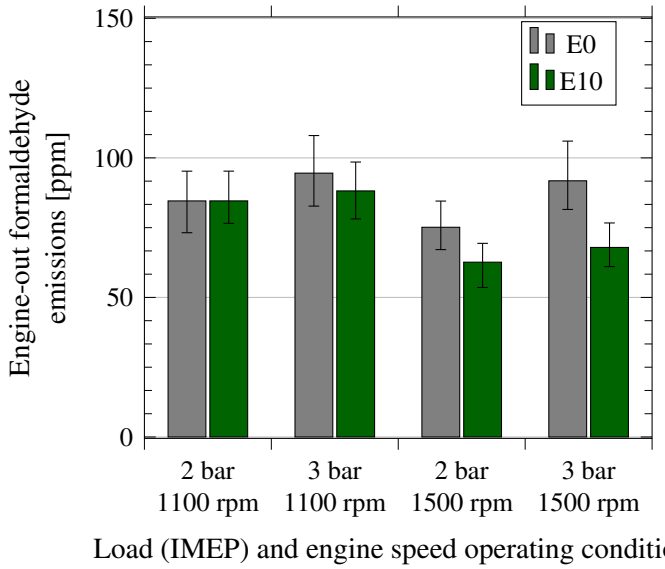

Figure 8.7: Engine-out formaldehyde emissions for E0 (gray) and E10 (green) at engine speeds of 1100 rpm and 1500 rpm and engine loads of 2 and 3 bar IMEP at stoichiometric conditions. Ignition timing was fixed for all fuels at -46.3 °CA aTDCf. Throttle position and fuel injection quantity were varied to maintain similar load (nIMEP). Error bars represent minimum and maximum emissions over three runs of 300 cycles each.

Interestingly, for most operating conditions except at 1100 rpm and 2 bar, a decrease in engine-out formaldehyde emissions was observed with E10 fuel compared to E0 fuel. This reduction was more visible at higher speeds and loads. The ignition timing for this work was consistently set at -46.3 °CA aTDCf across all fuels tested, as in Chapters 5 and 6. This consistent timing may have favoured the combustion characteristics of ethanol-containing fuels. The higher ethanol content can also enhance combustion efficiency, particularly at later ignition timings. This improved combustion with E10 fuel might lead to more complete oxidation, therefore reducing the formation of formaldehyde. Nevertheless, acetaldehyde was detected as will be discussed in the following section.

Acetaldehyde

Acetaldehyde was detected as an engine-out emission, albeit at low quantities, across all operating conditions and for both E0 and E10 fuels. Interestingly, acetaldehyde emissions were observed even for the E0 fuel. This could be attributed to its formation from non-oxygenate components such as iso-octane, as shown in Chapter 5 [188]. Iso-octane made up 20 % of the iso-paraffin content for the E0 fuel, whereas only 7 % for the

E10 fuel, as shown in the full detailed hydrocarbon analysis of these fuels in Appendix C. These results are different from Agarwal *et al.* [195], where they did not detect acetaldehyde emissions from E0 gasoline. Figure 8.8 showed that for both speed and load conditions, the acetaldehyde emissions increased for the E10 fuel. As the speed increased, the acetaldehyde emissions when using either the E0 or E10 decreased, similar to the previous findings at the same operating conditions form this study (detailed in Chapters 5 and 6). At the lower speed (1100 rpm) conditions, the acetaldehyde emissions increased by approximately 70 %, whereas, at 1500 rpm, the increase was only around 30 %.

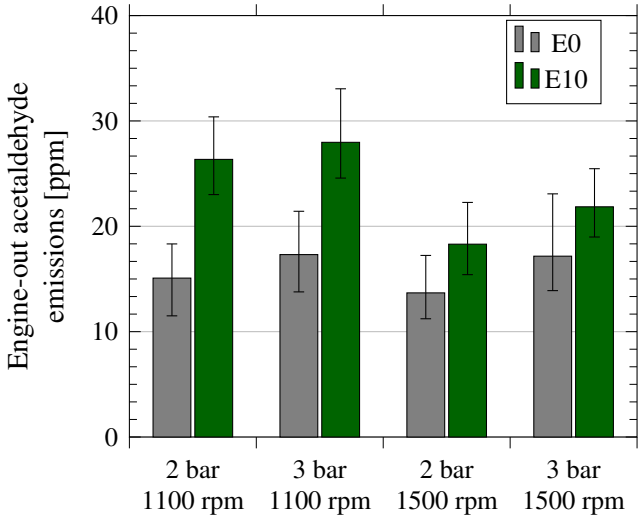

Figure 8.8: Engine-out acetaldehyde emissions for E0 (gray) and E10 (green) at engine speeds of 1100 and 1500 rpm and engine loads of 2 and 3 bar IMEP at stoichiometric conditions. Ignition timing was fixed for all fuels at -46.3 °CA aTDCf. Throttle position and fuel injection quantity were varied to maintain similar load (nIMEP). Error bars represent minimum and maximum emissions over three runs of 300 cycles each.

In real-driving scenarios, these conditions can be translated to when the vehicle starts and the engine is not fully warmed up, such as the cold-start (CS) phase, and during urban or rural conditions where the vehicles start/stop more frequently and move at lower speeds.

8.4 Summary

The capability of Emissions Analytics proprietary portable VOCs emissions measuring system was investigated with two scoping studies and a detailed study on the impact

of ethanol addition to gasoline on aldehyde emissions and their precursors, alcohols. Additionally, upcoming regulated emissions were investigated to explore the link to aldehydes, and the regulated emissions were analysed to ensure the overarching behaviour of the vehicles with the different fuels was captured correctly by the equipment. These are detailed in Appendix A.

A 30 % increase in tailpipe exhaust formaldehyde emissions for E10 compared to E0 for Cars 1, 2, and 4, with the greatest proportion and rate of increase between E0 and E10 at the cold-start conditions. However, for Car 3, the formaldehyde emissions decreased by 12 %. Tailpipe exhaust acetaldehyde emissions were below the detectable threshold limit across the different driving segments and cars for both E0 and E10 fuels. This finding differs from literature, which frequently combines data from real-driving emissions across the whole drive cycle, therefore, increasing the probability for detection. Nevertheless, when testing the same fuels in the single-cylinder engine test cell, the engine-out acetaldehyde emissions increased for E10 compared to E0.

This study shows the importance of having a standardised test comparing known fuel compositions. Furthermore, a significant proportion of the emissions are formed at the cold-start condition and the ability to observe this effect may be weakened when combined with the overall drive cycle. These results, supplemented by the findings on additional emissions, discussed in Appendix A, were published and presented at the SAE Energy & Propulsion Conference [196].

9

Conclusions and further work

Contents

9.1 Conclusions

This work covered a comprehensive range of studies, spanning from fundamental modelling and laboratory-based engine experiments to real-driving emissions measurements, all centred around the impact of fuel composition on aldehyde emissions. This concluding chapter consolidates the key insights from each part of the research, providing an integrated summary of the principal outcomes. Furthermore, it identifies potential directions for future research that build upon the insights gained from this investigation.

Firstly, the experimental work assessed the impact of an exhaustive matrix of research and surrogate fuel compositions on aldehyde emissions from a single-cylinder engine. For all the tested fuels, the ignition timing was fixed at -46.3 °CA aTDCf. This was also kept constant across the fuel-air equivalence ratio (ϕ) range. To maintain the same load (nIMEP) and account for fuel-specific behaviour when testing different fuels, the throttle

position and fuel injection quantities were varied. Based on the conditions, the following observations were made:

- Iso-octane, toluene, and n-heptane were found to inhibit aldehyde formation from fuel mixtures, particularly when blended with ethanol. Toluene showed a stronger effect on formaldehyde suppression, whereas n-heptane showed a strong effect on suppressing acetaldehyde.
- Toluene, when used as a pure fuel, produced negligible quantities of aldehydes.
- Iso-octane produced greater formaldehyde emissions than acetaldehyde.
- Across the fuel-air equivalence ratio range, ethanol showed a reduction in aldehyde emissions at both lean and rich conditions compared to stoichiometric.
- Across the fuel-air equivalence ratio range, iso-octane and toluene exhibited lower aldehyde emissions at stoichiometric conditions, and an increase in aldehyde emissions at both rich and lean conditions compared to stoichiometric. Similarly, all other fuel mixtures tested displayed the same trend, even when the fuel blend contained ethanol.
- Incorporating toluene in surrogate fuels decreases the average aldehyde emissions.
- With an increase in engine load (nIMEP) from 1.95 bar to 3.00 bar, an increase in aldehyde emissions is observed and the FA:AA ratio is maintained.
- With an increase in engine speed from 1100 rpm to 1500 rpm, a decrease in aldehyde emissions is observed and the FA:AA ratio maintained.
- Aldehyde emissions exhibit opposite trends to NMHC emissions. This was particularly noticed for fuels containing ethanol. Therefore, in future legislation, not coupling aldehyde emissions with THC or NMHC would be improve accuracy.

The modelling results in this study were used to support the experimental findings by assessing the same fuel matrix in fundamental reactors which can isolate the chemical kinetic processes. The key findings include:

- Validating mechanisms against relevant parameters for this work prior to their extensive use in models with novel fuel compositions is crucial:
  - Mechanism M1 [167] showed higher accuracy in predicting LBV, a fundamental combustion property, under lower pressure conditions. However, it was less accurate for species concentration studies due to a limited number of elementary reactions.
  - Mechanism M2 [169] was accurate in species concentration analysis and LBV prediction, but only at higher pressures. M2's larger list reactions, though still a skeletal mechanism, made it suitable for further studies on the fuel compositions from this work.
- The impact of ethanol on formaldehyde production was not fully captured in mechanism M2's predictions, indicating a need for the mechanism to incorporate additional reactions or investigate existing reaction rates in ethanol's oxidation pathways.
- There can be an overlap in the reactions influencing combustion properties (such as LBV) and those affecting aldehyde formation, particularly in fuels containing ethanol.
- Iso-octane, n-heptane, and toluene displayed a suppressive effect on aldehyde emissions, supporting the experimental findings. Nevertheless, the amount of suppression of each of the fuel components on the aldehydes was inaccurate. Additionally, their distinct effects on the formation of formaldehyde and acetaldehyde was not fully captured.
- Engine model predictions of the aldehyde emissions were several orders of magnitude lower than expected despite the combustion behaviour as anticipated. The model predictions had no observable trends, suggesting the necessity for model improvements to align with real-world data.

Finally, the results from real-driving emissions measurements provided the following insights:

- The VOCs system, successfully detected formaldehyde across all four vehicles with both E0 and E10 fuels.
- No acetaldehyde emissions were detected at the tailpipe for all four vehicles with both E0 and E10 fuels.
- A 30 % increase in tailpipe exhaust formaldehyde emissions for E10 compared to E0 for Cars 1, 2, and 4 with a significant increase observed during cold-start conditions. However, Car 3 showed a 12 % decrease with E10 compared to E0. This suggests that ethanol content in fuel has an impact on formaldehyde emissions.
- Emissions measured during the cold-start phase were significantly higher than those in other driving phases. Urban conditions resulted in the second-highest emission levels.
- The correlation between alcohol and aldehyde emissions was found to be less visible with E10 fuel, indicating that ethanol addition affected the emission formation.
- With the E10 fuel, the benzaldehyde-to-toluene ratio was lower across all driving phases, suggesting that ethanol presence in fuel could alter the relative proportions of these emissions.

9.2 Further work

This work provided a strong foundation focussing exclusively on the effects of fuel composition on aldehyde formation, consumption, and emissions. Building on this, there are several areas for additional research that could deepen the understanding of aldehyde emissions and potentially identify strategies for their mitigation:

- *Engine operating conditions*:
  - Expanding the range of steady state operating conditions, including higher loads and speeds, for realistic engine operation analysis, though this was explored in the RDE work.

  - Utilising the real-time capabilities (5 Hz) of the FTIR to observe the impact of transient conditions on engine-out aldehyde emissions from the single-cylinder engine test facility.
  - Leveraging the optical access to directly observe aldehyde formation and radical activity in the combustion chamber using laser induced fluorescence, integrated with temperature measurement for a comprehensive understanding of temperature's role in aldehyde dynamics.

- *Fuels*:
  - Exploring the combustion of other alcohols including methanol, propanol, and butanol. Methanol is an e-fuel candidate and can be directly linked to formaldehyde formation. Similarly, propanol and butanol could produce propionaldehyde and butyraldehyde, respectively. These compounds break down into smaller aldehydes like formaldehyde and acetaldehyde, which can be detected using the FTIR.
  - Incorporating additional gasoline surrogate components such as 1-hexene, an alkene, into the study to examine their impact on aldehyde emissions. As seen in the literature review (Section 2.2), this fuel type can also have impact on aldehyde emissions and it was not explored this work.

- *Real-driving emissions*:
  - Testing a wider range of modern vehicles with similar emissions specifications and conducting repeat experiments on them.
  - Exploring new technologies for aldehyde measurement on-board vehicles such as Horiba's next-generation QCL-IR which was introduced in Section 2.7.
  - Testing with refinery-made market-representative gasoline with increased ethanol concentrations (such as E20 or E25) on aldehyde emissions, as a consequence of upcoming legislative changes in countries like India.

- *Modelling*:
  - Refining the engine model to account heat loss as well as the cooler regions in the combustion chamber such as the crevices where increased aldehyde generation would be anticipated. One approach for this is to use a multi-zone combustion model.
  - Try larger chemical kinetic mechanisms in the engine model to examine whether the lack of formaldehyde and acetaldehyde generation was due to the model's inaccuracies or the mechanism's reduced capability.
  - Exploring a range of operating conditions for the PFR, particularly to study the impact of temperature changes on reaction progression.
  - Modifying conditions in the PSR to evaluate the impact of pressure variation over different temperature ranges.

Appendices

A

Additional analysis from real-driving emissions studies

A.1 Motivation

From the real-driving emissions data, several other emissions can be analysed too. The three main areas investigated include other low carbon molecules that could be formed instead of acetaldehyde, upcoming regulated emissions, and currently regulated emissions. Emissions in each of these categories were explored in this appendix.

A.2 Low carbon number molecules

As acetaldehyde was not detected in the real-driving emissions tests, other molecules with a low number of carbon atoms in the samples collected were investigated. No hydrocarbon molecules with one carbon atom were detected as they were too volatile and would oxidise to CO and CO_2. On the other hand, acetone ($(CH_3)_2CO$) and acetic acid (CH_3COOH) were two recurring low carbon molecules across all four driving phases and vehicles. Sarathy *et al.* [5] have also reported acetone emissions as a result of alcohol oxidation as further described in Section 2.2.4. Therefore, the impact of ethanol

in gasoline was reviewed on these unregulated emissions, that impact air quality, and compared to the behaviour of aldehydes.

The tailpipe exhaust acetone emissions were 5-fold greater for the cold-start than motorway conditions as shown in Figure A.1. Similarly, the cold-start acetone emissions were 2 and 4 times greater than rural and urban conditions, respectively. A reduction in acetone emissions was observed with the E10 fuel at the cold-start conditions for Cars 3 and 4.

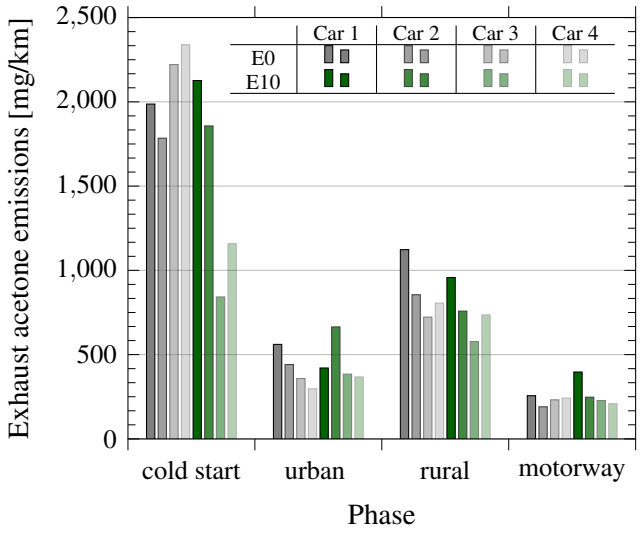

Figure A.1: Tailpipe exhaust acetone emissions for E0 (gray) and E10 (green) fuels with four cars (represented by varying shades of each colour) across four different driving modes.

For the urban condition, whilst Cars 2 to 4 had an increase in acetone emissions with the E10 fuel, Car 1 had a reduction. At the rural condition, a reduction of an average of 14 % was observed across all four vehicles with the E10 fuel compared to the E0. For the motorway condition, the acetone emissions increased with the E10 fuel for Cars 1 and 2 and decreased for Cars 3 and 4. The varied results between vehicles when comparing the E0 and E10 fuels are different to the findings reported by Sarathy *et al.* [5].

The rural driving conditions led to twice the tailpipe exhaust acetone emissions than the urban driving conditions for both fuels across all the cars. This distinction between urban and rural conditions was not as clear for the tailpipe exhaust formaldehyde emissions, however, the general behaviour amongst the driving phases was similar. The acetone

emissions were not recorded on the AVL FTIR, therefore laboratory-based engine-out emissions data are not available for these emissions.

Zervas *et al.* [197] found that exhaust acetic acid was slightly enhanced from the presence of oxygenated fuel components, such as ethanol. Therefore, the tailpipe exhaust acetic acid emissions were evaluated across the four cars and driving conditions for E0 and E10 as shown in Figure A.2. In line with the other emissions evaluated, the acetic acid emissions during cold-start were, on average, at least double the other conditions. Similarly, the motorway conditions produced the lowest emissions. These distinct findings emphasise the importance of segregating the real-driving emissions and investigating the driving conditions individually.

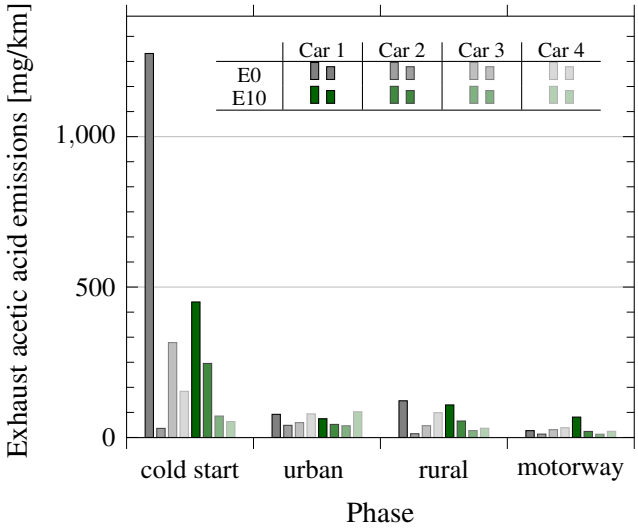

Figure A.2: Tailpipe exhaust acetic acid emissions for E0 (gray) and E10 (green) fuels with four cars (represented by varying shades of each colour) across four different driving modes.

Contrary to the consistency in the magnitude of the tailpipe exhaust emissions amongst the cars found in the previous investigations, there were significant discrepancies between the cars for acetic acid emissions. This was particularly evident for the cold-start condition with E0 fuel. The greater exhaust tailpipe acetic acid emissions for Car 1 with the E0 fuel during the cold-start conditions may be associated with the higher mileage of the vehicle and thus reduced functionality of the after-treatment system.

A.3 Upcoming regulated emissions

Given the high global warming potential of nitrous oxide (N_2O), it is being considered for upcoming regulations [198]. As real-driving emissions of N_2O were measured using the VOCs system, they were analysed, and the behaviour was compared against the aldehydes as they are formed at similarly low temperatures. Furthermore, ammonia (NH_3) emissions are also considered for upcoming light-duty vehicle legislation [198]. Although the equipment by Emissions Analytics did not measure tailpipe exhaust NH_3 emissions for this study, the engine-out emissions, which are less studied in the literature, were reviewed.

A.3.1 Nitrous oxide N_2O

The tailpipe exhaust N_2O emissions are presented for the different driving segments and vehicles with the E0 and E10 fuels, in Figure A.3 a) and b), respectively.

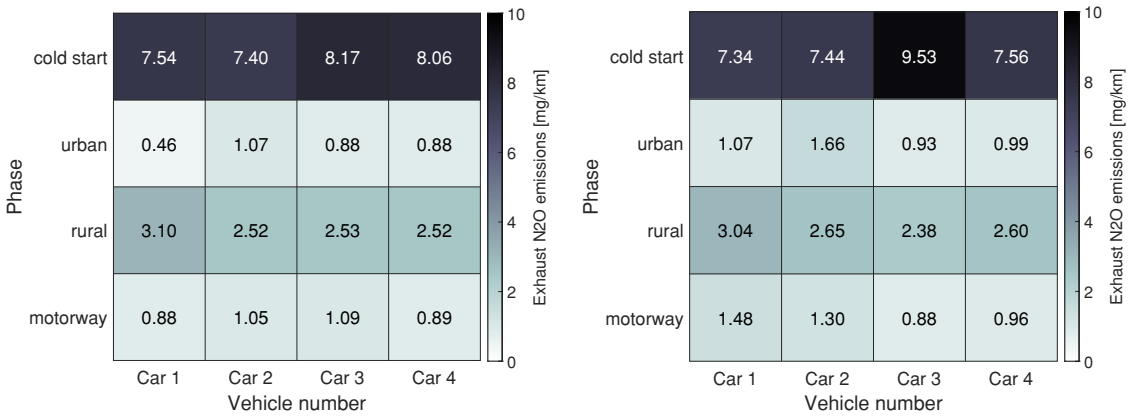

(a): N_2O with E0 fuel **(b):** N_2O with E10 fuel

Figure A.3: Tailpipe exhaust nitrous oxide N_2O emissions (mg/km) across the four different vehicles (columns) and driving conditions (rows) with the (a) E0 and (b) E10 fuels.

Figure A.3 shows that the cold-start N_2O emissions were 8 times greater than the motorway conditions for both fuels. This behaviour is expected, as the cold-start conditions reflect the period during which the exhaust after-treatment experiences catalyst light-off. The literature shows that at these low temperatures, the N_2O emissions are formed as the catalyst surface has not reached a sufficient temperature to completely reduce the NO [199]. These findings attribute the N_2O to be primarily associated with the

exhaust after-treatment system and not the fuel, although higher content ethanol-gasoline blends may produce different results.

Figure A.3 also shows that the N_2O emissions were approximately 3.5 times greater for rural driving conditions than in the urban phase. These results are similar to the observations made for acetone and acetic acid and different from the formaldehyde emissions. For the rural driving phase, the greater N_2O formation could be attributed to the reduction of NO by an alkane at higher temperatures in the exhaust after-treatment system as Wang *et al.* [200] reported. The relative magnitude and trends of tailpipe exhaust N_2O emissions for the E10 were similar to the E0 fuel across the four vehicles and driving conditions.

As N_2O formation is reported to primarily occur in the exhaust after-treatment system, the engine-out emissions were explored at 1100 rpm and 1500 rpm and at stoichiometric conditions with a load of 2 bar and 3 bar as shown in Figure A.4.

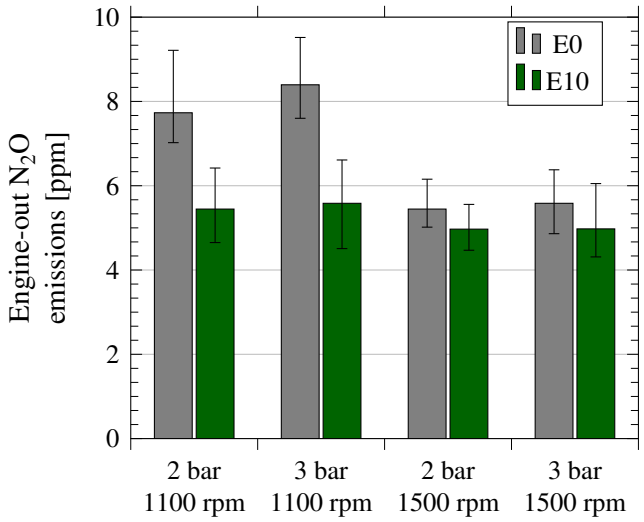

Figure A.4: Engine-out N_2O emissions for E0 (gray) and E10 (green) at engine speeds of 1100 and 1500 rpm and engine loads of 2 and 3 bar nIMEP at stoichiometric conditions. Ignition timing was fixed for all fuels at -46.3 °CA aTDCf across the speed and load range. Throttle position and fuel injection quantity were varied to maintain the expected loads (nIMEP). Error bars represent minimum and maximum emissions over three runs.

Comparing 2 bar and 3 bar, there was a marginal increase, although within the error bars. At the higher engine speed condition, the N_2O decreased for both fuels by approximately

30% and this could be attributed to the increased in-cylinder temperature. The N_2O emissions trends were similar to the aldehydes due to their low-temperature formation mechanisms. However, as the readings are below 10 ppm at engine-out, this affirms that primary N_2O formation occurs in the exhaust after treatment.

A.3.2 Ammonia NH_3

The engine-out NH_3 emissions for the E0 and E10 fuels are shown in Figure A.5. They were comparable across the two fuels, loads, and engine speeds, except for the higher speed (1500 rpm) and load (3 bar) where the E0 fuel led to greater emissions than the E10. Nevertheless, very low quantities of engine-out NH_3 emissions were recorded and significantly higher speed and load conditions need to be tested to verify this behaviour.

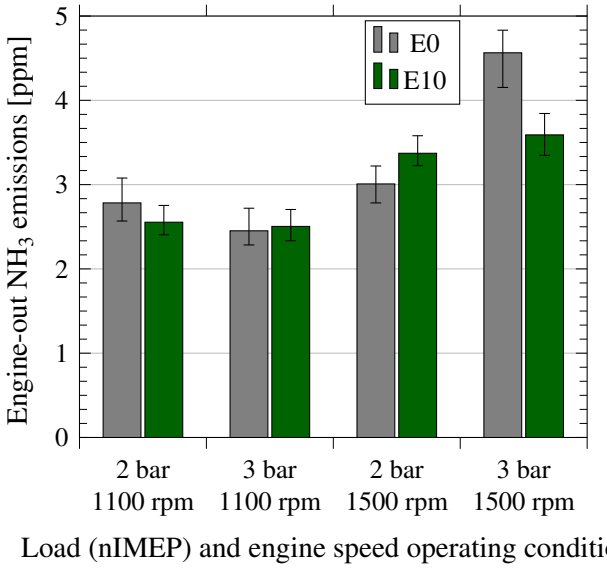

Figure A.5: Engine-out NH_3 emissions for E0 (gray) and E10 (green) at engine speeds of 1100 and 1500 rpm and engine loads of 2 and 3 bar nIMEP at stoichiometric conditions. Ignition timing was fixed for all fuels at -46.3 °CA aTDCf across the speed and load range. Throttle position and fuel injection quantity were varied to maintain the expected loads (nIMEP). Error bars represent minimum and maximum emissions over three runs.

To further understand the impact of fuel composition and engine operating conditions on ammonia generation, richer mixtures were tested. A two-zone thermodynamic spark ignition model was developed to run with the C3MechV3.3 mechanism [201] and was validated against the collected experimental data. Through this approach, it was found

that ammonia production occurred in two stages, increased engine load, and enriched conditions up to fuel-air equivalence ratio (ϕ) equal to 1.38 led to increased engine-out NH_3 emissions [202]. These trends were associated with third-body ammonia generation reactions whose reaction rates are affected by both temperature and pressure and the availability of OH radicals [202]. The latter also affects ethanol's OH radical scavenging pathways which then leads to stable aldehydes, as described in Section 2.2.4. However, the NH_3 formation seems to be formed at higher temperatures when N_2 reacts with H_2O to form amino NH_2 radicals. Whilst the ethanol content in the E10 fuel did not affect the NH_3 engine-out emissions, higher ethanol content in the fuel and transient engine operation with high load and rich conditions could affect the NH_3 production. Three-way catalysts can be a significant source of ammonia emissions, therefore real-driving emissions of NH_3 also need to be assessed.

This work was complemented by engine modelling and was published and presented at the SAE Energy & Propulsion Conference [202].

A.4 Regulated emissions

A.4.1 Nitrogen oxides NO_x

The current literature presents conflicting results on the impact of ethanol on NO_x emissions, therefore this study also examined these emissions across the range of driving conditions and vehicles. The opposite behaviour to N_2O, and thus aldehydes, was expected for NO emissions which would constitute a significant proportion of the NO_x emissions. Figure A.6 presents the tailpipe exhaust NO_x emissions for the four vehicles at each driving phase.

The NO forms a large share of the NO_x emissions. On average, the NO_x emissions were greatest at the cold-start and urban driving conditions and lower for the rural and motorway conditions. Across all the driving conditions except the motorway driving phase, the NO_x emissions were higher when the vehicles were fuelled with E10 compared to E0. An average increase of around 150 % across all four was observed with E10 compared to E0 at the cold-start and rural driving phases. In the urban driving phase, the

E10-fuelled vehicles led to an average of a 100 % increase in NO_x across all vehicles tested compared to E0. In the motorway driving conditions, the vehicles produced comparable NO_x emissions when using both E0 and E10 fuels.

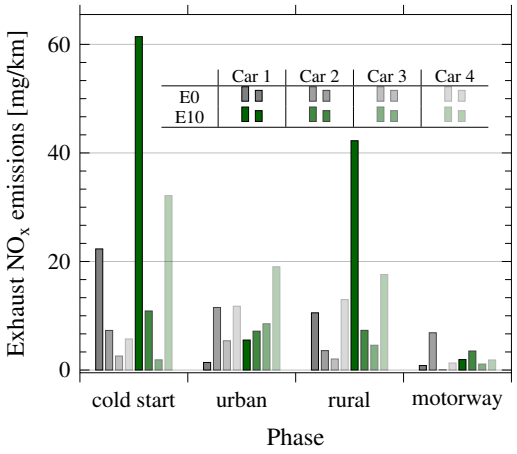

Figure A.6: Tailpipe exhaust NO_x emissions for E0 (gray) and E10 (green) fuels with four cars (represented by varying shades of each colour) across four different driving modes.

However, it should be noted that this increase was from very low levels and all vehicles have NO_x emissions lower than a third of the Euro 6 mandated and proposed Euro 7 values for emissions legislation. The formation of NO_x is complicated and primarily dependent on the temperatures, although the fuel chemistry can also play a role. Tests by O'Driscoll *et al.* also found that the NO_x emissions were higher during urban driving than motorway conditions by 200 % when measured using similar PEMs equipment [155]. Therefore, the results from these agree with the literature, affirming that tailor-made designed fuels have market-representative behaviour.

A.4.2 Carbon monoxide CO

Generally, the addition of ethanol content to gasoline would reduce the CO emissions. The additional fuel-bound oxygen in the ethanol is expected to contribute towards the oxidation of the CO emissions. Becker *et al.* [203] found a correlation between N_2O, thus aldehydes, and CO emissions and attributed this to the oxygen availability on the catalyst. However, Suarez-Bertoa *et al.* [204] also found an increase in CO emissions at lower temperatures, such as the cold-start condition, which could be prolonged with ethanol

content. Therefore, the tailpipe exhaust CO emissions from the real-driving conditions, collected by the PEMS, were evaluated.

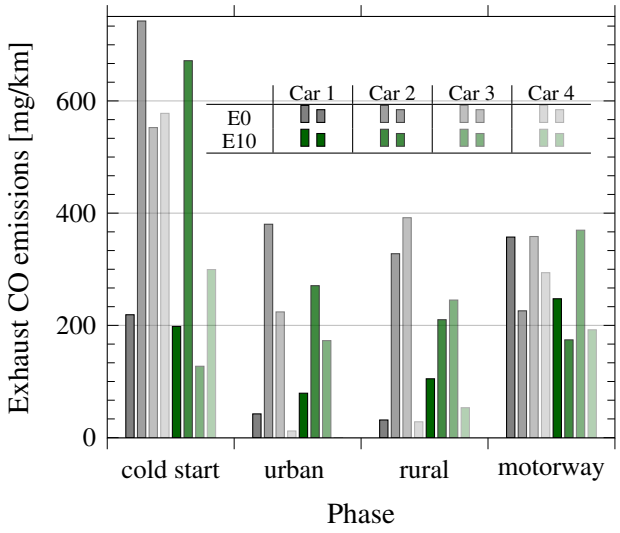

Figure A.7: Tailpipe exhaust CO emissions for E0 (gray) and E10 (green) fuels with four cars (represented by varying shades of each colour) across four different driving modes.

Overall, it was found that the E10-fuelled vehicles led to a 5 % reduction in CO emissions than the same vehicles with E0, in line with the expectations from literature. The CO emissions were greater for the cold-start and motorway conditions compared to the urban and rural. The cold-start, urban and motorway driving phases all showed that the vehicles with E10 fuel led to approximately 25 % lower CO emissions than E0, with a few exceptions such as Car 1 during urban and Car 3 during motorway driving phases. Nevertheless, the results also showed that an average 60 % increase with E10 compared E0 was observed at rural driving conditions. Though this data was skewed by Car 1, where the recorded emissions for E0 were significantly low, therefore a 3-fold rise in CO emissions was observed with E10. However, it should be noted this could be an anomaly, therefore, the E10 fuel led to reduced CO emissions than E0 across all four vehicles tested.

A.4.3 Carbon dioxide CO_2

The CO_2 emissions from the RDE tests are shown in Figure A.8. Generally, the CO_2 emissions with the E0 fuel were higher for vehicles with larger engine size and power

(Cars 1 and 2), except for the rural driving condition. Therefore, the CO_2 emissions agree with the literature that CO_2 savings could be made by downsizing gasoline engines, affirming the equipment by Emissions Analytics was capable of correctly distinguishing the impact of the vehicles [155].

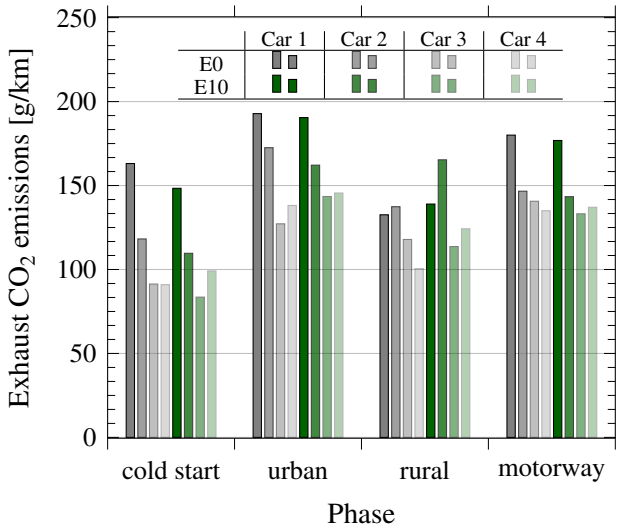

Figure A.8: Tailpipe exhaust CO_2 emissions for E0 (gray) and E10 (green) fuels with four cars (represented by varying shades of each colour) across four different driving modes.

The results show that the motorway and urban conditions led to greater CO_2 emissions across all vehicles and both fuels, whereas the cold-start and rural conditions had lower CO_2. During the cold-start and rural, there may be more stop/start and slow speed conditions which could lead to a lower exhaust temperature thus reducing the emissions fully oxidised to CO_2. Overall, the emissions were comparable across all vehicles with both fuels as E10 showed an average of a 2 % reduction in CO_2 compared to E0. Whilst for cold-start and motorway conditions, the vehicles with E0 fuel led to greater CO_2 emissions than the vehicles with E0, the opposite behaviour was observed for the urban and rural driving phases. Nevertheless, the differences were minimal, therefore difficult to attribute to specific behaviour.

A.5 Summary

- *Upcoming regulated emissions* - The cold-start emissions were 8 times greater than motorway conditions as N_2O forms at lower temperatures. Compared to the

aldehydes, the discrepancy between rural and urban driving conditions was greater with N_2O. The engine-out NH_3 formation was found to be dependent on OH radical availability which could be affected by fuel with higher ethanol content at richer and higher load conditions.

- *Regulated emissions* - The CO, CO_2, and NO_x emissions matched findings from the literature confirming the emissions measuring equipment's capability, fuel behaviour, and capturing the effect of the vehicles and driving conditions.

B

Additional information for the vehicles used in RDE chapter

B.1 Motivation

The objective of this Appendix is to provide additional information on the details of the vehicles used in the study

The fuel consumption (litres per 100 km) of the vehicles for each fuel during this study is shown in Table B.1. The results show that for all vehicles except the Citroen C3 Sense Puretech (Car 3), the fuel consumption improved with the E10 compared to the E0. On average, a 4.8 % reduction in fuel consumption was observed with the greatest reduction seen with the Renault Clio RS Line (Car 4).

Table B.1: Fuel consumption [liters per 100 kilometers (l/100 km)] for each vehicle with the E0 and E10 fuels

Vehicle	E0 (l/100 km)	E10 (l/100 km)
2020 Kia Sportage GT-line ISG	6.98	6.68
2022 Peugeot 2008 GT Premium PureTech	6.05	5.77
2022 Citroen C3 Sense PureTech	5.23	5.39
2022 Renault Clio RS Line TCe	5.07	4.48

The mileage at the time of testing for each vehicle is shown in Table B.2.

Table B.2: Mileage of each vehicle

Vehicle	Mileage (miles)
2020 Kia Sportage GT-line ISG	24332
2022 Peugeot 2008 GT Premium PureTech	8101
2022 Citroen C3 Sense PureTech	471
2022 Renault Clio RS Line TCe	1901

The transmission of the vehicles are shown in Table B.3.

Table B.3: Gearbox of each vehicle

Vehicle	Gearbox
2020 Kia Sportage GT-line ISG	Manual 6 gears
2022 Peugeot 2008 GT Premium PureTech	Automatic 8 gears
2022 Citroen C3 Sense PureTech	Manual 5 gears
2022 Renault Clio RS Line TCe	Manual 6 gears

C

Detailed hydrocarbon analysis of the E0 and E10 fuels

The detailed hydrocarbon analysis for the market representative E0 and E10 fuels are shown in the following tables, respectively.

Component	%v/v measured	%m/m measured
toluene	15.42	18.08
i-pentane	12.06	10.14
2,2,4-trimethylpentane (isooctane)	8.33	7.81
2-methylpentane	3.88	3.41
t-butylbenzene & 1,2,4-trimethylbenzene	3.13	3.65
n-butane	3.03	2.36
m-xylene	2.98	3.48
2-methylbut-2-ene (isoamylene isomer 2)	2.90	2.60
3-methylpentane	2.78	2.49
n-hexane	2.21	1.99
2,3,4-trimethylpentane	1.92	1.86
o-xylene	1.70	1.99
n-pentane	1.62	1.38
1-methyl-3-ethylbenzene	1.62	1.88
methylcyclopentane	1.45	1.46
i-butane	1.30	1.04
ethylbenzene	1.28	1.50
2,3-dimethylbutane	1.26	1.12

Continued on next page

Table C.1 – continued from previous page

Component	%v/v measured	%m/m measured
2,3-dimethyloctane	1.26	1.24
p-xylene	1.25	1.45
2,2-dimethylbutane	1.25	1.09
2-methylbut-1-ene (isoamylene isomer 1)	1.05	0.89
n-decane	0.92	0.91
2,3,3-trimethylpentane	0.89	0.86
1-methyl-2-ethylbenzene	0.85	0.99
cyclohexane	0.85	0.89
trans-2-pentene	0.78	0.69
1-methyl-4-ethylbenzene	0.77	0.90
2,5-dimethylhexane & 2,2,3-trimethylpentane	0.74	0.69
2,4-dimethylhexane	0.73	0.69
trans-but-2-ene	0.71	0.55
2,4-dimethylpentane	0.63	0.57
3-methylhexane	0.63	0.58
1-butene	0.60	0.48
2-methylhexane	0.59	0.54
1,2,3-trimethylbenzene	0.59	0.69
n-heptane	0.58	0.53
2,3-dimethylhexane	0.56	0.54
2,3-dimethylpentane	0.50	0.47
Others (<0.50 %v/v)	14.83	14.34

Component	%v/v measured	%m/m measured
toluene	24.91	28.94
i-pentane	11.86	9.88
Ethanol	10.17	10.78
n-hexane	7.60	6.78
3-methylpentane	6.48	5.74
2-methylpentane	5.32	4.63
hex-1-ene	3.65	3.29
2,2,4-trimethylpentane (iso-octane)	2.43	2.26
t-butylbenzene & 1,2,4-trimethylbenzene	1.64	1.90
n-butane	1.41	1.09
methylcyclopentane	1.38	1.38
m-xylene	1.29	1.50
2,3-dimethylbutane	0.91	0.80
n-pentane	0.90	0.76
n-heptane	0.89	0.81
1-methyl-3-ethylbenzene	0.85	0.98

Continued on next page

Table C.2 – continued from previous page

Component	%v/v measured	%m/m measured
2,3,4-trimethylpentane	0.78	0.75
o-xylene	0.75	0.87
2-methylbut-2-ene (isoamylene isomer 2)	0.72	0.64
i-butane	0.59	0.46
p-xylene	0.56	0.64
2,4-dimethylhexane	0.54	0.51
3-methylhexane	0.52	0.48
ethylbenzene	0.51	0.59
Others (<0.50 %v/v)	13.34	13.02

References

[1] International Transport Forum. *ITF Transport Outlook 2023*. 2023, p. 216. DOI: https://doi.org/https://doi.org/10.1787/b6cc9ad5-en.

[2] *Renewables 2023*. Jan. 2024.

[3] "Commission Delegated Regulation (EU) 2023/1640 of 5 June 2023 on the methodology to determine the share of biofuel and biogas for transport, produced from biomass being processed with fossil fuels in a common process". *Official Journal of the European Union* (June 2023).

[4] Azhaham Perumal Saravanan, Arivalagan Pugazhendhi, and Thangavel Mathimani. "A comprehensive assessment of biofuel policies in the BRICS nations: Implementation, blending target and gaps". *Fuel* 272 (2020), p. 117635. DOI: 10.1016/j.fuel.2020.117635.

[5] S. Mani Sarathy et al. "Alcohol combustion chemistry". *Progress in Energy and Combustion Science* 44 (2014), pp. 40–102. DOI: 10.1016/j.pecs.2014.04.003.

[6] Fushui Liu et al. "Experimental Investigation of Polycyclic Aromatic Hydrocarbons Growth Characteristics of Gasoline Mixed with Methanol, Ethanol, or n -Butanol in Laminar Diffusion Flames". *Energy & Fuels* 32.6 (June 2018), pp. 6823–6833. DOI: 10.1021/acs.energyfuels.8b00693.

[7] Daniel Schuch et al. "A two decades study on ozone variability and trend over the main urban areas of the São Paulo state, Brazil". *Environmental Science and Pollution Research* 26.31 (Nov. 2019), pp. 31699–31716. DOI: 10.1007/s11356-019-06200-z.

[8] Thiago Nogueira et al. "Formaldehyde and acetaldehyde measurements in urban atmosphere impacted by the use of ethanol biofuel: Metropolitan Area of Sao Paulo (MASP), 2012-2013". *Fuel* 134 (Oct. 2014), pp. 505–513. DOI: 10.1016/j.fuel.2014.05.091.

[9] Sérgio M. Corrêa, Eduardo M. Martins, and Graciela Arbilla. "Formaldehyde and acetaldehyde in a high traffic street of Rio de Janeiro, Brazil". *Atmospheric Environment* 37.1 (Jan. 2003), pp. 23–29. DOI: 10.1016/S1352-2310(02)00805-1.

[10] Rachel E. Dunmore et al. "Atmospheric ethanol in London and the potential impacts of future fuel formulations". *Faraday Discussions* 189 (July 2016), pp. 105–120. DOI: 10.1039/c5fd00190k.

[11] Roger Atkinson. "Atmospheric chemistry of VOCs and NO(x)". *Atmospheric Environment* 34 (Jan. 2000), pp. 2063–2101. DOI: https://doi.org/10.1016/S1352-2310(99)00460-4.

[12] Jeffrey S. Gaffney and Nancy A. Marley. "The impacts of combustion emissions on air quality and climate - From coal to biofuels and beyond". *Atmospheric Environment* 43.1 (Jan. 2009), pp. 23–36. DOI: 10.1016/j.atmosenv.2008.09.016.

[13] Dafni A. Missia et al. “Indoor exposure from building materials: A field study”. *Atmospheric Environment* 44.35 (Nov. 2010), pp. 4388–4395. DOI: 10.1016/j.atmosenv.2010.07.049.

[14] Thiago Nogueira et al. “Seasonal trends of formaldehyde and acetaldehyde in the megacity of São Paulo”. *Atmosphere* 8.8 (Aug. 2017), p. 144. DOI: 10.3390/atmos8080144.

[15] Pamela Dominutti et al. “One decade of VOCs measurements in São Paulo megacity: Composition, variability, and emission evaluation in a biofuel usage context”. *Science of the Total Environment* 738 (Oct. 2020). DOI: 10.1016/j.scitotenv.2020.139790.

[16] Isaac Schifter et al. “Assessment of Mexico’s program to use ethanol as transportation fuel: impact of 6% ethanol-blended fuel on emissions of light-duty gasoline vehicles”. *Environ Monit Assess* 173 (2011), pp. 343–360. DOI: 10.1007/s10661-010-1391-x.

[17] Mark Z. Jacobson. “Effects of ethanol (E85) versus gasoline vehicles on cancer and mortality in the United States”. *Environmental Science and Technology* 41.11 (2007), pp. 4150–4157. DOI: 10.1021/es062085v.

[18] Iyad Kheirbek et al. “Spatial variability in levels of benzene, formaldehyde, and total benzene, toluene, ethylbenzene and xylenes in New York City: a land-use regression study”. *Environmental Health* 11.1 (July 31, 2012), p. 51. DOI: 10.1186/1476-069X-11-51.

[19] Kang Chen et al. “Spatiotemporal mapping of atmospheric aldehydes over Beijing in summer during 20192021 via their source apportionment study”. *Atmospheric Research* 288 (2023), p. 106723. DOI: https://doi.org/10.1016/j.atmosres.2023.106723.

[20] EPA. “Environmental Protection Agency Control of Hazardous Air Pollutants From Mobile Sources; Final Rule”. *Federal Register* 72.37 (2007).

[21] IARC. “Diesel and Gasoline Engine Exhausts and Some Nitroarenes. Iarc Monographs on the Evaluation of Carcinogenic Risks To Humans”. *IARC monographs on the evaluation of carcinogenic risks to humans / World Health Organization, International Agency for Research on Cancer* 105 (2014), pp. 9–699.

[22] EPA. “Guidelines for Carcinogen Risk Assessment”. (2005).

[23] Michael Petroni et al. “Hazardous air pollutant exposure as a contributing factor to COVID-19 mortality in the United States”. *Environmental Research Letters* 15.9 (2020). DOI: 10.1088/1748-9326/abaf86.

[24] Mahdieh Delikhoon et al. “Characteristics and health effects of formaldehyde and acetaldehyde in an urban area in Iran”. *Environmental Pollution* 242 (Nov. 2018), pp. 938–951. DOI: 10.1016/j.envpol.2018.07.037.

[25] L. A. Díaz-Robles, J. S. Fu, and G. D. Reed. “Emission scenarios and the health risks posed by priority mobile air toxics in an Urban to regional area: An application in Nashville, Tennessee”. *Aerosol and Air Quality Research* 13 (2013), pp. 795–803. DOI: 10.4209/aaqr.2012.07.0165.

[26] G. Broustail et al. “Experimental determination of laminar burning velocity for butanol and ethanol iso-octane blends”. *Fuel* 90.1 (Jan. 2011), pp. 1–6. DOI: 10.1016/J.FUEL.2010.09.021.

[27] IARC. “Carcinogenicity of acrolein, crotonaldehyde, and arecoline”. *The Lancet Oncology* 22.1 (Jan. 2021), pp. 19–20. DOI: 10.1016/S1470-2045(20)30727-0.

[28] NJ Health. “Hazardous substance factsheet”. *New Jersey Department of Health and Senior Services* (2002).

[29] J Stanek et al. “Toxicological Review of Propionaldehyde”. *U.S. Environmental Protection Agency* 123 (2008).

[30] Navaporn Kanjanasiranont, Tassanee Prueksasit, and Daisy Morknoy. “Inhalation exposure and health risk levels to BTEX and carbonyl compounds of traffic policeman working in the inner city of Bangkok, Thailand”. *Atmospheric Environment* 152.December 2014 (2017), pp. 111–120. DOI: 10.1016/j.atmosenv.2016.11.062.

[31] Ramin Nabizadeh et al. “On the nature of airborne aldehydes in a middle eastern megacity: Tehran, Iran”. *Sustainable Cities and Society* 53 (Feb. 2020), p. 101895. DOI: 10.1016/j.scs.2019.101895.

[32] IARC. “IARC Monograph: Evaluation of carcinogenic risks to humans. Wood dust and Formaldehyde.” *IARC Monographs on the Evaluation of Carcinogenic Risks to Humans* 62 (1995), pp. 217–362.

[33] IARC. “IARC Monographs: Evaluation of Carcinogenic Risks to Humans Formaldehyde , 2-Butoxyethanol”. (2006).

[34] IARC. “IARC Monograph: Chemical agents and related occupations. A review of human carcinogens.” *IARC monographs on the evaluation of carcinogenic risks to humans / World Health Organization, International Agency for Research on Cancer* 100F (2012).

[35] IARC. “International Agency for Research on Cancer Monographs Volume 71”. 71.1985 (1999), pp. 319–335.

[36] EPA. “Acetaldehyde Hazard Summary”. *Acetaldehyde Hazard Summary* (Jan. 2000).

[37] IARC. “IARC Monographs on the Evaluation of Carcinogenic Risks to Humans: Outdoor Air Pollution”. *IARC monographs* 109 (2015).

[38] Thomas Wallner. “Correlation Between Speciated Hydrocarbon Emissions and Flame Ionization Detector Response for Gasoline/Alcohol Blends”. *Journal of Engineering for Gas Turbines and Power* 133.8 (Apr. 2011), p. 082801. DOI: 10.1115/1.4002893.

[39] Ricardo Suarez-Bertoa et al. “Intercomparison of ethanol, formaldehyde and acetaldehyde measurements from a flex-fuel vehicle exhaust during the WLTC”. *Fuel* 203 (2017), pp. 330–340. DOI: 10.1016/j.fuel.2017.04.131.

[40] *Control of Air Pollution From Motor Vehicles: Tier 3 Motor Vehicle Emission and Fuel Standards (79 FR 23414, April 28, 2014) (EPA-420-B-14-058)*. 2014.

[41] John German. *U.S. Tier 3 vehicle emissions and fuel quality standards, final rule - International Council on Clean Transportation*. Mar. 2014.

[42] *Resolução nž 492 de 26 de novembro de 2008*. 2008.

[43] Tim Dallmann. *Brazil PROCONVE L-7 and L-8 emission standards for light-duty vehicles - International Council on Clean Transportation*. Jan. 2020.

[44] *Enforcement Rules of the Air Quality Preservation Act*.

[45] European Commission. “Commission Regulation (EU) 2018/1832 of 5 November 2018 amending Directive 2007/46/EC of the European Parliament and of the Council, Commission Regulation (EC) No 692/2008 and Commission Regulation (EU) 2017/1151 for the purpose of improving the emission”. 1832.692 (2018), p. 301.

[46] Agency for Toxic Substances and Disease Registry (ATSDR). “Toxicological Profile for Endosulfan”. (2022).

[47] Dennis Schuetzle et al. “The Relationship between Gasoline Composition and Vehicle Hydrocarbon Emissions: A Review of Current Studies and Future Research Needs”. (1994).

[48] Sreshtha Sinha Majumdar, Josh A. Pihl, and Todd J. Toops. “Reactivity of novel high-performance fuels on commercial three-way catalysts for control of emissions from spark-ignition engines”. *Applied Energy* 255 (Dec. 2019), p. 113640. DOI: 10.1016/j.apenergy.2019.113640.

[49] H.J. Curran et al. “A comprehensive modeling study of iso-octane oxidation”. *Combustion and Flame* 129.3 (2002), pp. 253–280. DOI: https://doi.org/10.1016/S0010-2180(01)00373-X.

[50] Arvi Rauk et al. “Alkoxy radicals in the gaseous phase: β-scission reactions and formation by radical addition to carbonyl compounds”. *Canadian Journal of Chemistry* 81.6 (2003), pp. 431–442. DOI: 10.1139/v02-206.

[51] J.H. Knox. “A new mechanism for the low temperature oxidation of hydrocarbons in the gas phase”. *Combustion and Flame* 9.3 (1965), pp. 297–310. DOI: https://doi.org/10.1016/0010-2180(65)90095-7.

[52] G. Broustail et al. “Comparison of regulated and non-regulated pollutants with iso-octane/butanol and iso-octane/ethanol blends in a port-fuel injection Spark-Ignition engine”. *Fuel* 94 (2012), pp. 251–261. DOI: https://doi.org/10.1016/j.fuel.2011.10.068.

[53] Chenxu Jiang et al. “Influences of fuel injection strategies on combustion performance and regular/irregular emissions in a turbocharged gasoline direct injection engine: Commercial gasoline versus multi-components gasoline surrogates”. *Energy* 157 (Aug. 2018), pp. 173–187. DOI: 10.1016/j.energy.2018.05.160.

[54] D. J.M. Ray and D. J. Waddington. “Gas phase oxidation of alkenesPart II. The oxidation of 2-methylbutene-2 and 2,3-dimethylbutene-2”. *Combustion and Flame* 20.3 (June 1973), pp. 327–334. DOI: 10.1016/0010-2180(73)90024-2.

[55] Mohammed I. Sway and David J. Waddington. “Reactions of oxygenated radicals in the gas phase. Part 12. The reactions of isopropylperoxyl radicals and alkenes”. *Journal of the Chemical Society* 2 (Jan. 1983), pp. 139–143. DOI: 10.1039/P29830000139.

[56] Cesar L. Barraza-Botet and Margaret S. Wooldridge. “Combustion chemistry of iso-octane/ethanol blends: Effects on ignition and reaction pathways”. *Combustion and Flame* 188 (2018), pp. 324–336. DOI: https://doi.org/10.1016/j.combustflame.2017.10.011.

[57] Lars Seidel et al. “Comprehensive kinetic modeling and experimental study of a fuel-rich, premixed n-heptane flame”. *Combustion and Flame* 162.5 (2015), pp. 2045–2058. DOI: https://doi.org/10.1016/j.combustflame.2015.01.002.

[58] Henry Curran. *Generation of Detailed Chemical Kinetic Models for C 0 C 2 Hydrocarbon and Oxygenated Fuels*. Tech. rep. Princeton University, 2018.

[59] Eric Grosjean, Jailson Bittencourt De Andrade, and Daniel Grosjean. "Carbonyl Products of the Gas-Phase Reaction of Ozone with Simple Alkenes". *Environment Science and Technology* 30 (1996), pp. 975–983.

[60] Maryam Hajbabaei et al. "Impact of olefin content on criteria and toxic emissions from modern gasoline vehicles". *Fuel* 107 (May 2013), pp. 671–679. DOI: 10.1016/j.fuel.2012.12.031.

[61] Jiacheng Yang et al. "Impacts of gasoline aromatic and ethanol levels on the emissions from GDI vehicles: Part 1. Influence on regulated and gaseous toxic pollutants". *Fuel* 252 (Sept. 2019), pp. 799–811. DOI: 10.1016/j.fuel.2019.04.143.

[62] I. Schifter et al. "Influence of gasoline olefin and aromatic content on exhaust emissions of 15% ethanol blends". *Fuel* 265 (2020), p. 116950. DOI: https://doi.org/10.1016/j.fuel.2019.116950.

[63] Georgios Karavalakis et al. "Evaluating the Effects of Aromatics Content in Gasoline on Gaseous and Particulate Matter Emissions from SI-PFI and SIDI Vehicles". *Environmental Science & Technology* 49.11 (2015), pp. 7021–7031. DOI: 10.1021/es5061726.

[64] C. L. Goodfellow et al. "European Programme on Emissions, Fuels and Engine Technologies (EPEFE) - Gasoline Aromatics/E100 Study". *SAE Transactions* 105 (1996), pp. 503–526.

[65] E. Zervas, X. Montagne, and J. Lahaye. "Emission of alcohols and carbonyl compounds from a spark ignition engine. Influence of fuel and air/fuel equivalence ratio". *Environmental Science and Technology* 36 (Nov. 2002), pp. 2414–2421. DOI: 10.1021/es010265t.

[66] Jiacheng Yang et al. "Emissions from a flex fuel GDI vehicle operating on ethanol fuels show marked contrasts in chemical, physical and toxicological characteristics as a function of ethanol content". *Science of the Total Environment* 683 (Sept. 2019), pp. 749–761. DOI: 10.1016/j.scitotenv.2019.05.279.

[67] Mengzhu Zhang et al. "Effects of ethanol and aromatic compositions on regulated and unregulated emissions of E10-fuelled China-6 compliant gasoline direct injection vehicles". *Renewable Energy* 176 (2021), pp. 322–333. DOI: 10.1016/j.renene.2021.03.029.

[68] Zhuoyao He et al. "Effects of short chain aromatics in gasoline on GDI engine combustion and emissions". *Fuel* 297 (2021), p. 120725. DOI: https://doi.org/10.1016/j.fuel.2021.120725.

[69] Zhenyu Tian et al. "A detailed kinetic modeling study of toluene oxidation in a premixed laminar flame". *Proceedings of the Combustion Institute* 33.1 (2011), pp. 233–241. DOI: https://doi.org/10.1016/j.proci.2010.06.063.

[70] Sylvain Namysl et al. "Experimental and modeling study of benzaldehyde oxidation". *Combustion and Flame* 211 (2020), pp. 124–132. DOI: https://doi.org/10.1016/j.combustflame.2019.09.024.

[71] Gabriel Da Silvas et al. “Ethanol oxidation: Kinetics of the α-hydroxyethyl radical + O2 reaction”. *Journal of Physical Chemistry* 113.31 (Aug. 2009), pp. 8923–8933. DOI: 10.1021/jp903210a.

[72] Henry J. Curran. “Developing detailed chemical kinetic mechanisms for fuel combustion”. *Proceedings of the Combustion Institute* 37.1 (Jan. 2019), pp. 57–81. DOI: 10.1016/J.PROCI.2018.06.054.

[73] Gaurav Mittal et al. “Autoignition of ethanol in a rapid compression machine”. *Combustion and Flame* 161.5 (2014), pp. 1164–1171. DOI: https://doi.org/10.1016/j.combustflame.2013.11.005.

[74] Chiara Saggese et al. “An improved detailed chemical kinetic model for C3-C4 linear and iso-alcohols and their blends with gasoline at engine-relevant conditions”. *Proceedings of the Combustion Institute* 38.1 (2021), pp. 415–423. DOI: https://doi.org/10.1016/j.proci.2020.07.023.

[75] Matteo Pelucchi et al. “A Kinetic Modelling Study of Alcohols Operating Regimes in a HCCI Engine”. *SAE International Journal of Engines* 10.5 (2017), pp. 2354–2370. DOI: 10.4271/2017-24-0077.

[76] Francis M Haas, Marcos Chaos, and Frederick L Dryer. “Low and intermediate temperature oxidation of ethanol and ethanol PRF blends : An experimental and modeling study”. *Combustion and Flame* 156.12 (2009), pp. 2346–2350. DOI: 10.1016/j.combustflame.2009.08.012.

[77] Qian Zhao et al. “Chemical Kinetics of H-Atom Abstraction from Ethanol by H2: Implication for Combustion Modeling”. *The Journal of Physical Chemistry A* 123.5 (2019), pp. 971–982. DOI: 10.1021/acs.jpca.8b09074.

[78] Zhewen Lu, Yi Yang, and Michael J. Brear. “Impact of ethanol on oxidation of iso-octane at low and intermediate temperatures”. *Combustion and Flame* 214 (Apr. 2020), pp. 167–183. DOI: 10.1016/J.COMBUSTFLAME.2019.12.040.

[79] J. Li et al. “Chemical kinetics of ethanol oxidation”. *5th US Combustion Meeting 2007* 3 (2007), pp. 1361–1377.

[80] Zhewen Lu, Yi Yang, and Michael J. Brear. “Oxidation of PRFs and ethanol/iso-octane mixtures in a flow reactor and the implication for their octane blending”. *Proceedings of the Combustion Institute* 37.1 (2019), pp. 649–656. DOI: https://doi.org/10.1016/j.proci.2018.05.134.

[81] Hao Yuan et al. “Oxidation of ethanol and hydrocarbon mixtures in a pressurised flow reactor”. *Combustion and Flame* 199 (2019), pp. 96–113. DOI: https://doi.org/10.1016/j.combustflame.2018.10.011.

[82] Philippe Dagaut and Casimir Togbé. “Oxidation Kinetics of Mixtures of Iso-Octane with Ethanol or Butanol in a Jet-Stirred Reactor: Experimental and Modeling Study”. *Combustion Science and Technology* 184.7-8 (2012), pp. 1025–1038. DOI: 10.1080/00102202.2012.663993.

[83] Philippe Dagaut and Casimir Togbé. “Experimental and modeling study of the kinetics of oxidation of ethanol-n-heptane mixtures in a jet-stirred reactor”. *Fuel* 89.2 (2010), pp. 280–286. DOI: 10.1016/j.fuel.2009.06.035.

[84] P. Dagaut, G. Pengloan, and A. Ristori. "Oxidation, ignition and combustion of toluene: Experimental and detailed chemical kinetic modeling". *Physical Chemistry Chemical Physics* 4 (10 2002). DOI: 10.1039/b110282f.

[85] Frédérique Battin-Leclerc, John M Simmie, and Edward Blurock. *Cleaner Combustion*. Springer London, 2013. DOI: 10.1007/978-1-4471-5307-8_8.

[86] Nathan I D Hinton. "Measuring Laminar Burning Velocities using Constant Volume Combustion Vessel Techniques". PhD thesis. University of Oxford, 2014.

[87] Nathan Hinton, Richard Stone, and Roger Cracknell. "Laminar burning velocity measurements in constant volume vessels Reconciliation of flame front imaging and pressure rise methods". *Fuel* 211 (2018), pp. 446–457. DOI: https://doi.org/10.1016/j.fuel.2017.09.031.

[88] P. Dirrenberger et al. "Laminar burning velocity of gasolines with addition of ethanol". *Fuel* 115 (2014), pp. 162–169. DOI: https://doi.org/10.1016/j.fuel.2013.07.015.

[89] Alexander A. Konnov et al. "A comprehensive review of measurements and data analysis of laminar burning velocities for various fuel+air mixtures". *Progress in Energy and Combustion Science* 68 (2018), pp. 197–267. DOI: https://doi.org/10.1016/j.pecs.2018.05.003.

[90] Maris Gailis et al. "An Experimental Investigation on Aldehyde and Methane Emissions from Hydrous Ethanol and Gasoline Fueled SI Engine". *SAE Technical Papers* (2020), pp. 1–12. DOI: 10.4271/2020-01-2047.

[91] Thomas Wallner and Richard Frazee. "Study of regulated and non-regulated emissions from combustion of gasoline, alcohol fuels and their blends in a DI-SI engine". *SAE Technical Papers* (2010). DOI: 10.4271/2010-01-1571.

[92] Diego Golke et al. "Exploring the part load lean limit of a direct injection spark ignition engine fueled with ethanol". *International Journal of Engine Research* 24.4 (2023), pp. 1565–1577. DOI: 10.1177/14680874221092729.

[93] Yong Qian et al. "Improvement of combustion performance and emissions in a gasoline direct injection (GDI) engine by modulation of fuel volatility". *Fuel* 268 (Dec. 2020), p. 117369. DOI: 10.1016/j.fuel.2020.117369.

[94] Xiaobing Pang et al. "Carbonyls emission from ethanol-blended gasoline and biodiesel-ethanol-diesel used in engines". *Atmospheric Environment* 42.6 (2008), pp. 1349–1358. DOI: https://doi.org/10.1016/j.atmosenv.2007.10.075.

[95] Paola Helena Barros Zarante and José Ricardo Sodré. "Comparison of aldehyde emissions simulation with FTIR measurements in the exhaust of a spark ignition engine fueled by ethanol". *Heat and Mass Transfer* 54 (7 July 2018), pp. 2079–2087. DOI: https://doi.org/10.1007/s00231-018-2295-5.

[96] Rinaldo Antunes Amaral and José Ricardo Sodré. "Aldehyde emissions from an ethanol-fuelled vehicle as influenced by engine geometric parameters". *SAE Technical Papers* (2001). DOI: 10.4271/2001-01-1998.

[97] Rinaldo Antunes Amaral and Jose Ricardo Sodre. "Influence of engine operating parameters on aldehyde emissions from an ethanol-fueled vehicle". *Combustion Science and Technology* 174.7 (2002), pp. 153–165. DOI: 10.1080/00102200208984091.

[98] Enrico R. Malheiro de Oliveira, Caio Henrique Rufino, and Pedro Teixeira Lacava. "Effects of direct injection and mixture enleament on the combustion of hydrous ethanol and an ethanol-gasoline blend in an optical engine". *Fuel* 327 (2022), p. 125137. DOI: https://doi.org/10.1016/j.fuel.2022.125137.

[99] Ritchie Lewis Daniel. "Combustion and emissions performance of oxygenated fuels in a modern spark ignition engine". (May 2012).

[100] Yong Qian et al. "Combustion and regulated/unregulated emissions of a direct injection spark ignition engine fueled with C3-C5 alcohol/gasoline surrogate blends". *Energy* 174 (2019), pp. 779–791. DOI: https://doi.org/10.1016/j.energy.2019.03.021.

[101] Jun Li et al. "Emissions of Formaldehyde and Unburned Methanol from a Spark-Ignition Methanol Engine during Cold Start". *Energy & Fuels* 24.2 (2010), pp. 863–870. DOI: 10.1021/ef9009982.

[102] Xiang Qu et al. "Regulated and unregulated emissions from a DISI methanol engine under homogenous combustion and light load". *Fuel* 158 (2015), pp. 166–175. DOI: https://doi.org/10.1016/j.fuel.2015.05.033.

[103] Changming Gong et al. "Numerical study of effect of injection and ignition timings on combustion and unregulated emissions of DISI methanol engine during cold start". *Renewable Energy* 112 (Nov. 2017), pp. 457–465. DOI: 10.1016/j.renene.2017.05.055.

[104] Jiajun Liu et al. "Numerical study of formaldehyde and unburned methanol emissions of direct injection spark ignition methanol engine under cold start and steady state operating conditions". *Fuel* 202 (2017), pp. 405–413. DOI: https://doi.org/10.1016/j.fuel.2017.04.059.

[105] Changming Gong et al. "Detection and analysis of formaldehyde and unburned methanol emissions from a direct-injection spark-ignition methanol engine". *Fuel* 221 (2018), pp. 188–195. DOI: https://doi.org/10.1016/j.fuel.2018.02.115.

[106] "Effects of injection and spark timings on combustion, performance and emissions (regulated and unregulated) characteristics in a direct injection methanol engine". *Fuel Processing Technology* 247 (2023), p. 107758. DOI: https://doi.org/10.1016/j.fuproc.2023.107758.

[107] Saket Sahu, Parmod Kumar, and Atul Dhar. "Effect of injection timing on combustion, performance and emissions characteristics of methanol fuelled DISI engine: A numerical study". *Fuel* 322 (2022), p. 124167. DOI: https://doi.org/10.1016/j.fuel.2022.124167.

[108] P. Aakko-Saksa et al. "Comprehensive emission characterisation of exhaust from alternative fuelled cars". *Atmospheric Environment* 236 (2020), p. 117643. DOI: https://doi.org/10.1016/j.atmosenv.2020.117643.

[109] Fatemeh Kazemiparkouhi et al. "Comprehensive US database and model for ethanol blend effects on air toxics, particle number, and black carbon tailpipe emissions". *Atmospheric Environment: X* 16 (2022), p. 100185. DOI: https://doi.org/10.1016/j.aeaoa.2022.100185.

[110] Andreas Kolbeck and Ortwin Costenoble. "Engine tests with new types of biofuels and development of biofuel standards". *Horizon 2020 E10+ Project* (2019), pp. 1–16.

[111] Georgios Karavalakis et al. “Impacts of ethanol fuel level on emissions of regulated and unregulated pollutants from a fleet of gasoline light-duty vehicles”. *Fuel* 93 (Mar. 2012), pp. 549–558. DOI: 10.1016/j.fuel.2011.09.021.

[112] Georgios Karavalakis et al. “Assessing the impacts of ethanol and isobutanol on gaseous and particulate emissions from flexible fuel vehicles”. *Environmental Science and Technology* 48 (Dec. 2014), pp. 14016–14024. DOI: 10.1021/es5034316.

[113] Brian H West et al. “Intermediate Ethanol Blends Catalyst Durability Program”. *Office of Scientific and Technical Information (OSTI)* (Feb. 2012). DOI: 10.2172/1035578.

[114] Carolyn P. Hubbard, James E. Anderson, and Timothy J. Wallington. “Ethanol and Air Quality: Influence of Fuel Ethanol Content on Emissions and Fuel Economy of Flexible Fuel Vehicles”. *Environmental Science & Technology* 48.1 (2014), pp. 861–867. DOI: 10.1021/es404041v.

[115] Ingrid J. George et al. “Effects of Cold Temperature and Ethanol Content on VOC Emissions from Light-Duty Gasoline Vehicles”. *Environmental Science & Technology* 49.21 (2015), pp. 13067–13074. DOI: 10.1021/acs.est.5b04102.

[116] Georgios Karavalakis et al. “Evaluating the regulated emissions, air toxics, ultrafine particles, and black carbon from SI-PFI and SI-DI vehicles operating on different ethanol and iso-butanol blends”. *Fuel* 128 (2014), pp. 410–421. DOI: https://doi.org/10.1016/j.fuel.2014.03.016.

[117] Georgios Karavalakis et al. “The impact of ethanol and iso-butanol blends on gaseous and particulate emissions from two passenger cars equipped with spray-guided and wall-guided direct injection SI (spark ignition) engines”. *Energy* 82 (2015), pp. 168–179. DOI: https://doi.org/10.1016/j.energy.2015.01.023.

[118] Dongyoung Jin et al. “The impact of various ethanol-gasoline blends on particulates and unregulated gaseous emissions characteristics from a spark ignition direct injection (SIDI) passenger vehicle”. *Fuel* 209 (Dec. 2017), pp. 702–712. DOI: 10.1016/j.fuel.2017.08.063.

[119] Xin Wang et al. “Estimating Ozone Potential of Pipe-out Emissions from Euro-3 to Euro-5 Passenger Cars Fueled with Gasoline, Alcohol-Gasoline, Methanol and Compressed Natural Gas”. *SAE Technical Papers* 2016-April (April Apr. 2016). DOI: 10.4271/2016-01-1009.

[120] Mengzhu Zhang et al. “Effects of ethanol and aromatic contents of fuel on the non-regulated exhaust emissions and their ozone forming potential of E10-fueled China-6 compliant vehicles”. *Atmospheric Environment* 264 (2021), p. 118688. DOI: https://doi.org/10.1016/j.atmosenv.2021.118688.

[121] M. Clairotte et al. “Effects of low temperature on the cold start gaseous emissions from light duty vehicles fuelled by ethanol-blended gasoline”. *Applied Energy* 102 (2013). Special Issue on Advances in sustainable biofuel production and use - XIX International Symposium on Alcohol Fuels - ISAF, pp. 44–54. DOI: https://doi.org/10.1016/j.apenergy.2012.08.010.

[122] R. Suarez-Bertoa et al. “Impact of ethanol containing gasoline blends on emissions from a flex-fuel vehicle tested over the Worldwide Harmonized Light duty Test Cycle (WLTC)”. *Fuel* 143 (Mar. 2015), pp. 173–182. DOI: 10.1016/j.fuel.2014.10.076.

[123] R. Suarez-Bertoa et al. “Primary emissions and secondary organic aerosol formation from the exhaust of a flex-fuel (ethanol) vehicle”. *Atmospheric Environment* 117 (Sept. 2015), pp. 200–211. DOI: 10.1016/j.atmosenv.2015.07.006.

[124] R. Suarez-Bertoa and C. Astorga. “Unregulated emissions from light-duty hybrid electric vehicles”. *Atmospheric Environment* 136 (2016), pp. 134–143. DOI: https://doi.org/10.1016/j.atmosenv.2016.04.021.

[125] P Anselmi et al. “Ethanol fuel content impact on regulated and non-regulated emissions on EU6c and EU6d-Temp vehicles”. Jan. 2022.

[126] J-F. Fortune et al. “Impact of fuel ethanol content on regulated and non-regulated emissions monitored by various analytical techniques over flex-fuel and conversion kit applications”. *Fuel* 334 (2023), p. 126669. DOI: https://doi.org/10.1016/j.fuel.2022.126669.

[127] Piotr Bielaczyc et al. “An examination of the effect of ethanol-gasoline blends’ physicochemical properties on emissions from a light-duty spark ignition engine”. *Fuel Processing Technology* 107 (2013), pp. 50–63. DOI: 10.1016/j.fuproc.2012.07.030.

[128] Ahmad O. Hasan et al. “Formaldehyde, acetaldehyde and other aldehyde emissions from HCCI/SI gasoline engine equipped with prototype catalyst”. *Fuel* 175 (July 2016), pp. 249–256. DOI: 10.1016/j.fuel.2016.02.005.

[129] S. G. Poulopoulos, D. P. Samaras, and C. J. Philippopoulos. “Regulated and unregulated emissions from an internal combustion engine operating on ethanol-containing fuels”. *Atmospheric Environment* 35 (Sept. 2001), pp. 4399–4406. DOI: 10.1016/S1352-2310(01)00248-5.

[130] Ricardo Suarez-Bertoa et al. “Laboratory and On-Road Evaluation of a GPF-Equipped Gasoline Vehicle”. *Catalysts* 9.8 (2019). DOI: 10.3390/catal9080678.

[131] Päivi T. Aakko-Saksa, Leena Rantanen-Kolehmainen, and Eija Skyttä. “Ethanol, Isobutanol, and Biohydrocarbons as Gasoline Components in Relation to Gaseous Emissions and Particulate Matter”. *Environmental Science & Technology* 48.17 (2014), pp. 10489–10496. DOI: 10.1021/es501381h.

[132] Kawsar Mehsein et al. “Minimizing secondary pollutant formation through identification of most influential volatile emissions in gasoline exhausts: Impact of the vehicle powertrain technology”. *Atmospheric Environment* 226 (2020), p. 117394. DOI: https://doi.org/10.1016/j.atmosenv.2020.117394.

[133] Luis Carlos Monteiro Sales and José Ricardo Sodré. “Cold start emissions of an ethanol-fuelled engine with heated intake air and fuel”. *Fuel* 95 (2012), pp. 122–125. DOI: https://doi.org/10.1016/j.fuel.2011.11.067.

[134] Charlotte Sandstroem-Dahl et al. “Measurement methodologies for hydrocarbons, ethanol and aldehyde emissions from ethanol fuelled vehicles”. *SAE Technical Papers* 3 (2010), pp. 453–466. DOI: 10.4271/2010-01-1557.

[135] US EPA. *Compendium of Methods for the Determination of Toxic Organic Compounds in Ambient Air Second Edition Compendium Method TO-11A Determination of Formaldehyde in Ambient Air Using Adsorbent Cartridge Followed by High Performance Liquid Chromatography (HPLC)*. Tech. rep. 1999.

[136] Barouch Giechaskiel and Michaël Clairotte. "Fourier Transform Infrared (FTIR) Spectroscopy for Measurements of Vehicle Exhaust Emissions: A Review". *Applied Sciences* 11.16 (2021). DOI: 10.3390/app11167416.

[137] "Measurement Principle using an FTIR (Fourrier Transform Infra Red) Spectrometer (AVL SESAM FTIR)". ().

[138] Nick Molden. "Innovative Emissions Measurement and Perspective on Future Tailpipe Regulation : Real-world measurement and role of VOCs and N_2O emissions". *Johnson Matthey Technology Review* (Oct. 2022). DOI: 10.1595/205651323X16650512926820.

[139] Manni Zhu et al. "A New Portable Instrument for Online Measurements of Formaldehyde: From Ambient to Mobile Emission Sources". *Environmental Science & Technology Letters* 7.5 (2020), pp. 292–297. DOI: 10.1021/acs.estlett.0c00169.

[140] Ricardo Suarez-Bertoa et al. "Real-Time Measurements of Formaldehyde Emissions from Modern Vehicles". *Energies* 15.20 (2022). DOI: 10.3390/en15207680.

[141] Kenji Hara et al. "Formaldehydes Measurement Using Laser Spectroscopic Gas Analyzer". *SAE Technical Papers* (2021 2021). DOI: 10.4271/2021-01-0604.

[142] Yosuke Kondo et al. "Development Of On-board Multi-component Gas Analyzer Toward Euro 7". *SAE Technical Paper Series* 1 (Aug. 2023). DOI: 10.4271/2023-32-0026.

[143] Cécile Pera and Vincent Knop. "Methodology to define gasoline surrogates dedicated to auto-ignition in engines". *Fuel* 96 (2012), pp. 59–69. DOI: https://doi.org/10.1016/j.fuel.2012.01.008.

[144] Vincent Knop et al. "A linear-by-mole blending rule for octane numbers of n-heptane/iso-octane/toluene mixtures". *Fuel* 115 (2014), pp. 666–673. DOI: https://doi.org/10.1016/j.fuel.2013.07.093.

[145] European Union Science Hub. "EN 228: Automotive fuels-Unleaded petrol-Requirements and test methods". *European Commission* (2008).

[146] Rakesh Sarwal et al. "Ethanol blending in India - 2020-25 Roadmap". *Report of the Expert Committee, Government of India* (2021).

[147] National Renewable Energy Lab (NREL). "Ethanol Blends: Providing a Renewable Fuel Choice". *USDOE Office of Energy Efficiency and Renewable Energy (EERE)* (Aug. 2022).

[148] "Leading Supplier Of Bespoke Fuels and Blended Fuel Design". *Coryton* ().

[149] Sunnarborg; Duane A. "Quick release engine cylinder". *Sandia Corporation (Livermore, CA)* (1997).

[150] J. Baronick et al. "Modal measurement of raw exhaust volume and mass emissions by SESAM". *SAE Technical Papers* (1998). DOI: 10.4271/980047.

[151] Christine A. Gierczak et al. "Measuring NMHC and NMOG emissions from motor vehicles via FTIR spectroscopy". *Atmospheric Environment* 150 (2017), pp. 425–433. DOI: https://doi.org/10.1016/j.atmosenv.2016.11.038.

[152] SEMTECH. "SEMTECH DS+ module specifications". *SEMTECHő* (2023).

[153] Martin Weiss et al. "Will Euro 6 reduce the NOx emissions of new diesel cars? Insights from on-road tests with Portable Emissions Measurement Systems (PEMS)". *Atmospheric Environment* 62 (Dec. 2012), pp. 657–665. DOI: 10.1016/J.ATMOSENV.2012.08.056.

[154] Rosalind O'Driscoll et al. "A Portable Emissions Measurement System (PEMS) study of NOx and primary NO_2 emissions from Euro 6 diesel passenger cars and comparison with COPERT emission factors". *Atmospheric Environment* 145 (2016), pp. 81–91. DOI: https://doi.org/10.1016/j.atmosenv.2016.09.021.

[155] Rosalind O'Driscoll et al. "Real world CO_2 and NOx emissions from 149 Euro 5 and 6 diesel, gasoline, and hybrid passenger cars". *Science of The Total Environment* 621 (2018), pp. 282–290. DOI: https://doi.org/10.1016/j.scitotenv.2017.11.271.

[156] Marina Kousoulidou et al. "Use of portable emissions measurement system (PEMS) for the development and validation of passenger car emission factors". *Atmospheric Environment* 64 (2013), pp. 329–338. DOI: https://doi.org/10.1016/j.atmosenv.2012.09.062.

[157] Nick Molden and D.D. Booker. "Apparatus and Method for Sampling an Exhaust Gas". (2022).

[158] Sepsolve. "INSIGHTő- Outstanding performance for routine GCŒGC applications". *Sepsolve Analytical* (2023).

[159] Markes. "Markes International launches worlds first range of hydrogen-certified, Multi-Gas enabled thermal desorption instruments". *Markes International* (2023).

[160] Agilent. "Analytical HPLC systems - Agilent 1220 Infinity II Liquid Chromatography". *Aglient* (2023).

[161] R. J. Kee, F. M. Rupley, and J. A. Miller. *Chemkin-II: A Fortran chemical kinetics package for the analysis of gas-phase chemical kinetics*. Sept. 1989. DOI: 10.2172/5681118.

[162] J Warnatz, ů U Maas, and ů R W Dibble. *Combustion*. 4th ed. Springer, Apr. 2006.

[163] Alexander Burcat. "Thermochemical Data for Combustion Calculations". *Combustion Chemistry* (1984), pp. 455–473. DOI: 10.1007/978-1-4684-0186-8_8.

[164] Alison S. Tomlin. "The role of sensitivity and uncertainty analysis in combustion modelling". *Proceedings of the Combustion Institute* 34.1 (Jan. 2013), pp. 159–176. DOI: 10.1016/J.PROCI.2012.07.043.

[165] Reaction Design. "Chemkin Theory Manual Chemkin ő Software". (2016).

[166] XiaoHang Fang, Nikola Sekularac, and Martin H. Davy. "Parametric Studies of a Novel Combustion Modelling Approach for Low Temperature Diesel Spray Simulation". *Proceedings of the ASME 2020 Internal Combustion Engine Division Fall Technical Conference*. ASME, 2020. DOI: 10.1115/ICEF2020-2924.

[167] Yang Li et al. "Development of a reduced four-component (toluene/n-heptane/iso-octane/ethanol) gasoline surrogate model". *Fuel* 247 (2019), pp. 164–178. DOI: https://doi.org/10.1016/j.fuel.2019.03.052.

[168] Mani Sarathy et al. "Reduced Gasoline Surrogate (Toluene/n-Heptane/iso-Octane) Chemical Kinetic Model for Compression Ignition Simulations". *WCX World Congress Experience*. SAE International, Apr. 2018. DOI: https://doi.org/10.4271/2018-01-0191.

[169] Yunchao Wu et al. "A skeletal chemical kinetic mechanism for gasoline and gasoline/ethanol blend surrogates for engine CFD applications". *International Conference on Chemical Kinetics*. Chicago, IL, May 2017.

[170] Marco Mehl et al. “Kinetic modeling of gasoline surrogate components and mixtures under engine conditions”. *Proceedings of the Combustion Institute* 33.1 (2011), pp. 193–200. DOI: https://doi.org/10.1016/j.proci.2010.05.027.

[171] L.R. Cancino et al. “Ignition delay times of ethanol-containing multi-component gasoline surrogates: Shock-tube experiments and detailed modeling”. *Fuel* 90.3 (2011), pp. 1238–1244. DOI: https://doi.org/10.1016/j.fuel.2010.11.003.

[172] Philippe Dagaut and Casimir Togbé. “Experimental and Modeling Study of the Kinetics of Oxidation of EthanolGasoline Surrogate Mixtures (E85 Surrogate) in a Jet-Stirred Reactor”. *Energy & Fuels* 22.5 (2008), pp. 3499–3505. DOI: 10.1021/ef800214a.

[173] Zhewen Lu et al. “A high-pressure plug flow reactor for combustion chemistry investigations”. *Measurement Science and Technology* 28.10 (Sept. 2017), p. 105902. DOI: 10.1088/1361-6501/aa8023.

[174] S.P. Marshall et al. “Laminar burning velocity measurements of liquid fuels at elevated pressures and temperatures with combustion residuals”. *Combustion and Flame* 158.10 (2011), pp. 1920–1932. DOI: https://doi.org/10.1016/j.combustflame.2011.02.016.

[175] Congcong Liu et al. “Flammability and Propagation Dynamics of Planar Freely Propagating Dimethyl Ether Premixed Flame”. *ACS Omega* 5.19 (2020), pp. 10965–10976. DOI: 10.1021/acsomega.0c00792.

[176] Zhewen Lu, Yi Yang, and Michael J. Brear. “Impact of ethanol on oxidation of iso-octane at low and intermediate temperatures”. *Combustion and Flame* 214 (2020), pp. 167–183. DOI: https://doi.org/10.1016/j.combustflame.2019.12.040.

[177] Philippe Dagaut, Marcelline Reuillon, and Michel Cathonnet. “Experimental study of the oxidation of n-heptane in a jet stirred reactor from low to high temperature and pressures up to 40 atm”. *Combustion and Flame* 101.1 (1995), pp. 132–140. DOI: https://doi.org/10.1016/0010-2180(94)00184-T.

[178] S. Jerzembeck et al. “Laminar burning velocities at high pressure for primary reference fuels and gasoline: Experimental and numerical investigation”. *Combustion and Flame* 156.2 (2009), pp. 292–301. DOI: https://doi.org/10.1016/j.combustflame.2008.11.009.

[179] Tobias Knorsch et al. “Comparison of Different Gasoline Alternative Fuels in Terms of Laminar Burning Velocity at Increased Gas Temperatures and Exhaust Gas Recirculation Rates”. *Energy & Fuels* 28.2 (2014), pp. 1446–1452. DOI: 10.1021/ef4021922.

[180] A.P. Kelley et al. “Laminar flame speeds, non-premixed stagnation ignition, and reduced mechanisms in the oxidation of iso-octane”. *Proceedings of the Combustion Institute* 33.1 (2011), pp. 501–508. DOI: https://doi.org/10.1016/j.proci.2010.05.058.

[181] A.P. Kelley et al. “Laminar flame speeds of C5 to C8 n-alkanes at elevated pressures: Experimental determination, fuel similarity, and stretch sensitivity”. *Proceedings of the Combustion Institute* 33.1 (2011), pp. 963–970. DOI: https://doi.org/10.1016/j.proci.2010.06.074.

[182] Zhongwei Meng, Kun Liang, and Jia Fang. “Laminar burning velocities of iso-octane, toluene, 1-hexene, ethanol and their quaternary blends at elevated temperatures and pressures”. *Fuel* 237 (2019), pp. 630–636. DOI: https://doi.org/10.1016/j.fuel.2018.10.072.

[183] Guoqing Wang et al. “Investigation on laminar burning velocities of benzene, toluene and ethylbenzene up to 20 atm”. *Combustion and Flame* 184 (2017), pp. 312–323. DOI: https://doi.org/10.1016/j.combustflame.2017.06.017.

[184] V. Shankar et al. “Effect of ethanol addition on the laminar burning velocities of gasoline surrogates”. *Fuel* 327 (2022), p. 125186. DOI: https://doi.org/10.1016/j.fuel.2022.125186.

[185] N. Hinton et al. “Aqueous ethanol laminar burning velocity measurements using constant volume bomb methods”. *Fuel* 214 (2018), pp. 127–134. DOI: https://doi.org/10.1016/j.fuel.2017.10.113.

[186] E. Ranzi et al. “Hierarchical and comparative kinetic modeling of laminar flame speeds of hydrocarbon and oxygenated fuels”. *Progress in Energy and Combustion Science* 38.4 (2012), pp. 468–501. DOI: https://doi.org/10.1016/j.pecs.2012.03.004.

[187] Varun Shankar et al. “Effect of Ethanol Addition on the Laminar Burning Velocity of Gasoline Surrogates With Toluene”. Vol. ASME 2022 ICE Forward Conference. Internal Combustion Engine Division Fall Technical Conference. V001T02A006. Oct. 2022. DOI: 10.1115/ICEF2022-90452.

[188] Varun Shankar and Felix Leach. “Effects of oxygenate and aromatic content on engine-out aldehyde emissions from pure, binary, and ternary mixtures of ethanol, toluene, and iso-octane”. *JSAE/SAE Powertrains, Energy and Lubricants International meeting*. SAE International, Sept. 2023. DOI: doi.org/10.4271/2023-32-0029.

[189] Qinhao Fan et al. “Investigation into pressure dependence of flame speed for fuels with low and high octane sensitivity through blending ethanol”. *Combustion and Flame* 212 (Feb. 2020), pp. 252–269. DOI: 10.1016/J.COMBUSTFLAME.2019.10.040.

[190] Yanju Wei et al. “Aldehydes and Methanol Emission Mechanisms and Characteristics from a Methanol/Gasoline-Fueled Spark-Ignition (SI) Engine”. *Energy & Fuels* 23.12 (2009), pp. 6222–6230. DOI: 10.1021/ef900721v.

[191] Sergio Manzetti and Otto Andersen. “A review of emission products from bioethanol and its blends with gasoline. Background for new guidelines for emission control”. *Fuel* 140 (2015), pp. 293–301. DOI: https://doi.org/10.1016/j.fuel.2014.09.101.

[192] E. Zervas. “Formation of Oxygenated Compounds from Isooctane/Toluene Flames”. *Energy & Fuels* 19.5 (2005), pp. 1865–1872. DOI: 10.1021/ef050059x.

[193] E. Zervas, X. Montagne, and J. Lahaye. “Influence of fuel and air/fuel equivalence ratio on the emission of hydrocarbons from a SI engine. 2. Formation pathways and modelling of combustion processes”. *Fuel* 83.17 (2004), pp. 2313–2321. DOI: https://doi.org/10.1016/j.fuel.2004.06.028.

[194] Roger Magnusson, Calle Nilsson, and Barbro Andersson. “Emissions of Aldehydes and Ketones from a Two-Stroke Engine Using Ethanol and Ethanol-Blended Gasoline as Fuel”. *Environmental Science & Technology* 36.8 (2002), pp. 1656–1664. DOI: 10.1021/es010262g.

[195] Avinash Kumar Agarwal et al. “Unregulated emissions from a gasohol (E5, E15, M5, and M15) fuelled spark ignition engine”. *Applied Energy* 154 (2015), pp. 732–741. DOI: https://doi.org/10.1016/j.apenergy.2015.05.052.

[196] Varun Shankar et al. “Comparing Real Driving Emissions from Euro 6d-TEMP Vehicles Running on E0 and E10 Gasoline Blends”. *SAE Technical Papers* (Oct. 2023). DOI: 10.4271/2023-01-1662.

[197] E. Zervas, X. Montagne, and J. Lahaye. “C1 - C5 Organic Acid Emissions from an SI Engine: Influence of Fuel and Air/Fuel Equivalence Ratio”. *Environmental Science & Technology* 35.13 (2001), pp. 2746–2751. DOI: 10.1021/es000237v.

[198] European Commission. “Regulation of the European Parliament and of the Council on type-approval of motor vehicles and engines of systems, components, and separate technical units intended for such vehicles, with respect to their emissions and battery durability (Euro 7) and repealing Regulations (EC) No 715/2007 and (EC) No 595/2009”. (2022).

[199] T.J. Wallington and P. Wiesen. “N_2O emissions from global transportation”. *Atmospheric Environment* 94 (2014), pp. 258–263. DOI: https://doi.org/10.1016/j.atmosenv.2014.05.018.

[200] Xiaochen Wang et al. “Evaluation of hydrous ethanol as a fuel for internal combustion engines: A review”. *Renewable Energy* 194 (2022), pp. 504–525. DOI: https://doi.org/10.1016/j.renene.2022.05.132.

[201] Shijun Dong et al. “A new detailed kinetic model for surrogate fuels: C3MechV3.3”. *Applications in Energy and Combustion Science* 9 (2022), p. 100043. DOI: 10.1016/j.jaecs.2021.100043.

[202] Abdullah Bajwa, Varun Shankar, and Felix Leach. “Engine-out Ammonia Emissions from a Gasoline Direct Injection Engine”. SAE Technical Papers, 2023. DOI: doi.org/10.4271/2023-01-1655.

[203] K. H. Becker et al. “Nitrous Oxide (N_2O) Emissions from Vehicles”. *Environmental Science & Technology* 33.22 (1999), pp. 4134–4139. DOI: 10.1021/es9903330.

[204] Ricardo Suarez-Bertoa and Covadonga Astorga. “Impact of cold temperature on Euro 6 passenger car emissions”. *Environmental Pollution* 234 (2018), pp. 318–329. DOI: https://doi.org/10.1016/j.envpol.2017.10.096.